NOVEL DONOR-ACCEPTOR-SUBSTITUTED BUTADIENE SYSTEMS: PHOTOCHEMICAL AND PHOTOPHYSICAL PROPERTIES IN SOLUTION, LIQUID CRYSTALLINE AND CRYSTALLINE PHASES

THESIS SUBMITTED TO
THE UNIVERSITY OF KERALA
FOR THE DEGREE OF
DOCTOR OF PHILOSOPHY
IN CHEMISTRY
UNDER THE FACULTY OF SCIENCE

By
RIJU DAVIS

PHOTOSCIENCES AND PHOTONICS DIVISION
REGIONAL RESEARCH LABORATORY (CSIR)
TRIVANDRUM – 695 019
KERALA, INDIA

NOVEMBER 2002

I dedicate this to .....

My Parents

and

My Sister

STATEMENT

I hereby declare that the matter embodied in the thesis entitled: *"Novel Donor-Acceptor-Substituted Butadiene Systems: Photochemical and Photophysical Properties in Solution, Liquid Crystalline and Crystalline Phases,"* is the result of investigations carried out by me at the Photosciences and Photonics Division of the Regional Research Laboratory (CSIR). Trivandrum, under the supervision of Dr. Suresh Das and the same has not been submitted elsewhere for a degree.

In keeping with the general practice of reporting scientific observations, due acknowledgement has been made wherever the work described is based on the findings of other investigators.

Riju Davis

1

PHOTOSCIENCES AND PHOTONICS DIVISION
REGIONAL RESEARCH LABORATORY (CSIR)
TRIVANDRUM-695 019, INDIA

Dr. SURESH DAS
HEAD

Tel: 91-471-515318(O), 544309(R)
Fax: 91-471-490186
Email: sdaas@rediffmail.com

November 11, 2002

CERTIFICATE

This is to certify that the work embodied in the thesis entitled: *"Novel Donor-Acceptor-Substituted Butadiene Systems: Photochemical and Photophysical Properties in Solution, Liquid Crystalline and Crystalline Phases,"* has been carried out by Mr. Riju Davis under my supervision and the same has not been submitted elsewhere for a degree.

Suresh Das

Thesis Supervisor

ACKNOWLEDGEMENTS

I have great pleasure in placing on record my deep sense of gratitude to Dr. Suresh Das, my thesis supervisor, for suggesting the research problem and for his guidance, support and encouragement, leading to the successful completion of this work.

I would like to express my sincere thanks to Professor M. V. George for his constant encouragement, inspiration and useful discussions during the tenure of this work.

I wish to thank Professor Javed Iqbal and Dr. G. Vijay Nair, Director and former Director, respectively, Regional Research Laboratory, Trivandrum for providing necessary facilities for carrying out the work.

I sincerely thank Dr. A. Ajayaghosh, Dr. K. R. Gopidas, Dr. D. Ramaiah and Dr. K. George Thomas, Scientists of Photosciences and Photonics Division, for all help and support extended to me.

I thank all the members of Photosciences and Photonics Division and in particular, Dr. Mathew George, Dr. V. Suresh, Dr. V. Ajaya Mallia, Mr. Robert Philip, Mr. Shibu Abraham and Mrs. Sarada Nair for their help and cooperation. I also thank my friends in other divisions of Regional Research Laboratory, Trivandrum for their cooperation.

Also, I wish to thank Professor Klass A. Zachariasse, Max-Planck- Institut für biophysikalische Chemie, Göttingen, Germany for useful discussions.

I am deeply grateful to my parents and my other family members for their constant love and care which has been a great source of motivation.

Riju Davis

CONTENTS

Chapter 3. Reversible Photochemical Phase Transition Behaviour of Alkoxy-Cyano-Substituted Diphenylbutadiene Liquid Crystals

V

Chapter 4. *Study of the Fluorescence of Alkoxy-Cyano and Alkylamino-Cyano-Substituted Diphenylbutadienes in Solution and Crystalline Phases*

PREFACE

The design and study of photoresponsive materials has been attracting increasing attention due to their potential application in memory storage, optical computing, high-speed communications and display devices. Liquid crystals form a class of materials that are highly suited for the design of photoresponsive materials, since the cooperative behaviour of liquid crystalline molecules and their long-range order help to amplify relatively weak photochemical processes occurring at the molecular level into macroscopic phenomena. Most liquid crystalline systems designed for such applications have utilized the trans-cis photoisomerization of the azobenzene chromophore, since its rod-shaped trans isomer is known to stabilize the liquid crystalline phase whereas, the cis isomer destabilizes it. Although the azobenzene chromophore has several advantages, development of photoswitchable liquid crystals using alternate chromophores is desirable. The major focus of this thesis has been to study the detailed photochemical and photophysical properties of some donor-acceptor (DA)-substituted butadienes and to develop photoresponsive materials based on this chromophore, including liquid crystals and solid state fluorescent materials.

Chapter 1 provides a review of the recent work on the design and study of photoresponsive liquid crystals. A brief description of various aspects regarding photoisomerization in polyenes, its role in vision as well as its potential aspects in the design of photoresponsive liquid crystals are also presented.

*Chapter 2 describes a detailed study on the photophysical and photochemical properties of some DA-substituted butadiene derivatives containing various amines as donors and indane-1,3-dione as the acceptor. These model compounds were selected in order to gain an insight into the role of donor and acceptor groups in controlling the excited state behavior of the butadiene chromophore. Four of these derivatives, **BN5**, **BN6**, **BNDE** and **BN5AN** showed the anomalous property of dual fluorescence. This could be attributed to emissions arising from a locally excited (LE) state and from a considerably more polar intramolecular charge transfer (ICT) state. The presence of an amine substituent with the nitrogen atom directly attached to the butadiene chain was found to be essential for observing dual fluorescence in this class of compounds. The*

quantum efficiency of E-Z photoisomerization from the excited singlet state of these compounds was about 0.1 in benzene at room temperature. The triplet excited state properties of the butadiene derivatives have been characterized via triplet-triplet sensitization with benzophenone as the triplet energy donor, since the intersystem crossing efficiency was negligible for this class of compounds. Whereas photoisomerization of the derivatives with five-membered alicylic amine donors occurred quantitatively from the singlet state, those containing six- membered or aliphatic amines as the donor moiety underwent photoisomerization more efficiently from their triplet states. The Z-E thermal isomerization of the derivatives with nitrogen atoms directly linked to the butadiene chain occurred at rates, which were several orders of magnitude higher than that of the derivative containing a phenyl linker between the amine and the butadiene groups.

Earlier work on the design of photoswitchable liquid crystals have mostly used the photoisomerization of the azobenzene chromophore. A major drawback associated with the use of the azobenzene chromophore is its ability to undergo thermal cis-trans isomerization, which makes long-term storage of information difficult. Chapter 3 describes our work on the design and synthesis of photoresponsive liquid crystals based on the butadiene chromophore. The EE isomers of the monoalkoxy-cyano-substituted diphenylbutadiene derivatives were found to undergo isomerization on photolysis with 360 nm light, to yield thermally stable EZ and ZE isomers, which could be transformed back to the EE isomer by photolysis using 266 nm light. Photolysis of the liquid crystalline EE isomers of monoalkoxy derivatives resulted in isothermal phase transition to the isotropic phase due to the formation of the non-liquid crystalline EZ and ZE isomers. The thermal stability of the EZ and ZE isomers ensured that reverse switching of these materials to the liquid crystalline phase occurred only on photolysis with 266 nm light.

Chapter 4 describes the solution and solid state fluorescence of mono- and tri-alkoxy-cyano-substituted diphenylbutadienes, as well as that of some alkylamino-cyano-substituted diphenylbutadiene derivatives. In solution, the fluorescence properties of the alkoxy derivatives were nearly indistinguishable, showing an emission in the blue region with emission maxima centered on ~450 nm. In the solid state however, the

*fluorescence properties of the monoalkoxy-cyano-substituted diphenylbutadiene derivatives were observed to be highly dependent on the nature of the alkoxy substitution. Whereas the short alkoxy chain derivatives exhibited green emission (λ_{max}~520 nm) the long-chain derivatives showed blue emission (λ_{max}~450 nm). The drastic difference in fluorescence properties with the change of their alkoxy substituent has been attributed to the way in which molecules pack in the solid state, which in turn affects the exciton coupling. Single crystal and powder X-ray diffraction (XRD) analyses show that in the solid state these molecules are held in a three dimensional lattice by both π-stacking and hydrogen bonding. By bringing about suitable structural modifications of the butadiene chromophore it has been possible to tune the solid state fluorescence of these materials almost over the entire visible range, with the alkoxy-cyano-substituted diphenylbutadienes emitting in the blue-green region and the alkylamino-cyano derivatives emitting in the yellow-red region. The solid state fluorescence of these derivatives was also found to be highly sensitive to temperature, decreasing in its intensity with increasing temperature. The thermal sensitivity of these materials makes them potentially useful as temperature sensors. One of these derivatives, **BC8** when obtained freshly from its melt exhibited green fluorescence (~500 nm) which changes back to its original blue fluorescing state over a period ~6 h at 27 °C. Powder XRD analyses clearly show that these changes are due to distinctly different crystal packing. Photoisomerization of the butadiene chromophore in these derivatives could also be utilized for storing fluorescent images in the their solid films.*

Chapter 1

Photoresponsive Liquid Crystals and The Role of Photoisomerization Reactions for Their Design

1.1. Abstract

Photochemical transformations of molecules in liquid crystalline media can lead to changes in their phase transition characteristics or alignment. The ability of liquid crystals to amplify molecular level processes into macroscopic phenomena arises due to their cooperative interactions and long-range ordering. This chapter provides an overview of various aspects regarding the use of the photoisomerizable azobenzene chromophore for the design and study of photoresponsive liquid crystals. Another class of chromophores that can be used for the design of photoresponsive materials are polyenes. A brief description of various aspects regarding photoisomerization in polyenes, its role in vision as well as its potential application in the design of photoresponsive liquid crystals is also presented.

1.2. Introduction

Interest in the study of photochemical and photophysical processes in organized assemblies has largely been driven by efforts to use the constrained matrices provided by such assemblies to control the excited state properties of guest molecules. For example, the rigid environment provided by some of the microassemblies can be utilized for carrying out photochemical reactions in a stereo-, regio- and enantiospecific manner.[1-4] Similarly, variations in viscosity, polarity and pH in constrained media can be used to control the excited state lifetimes and luminescence properties of guest molecules.[4-7] In tune with these studies, earlier reports on photochemical and photophysical processes in liquid crystalline (LC) media have also mainly concentrated on utilizing the anisotropic and constrained environment of LCs to control the excited state behaviour of guest molecules.[8-11] Most of these studies have been reviewed.[4,8]

A far more interesting aspect of the study of photochemical processes in liquid crystalline media is where the photochemical transformations can bring about modifications in the alignment or phase transition properties of the liquid crystalline host.[12-14] In these systems, weak photochemical processes occurring at the molecular level are translated into macroscopic phenomena due to the cooperative interactions and long-range ordering of liquid crystalline molecules, leading to amplification of the signals. Currently available display devices based on liquid crystals use electric field induced

switching, which possess switching times in the order of several milliseconds. In photoresponsive liquid crystals, switching rates can be several orders of magnitude higher making them potentially important in a number of advanced photonic applications such as memory storage, optical computing, high-speed communication and real-time holography.

1.3. Classification and Optical Properties

The structure and properties of liquid crystals have been extensively reviewed[15-24] and only a brief description is provided here. Liquid crystals form a class of condensed phase where the molecules possess a degree of orientation, intermediate to that of highly ordered crystals and isotropic liquids. They form supramolecular assemblies with unidirectional orientation of their molecular axes to give rise to optical anisotropy. Liquid crystals can be broadly classified as lyotropic, where the mesomorphic phase formation is solvent induced and thermotropic, where the mesophase formation is thermally induced. This account mainly deals with the photoresponsive aspects of thermotropic LCs. Thermotropic LC phases are predominantly observed in organic compounds, which are rod-, disc- or board- shaped. According to their microscopic organization, liquid crystalline phases are broadly grouped into four major classes namely nematics, cholesterics, smectics, and discotics (Figure 1.1). In the nematic mesophase, the molecules are aligned with their long axes parallel to each other. Cholesteric or chiral

nematic phases are observed in optically active molecules or by nematic liquid crystals containing optically active dopants. In this phase the director (a unit vector signifying the average direction of the molecular long axis) of an individual layer is twisted through a small angle with respect to the director of the adjacent layer resulting in a helical arrangement of the layers. The thickness required for the director to turn through 360° represents the pitch length (p) of the helical arrangement in cholesterics. In a smectic mesophase, the molecules are not only aligned parallel but are also arranged in such a way that the centers of adjacent molecules lie in a plane. Smectic phases can be further differentiated depending upon the packing arrangement of the molecules within the layers and the angle of the directors to the layer plane. Discotic phases are generally exhibited by disc shaped molecules where these molecules can pack in a nematic-like arrangement or as vertically stacked columns.

Nematic   Cholesteric

Smectic   Discotic
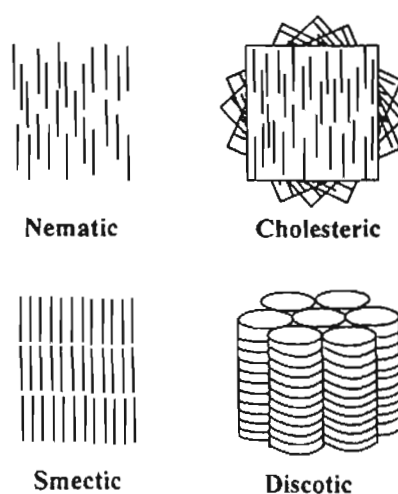
Figure 1.1. Pictorial representations of the molecular shapes and orientations of the major liquid crystalline phase types.

The anisotropic packing of liquid crystals imparts unique optical properties to this class of materials.[16,25,26] Most mesophases exhibit birefringence whose intensity is dependent upon the difference of the refractive index parallel and perpendicular to the director, angle of incidence of light on the surface and wavelength of light. As a result, the polarization of light can be altered as it passes through the mesophase. Normally mesophases exist in a non-oriented fashion containing domains of differing alignment (Figure 1.2), and these generally possess a milky and non-transparent appearance due to internal light scattering.
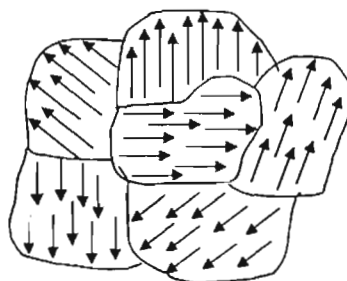
Figure 1.2. Representation of several domains in a mesophase having different alignment.

Liquid crystals can however be oriented macroscopically using mechanical, electric or magnetic forces, to form optically clear films.[25] A typical example of a macroscopically oriented liquid crystal cell is shown in Figure 1.3a, where the top and bottom surfaces of the liquid crystal cell that have been treated to align the molecules perpendicular to each other. The intervening layers arrange themselves in a twisted manner as shown in the figure, due to the influence of the neighboring molecules. In such a cell, known as the twisted nematic cell, which is normally used in conventional liquid crystal display devices, the plane of polarization of

transmitted light will also be twisted by 90° as depicted in Figure 1.3a.[27] The unique helical ordering of cholesteric liquid crystal molecules on the other hand induces selective reflection of the wavelengths satisfying the relationship, $\lambda = np$, where n is the refractive index of the liquid crystalline material and p is the helical pitch length (Figure 1.3b).[28] The ability to control these and other unique optical properties of liquid crystals by modifying their alignment and phase transition behaviour forms the principal basis for design of liquid crystal based optical switches.
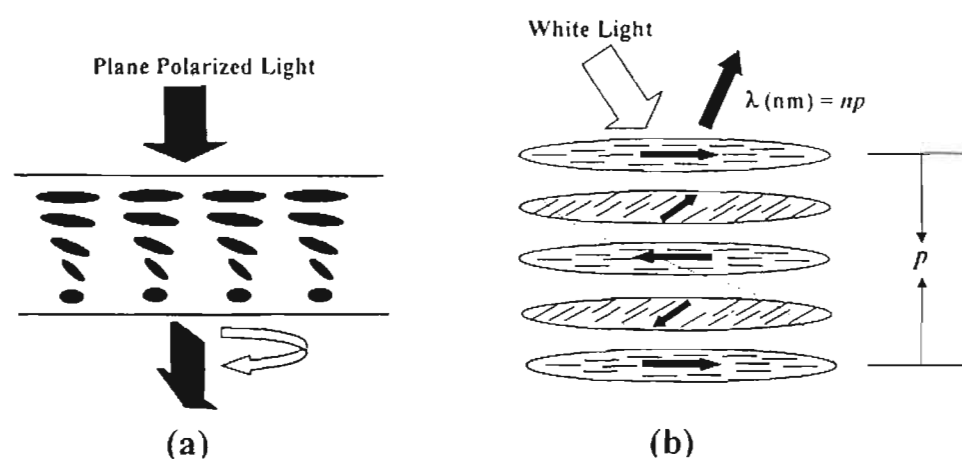
Figure 1.3. Pictorial representation of a) a typical twisted nematic liquid crystal cell and b) helical ordering of layers and selective reflection of light in cholesteric liquid crystals.

1.4. Photoswitching in Liquid Crystals

Photophysical and photochemical processes in liquid crystals can bring about changes in the alignment or phase transition properties. Earlier studies utilized the heat content (thermal-mode switching) of light to bring about such changes. More recently, it has been shown that photochemical changes

(photochemical-mode) can be utilized to bring about these transformations in a more selective manner.

1.4.1. Thermal-Mode Switching

In thermal-mode switching, regions of local overheating are created with a laser beam in homeotropically-aligned smectic, cholesteric or smectic/cholesteric mixtures held between transparent indium tin oxide (ITO) coated glass plates.[29,30] In these local regions, the liquid crystalline phase changes to an isotropic melt thereby destroying the homeotropic alignment. On cooling, scattering polydomains are formed in this region (Figure 1.4). Such laser addressed liquid crystal light valves can generate stable images with high spatial resolution and contrast ratio.[31] The image can be erased by applying an electrical field as depicted in Figure 1.4. The long-term stability of images could be significantly improved by using polymeric LCs.[32,33]
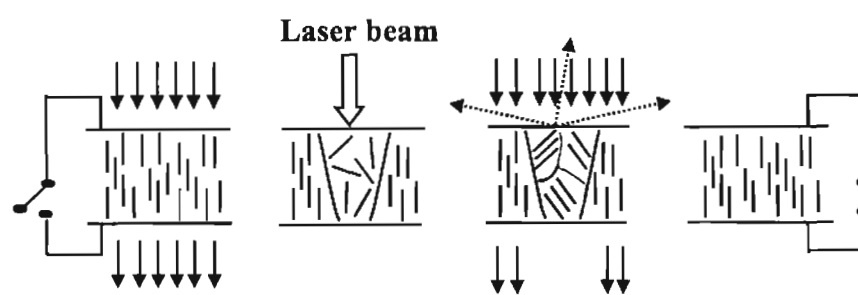
Figure 1.4. Representation of thermal-mode imaging on oriented nematic LC film. Adapted from reference 32.

In the earlier devices optically transparent ITO electrodes were used to absorb the laser light and convert it into heat. The heat thus generated is conducted

into the LC layer resulting in local isotropization. However in these systems the necessity for heat transfer from the glass substrate to the LC layer results in an increase in the write-in time, and the spread in heat energy results in the loss of resolution of the images. Imaging by thermal-mode switching could be substantially improved by doping the LCs with a light absorbing dye such as Ni chelates, which are photochemically inert and nonfluorescent. The predominant pathway for loss of excitation energy in these Ni chelates is via radiation (thermal) processes with lifetimes of 10^{-11} to 10^{-13} s. These complexes can rapidly 'dump' heat uniformly into the LC medium. Further improvement in the resolution of the image in the 'thermal-mode' switching could be obtained by doping the LCs with photochemically inert dyes possessing high dichroic ratios.[34]

1.4.2. Photochemical Switching

In contrast to thermal-mode switching, photochemical switching is brought about by chemical transformations of either the guest molecules dissolved in LC matrices or of the LC molecules themselves. Both reversible and irreversible photochemical transformations can be utilized for switching applications. For example, photodecomposition of cholesteryl iodide in LC mixtures comprising of cholesteryl iodide and cholesteryl nonanoate resulted in a change in their selective reflectivity.[35] Due to the irreversible nature of this photoreaction, it is not possible to erase images stored in this manner. Phase transitions as well as alignment changes of LCs brought about by photochemical transformations which are

thermally or photochemically reversible are of more interest since they can be used for the design of erasable-direct-read-after-write (EDRAW) systems.[13,36-42]

1.5. Photoinduced Phase Transitions

1.5.1. Host-Guest Systems

The presence of extraneous molecules can reduce the isotropization temperatures of LCs, and the extent of reduction can vary with the shape of the molecule. For example, when nematic or smectic LCs are doped with rod-shaped *trans*-isomers of azobenzenes the isotropization temperature of the host LCs are not significantly altered, whereas large depression in the isotropization temperatures can be observed when the bent *cis*-isomers of azobenzenes are used as dopants.[12,41] Thus photoisomerization of *trans* azobenzenes dissolved in LC matrices held close to their isotropization temperatures can result in isotropization. Recovery of the LC phase becomes possible by reconversion of the *cis*-isomers of azobenzenes to their *trans*-form either thermally or photochemically. Since photochemically induced phase transitions do not involve a change in temperature, they are termed as isothermal phase transitions. Apart from azobenzenes, photochromic molecules such as spiropyrans, fulgides and stilbenes, which can undergo significant changes in their molecular shapes, can be used as dopants to bring about photoinduced isothermal phase transitions.[43,44] The various parameters that control photoinduced isothermal phase transitions in host-guest systems,

such as the nature of the host LCs, photochromic guest, concentration of the guest as well as temperature, have been extensively investigated.[45-48] Photochemical phase transitions in host-guest systems where the host is a liquid crystalline polymer has also been extensively investigated.[49]

The dynamics of phase transition in LCs doped with azobenzenes has been examined by Ikeda and co-workers using time-resolved birefringence measurements.[50] Excitation by 355 nm pulsed laser resulted in photoisomerization of the azobenzene dopant which leads to the isotropization of the LC host. Loss of birefringence in the irradiated region resulted in reduction in the transmission of light through the crossed polarizers. The time required for total loss of transmittance, which corresponds to the time required for the isothermal phase transition was observed to be ~100 ms. Confirmation that the phase transition was indeed due to photochemical transitions and not due to 'thermal-mode' switching, was obtained by the absence of isotropization when a model azobenzene derivative, which does not undergo photoisomerization, was used as the dopant. The time required for nematic-isotropic switching was the same for LC polymers doped with azobenzene derivatives.

Photoswitching between nematic and cholesteric phases have been investigated using chiro-optical molecular switches. Nematic liquid crystals can be converted into cholesterics using chiral dopants.[51] By doping the nematic LC with just sufficient amount of chiral dopant needed for the

formation of cholesteric phase only in one photostate, a reversible nematic to cholesteric photoswitching can be produced. For example, the photoisomerization of enantiomerically pure bisimine (Scheme 1.1) doped in a commericially available nematic LCs, such as ZL1-389 and K_{15} resulted in reversible switching between cholesteric and nematic phases.[51]
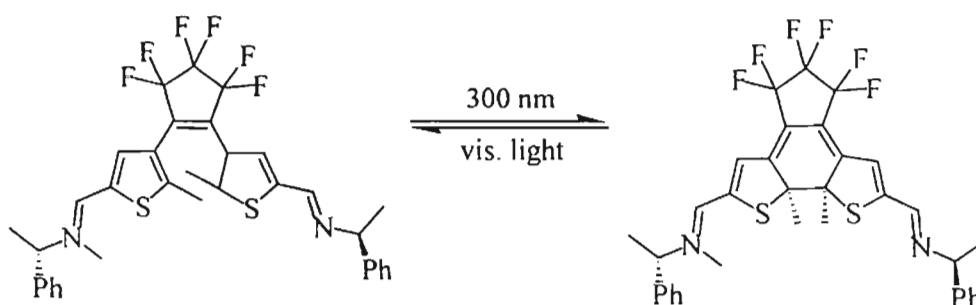
Scheme 1.1. Photoisomerization of enantiomerically pure bisimines. Adapted from reference 51.

Irradiation of the nematic LCs doped with the acrylic ester-substituted bicyclic ketones (Chart 1.1) using circularly polarized light resulted in a nematic to cholesteric phase transition due to formation of enantiomeric excess of the dopant.[52]
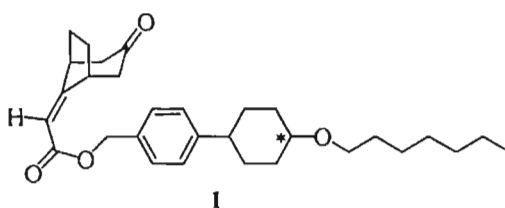
Chart 1.1

1.5.2. Intrinsically Photoactive Liquid Crystals

Photoisomerization of azobenzene derivatives is a very fast process and generally occurs in the picosecond time domain. The relatively long time required for photoinduced isothermal phase transitions in azobenzene doped LCs can be attributed to the time required for the host LC molecules to react to the formation of the *cis*-isomer of the azobenzene dopant. It would therefore be possible to reduce the response or switching times for photoinduced isothermal phase transitions by designing LC molecules, which are intrinsically photoactive.

The azobenzene chromophore is ideally suited for the design of intrinsically photoactive liquid crystals, since its *trans*-isomer stabilizes the LC phase whereas its *cis*-isomer destabilizes it. Ikeda and coworkers have developed monomeric and polymeric azobenzene derivatives (Chart 1.2) which are nematic in their *trans*-form and isotropic in their *cis*-form.[41,53-55] Photolysis of thin films (~200 nm) of the *trans*-isomer of the low molecular weight azobenzene derivatives leads to isotropization due to the formation of the *cis*-isomer. Time-resolved measurements of the changes in the birefringence indicated that the photoinduced isothermal phase transition occurred in about 200 μs, which is several orders of magnitude faster than the rate of photoswitching observed in host-guest systems. In these systems, the

thermal *cis-trans* isomerization is very fast (~30 s) and hence long-term storage of the image is not possible.

$n\text{-}C_4H_9$—⬡—N=N—⬡—OCH_3

2

K 35°C N 48°C I

$n\text{-}C_8H_{17}O$—⬡—N=N—⬡—$O\text{-}n\text{-}C_8H_{17}$

3

K 99°C N 113°C I

$+CH_2\text{-}CH+_n$
|
C=O
|
O-$(H_2C)_6$-O—⬡—N=N—⬡—OC_2H_5

4

G 45°C N 155°C I $Mn = 9100$
                      $Mw/Mn = 1.3$
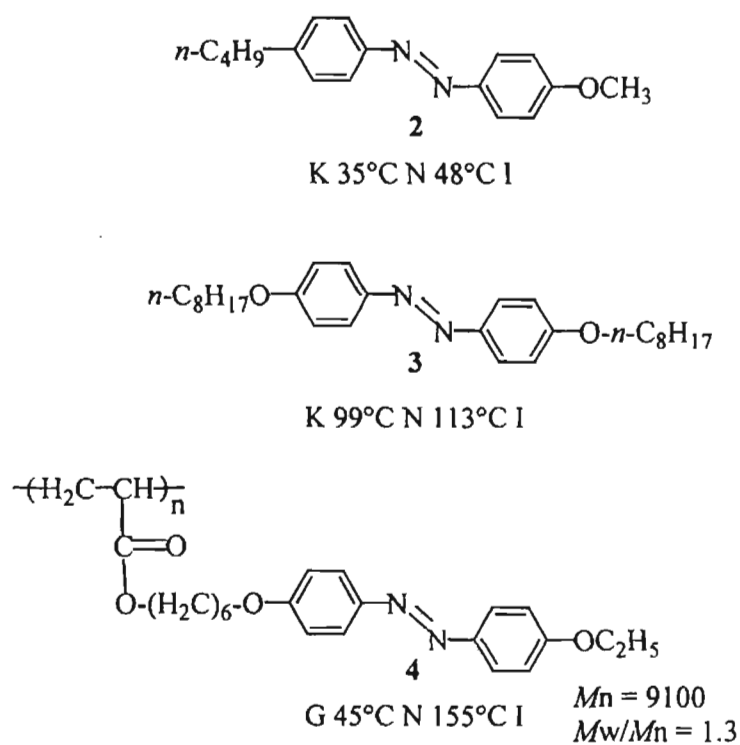
Chart 1.2

The polymeric LC (PLC), **4**(Chart 1.2) possess a much larger nematic temperature range. Irradiation of the PLC derivative also led to isothermal phase changes and the rate of change was similar to that reported for the low-molecular weight LCs. Interestingly, a nematic to isotropic phase transition with similar switching times could also be observed on irradiation of the PLC below its glass transition temperature (T_g).[41,55] Although at room temperature the thermal *cis-trans* isomerization occurred within about 24 h the image formed remains stable for extended periods of over a year. The images could be erased however by heating the polymer film above its T_g. Based on the

changes in the dichroic ratios of the azobenzene chromophore between the various states, the mechanism shown in Figure 1.5 was proposed to explain the storage of information in the PLC below its T_g.[41]
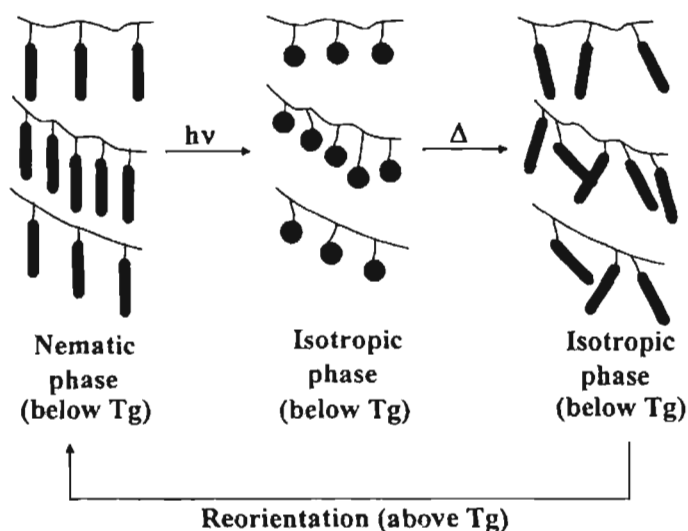
Figure 1.5. Orientation of *trans*-azobenzene mesogens after the *trans-cis-trans* cycles. The orientation of the *trans*-azobenzene mesogens is random after the thermal *cis-trans* back isomerization and this random orientation is fixed below the Tg of the polymer. The nematic phase can be restored if the temperature is raised above Tg. Adapted from reference 41.

In the glassy state (below Tg) the azobenzene chromophores exist in an ordered state as in the nematic phase. Irradiation resulted in a *trans-cis* isomerization of the azobenzene chromophore, which leads to a loss in the dichroic ratio as shown schematically in Figure 1.5. The dichroic ratio did not recover even after the thermal *cis-trans* isomerization was complete, indicating that the *trans-* isomers were reformed in a randomly aligned manner. The randomly aligned azobenzene chromophores could not reorient due to the rigidity of the PLC film below its T_g and thus forming a stable

image. Above the T_g of the polymer the chromophore realign leading to erasure of the stored image.

The optical switching behaviour of polymer azobenzene LCs has been investigated using reflection-mode analysis. Optical switching observed in the reflection-mode could be repeated over ten thousand cycles, which was ten times more stable than that observed in the transmission-mode analysis. Although the response time in the switching was 100 μs, which was similar to that observed in the transmission-mode the recovery of the nematic phase occurred in 1 ms which was about six times faster.[54]

LC materials can also be obtained through non-covalent interactions such as hydrogen bonding, ionic, charge-transfer and ion-dipolar interactions between complimentary structural elements. Photoswitchable LCs can be designed by selecting a photoresponsive chromophore as one of the elements. Kato *et al.* have reported on a hydrogen bonded liquid crystalline polymer complex between a polymeric hydrogen bond acceptor **5** (Chart 1.3) and 6-[(4-octlphenylazo)phenoxy]hexanoic acid (**6**).[56] The hydrogen bonded complex between the acceptor and 6-[(4-octylphenylazo)phenoxy]hexanoic acid exhibited a nematic phase between 47-93 °C. Sequential UV and visible light irradiation caused reversible photochemically induced nematic-isotropic phase transitions.
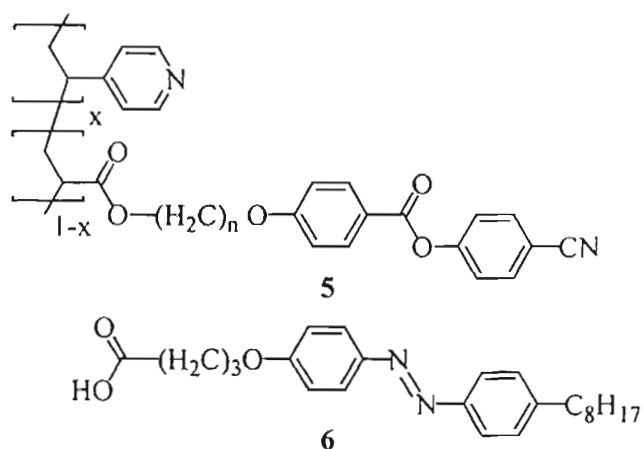
Chart 1.3

The liquid crystalline behaviour and photoswitching characteristics of LCs formed via hydrogen bonding between 4,4'-azobipyridine and 4-alkylbenzoic acids have been reported (Chart 1.4). On photolysis the supramolecular hydrogen bonded assemblies undergo a smectic to crystalline phase transition.[57] A number of other hydrogen bonded LCs containing substituted 4'-azopyridine as the hydrogen bond acceptor have been synthesized and investigated.[58] Photoinduced phase transitions were not observed in these systems and this could be attributed to substantial enhancement in thermal *cis-trans* isomerization of the chromophore on hydrogen bonding, which did not allow sufficient amounts of the *cis*-isomer to build up on irradiation.

$R = C_4H_9, C_6H_{13}, C_8H_{17}, C_{10}H_{21}, C_{12}H_{25}$
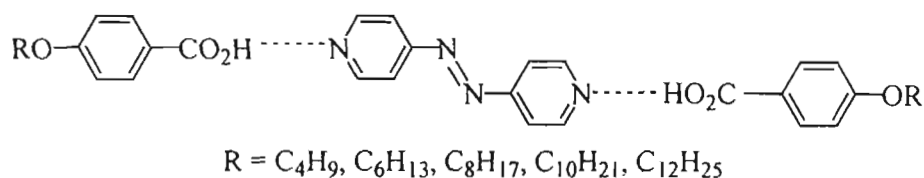
7

Chart 1.4

1.6. Photoinduced Alignment Changes in Liquid Crystals

Photochemically induced changes in alignment of LCs have been extensively investigated in recent years. Both in-plane and out-of-plane alignment of LCs can be achieved allowing two- and three-dimensional storage of information. Various aspects regarding photoinduced alignment have been recently reviewed.[12,13]

Reversibly isomerizable chromophores such as azobenzene are known to undergo reorientation when irradiated with plain polarized light in rigid polymeric media. The change in alignment can be easily discerned on measuring the angular dependence of absorbance of the chromophore at its absorption maximum using polarized light, which arises due to the dichroic nature of the molecule.[59-63] The dichroic ratio (R) of a molecule is given by.

$$R = A_\parallel / A_\perp \qquad (1.1)$$

where, $A_\parallel$ and $A_\perp$ are the absorbance measured with the polarized beam parallel and perpendicular to the optical axis of the molecule. The dichroic ratio of azobenzene derivatives are fairly high.[64,65] A schematic representation of the change in angular dependence of absorption before and after irradiation of azobenzene in a polymeric film using plane-polarized light is given in Figure 1.6. Before irradiation the azobenzene chrompohores are randomly aligned and the absorbance is the same in all directions as represented by the radius of the circle. Following irradiation, the intensity of

absorption perpendicular to the plane of polarization of light increases whereas the absorption parallel to it decreases. This is caused by selective absorption of light by the azobenzene chromophore aligned parallel or closely parallel to the plane of polarization of the irradiation source and conversion of these molecules to their *cis*-form. Thermal isomerization of the *cis*-isomer will lead to randomly aligned *trans*-isomers, which due to the rigidity of the medium will be frozen into the new alignment until excited again. On prolonged irradiation, chromophores possessing their molecular axis aligned closely parallel to the plane of polarization will undergo repeated *trans-cis-trans* isomerization whereas those with their molecular axis aligned perpendicular would remain unaffected. This eventually results in most of the azobenzene molecules being perpendicularly aligned to the plane of polarization of light. Heating the polymers above their T_g can erase the induced alignment.

Direction of polarization of irradiation light
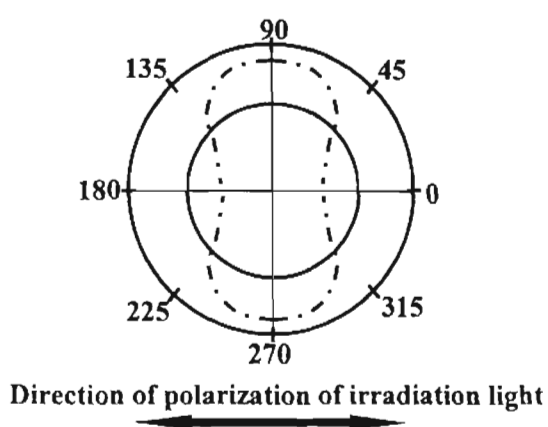
Figure 1.6. Schematic representation of angular dependence of absorption of plane polarized light by azobenzene in polymer film before (inner circle) and after irradiation (dotted curve).

The ability of photoresponsive molecules like azobenzene derivatives to undergo reorientation on irradiation by polarized light can be utilized to bring about photoalignment of LCs.[13] This can be achieved either by doping the LCs with photoresponsive molecules or incorporation of such molecules on the surface of cells containing the LCs. The mechanism of photoalignment in LCs doped with a photoresponsive molecule on irradiation is shown schematically in Figure 1.7.

● Photoresponsive molecule ◯ LC molecule
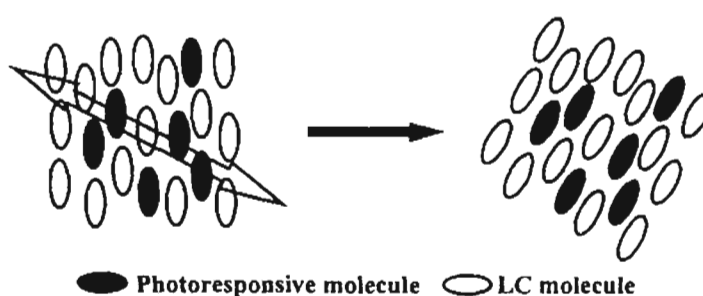
Figure 1.7 Molecular reorientation of photochromic LCs irradiated with linearly polarized light resulting in a cooperative photo-reorientation of LC molecules. Adapted from reference 13.

Irradiation of azobenzene doped LCs results in alignment of the axes of the azobenzene molecules perpendicular to the plane of polarization. Due to the cooperative interaction and long-range ordering of LCs the host LC molecules also align their axes parallel to that of the photochromic molecules. The photoinduced alignment is short-lived in low-molecular weight LCs. This is due to thermal randomization of the *trans*-isomers of azobenzene due to the fluid like nature of low-molecular weight LCs. Stable alignment could be obtained by incorporating the azobenzene chromophores as pendants in cross-linked polymers.[66] The efficiency and stability of

alignment is dependent on the nature of the LC host, photoresponsive molecule, temperature and intensity of light.[67-71]

Undoped liquid crystals as well as liquid crystals doped with photochemically inert dyes are also known to undergo reorientation. Reorientation in such systems is proposed to arise from the local electric field induced by the irradiation source.[72,73]

An interesting effect arises when polymeric films containing azobenzene chromophores are irradiated using unpolarized light. This result in the realignment of the azobenzene chromophores along the direction of propagation of light, since this is the only direction in which the azobenzene chromophore cannot absorb unpolarized light. Using this method three-dimensional control of alignment of photoresponsive molecules becomes achievable. Further control in the three-dimensional alignment can be obtained by varying the incident direction of the irradiation light. This type of three-dimensional alignment, which has potential use in the development of high-density information storage devices, has been reported in a large number of PLCs.[74]

Another interesting effect of *trans-cis* photoisomerization of azobenzene doped in smectic hosts is the reversible increase in the smectic A layer spacing.[42,75,76] Experimental and computer simulation studies suggest that the effect can be attributed to the photochemically formed *cis*-isomers

being driven from within the smectic layers to locations between the layers as depicted in Figure 1.8.
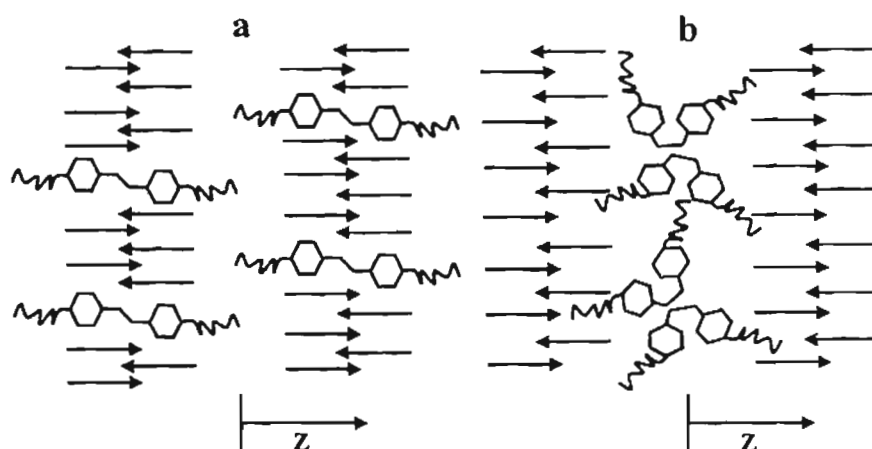
Figure 1.8. Schematic representation of the exclusion of *cis*-isomers of azobenzene derivatives from the smectic layers. Adapted from reference 42.

The observed photomodulation of ferroelectric polarization in ferroelectric smectic C LCs doped with chiral azobenzenes[77,78] has also been attributed to this effect.[42] The *trans*-isomers of the chiral azobenzene are incorporated into the smectic layers contributing to the overall ferroelectric polarization of the material. On *trans-cis* photoisomerization however, the *cis*-isomer is expelled from the layers and their contribution to ferroelectric polarization becomes zero. The possibility of manipulating organic materials at the nanometre scale in this manner can have variety of applications in nanotechnology including development of low-power, high-resolution optical data storage systems.[42]

Photochemical switching of alignment in ferroelectric liquid crystals have been extensively investigated by Ikeda and co-workers.[77,78] As discussed above, photoisomerization of azobenzene derivatives doped into ferroelectric LCs results in a decrease in the switching potential of the ferroelectric host (Chart 1.5).
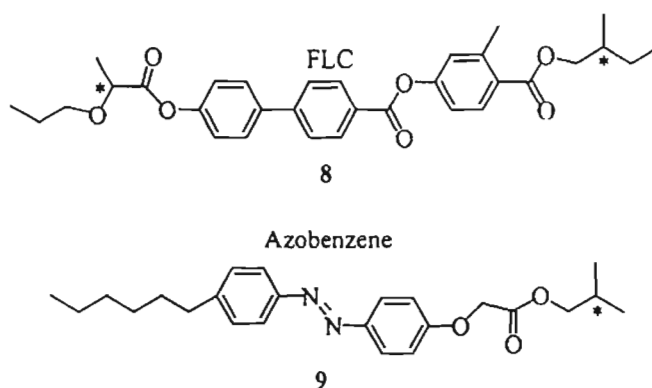
Chart 1.5

The working principle of an imaging device, which makes use of this effect, is shown schematically in Figure 1.9. The polarization of ferroelectric LC is aligned using an electric field. A weak electric field is then applied in the opposite direction such that it is not sufficient to disturb the polarization of the FLC arrangement due to cooperative interaction of LC molecules. On irradiation of selected portions, the threshold voltage for switching drops significantly due to *trans-cis* photoisomerization of the azobenzene chromophore, and polarization flips into the opposite direction in these regions.
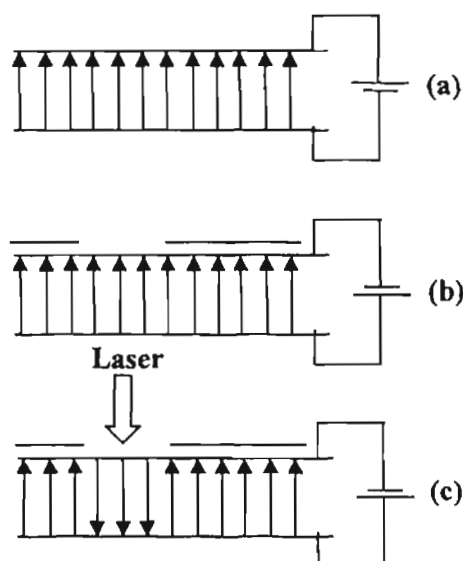
Figure 1.9. Schematic representation of photochemical flip of the polarization in ferroelectric LCs doped with azobenzene derivatives (a) Electric field induced alignment of FLC, (b) Application of weaker reverse electric field which maintain the initial polarization, (c) polarization flips due to reduction in threshold voltage caused by the photoisomerization of the azobenzene derivatives. Adapted from reference 78.

1.6.1. Surface-Controlled Photoalignment

LCs can be aligned parallel and perpendicular to the cell surface using suitably modified cell surfaces.[13,79,80] If the cell surfaces are modified using photochemically active chromophores, then surface-controlled photoswitching becomes possible. Such surfaces which can be used to switch the alignment of LCs have been termed as 'command surfaces'. Figure 1.10 shows a schematic representation of photoswitching in nematic LC cells where surfaces contain immobilized azobenzene derivatives. *Trans-cis* photoisomerization of the immobilized azobenzenes result in switching between the homeotropic and planar alignments.[81-83]
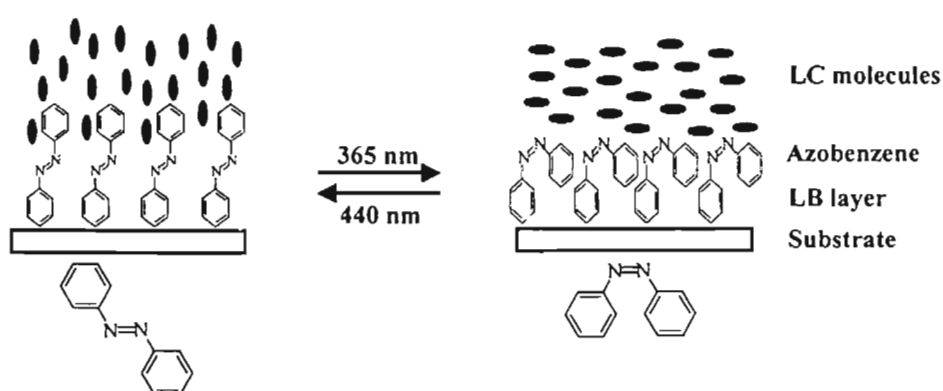
Figure 1.10. Schematic illustration of the photochromic reaction-induced alignment changes of nematic LC (command surfaces). Adapted from reference 13.

Photoswitching between parallel and perpendicular orientations can also be achieved by irradiation of suitably modified cell surfaces using plane polarized light. Gibbons *et al.* reported photoswitching using cell surfaces coated with a polyimide copolymer doped with a diazodiamine dye, **10** (Chart 1.6).[84] The cell used is schematically shown in Figure 1.11. One of the surfaces contained the polymer/dye coating while the other surface was coated with the polymer alone.

10
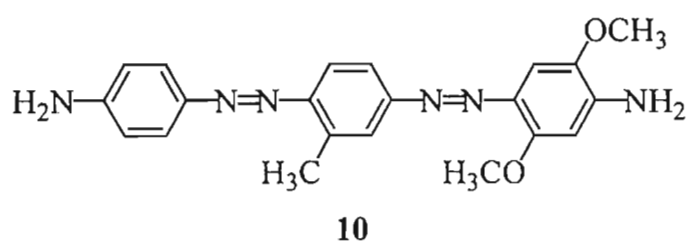
Chart 1.6

Both surfaces were rubbed with a cloth to provide homogeneous alignment of the nematic LC. On irradiation of the cell with plane polarized light, the nematic LCs close to the surface coated with the dye reorient

perpendicular to the plane of polarization of light, while the molecules close to the other side remain unaffected. Thus the irradiated portions acquire a twisted nematic alignment, and can be viewed as images when the cell is placed between polarizers.
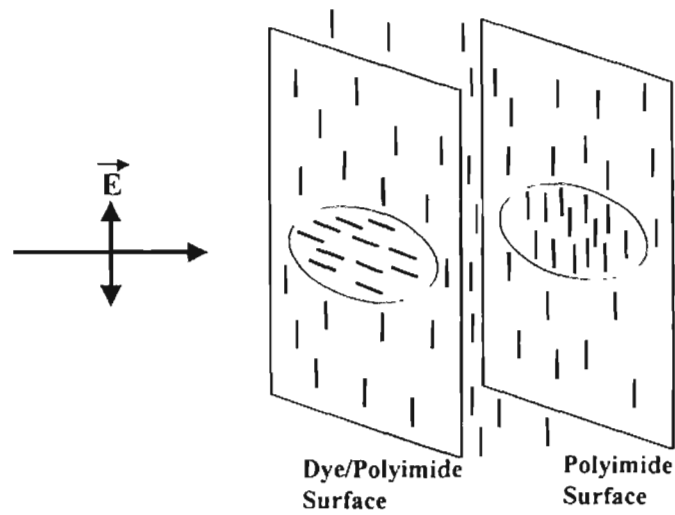
Figure 1.11. The geometry of the illuminated liquid crystal cell. The rods represent the liquid crystal orientation near the substrates before and after illumination. The oblong markings represent the illuminated portion. Adapted from the reference 84.

Control of liquid crystal alignment could also be achieved by illuminating the dye-doped polyimide substrate before filling the cell with the nematic LC. Using similar surface controlled optical alignment high-resolution continuous gray scale images could also be recorded.[85] This was achieved by focussing the light beam to a size comparable to its wavelength and varying the twist angle of the liquid crystal by varying the polarization direction of the write beam. Varying the polarization of the write beam the orientation of the LC molecules close to the surface coated with dye doped

polyimide can be continuously varied from 0-90°, which can provide images with a continuous gray scale when viewed between polarizers. Photoalignment using surfaces modified with chromophores can be fully reversible by irradiation using suitably polarized light.

As with dye-doped LCs, out-of-plane photoalignment of LCs is also possible using such 'command surfaces.' Reversible *cis-trans* photoisomerization of azobenzene side chain attached to vinyl polymers by irradiating them alternately with UV and visible light can bring about reversible out-of-plane alignment of the LC medium.[86,87]

1.6.2. Photochemical Switching in Cholesteric Liquid Crystals

The pitch of cholesteric LCs is sensitive to temperature, pressure and the presence of dopants.[88-91] From the point of view of photoswitching, it is interesting to note that the pitch of cholesteric LCs is very sensitive to the nature of the dopants. Thus a dopant that can be photochemically switched between two different forms can be utilized to optically switch the pitch of the cholesteric host. Sackman reported on changes in the pitch of cholesteric LCs induced by photoisomerization of azobenzene and stilbene in a mixture of cholesteryl chloride and cholesteryl nonanoate.[43] Photoactive chiral dopants, which can induce cholesteric phases in nematic LCs have also been used to bring about photoinduced pitch changes. For example, (-)-2-arylideine-*p*-menthane-3-ones induce a cholesteric phase when doped into nematic LCs. Photoisomerization of

(-)-2-arylidcine-*p*-menthane-3-ones (Scheme 1.2) results in lengthening of the pitch, which is proportional to the extent of photoisomerization.[92]

R = Ph. OMe. NMe2. Cl. CN. NO2
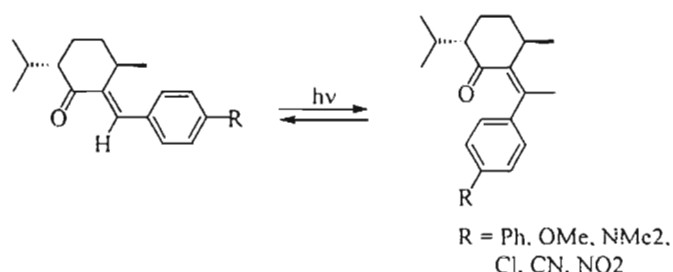
Scheme 1.2. Photochemical isomerization of (-)-2-arylidene-*p*-menthane-3-one.

Ikeda and co-workers investigated reversible photoinduced pitch changes in nematic LCs doped with a chiral molecule, **11** and photoactive dopant, **12** (Chart 1.7).[93] The presence of the chiral dopant induced a cholesteric phase in the nematic LC, while photoisomerization of the azobenzene dopant resulted in a reduction of the pitch of the cholesteric mixture. Blue-shift in the reflectance maximum from 640 to 475 nm was observed.
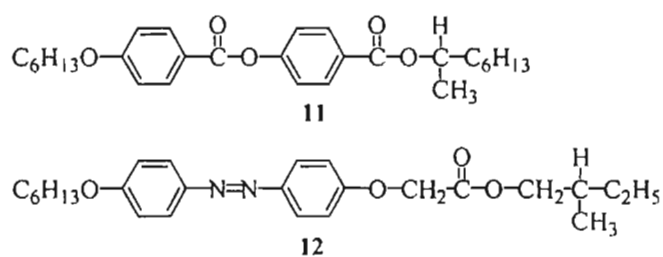
Chart 1.7

Photoisomerization of the azochromophores in cholesterol-linked azobenzene dopants, **13a,b** (Chart 1.8) in cholesteric LC mixture consisting of cholesteryl chloride, cholesteryl nonanoate and cholesteryl oleate resulted in elongation of the pitch and associated red-shift in the reflection band.[94]

13a,b

a, R = NO$_2$
b, R = n-C$_4$H$_9$
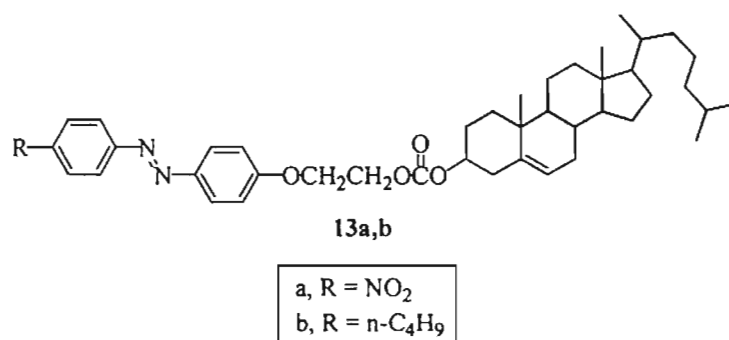
Chart 1.8

Photoisomerization of **13a** in the cholesteric mixture resulted in a 110 nm red-shift of the reflectance band maximum. In most of the above mentioned studies the change in pitch occurs rapidly and hence under steady-state or constant-wave irradiation conditions the photochemical transformation and change in pitch are indistinguishable. The dynamics of pitch change induced by photoisomerization of the cholesterol-linked azobenzene dopant **13b** in the cholesterol mixture consisting of cholesterol chloride, cholesteryl nonanoate and cholesterol oleate has been studied using time-resolved spectroscopy. The pitch change following isomerization was found to occur in the time-scale of 80-100 ms.[94] Laser induced heating can also result in temporal changes in the pitch of cholesteric LCs.[95] Pulsed laser irradiation of similar cholesteric mixtures doped with a photochemically inert copper complex which could dump heat following laser excitation, indicated that the reorientation of the LC molecules and change in the pitch, occurred over a time-scale of 300-600 µs.[11]

Due to the fluidity of low-molecular weight LCs, their use in long-term storage of photoinduced images is not feasible. In order to try and overcome this

problem, photoinduced changes in the pitch have also been investigated in polymeric LCs. Irradiation of a cholesteryl polymer containing the photoactive (-)-2-arylidine-*p*-menthane-3-one as pendants (Scheme 1.3) results in elongation of the pitch resulting in a red-shift and broadening of the reflectance band.[96,97]
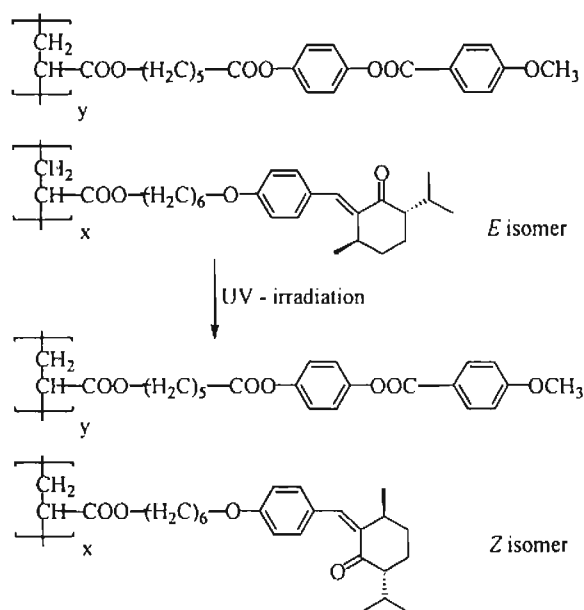
Scheme 1.3. Photoisomerization of cholesteric polymer with photoactive (-)-2-arylidine-*p*-menthane-3-one as pendants.

The use of polymeric LCs for imaging via photoinduced pitch changes also suffer form several drawbacks including, slow switching times, broadening of the reflectance bands and difficulty in erasure of stored images.[98,99]

Tamaoki and co-workers have made elegant use of the glass forming abilities of some cholesteric liquid crystals to overcome the problems associated with photoswitching in low-molecular weight and polymeric LCs.[14,100-103] Glassy liquid crystals can be obtained when the cholesteric phase is solidified by rapid cooling without allowing it to recrystallize, i.e. the macroscopic long-range helical

ordering is preserved in the solid state.[14] The glassy materials so obtained retain all the optical characteristics such as selective reflection and selective transmittance of circularly polarized phase. Glassy liquid crystals can also be obtained by polymerizing the cholesteric phase. However in such systems the pitch is not amenable to changes using photochemical transformations. Tamaoki and co-workers have prepared several dicholesteric esters (Chart 1.9) with molecular weights over 1000 which could be reversibly transformed into glassy and cholesteric LCs both of which showed the iridescent colour characteristic of cholesteric LCs. The stored colour in the glassy state could be tuned by controlling the cooling rate. Glassy LCs could also be obtained by spin-coating the dicholesteryl esters dissolved in dichloromethane.

Chart 1.9

$$H(H_2C)_n \underset{N}{\overset{N}{\diagdown}} (CH_2)_n H$$

19   (n = 4,7,11-16)
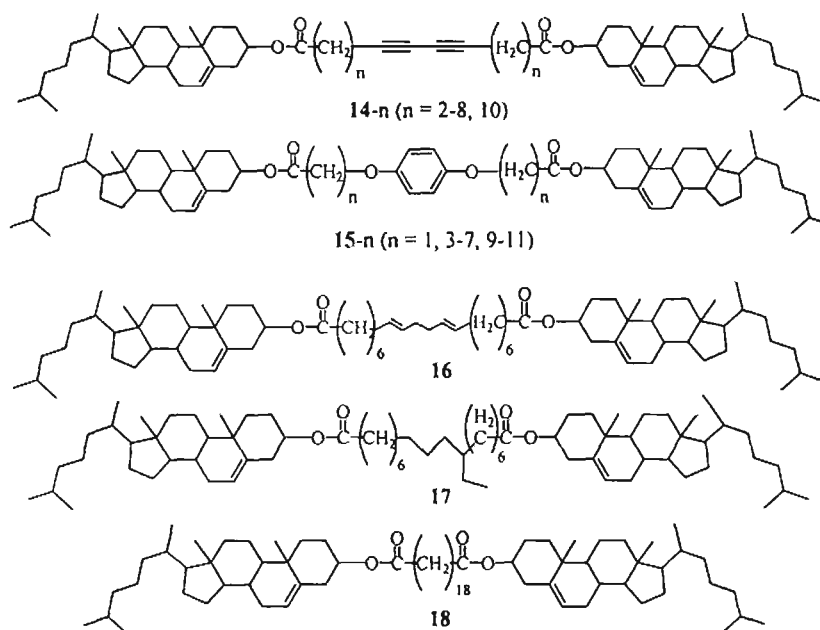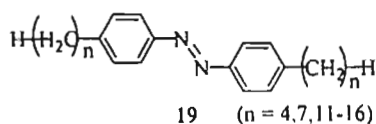
Chart 1.10

Photoinduced changes in the pitch and fixation of the images could be achieved using azobenzene doped dicholesteryl esters. Thus a thin film of the cholesteric phase of mixture consisting of **14**(n=8) and photochromic azobenzene derivative, **19**(n = 12) (Chart 1.10) in a 98:2 weight ratio form a red coloured film at 87 °C. Irradiation using 366 nm caused a shift in the reflectance band resulting in blue colouration of the film. Rapid cooling of the film to 0 °C resulted in storage of the photoinduced colour change. The change in colour could be controlled by varying the period of irradiation. The images could be conveniently erased by heating the film above their T_g. The stored images were found to be extremely stable (>1 year). These studies have shown the feasibility of developing full-colour rewritable images using both thermal and photochemical modes.

Non-covalent interactions such as hydrogen bonding and metallomesogens containing photoisomerizable azo chromophores capable of forming glassy liquid crystals have also been reported.[104,105]

Cholesterol linked azobenzene derivatives have been extensively investigated for their sol-gel formation,[106-108] nonlinear optics[109] and use as photoswitching dopants.[94] Recently, Moriyama and Tamaoki have shown that by suitably controlling the nature of the linker between the azobenzene and

cholesterol moieties glass forming LCs can be obtained. Imaging in such intrinsically photoactive LC glasses **20, 21** and **22** (Chart 1.11) have been reported.[110]

20, R = H 21, R = C₇H₁₅

22
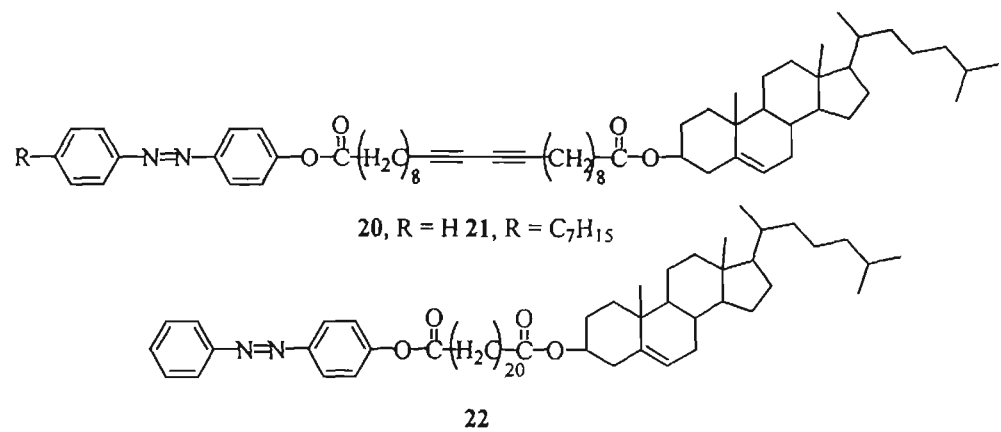
Chart 1.11

Owing to the characteristic cooperative interactions and long-range forces exhibited by liquid crystals, these materials have become highly sought as important elements in innumerable devices. Photon-based control of the material properties of liquid crystals described above make them highly suited for a variety of applications such as optical switches, imaging devices, holographic materials, optoelectronics and telecommunications. The photoinduced molecular amplification in these materials has employed the *trans-cis* photoisomerization of the azobenzene chromophore with few reports making use of spiropyran, fulgides and stilbenes. The extensive use of azobenzene has primarily been due to the fact that their *trans*-form stabilizes liquid crystalline phase whereas the *cis*-form destabilizes it. Another important factor is that its photoisomerization mechanism involves an

inversion of nitrogen which requires only small volumes unlike in chromophores with C=C double bond, where isomerization proceeds through a rotation mechanism requiring a larger free volume. Photoisomerization of azobenzene derivatives are not very sensitive to the viscosity of the medium and occur very efficiently even in rigid media. A major drawback associated with the use of azobenzene has been their thermal back (*cis-trans*) isomerization, which causes erasure of stored information. Additional factors such as use of polymeric matrices or vitrification are required for permanent storage of information. It is therefore desirable to look for alternative chromophores, which possess thermally stable photoisomers, which can only be reverted photochemically. A class of compounds, which could be used for such applications, is polyenes. Photoisomerization in alkenes and polyenes have been extensively studied specially for understanding the primary processes involved in vision. The photochemistry of polyenes and its role in vision are briefly described below.

1.7. Photochemistry of Polyenes and Its Role in Vision

The process of vision is initiated by light absorption by pigments consisting of a chromophore, 11-cis retinal, covalently bound to a lysine residue in an apoprotein, opsin in the form of a Schiff base. These proteins are hydrophobic and transmembranous in disc-like membrane sheets of specialized cells. These cells are of two kinds called rods and cones according to their shapes. Rods function in

dim light and cones perceive colour. In a human retina there are ~3 x 10^6 cones and ~10^9 rods, which are arranged in multilayers in the retina and are connected through bipolar cells to the optic nerve.

The planes of the disc-like membrane sheets are perpendicular to the long axis of the cells and to the direction of the incident light. There are three regions associated with the rod outer segments (ROS) as shown in Figure 1.12; extracellular, intracellular and intradisc. The action of light is to induce a structural change in rhodopsin molecules in the disc membrane, which triggers a sequence of molecular transformations that have not been completely elucidated. This is followed by a release of a diffusible transmitter substance able to couple a signal from the photolysed rhodopsin in the disc membrane to the outer plasma membrane. The nature of the transmitter mediating between rhodopsin and the plasma membrane is still controversial. Two candidates have been proposed. The first is calcium ions. In this model, illustrated by Figure 1.12a, sodium channels of the plasma membrane close when the level of Ca^{2+} ions is raised by rhodopsin photolysis. The second candidate is cyclic guanosine monophosphate (c GMP). In this model, shown in Figure 1.12b, c GMP would play a role of a 'negative' transmitter. Light activates a phosphodiesterase that hydrolyses c GMP and the lowered level of c GMP closes the sodium channels in the plasma membrane. The role of rhodopsin in the transmitter release is not clear. The partial modification of the permeability of the plasma membrane decreases the flow rate of Na^+ ions into

the outer segment of the cell causing a change in the electric potential of the cell

membrane and this signal is finally transmitted to the brain by the optic nerve.
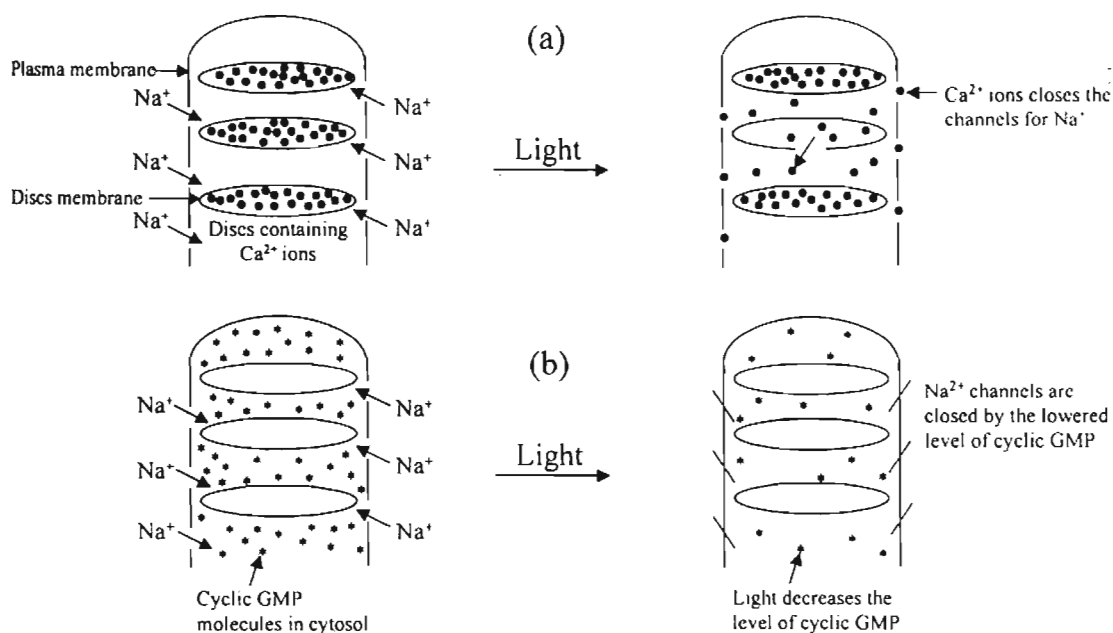
Figure 1.12. Part of rod outer segment and events triggered by light. Rhodopsin molecules float in the disc membrane. The change of their conformations on light excitation causes (a) release of Ca^{2+} ions, or (b) a decrease in the level of cyclic GMP.

The regiospecific geometrical isomerization upon photoexcitation of the

retinyl chromophore, is the primary photochemical event in both visual reception

and light-harvesting processes.[111] Hence polyene chemistry has been the

molecular basis of light transduction in visual receptors and light-harvesting in

bacteria.[112] Whereas the retinyl chromophore in rhodopsin undergoes 11-*cis* to *all-*

trans isomerization to initiate a chain of events in vision chemistry, the *all-trans* to

13-*cis* isomerization in BR leads to energy storage.[112,113] An understanding of the

photophysical properties of the chromophore in the protein environment requires a

fundamental knowledge of the photophysical properties of the free chromophore.

As a result, innumerable studies have been carried out to understand the ground and excited state properties of the visual chromophores and related polyenes.[112-119]

It is interesting to try and understand the reasons why natural selection has converged upon the 11-*cis* retinal for its use as the visual chromophore. A visual receptor should efficiently convert a photon of light into a nerve impulse, while preventing such a process in the dark. The 11-*cis* to 11-*trans* isomerization in the ground state has a large barrier ($\sim$45 kcal mol^{-1}), whereas it is barrierless in the excited state. This barrierless excited state potential surface diminishes the probability of radiationless processes competing with the isomerization. The primary photochemical process in vision which occurs with high quantum efficiency ($\Phi = 0.6$) is also highly regiospecific. Apart from these factors the visual pigment is a highly efficient photon collector. With respect to efficiency and regioselectivity of photoisomerization as well as absence of dark reactions the 11-*cis* isomer compares much more favourably than the other isomers of retinal.[112]

Time-resolved vibrational spectroscopy has played a crucial role in helping to understand the isomerization dynamics of retinal. In a recent study, Yamaguchi and Hamaguchi have proposed that isomerization from the all-*trans* to 13-*cis* isomer proceeds directly from the S_2 state to the S_0 state through a perpendicular intermediate on the basis of their femtosecond absorption data.[119] In a further study, Shimojima and Tahara have observed that *cis-trans* isomerization of 13-*cis* is unique compared to the other mono-

cis isomers of retinal.[113] It has been found that the 7-*cis*, 9-*cis* and 11-*cis* isomers undergo isomerization to the all-*trans* form through their excited triplet states, which are identical to the triplet excited state of the all-*trans* isomer. The 13-*cis* isomer on the other hand isomerizes to the all-*trans* thought an excited singlet state. They proposed that both the all-*trans* to 13-*cis* and the reverse isomerization processes proceed through singlet states.

The photochemistry of 1,3-dienes has also been extensively investigated.[120-122] It was found that direct irradiation of 1,3-dienes in dilute solution at room temperature results mostly in cyclobutene formation[123,124] (Scheme 1.4) and double bond isomerization.[125,126] Both the processes were found to proceed through the first excited singlet state.[127-129] Most acyclic 1,3-dienes exist as a mixture of two conformers[130,131] with the stable conformation being planar and *s-trans* about the central bond,[132,133] while the minor form has a *s-cis* configuration.
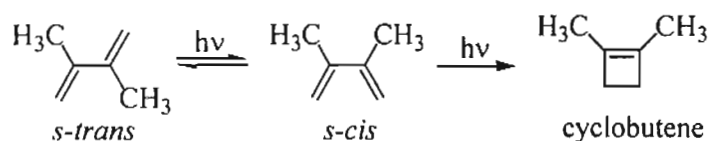
Scheme 1.4. Electrocyclic reactions of 1,3-dienes.

Although much of the thermal and photochemical reactions of 1,3-dienes proceed through the *s-cis* conformer, direct examination of *s-cis* chemistry has been limited because of its high energy relative to the *s-trans* isomer and the small barrier separating the *s-cis* from the *s-trans* isomer. The double bond isomerization

in 1,3-dienes has been proposed to be accompanied by a simultaneous *s-trans-s-cis*

isomerization. This 'space-saving' isomerization process has conceptualized as the

popular 'Hula-Twist mechanism,' proposed and explored by Liu and co-

workers.[134-136] It has been proposed that such a mechanism is involved in the

isomerization of the opsin-bound retinal in the vision chemistry.

α,ω-Diphenylpolyenes and in particular diphenylbutadiene, have been

extensively investigated using experimental[129,136-151] and theoretical[152-157]

techniques in order to gain an understanding of the photoprocesses occurring in

the natural systems such as vision. Saltiel and co-workers have extensively studied

the photochemistry of stilbenes.[122,158] Stilbene has served as a prototype for

understanding isomerization of the other olefins. *Trans*-stilbene can form

phenanthrene via the formation of the *cis*-isomer and dihydrophenanthrene

(Scheme 1.5). Diphenylbutadiene and diphenylhexatriene also undergo cyclization

to give phenyl naphthalene and chrysene, respectively (Scheme 1.5).
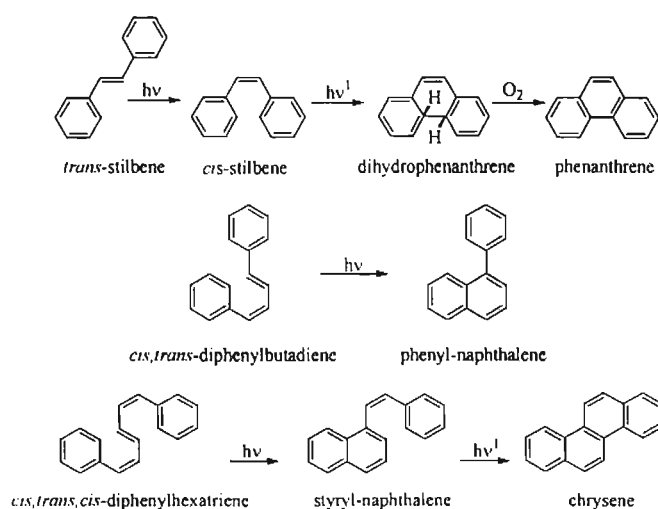
Scheme 1.5. Cyclization reactions of diphenylpolyenes.

Fluorescence and isomerization via the singlet state are the principal paths of deexcitation for diphenylpolyenes. Diphenylpolyenes are nominally planar molecules with substantial π-electron resonance stabilization. Thermally activated rotation about the phenyl-α-carbon single bond reduces the extent to which π bonding is delocalized within a diphenylpolyene chromophore. Calculations by Rulliere et al. suggest that in the equilibrium geometry of ground-state diphenylbutadiene, the phenyl rings are twisted 75° out of the polyene plane.[159] As the length of the polyene chain increases, there is an increase in the resonance delocalization of the π electrons causing a reduction in the energy of the π,π^* transition. Upon increasing the number of double bonds in a diphenylpolyene, the corresponding absorption spectrum becomes progressively red-shifted.

Sonoda *et al.* have reported on photocylcoaddition of substituted diphenylehexatrienes.[160] Formyl- and cyano- substituted dipheynylhexatrienes underwent intermolecular [2+2] photocycloaddition to yield mirror symmetric dimers (Scheme 1.6).

R = CHO
R = CN
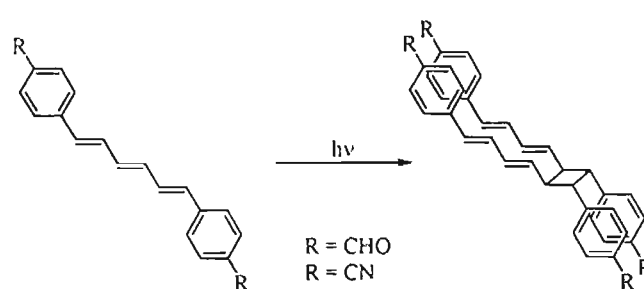
Scheme 1.6. Photocycloaddition reactions of diphenylhexatrienes.

Polyenes are highly versatile compounds. For example, long polyenic chains appear in vitamins and antibiotics. The polymeric form, namely

polyacetylene, is naturally photoconductive and becomes conductive with conductivities close to that of copper upon suitable doping. Polyenes are also known for their fluorescence and nonlinear optical properties.[161] Diphenylpolenes are also often used as scintillators.

1.8. Objectives of the Present Work

In the process of vision, a photochemical transformation at the molecular level results in changes in the macroscopic level due to a chemical amplification of the initial photochemical signal. An amplification of the photochemical processes also occurs in photoresponsive LCs, although in this case the amplification is due to a physical transformation, which arises due to the cooperative interaction and long-range order of LCs. Photoresponsive LCs, can therefore be seen as artificial method of mimicking vision. It is possible to envisage that with the proper choice of chromophore and LC medium, real-time imaging including real-time holography could be achieved. Nature has selected polyene as the chrompohore for vision. It would therefore be of interest to examine the use of polyene photochemistry for the design of photoresponsive LCs. Interestingly, this aspect of polyene chemistry has not been actively pursued. This thesis describes our efforts to understand the photophysical and photochemical properties of donor-acceptor-substituted butadienes and to use the butadiene chromophore for designing photoresponsive LCs. Some of these butadiene derivatives showed intense solid state fluorescence, which could be reversibly

switched using light. Our efforts to elucidate the molecular basis for the bulk properties of the butadiene based molecules are also discussed.

1.9. References

1) *Photochemistry in organized and constrained media*; V. Ramamurthy (Ed.) VCH Publishers, Inc.: New York, 1991.

2) Ramamurthy, V.; Venkatesan, K. *Chem. Rev.* **1987**, *87*, 433.

3) Ogawa, M.; Kuroda, K. *Chem. Rev.* **1995**, *95*, 399.

4) Kalyanasundaram, K. *Photochemistry in Microheterogeneous Systems*; Academic Press: New York, 1987.

5) Kalyanasundaram, K. *Chem. Soc. Rev.* **1978**, *7*, 453.

6) Whitten, D. G.; Russell, J. C.; Schmehl, R. H. *Tetrahedron* **1982**, *38*, 2455.

7) Bhattacharyya, K. *Proc. Indian Acad. Sci. (Chem. Sci.)* **2000**, *66*, 199.

8) Weiss, R. G. *Photochemical Processes in Liquid Crystals*; Ramamurthy, V., Ed.; VCH Publishers, Inc.: New York, 1991, pp 603-690.

9) Lin, Y. C.; Kachar, B.; Weiss`, R. G. *J. Am. Chem. Soc.* **1989**, *111*, 5542.

10) Anderson, V. C.; Craig, B. B.; Weiss, R. G. *J. Am. Chem. Soc.* **1982**, *104*, 2972.

11) Das, S.; Lenoble, C.; Becker, R. S. *J. Am. Chem. Soc.* **1987**, *109*, 4349.

12) Ikeda, T.; Kanazawa, A. *Molecular Switches*; Wiley-VCH: Weinheim, 2001.

13) Ichimura, K. *Chem. Rev.* **2000**, *100*, 1847.

14) Tamaoki, N. *Adv. Mater.* **2001**, *13*, 1135.

15) Demus, D. *Liquid Crystals-Applications and Uses*; Bahadur, B. Ed., World Scientific: Singapore, 1995; Vol. 1.

16) Chandrasekhar, S. *Liquid Crystals*; Cambridge University Press: Cambridge, 1977.

17) Kelker, H.; Hatz, R. *Hand book of liquid crystals,* Verlag Chemie: Weinheim, 1980.

18) Gennes, P. G. d. *The Physics of Liquid Crystals*; Oxford: Clarendon, 1974.

19) Demus, D.; Richter, L. *Texture of Liquid Crystals*; Weinheim, New York, 1978.

20) Gray, G. W.; Goodby, J. W. *Smectic Liquid Crystals*; Leonard Hill, Glasgow.London and Heyden & Son Inc.: Philadelphia, 1984.

21) Brown, G. H. *Advances in Liquid Crystals*; Academic Press: New York, San Francisco, London, 1983; Vol. 1-6.

22) Blumstein, A. *Polymeric Liquid Crystals*; Plenum: New York, 1985.

23) Demus, D. *Liq. Cryst.* **1989**, *5*, 75.

24) Wunderlich, B.; Moller, M.; Wiedemann, H. G. *Mol. Cryst. Liq. Cryst.* **1986**, *140*, 211.

25) Pohl, L.; Finkenzeller, U. *Liquid Crystals - Applications and Uses*; Bahadur, B., Ed.; World Scientific: Singapore, 1995; Vol. 1, pp 140-169.

26) Palffy-Muhoray, P. *Liquid Crystals-Applications and Uses*; Bahadur, B., Ed.; World Scientific: Sinngapore, 1995; Vol. 1, pp 494-538.

27) Scheffer, T.; Nehring, J. *Liquid Crystals-Applications and Uses*; Bahadur, B., Ed.; World Scientific: Singapore, 1995; Vol. 1, pp 232-270.

28) Bahadur, B. *Liquid Crystals-Applications and uses*; World Scientific: Singapore, 1995; Vol. 1.

29) Kahn, F. *Appl. Phys. Lett.* **1973**, *22*, 111.

30) Nakamura, K.; Oda, Y.; Sugimoto, M. *J. Appl. Phys.* **1986**, *59*, 593.

31) Shields, S. E.; Bleha, W. P. *Liquid Crystals-Applications and Uses*; World Scientific: Singapore, 1995; Vol. 1.

32) Shibaev, V. P.; Kostromin, S. G.; Plate, N. A.; Ivanov, S. A.; Vetrov, V. Y.; Yakovlev, I. A. *Polym. Commun.* **1983**, *24*, 364.

33) Coles, H. J.; Simon, R. *Polymer* **1985**, *26*, 1801.

34) Urabe, T.; Arai, K.; Ohkoshi, A. *J. Appl. Phys.* **1983**, *54*, 1552.

35) Haas, W.; Adams, J.; Wysocki, J. *Mol. Cryst. Liq. Cryst.* **1969**, *7*, 371.

36) Emmelius, M.; Pawlowski, G.; Vollman, H. W. *Angew. Chem. Int. Ed. Engl.* **1989**, *28*, 1445.

37) Cabrera, I.; Engel, M.; Haübling, L.; Mertisdorf, C.; Ringsdorf, H. *Photoinduced Structural Changes in Organized Supramolecular Systems: Frontiers in Supramolecular Organic Chemistry and Photochemistry*; Schneider, H. and Dürr, H., Ed.; Weinheim: New York, 1991.

38) Ringsdorf, H.; Carbrera, I.; Dittrich, A. *Angew. Chem. Int. Ed. Engl.* **1991**, *30*, 76.

39) Suarez, M.; Schuster, G. B. *J. Am. Chem. Soc.* **1995**, *117*, 6732.

40) Zhang, M.; Schuster, G. B. *J. Org. Chem.* **1994**, *59*, 1855.

41) Ikeda, T.; Tsutsumi, O. *Science* **1995**, *268*, 1873.

42) Lansac, Y.; Glaser, M. A.; Clark, N. A.; Lavrentovich, O. D. *Nature* **1999**, *398*, 54.

43) Sackman, E. *J. Am. Chem. Soc.* **1971**, *93*, 7088.

44) Kobayashi, T.; Degenkolb, E. O.; Rentzepis, P. M. *J. Phys. Chem.* **1979**, *83*, 2431.

45) Kurihara, S.; Ikeda, T.; Tazuke, S. *Mol. Cryst. Liq. Cryst.* **1990**, *178*, 117.

46) Ikeda, T.; Miyamoto, T.; Kurihara, S.; Tazuke, S. *Mol. Cryst. Liq. Cryst.* **1990**, *188*, 223.

47) Ikeda, T.; Miyamoto, T.; Kurihara, S.; Tazuke, S. *Mol. Cryst. Liq. Cryst.* **1990**, *188*, 235.

48) Ikeda, T.; Miyamoto, T.; Kurihara, S.; Tsukada, M.; Tazuke, S. *Mol. Cryst. Liq. Cryst.* **1990**, *182B*, 357.

49) Kurihara, S.; Ikeda, T.; Sasaki, T.; Kim, H.-B.; Tazuke, S. *Mol. Cryst. Liq. Cryst.* **1991**, *195*, 251.

50) Kurihara, S.; Ikeda, T.; Sasaki, T.; Kim, H.-B.; Tazuke, S. *J. Chem. Soc. Chem. Commun.* **1990**, 1751.

51) Denekamp, C.; Feringa, B. L. *Adv. Mater.* **1998**, *10*, 1080.

52) Burnham, K. S.; Schuster, G. B. *J. Am. Chem. Soc.* **1999**, *121*, 10245.

53) Shishido, A.; Tsutsumi, O.; Kanazawa, A.; Shiono, T.; Ikeda, T. *J. Phys. Chem. B* **1997**, *101*, 2806.

54) Shishido, A.; Tsutsumi, O.; Kanazawa, A.; Shiono, T.; Ikeda, T.; Tamai, N. *J. Am. Chem. Soc.* **1997**, *119*, 7791.

55) Tsutsumi, O.; Shiono, T.; Ikeda, T.; Galli, G. *J. Phys. Chem. B* **1997**, *101*, 1332.

56) Kato, T.; Hirota, N.; Fujishima, A.; Frechet, J. M. J. *J. Polym. Sci. A Polym. Chem.* **1996**, *34*, 57.

57) Mallia, V. A.; George, M.; Das, S. *Chem. Mater.* **1999**, *11*, 207.

58) Mallia, V. A.; Das, S. *Liq. Cryst.* **2001**, *28*, 259.

59) Michl, J.; Thulstrup, E. W. *Spectroscopy and Polarized Light*, VCH Publishers: New York, 1995, pp 198.

60) Dumont, M. *Mol. Cryst. Liq. Cryst.* **1996**, *282*, 437.

61) Sekkat, A.; Dumon, M. *Synth. Met.* **1993**, *54*, 373.

62) Sekkat, Z.; Wood, J.; Knoll, W. *J. Phys. Chem.* **1995**, *99*, 17226.

63) Hore, D.; Natansohn, A.; Rochon, P. *Can. J. Chem.* **1998**, *76*, 1684.

64) Jones, F.; Reeve, T. J. *J. Soc. Dyers Col.* **1979**, 352.

65) Jones, F.; Reeve, T. J. *Mol. Cryst. Liq. Cryst.* **1980**, *60*, 99.

66) Morino, S.; Kaiho, A.; Ichimura, K. *Appl. Phys. Lett.* **1998**, *73*, 1317.

67) Stumpe, J.; Geue, T.; Fischer, T.; Menzel, H. *Thin Solid Films* **1996**, 60.

68) Fischer, T.; Lasker, L.; Stumpe, J.; Kostromin, S. *J. Photochem. Photobiol. A: Chem.* **1994**, *80*, 453.

69) Lasker, L.; Stumpe, J.; Fischer, T.; Rutloh, L.; Kostromin, S.; Ruhmann, R. *Mol. Cryst. Liq. Cryst.* **1995**, *261*, 371.

70) Lasker, L.; Fischer, T.; Stumpe, J.; Kostromin, S.; Ivanov, S.; Shibaev, V. P.; Ruhmann, R. *Mol. Cryst. Liq. Cryst.* **1994**, *253*, 1.

71) Wu, Y.; Demachi, Y.; Tsutsumi, O.; Kanazawa, A.; Shiono, T.; Ikeda, T. *Macromolecules* **1998**, *31*, 349.

72) Bartkiewics, S.; Miniewics, A. *Adv. Mater. Opt. Electron.* **1996**, *6*, 219.

73) Bartkiewics, S.; Januszko, A.; Miniewics, A.; Parka, J. *J. Pure. Appl. Opt.* **1996**, *5*, 799.

74) Yoshimoto, N.; Morino, S.; Kaiho, A.; Ichimura, K. *Chem. Lett.* **1999**, 711.

75) Folks, W. R.; Reznikov, Y. A.; Yarmolenko, S. N.; Lavrentovich, O. D. *Mol. Cryst. Liq. Cryst.* **1997**, *292*, 183.

76) Krentsel, T. A.; Lavrentovich, O. D.; Kumar, S. *Mol. Cryst. Liq. Cryst.* **1998**, *320*, 77.

77) Sasaki, T.; Ikeda, T.; Ichimura, K. *J. Am. Chem. Soc.* **1994**, *116*, 625.

78) Ikeda, T.; Sasaki, T.; Ichimura, K. *Nature* **1993**, *361*, 428.

79) Kawatsuki, N.; Ono, H.; Takatsuka, H.; Yamamoto, T.; Sangen, O. *Macaromolecules* **1997**, *30*, 6680.

80) Schadt, M.; Seiberle, H.; Schuster, A. *Nature* **1996**, *381*, 212.

81) Ichimura, K.; Suzuki, Y.; Seki, T.; Hosoki, A.; Aoki, K. *Langmuir* **1988**, *4*, 1214.

82) Ichimura, K.; Suzuki, Y.; Seki, T.; Kawanishi, A.; Aoki, K. *Macromol. Chem. Rapid Commun.* **1989**, *10*, 5.

83) Seki, T.; Sakuragi, M.; Kawanishi, A.; Tamaki, T.; Fukuda, R.; Ichimura, K. *Langmuir* **1993**, *9*, 211.

84) Gibbons, W. M.; Shannon, P. J.; Sun, S. T.; Swetlin, B. J. *Nature* **1991**, *351*, 49.

85) Gibbons, W. M.; Kosa, T.; Palffy-Muhoray, P.; Shannon, P. J.; Sun, S. T.; Swetlin, B. J. *Nature* **1995**, *377*, 43.

86) Aoki, K.; Seki, T.; Suzuki, Y.; Tamaki, T.; Hosoki, A.; Ichimura, K. *Langmuir* **1992**, *8*, 1007.

87) Kawanishi, Y.; Tamaki, T.; Sakuragi, M.; Seki, T.; Suzuki, Y.; Ichimura, K. *Langmuir* **1992**, *8*, 2601.

88) Fergason, J. L. *Appl. Opt.* **1968**, *7*, 1729.

89) Fergason, J. L. *Sci. Am.* **1964**, *211*, 76.

90) Muller, J. H. *Mol. Cryst.* **1966**, *2*, 167.

91) Keating, P. N. *Mol. Cryst. Liq. Cryst.* **1969**, *8*, 315.

92) Yarmolenko, S. N.; Kutulya, L. A.; Vashchenko, V. V.; Chepeleva, L. V. *Liq. Cryst.* **1994**, *16*, 877.

93) Lee, H.-K.; Doi, K.; Harada, H.; Tsutsumi, O.; Kanazawa, A.; Shiono, T.; Ikeda, T. *J. Phys. Chem. B* **2000**, *104*, 7023.

94) George, M.; Mallia, V. A.; Antharjanam, P. K. S.; Saminathan, M.; Das, S. *Mol. Cryst. Liq. Cryst.* **2001**, *350*, 125.

95) Becker, R. S.; Chakravorti, S.; Das, S. *J. Chem. Phys.* **1989**, *90*, 2802.

96) Brehmer, M.; Lub, J.; Witte, P. v. d. *Adv. Mater.* **1998**, *10*, 17.

97) Witte, P. v. d.; Galan, J. C.; Lub, J. *Liq. Cryst.* **1998**, *24*, 819.

98) Bobrovski, A. Y.; Boiko, N. I.; Shibaev, V. P.; Spriger, J. **2000**, *12*, 16.

99) Bobrovski, A. Y.; Boiko, N. I.; Shibaev, V. P. **1998**, *25*, 679.

100) Tamaoki, N.; Moriyama, M.; Matsuda, H. *Angew. Chem. Int. Ed. Engl.* **2000**, *39*, 509.

101) Tamaoki, N.; Parfenov, A. V.; Masaki, A.; Matsuda, H. *Adv. Mater.* **1997**, *9*, 1102.

102) Tamaoki, N.; Kruk, G.; Matsuda, H. *J. Mater. Chem.* **1999**, *9*, 2381.

103) Tamaoki, N.; Song, S.; Moriyama, M.; Matsuda, H. *Adv. Mater.* **2000**, *12*, 94.

104) Mallia, V. A.; Antharjanam, P. K. S.; Das, S. *Chem. Lett.* **2001**, 752.

105) Antharjanam, P. K. S.; Mallia, V. A.; Das, S. *Chem. Mater.* **2002**, *14*, 2687.

106) Kawabata, H.; Murata, K.; Harada, T.; Shinkai, S. *Langmuir* **1995**, *11*, 623.

107) Murata, K.; Aoki, M.; Shinkai, S. *Chem. Lett.* **1992**, 739.

108) Murata, K.; Aoki, M.; Suzuki, T.; Harada, T.; Kawabata, H.; Komori, T.; Ohseto, F.; Ueda, K.; Shinkai, S. *J. Am. Chem. Soc.* **1994**, *116*, 6694.

109) George, M.; Das, S. *Chem. Lett.* **1999**, 1081.

110) Moriyama, M.; Tamaoki, N. *Chem. Lett.* **2001**, 1142.

111) Liu, R. S. H. ; Ramamurthy, V., Ed.; VCH Publishers Inc.: New York, 1991.

112) Birge, R. R. *Ann. Rev. Biophys. Bioeng.* **1981**, *10*, 315.

113) Shimojima, A.; Tahara, T. *J. Phys. Chem. B* **2000**, *104*, 9288.

114) Birge, R. R. *Annu. Rev. Phys. Chem.* **1990**, *41*, 683.

115) Mathies, R. A.; Lin, S. W.; Ames, J. B.; Pollard, W. T. *Annu. Rev. Biophys. Biophys. Chem.* **1991**, *20*, 491.

116) Warshel, A.; Barboy, N. *J. Am. Chem. Soc.* **1982**, *104*, 1469.

117) Liu, R. S. H.; Shichida, Y. *Constrained Media*; Ramamurthy, V., Ed.; VCH Publishers Inc.: New York, 1991, pp 817-840.

118) Hendrickx, E.; Clays, K.; Persoons, A.; Dehu, C.; Bredas, J. L. *J. Am. Chem. Soc.* **1995**, *117*, 3547.

119) Yamaguchi, S.; Hamaguchi, H.-O. *J. Chem. Phys.* **1998**, *109*, 1397.

120) Srinivasan, R. *J. Am. Chem. Soc.* **1960**, *82*, 5063.

121) Srinivasan, R. *Adv. Photochem.* **1966**, *4*, 113.

122) Saltiel, J.; D'Agostino, J. T.; Megarity, E. D.; Mett, L.; Neuberger, K. R.; Wrighton, M.; Zafiriou, O. C. *Org. Photochem.* **1973**, *3*, 1.

123) Srinivasan, R. *J. Am. Chem. Soc.* **1962**, *84*, 4141.

124) Srinivasan, R.; Boue, S. *J. Am. Chem. Soc.* **1971**, *93*, 550.

125) Srinivasan, R. *J. Am. Chem. Soc.* **1968**, *90*, 4498.

126) Vanderlinden, P.; Boue, S. *J. Chem. Soc. Chem. Commun.* **1975**, 932.

127) Srinivasan, R. *J. Am. Chem. Soc.* **1963**, *85*, 4045.

128) Dauben, W. G.; Cargill, R. L.; Coates, R. M.; Saltiel, J. *J. Am. Chem. Soc.* **1966**, *88*, 2742.

129) Squillacote, M.; Semple, T. C. *J. Am. Chem. Soc.* **1990**, *112*, 5546.

130) Huckel, E. *Z. Phys.* **1932**, *76*, 628.

131) Aston, J. G.; Szasz, G.; Woolley, H. W.; Brickwedde, F. G. *J. Chem. Phys.* **1946**, *14*, 67.

132) Almenningen, A.; Traetteburg, M. *Acta. Chem. Scand.* **1958**, *12*, 1221.

133) Aten, C. F.; Hedberg, L.; Hedberg, K. *J. Am. Chem. Soc.* **1968**, *90*, 2463.

134) Liu, R. S. H.; Asato, A. E. *Proc. Natl. Acad. Sci. U. S. A.* **1985**, *82*, 259.

135) Liu, R. S. H.; Browne, D. T. *Acc. Chem. Res.* **1986**, *19*, 42.

136) Liu, R. S. H. *Acc. Chem. Res.* **2001**, *34*, 555.

137) Görner, H. *J. Photochem.* **1982**, *19*, 343.

138) Allen, M. T.; Whitten, D. G. *Chem. Rev.* **1989**, *89*, 1691.

139) Kawski, A.; Kuklinski, B.; Kubicki, A. *Z. Naturfosch.* **1993**, *48a*, 1177.

140) Wallace-Williams, S. E.; Møller, S.; Goldbeck, R. A.; Hanson, K. M.; Lewis, J. W.; Yee, W. A.; Kliger, D. S. *J. Phys. Chem.* **1993**, *97*, 9587.

141) Wallace-Williams, S. E.; Schwartz, B. J.; Møller, S.; Goldbeck, R. A.; Yec. W. A.; El-Bayoumi, M. A.; Kliger, D. S. *J. Phys. Chem.* **1994**, *98*, 60.

142) Jr., D. L. M.; Gustafson, T. L. *J. Phys. Chem.* **1994**, *98*, 6725.

143) Oberle, J.; Abraham, E.; Ivanov, A.; Jonusauskas, G.; Rulliere, C. *J. Phys. Chem.* **1996**, *100*, 10179.

144) Spalletti, A.; Bartocci, G.; Galiazzo, G.; Macchioni, A.; Mazzucato, U. *J. Phys. Chem. A* **1999**, *103*, 8994.

145) Braatz, H.; Hecht, S.; Seifert, H.; Helm, S.; Bendig, J.; Rettig, W. *J. Photochem. Photobiol. A: Chem.* **1999**, *123*, 99.

146) Singh, A. K.; Krishna, T. S. R. *J. Photosci.* **1998**, *5*, 47.

147) Singh, A. K.; Krishna, T. S. R. *J. Phys. Chem. A* **1997**, *101*, 3066.   6/21 15

148) Singh, A. K.; Darshi, M.; Kanvah, S. *New. J. Chem.* **1999**, *23*, 1075.

149) Singh, A. K.; Darshi, M.; Kanvah, S. *J. Phys. Chem. A* **2000**, *104*, 464.

150) Singh, A. K.; Kanvah, S. *New J. Chem.* **2000**, *24*, 639.

151) Singh, A. K.; Darshi, M.; Kanvah, S. *J. Phys. Chem. A* **2000**, *104*, 464.

152) Orlandi, G.; Zerbetto, F.; Zgierski, M. Z. *Chem. Rev.* **1991**, *91*, 867.

153) Anderton, R. M.; Kauffman, J. F. *J. Phys. Chem.* **1995**, *99*.

154) Maré, G. R. D.; Panchenko, Y. N.; Auwera, J. V. *J. Phys. Chem. A* **1997**, *101*, 3998.

155) Bunker, C. E.; Lytle, C. A.; Rollins, H. W.; Sun, Y.-P. *J. Phys. Chem. A* **1997**, *101*, 3214.

156) Maroulis, G.; Makris, C.; Hohm, U.; Wachsmuth, U. *J. Phys. Chem. A* **1999**, *103*, 4359.

157) Lappe, J.; Cave, R. J. *J. Phys. Chem. A* **2000**, *104*, 2294.

158) Saltiel, J.; Charlton, J. L. *In Rearrangements in Ground and Excited States*; deMayo, P., Ed.; Academic Press: New York, 1980.

159) Rulliere, C.; Declemy, A.; Kottis, P.; Ducasse, L. *Chem. Phys. Lett.* **1985**, *117*, 583.

160) Sonoda, Y.; Miyazawa, A.; Hayashi, S.; Sakuragi, M. *Chem. Lett.* **2001**, 410.

161) Christopher, R. M.; Robert, J. T.; Lee, V. Y.; Swanson, S. A.; Betterton, K. M.; Miller, R. D. *J. Am. Chem. Soc.* **1993**, *115*, 12599.

Chapter 2

Intramolecular Charge Transfer and Photochemical Isomerization in Donor-Acceptor-Substituted Butadienes

2.1. Abstract

Intramolecular charge transfer, triplet state properties and photoisomerization of five donor-acceptor- (DA) substituted butadienes, were investigated. Four of these derivatives, **BN5, BN6, BNDE** *and* **BN5AN** *show dual fluorescence arising from a locally excited (LE) state and a considerably more polar intramolecular charge transfer (ICT) state. The presence of an amine substituent with the nitrogen atom directly attached to the butadiene chain is essential for the dual fluorescence in this class of compounds.* **BAN**, *containing only an aromatic amino substituent connected to the butadiene chain does not show dual fluorescence. The quantum yields of fluorescence of these derivatives were found to be very low. These compounds undergo E-Z photoisomerization from the excited singlet state with a quantum efficiency of about 0.1 in benzene at room temperature. The intersystem crossing efficiency for these compounds is negligible. The triplet excited state properties of the five butadienes have been studied via triplet-triplet sensitization with benzophenone as the triplet energy donor.*

2.2. Introduction

The synthesis and study of new organic molecules possessing second-order nonlinear optical (NLO) properties have been a subjects of intense activity due to the potential applications of these molecules in integrated optics, such as optical modulation, optical switching and optical data-processing.[1-8] The ability to optimize the NLO properties of organic materials relies on a fundamental understanding of the interrelationships between chemical structure and molecular nonlinearities.[1-4] Materials capable of second harmonic generation are associated with highly polarizable molecules, with large second-order molecular polarizability (β) values. Such molecules can be obtained by linking strong electron donor (D) and acceptor (A) groups through polarizable π-conjugated bridges. DA molecules are usually characterized by large oscillator strengths for the ground to excited state transition, large dipole moment change between the ground and excited states and intramolecular charge transfer (ICT) transitions at relatively low energies. There has been a growing interest in the design of molecular systems in which the second-order nonlinear optical property can be switched on and off using external light or electric stimuli.[9]

DA-substituted butadienes are reported to have good NLO properties.[10,11] Intramolecular charge transfer has also been recently reported for nitro and cyano-substituted 1,4-diphenylbutadienes.[12] Nonlinear optical properties of some donor-acceptor-substituted butadienes, containing L-prolinol as the donor have been

reported.[11] One of these molecules shows an anomalous red-shifted fluorescence band in addition to the normal Stokes-shifted band. Several molecules in which ICT transitions take place show the phenomenon of dual luminescence. The origin of these processes is presently under debate.[13-18] In order to explore the mechanism of dual luminescence exhibited by the DA-substituted butadienes, a series of such compounds containing different amine groups as donor substituents and 1,3-indanedione as the acceptor moiety (Chart 2.1) have been investigated. These molecules are also capable of undergoing photoisomerization, which makes them potentially useful for designing photoswitchable NLO materials. Photoisomerization in linear polyenes is also of interest in view of the related processes that occur in retinal polyenes.[19-21] Here, we report the detailed study of the intramolecular charge transfer process as well as photoisomerization from the excited singlet and triplet states of this class of DA-substituted butadienes.
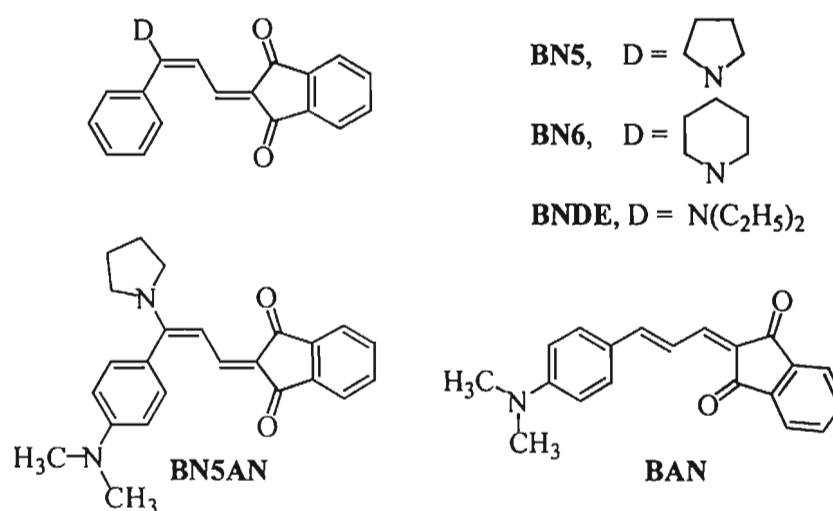
Chart 2.1

2.3. Results and Discussion

2.3.1. Synthesis of Butadiene Derivatives

The DA-substituted butadiene derivatives (Chart 2.1) were synthesized as per Schemes 2.1 and 2.2. The details of the synthetic procedure and spectral characterization of these derivatives are given in the Experimental Section (2.5).
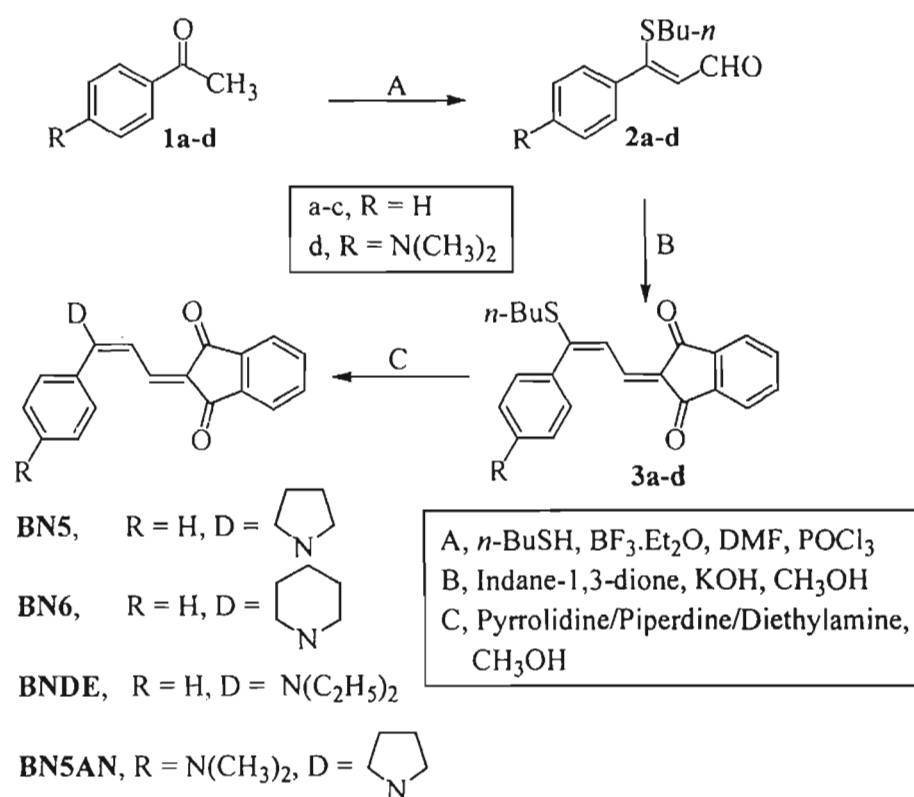
Scheme 2.1
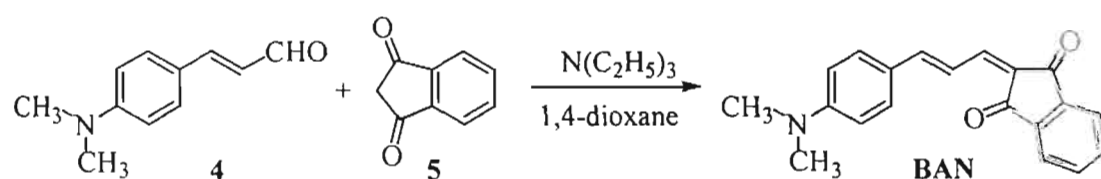
Scheme 2.2

2.3.2. Molecular Structure

The molecular structure of **BN5** was determined by X-ray crystal analysis[22] (Annexure A.1) for which good quality crystals could be obtained from a 1:9 solvent mixture of methanol and chloroform. The molecular geometry of **BN5** with the atomic labeling is shown in Figure 2.1. It is evident from Figure 2.1 that the *E* isomer is the thermodynamically preferred species. It is seen that the pyrrolidine and the indanedione moieties are largely coplanar, with the dihedral angles N(15)C(1)C(2)C(3), C(1)C(2)C(3)C(4) and C(2)C(3)C(4)C(5) equal to 175.2°, 175.6° and 1.8°, respectively. The phenyl group, on the other hand, is perpendicularly twisted out of this plane, with the dihedral angle C(2)C(1)C(20)C(21) equal to 85.2°.
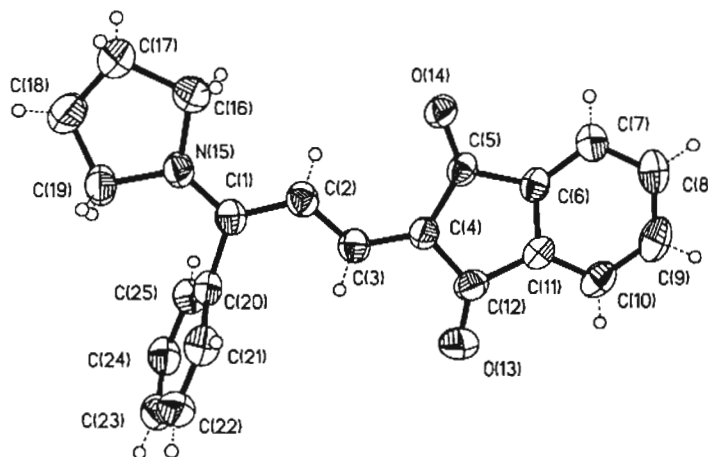
Figure 2.1. ORTEP diagram of **BN5**.

The C(1)-N(15) bond length is very short for a single bond (1.334 (3) Å), indicating that the pyrrolidine group is in strong conjugation with the indanedione moiety through the butadiene chain. This is also supported by the lack of bond

length alternation in the buatadiene chain, with the C(1)-C(2), C(2)-C(3) and C(3)-C(4) bonds as 1.396 (3) Å, 1.387 (4) Å and 1.391 (3) Å, respectively.[4]

2.3.3. Absorption and Fluorescence

The absorption spectrum of **BN6** in acetonitrile as well as its fluorescence spectra in diisopropyl ether and acetonitrile at 25 °C are shown in Figure 2.2.
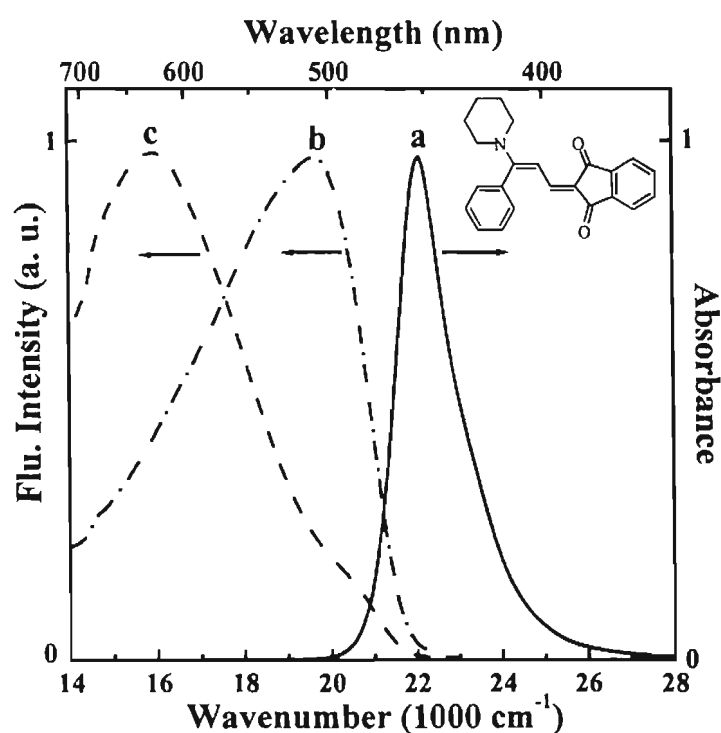
Figure 2.2. Absorption and fluorescence spectra of **BN6**; (a) absorption spectrum in acetonitrile, (b) fluorescence spectrum in diisopropyl ether and (c) fluorescence spectrum in acetonitrile.

The maximum of the absorption band is practically independent of solvent polarity (Table 2.1). Similar observations were made in the case of compounds **BN5**, **BNDE** and **BN5AN**, which can be attributed to a negligible change in the dipole moments between the ground and the Franck-Condon (FC)

excited state of these molecules. The absorption maximum of **BAN**, on the other hand, shows a bathochromic shift with increasing solvent polarity, indicating an increase in the dipole moment in the excited FC state for this compound. The absorption and fluorescence properties of the compounds studied are summarized in Table 2.1.

The compounds **BN5**, **BN6**, **BNDE** and **BN5AN** have low fluorescence quantum yields between 3×10^{-3} and 10^{-4} (Table 2.1). Unlike the negligible effect of solvent polarity on their absorption spectra, the effect on their fluorescence spectra is quite significant. In a weakly polar solvent such as diisopropyl ether ($\varepsilon =$ 3.88 (25 °C)), the emission spectrum shows a maximum around 500 nm and a broad tail in the longer wavelength region (Figure 2.2, curve b). With increasing solvent polarity, there is a relative increase in intensity at longer wavelengths and in a highly polar solvent such as acetonitrile ($\varepsilon = 37.5$ (25 °C)), two distinct fluorescence bands are clearly visible (Figure 2.2, curve c).

Dual fluorescence in molecules possessing ICT transitions can generally be described on the basis of the mechanism shown in Scheme 2.3.[15]

$$
\mathrm{LE} \underset{k_d}{\overset{k_a}{\rightleftharpoons}} \mathrm{ICT}
$$
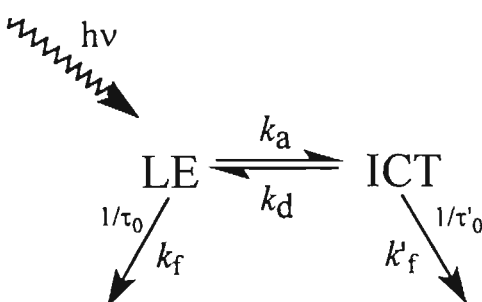
Scheme 2.3

According to this mechanism, the dual emission arises from two states, termed as locally excited (LE) and intramolecular charge transfer (ICT) states, which are in equilibrium. The LE state refers to a state which can be reached directly by absorption from S_0. In the ICT excited state, which originates from the LE state, considerable charge separation between the donor and the acceptor groups is expected. The separated LE and ICT fluorescence bands of **BN6** in diisopropyl ether and acetonitrile are shown in Figure 2.3. Similarly, distinct LE and ICT bands were also observed for the compounds **BN5** and **BN6**.

The kinetics of the dual fluorescence can be treated on the basis of the mechanism shown in Scheme 2.3., where k_a and k_d are the rate constants of the forward and backward ICT reactions, $\tau_0(LE)$ and $\tau'_0(ICT)$ are the fluorescence lifetimes. The radiative rate constants, $k_f(LE)$ and $k'_f(ICT)$ have also been indicated.
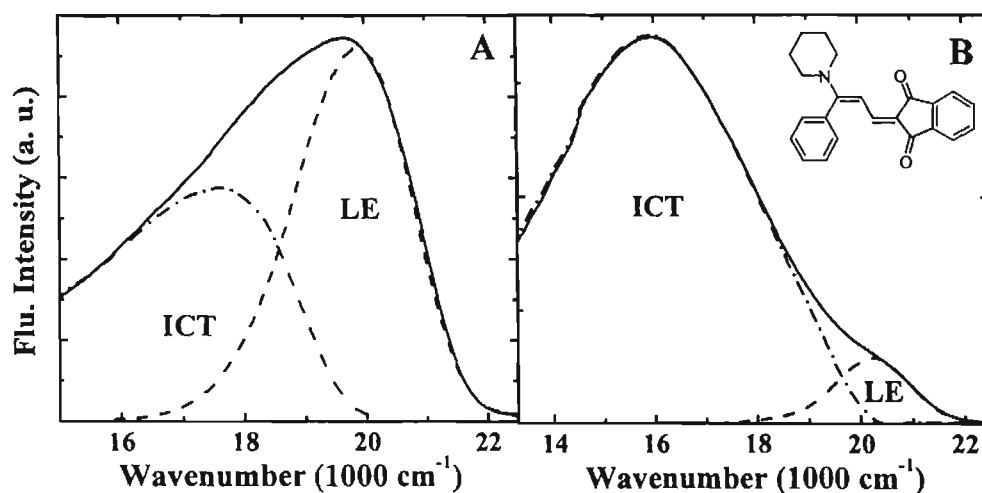
Figure 2.3. Fluorescence spectra of **BN6** in (A) diisopropyl ether and (B) acetonitrile. The separate emissions from the LE and ICT states are indicated.

Table 2.1. Absorption and emission properties of the butadiene derivatives (Chart 2.1) in various solvents (in cm^{-1}).

Compound	Toluene		Diisopropyl ether		Acetonitrile		DMSO		$\Phi_{fluorescence}$ * (x 10^{-4})
	Abs.	Ems.	Abs.	Ems.	Abs.	Ems.	Abs.	Ems.	
BN5	21978	20533	22222	20325	22222	20703, 16583	21978	20661, 16286	4.0
BN6	21978	20325	22222	20120	22222	20202, 16750	21978	20408, 16556	2.0
BNDE	21978	20764	22222	20283	22222	20746, 16750	21978	20202, 16420	3.0
BN5AN	21739	19493	21978	19417	21978	16420	21739	16000	30.0
BAN	19230	17006	19607	16863	19047	15625	18018	15220	300.0

* measured in toluene

The forward and backward reactions represented by this scheme commonly involve an orientational relaxation of the solvent molecules, following the changes in charge distribution.

2.3.4. Dipole Moments

Figure 2.4 shows the plot of the LE and ICT fluorescence band maxima of BN6 against the solvent polarity parameter (f-f') (eq 2.1).

$$(f-f') = [\varepsilon-1/2\varepsilon+1] - [n^2-1/2n^2+1] \tag{2.1}$$

The solvatochromic shift of the fluorescence (v_{flu}) maxima of the LE and ICT bands can be expressed by the following equation (2.2),[23-29]

$$v_{flu} = (-1/4\pi\varepsilon_0).(2/hca^3).\mu_e^{ex}(\mu_e^{ex}-\mu_g) (f-f') + const.'$$

$$= m(flu) (f-f') + const.' \tag{2.2}$$

where, a is the equivalent spherical radius of the solute (Onsager radius) and ε, ε_0 and n are the dielectric constant, the vacuum permittivity and the refractive index of the solvent, respectively. μ_g is the ground state dipole moment and μ_e^{ex} refers to the dipole moment of the LE or ICT state.

The Onsager radius a (5.1 Å), was determined from the Avogadro number, assuming that the molecular density of BN6 is equal to 1.0.[27] For the ground state dipole moment of BN6 a value of μ_g= 6.0 D was calculated.[30,31] From the slope m(flu) for the ICT fluorescence obtained from Figure 2. 4, μ_e^{ICT} was calculated to be 13.6 D. Similarly, from the slope for the LE fluorescence in Figure 2.4, the dipole moment of the LE state (μ_e^{LE}) was estimated as 8.1 D.
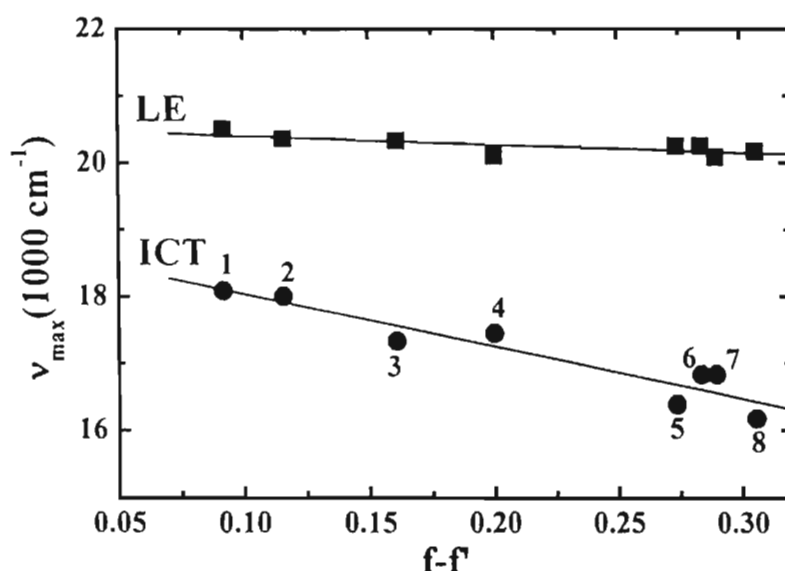
Figure 2.4. Solvatochromic plots of the emission maxima of the locally excited state (■) and the ICT state (●) of **BN6** versus the macroscopic solvent polarity parameter, f-f' (eq 2.3). Solvents:1) di(*n*-butyl) ether, 2) di(*n*-propyl) ether, 3) diethyl ether, 4) ethyl acetate, 5) acetone, 6) dimethyl formamide, 7) propionitrile and 8) acetonitrile.

2.3.5. Effect of Temperature on the Fluorescence Spectra

The effect of temperature on the fluorescence spectra of **BN6** and **BN5AN** in acetonitrile is shown in Figure 2.5 For **BN6** (Figure 2.5A), an increase in temperature results in a relative increase in intensity of the LE band, which is accompanied by a decrease in the intensity of the ICT band around 625 nm. This temperature dependence is attributed to the low-lying ICT being energized back to the LE state with increasing temperature (see Scheme 2.3). Similar observations were made for the solvent and temperature dependence of the fluorescence of **BN5** and **BNDE**.

In most compounds that contain an amine group, which show dual luminescence, this phenomenon has been attributed to conformational changes of

the amine substituent.[13-18] Comparison of the fluorescence properties of **BN5AN** and **BAN** helps to determine the role of the amine group in the dual emission of the DA-substituted butadienes discussed here. Compound **BN5AN** contains a dimethylamino group on the phenyl ring in addition to the pyrrolidine substituent, the latter being absent in **BAN**. The solvent effect on the emission spectrum of **BN5AN** indicates qualitative similarities with those of **BN5, BN6** and **BNDE**. The LE band is more prominent in non-polar solvents whereas the ICT band predominates in polar solvents. The fluorescence maxima of **BN5AN** in various solvents are listed in Table 2.1. Significant differences can however be observed on comparing the effect of temperature on the fluorescence of **BN5AN** with that found for **BN5, BN6** and **BNDE**. Figure 2.5B shows that with increasing temperature, the overall fluorescence intensity of **BN5AN** in the LE and ICT spectral region increases unlike what was observed for **BN6** (Figure 2.5A).

Addition of trifluoroacetic acid (TFA) has an interesting effect on the shape and temperature dependence of the fluorescence spectrum of **BN5AN** (Figure 2.5C). The response of the fluorescence spectrum of **BN5AN** to temperature in presence of TFA is similar to that of **BN6** (Figure 2.5.(A)). With increasing temperature, there is a decrease in the intensity of the ICT band and an enhancement in the intensity of the LE band. This indicates that addition of TFA leads to protonation of the aromatic dimethylamine group of **BN5AN**.
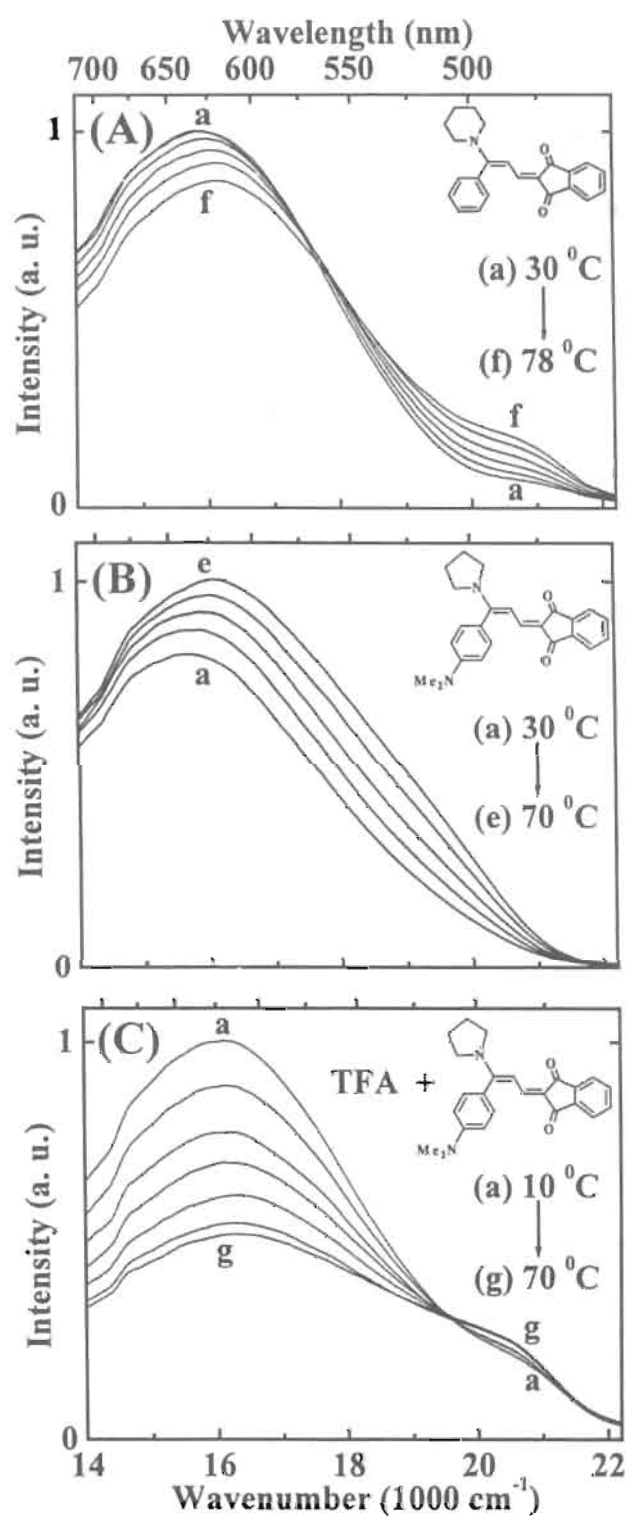
Figure 2.5. Temperature dependence of the fluorescence of (A) **BN6** in acetonitrile, (B) **BN5AN** in acetonitrile, (C) **BN5AN** in acetonitrile containing 43 mM of trifluoroacetic acid. Temperature increase is in steps of 10 °C.

With the lone pair of the aromatic amine blocked by protonation and thus unable to partake in the ICT process, the compound behaves very much like the derivatives, **BN5**, **BN6** and **BNDE**, which do not have a dimethylamino group on the phenyl ring. The dual fluorescence observed in these compounds, **BN5**, **BN6**, **BNDE** and **BN5AN** can therefore be attributed to conformational changes of the amine group, which is directly connected to the butadiene chain.

The role of this amine group in the dual fluorescence of, **BN5**, **BN6**, **BNDE** and **BN5AN**, was further confirmed by studying the fluorescence properties of **BAN**. For this compound, increase in solvent polarity results in a bathochromic shift in the fluorescence spectrum (Table 2.1), whereas increase in temperature results only in a decrease in the fluorescence intensity (Figure 2.6).
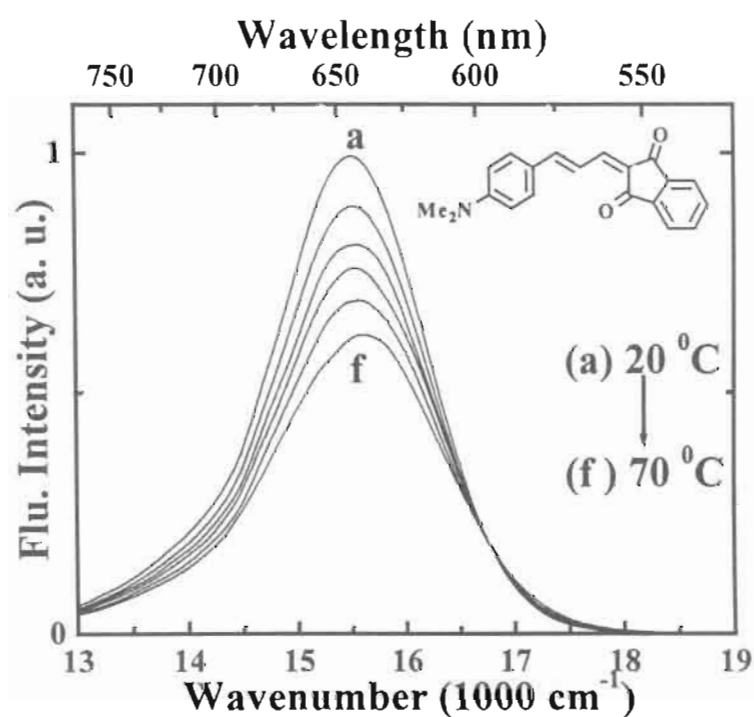
Figure 2.6. Temperature dependence of the fluorescence spectra of **BAN**. Temperature increase is in steps of 10 °C.

Hence there was no evidence of dual luminescence in the case of **BAN**. This again confirms that the amine group directly connected to the butadiene chain is responsible for the dual fluorescence in, **BN5, BN6, BNDE** and **BN5AN**

Figure 2.7 shows the Stevens-Ban plot of ln I'(ICT)/I(LE) versus the reciprocal absolute temperature for **BN5** in butyronitrile, where I'(ICT) is the intensity of the ICT emission band corrected for the increase in the band-width with increasing temperature and I(LE) is the intensity of the LE band. The plot shows the pattern normally observed in the high-temperature limit (HTL) of a reversible ICT reaction described in Scheme 2.3, for which $k_d \gg 1/\tau'_0$.[32] The data points in Figure 2.7 were fitted to equation 2.3 by the nonlinear least squares method.[32]
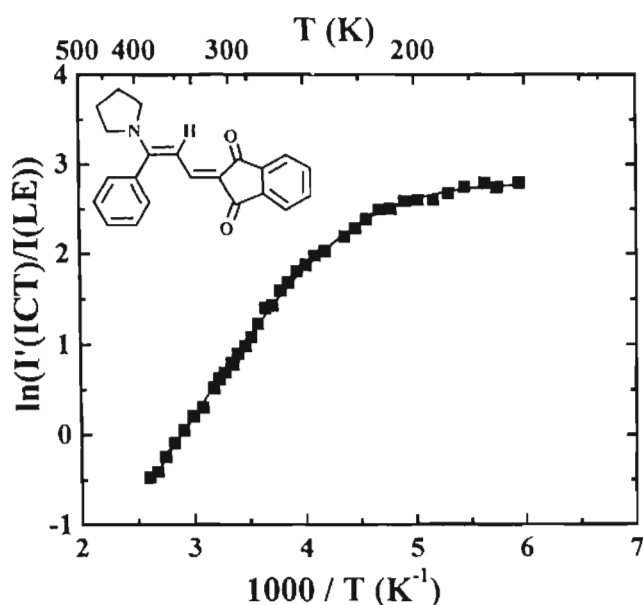
Figure 2.7. Stevens-Ban plot of the natural logarithm of the LE/ICT fluorescence intensity ratio I'(ICT)/I(LE), determined at the maxima of the ICT and LE emission bands, versus the reciprocal of absolute temperature, for **BN5** in butyronitrile. The data points are fitted by a curve described by equation 2.3.

$\phi'(ICT)/\phi(LE) \cong I'(ICT)/I(LE)$

$$= k'_f.[ICT] / k_f.[LE] = k'_f/k_f . k_a/(k_d + 1/\tau'_0) \qquad (2.3.)$$

The good fit of the data points to equation 2.3. supports our interpretation that dual emission in, **BN5, BN6, BNDE** and **BN5AN** originates from a reversible ICT reaction as represented by Scheme 2.3. The fit suggests a value approaching zero (0.2 ± 0.4 kJ/mol) for the activation energy, E_a of the forward ICT rate constant k_a.

2.3.6. Fluorescence Lifetimes

The picosecond fluorescence decay of compound **BN5** was measured at -40 °C in three alkyl nitriles of different polarity, acetonitrile (MeCN), propionitrile (EtCN) and butyronitrile (PrCN). The measurements were carried out at two wavelengths, one corresponding to the LE emission (480 nm) and the other at the maximum of the ICT fluorescence (650 nm), see Figure 2.8.

Table 2.2. Fluorescence decay times τ_1 and τ_2 and their amplitude ratios (equations 2.4 and 2.5) measured at the ICT (650 nm) and LE (480 nm) fluorescence bands of **BN5** in three solvents at −40 °C.

Solvent[a]	$\tau_2(ICT)$ [ps]	$\tau_1(ICT)$ [ps]	$-A_{22}/A_{21}$	$\tau_2(LE)$ [ps]	$\tau_1(LE)$ [ps]	A_{12}/A_{11}
MeCN	6.7	208	0.97	2.7	245	2100
EtCN	6.1	307	1.01	2.8	276	1000
PrCN	6.0	355	1.03	3.2	306	500

[a]MeCN: acetonitrile; EtCN: propionitrile; PrCN: butyronitrile

The fluorescence response function obtained at the maximum of the ICT emission band of **BN5** in the three alkyl nitriles (Table 2.2.) can be fitted with two exponentials (equations 2.4 and 2.5). A growing-in with a decay time τ_2 between 6 and 7 ps is observed, whereas the longer decay time τ_1 increases with decreasing solvent polarity, 208 ps (MeCN), 307 ps (EtCN) and 355 ps (PrCN) (Table 2.2). The amplitude ratio $-A_{22}/A_{21}$ equals unity, which shows that the ICT state cannot be reached by direct light absorption from S_0 (Scheme 2.3).[33]

$$i_f(\text{LE}) = A_{11}\exp(-t/\tau_1) + A_{12}\exp(-t/\tau_2) \tag{2.4}$$

$$i_f(\text{ICT}) = A_{21}\exp(-t/\tau_1) + A_{22}\exp(-t/\tau_2) \tag{2.5}$$

The LE fluorescence decays, on the other hand, are practically single exponential in all three solvents, with a decay time τ_2 around 3 ps (at the limit of the time resolution of our SPC setup, see Experimental Section) and a longer decay time τ_1 similar to that of the ICT decays, but with a large amplitude ratio A_{12}/A_{11} between 2100 and 500 (Figure 2.8 and Table 2.2). Somewhat surprisingly, the LE and ICT decay times of **BN5** in PrCN are practically independent of temperature over the entire temperature range between −20 and −100 °C, measured at intervals of 20 °C. The same temperature independence was found for **BN5** in MeCN at 25 and −40 °C. With **BN6** in MeCN, similar decay times τ_1 were obtained at these temperatures. Whereas the LE decay time τ_2 of ~3 ps seems to be in accord with the ICT activation energy, E_a of smaller than 1 kJ/mol (Table 2.2), the fact that the ICT rise-time τ_2 (6 to 7 ps) is different from the LE decay time is

in conflict with the requirements of Scheme 2.3. This difference may be interpreted in terms of an additional intermediate species[34] or a time dependent Stokes-shift. However, at the present stage of investigation no direct evidence is available on the involvement of either of these two processes.
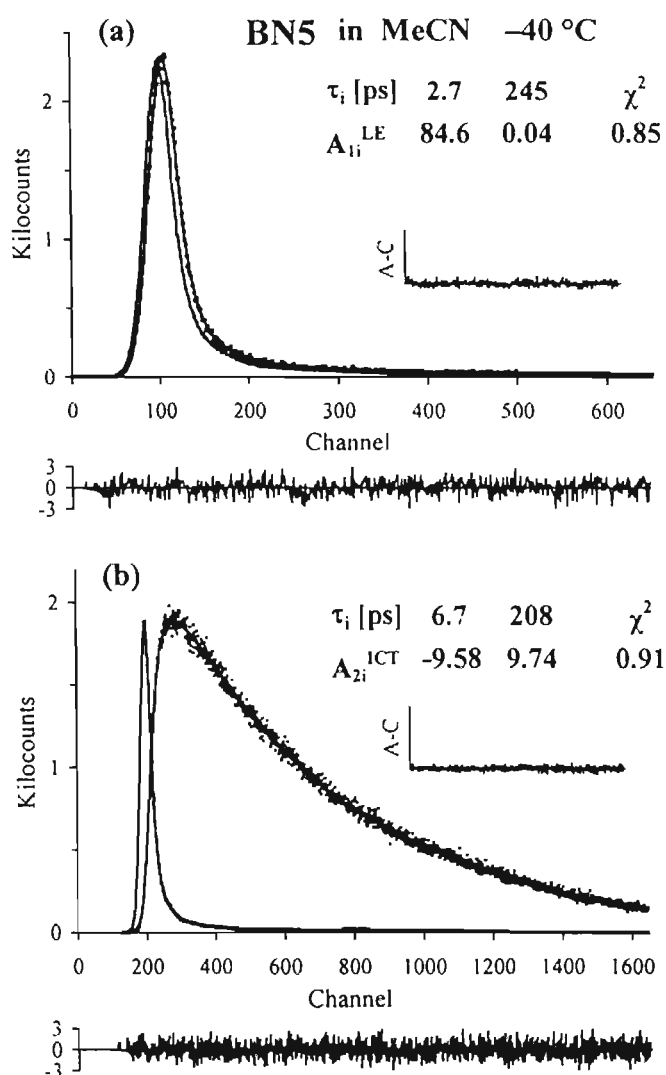
Figure 2.8. LE (a) and ICT (b) fluorescence response functions of **BN5** in acetonitrile at −40 °C. The decay times (τ_1, τ_2) and their pre-exponential factors A_{1i}^{LE} and A_{2i}^{ICT} are given in equations 2.4 and 2.5. The shortest decay time τ_2 is listed first. The weighted deviations expressed in σ(expected deviations), the autocorrelation functions A-C, and the values for χ^2 are also shown. Excitation wavelength, 413 nm.

2.3.7. Photoisomerization

Direct excitation of **BN6** in benzene using a 355 nm laser pulse gives the transient absorption spectrum shown in Figure 2.9.
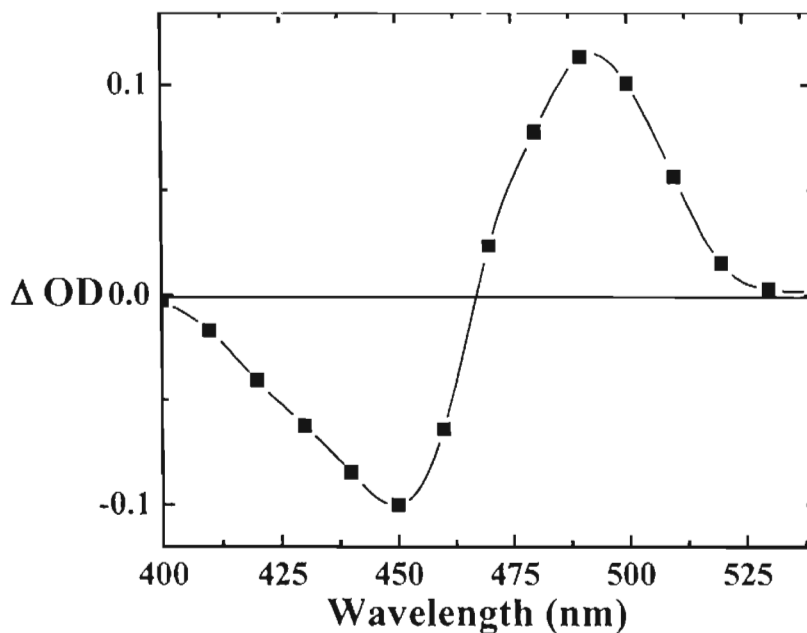
Figure 2.9. Transient absorption spectrum measured immediately following 355 nm laser pulse excitation of a solution of **BN6** in benzene.

The depletion, observed around 450 nm corresponds to the ground-state absorption maximum of **BN6**. The transient absorption maximum at 490 nm decays back to the baseline by a first order process, simultaneous with the recovery of the ground-state absorption of **BN6** around 450 nm (Figure 2.10). No change in the nature of the transient absorption or rate of transient decay was observed on using solutions saturated with oxygen, which indicates that the observed changes cannot be due to the formation of the triplet excited state of **BN6**. The fully reversible phototransformation observed on laser excitation may be attributed to isomerization of the butadiene moiety.
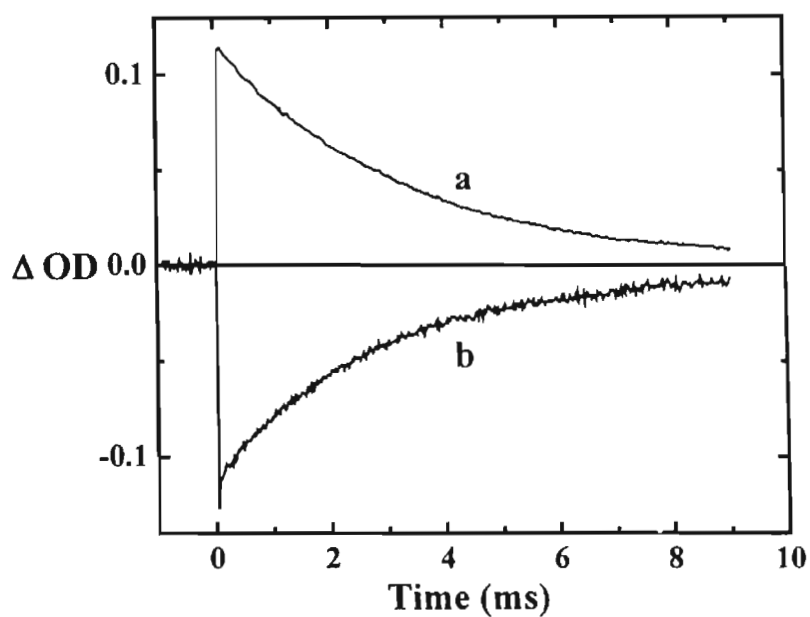
Figure 2.10. Transient absorption profile recorded immediately following 355 nm laser pulse excitation of a solution of **BN6** in benzene, (a) 490 nm and (b) 450 nm.

The *trans* to *cis* photoisomerization of diphenylbutadienes has been extensively studied.[35-37] The most likely transformation in the present DA-substituted butadienes is therefore the photoisomerization from the E to the Z isomer (E-Z), as shown in Scheme 2.4. It may be noted that isomerization around the double bond connected to the indane-1,3-dione moiety would not lead to any change in the absorption spectrum due to the symmetry of this group.
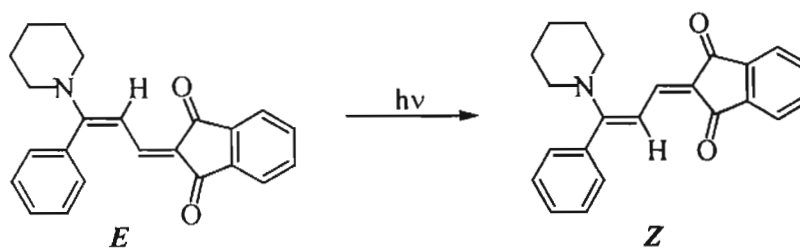
Scheme 2.4. *E-Z* photoisomerization in **BN6**.

The transient absorption spectrum (Figure 2.9) shows a shift of about 40 nm in the absorption maximum of the Z isomer, compared to that of the E isomer. Similar bathochromic shifts on E-Z isomerization have been reported for several substituted olefins.[38-42]

2.3.8. Triplet Excited States

As discussed above, direct excitation of **BN6** does not lead to the formation of its triplet excited state. In order to study its triplet state properties, benzophenone (**BP**) was used as a triplet sensitizer. Figure 2.11 shows the transient absorption spectra measured on 355 nm laser pulse excitation of a solution of **BN6** in benzene, containing benzophenone.

Under these conditions the radiation is predominantly absorbed by benzophenone. The transient absorption spectrum obtained immediately after the laser pulse (Figure 2.11, curve a) can be attributed to the triplet excited state of benzophenone, by comparison with spectral features reported earlier.[43]

The triplet of benzophenone is quenched by **BN6**, to yield the transient spectrum with a broad absorption in the region of 480-600 nm and a depletion around 450 nm (Figure 2.11, curve b). The rates of benzophenone triplet decay and growth of transient species are identical. From the dependence of observed rate constant for decay of the benzophenone triplet on the concentration of **BN6** (Figure 2.12), a rate constant, $k = 1.0 \times 10^{10}$ M^{-1} s^{-1} is obtained, indicating a diffusion-controlled process.
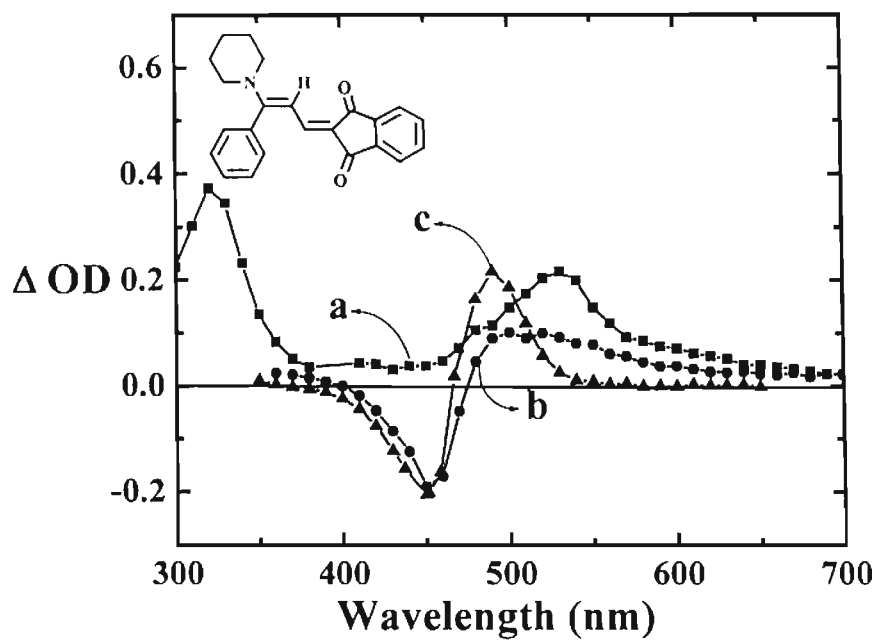
Figure 2.11. Transient absorption spectrum measured after 355 nm laser pulse excitation of argon-degassed solution of **BN6** and benzophenone in benzene: (a) 0.1 s, (b) 5 s and (c) 10 s.
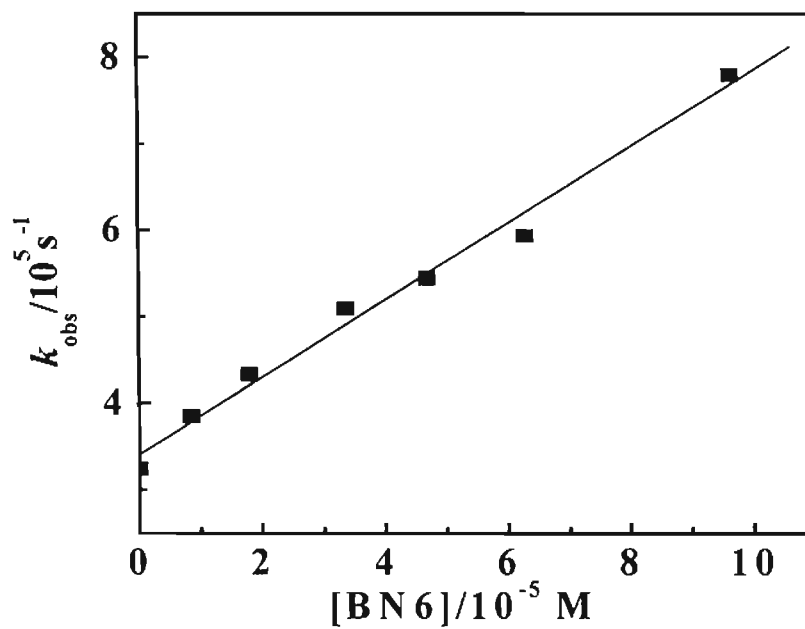
Figure 2.12. The plot of rate constant for decay of benzophenone triplet at 320 nm versus concentration of **BN6**.

Benzophenone is known to sensitize the triplet state of organic molecules and the transient absorption following the quenching process can be attributed to the triplet state of **BN6**. The triplet excited state of **BN6** decays by a first order process with a lifetime of 9 μs, to yield a fairly long-lived transient (Figure 2.11, curve c). The transient spectrum of this long-lived species is identical to the transient spectrum obtained on direct excitation of **BN6** (Figure 2.9). The decay of this species occurs by a first-order process with a lifetime of 3 ms, which is identical to the decay of the transient species formed on direct excitation of **BN6** (Figure 2.9 and Table 2.3). These results indicate that the triplet excited state of **BN6** decays to the Z isomer of **BN6**. Oxygen-saturated solutions were studied in order to confirm that the **BN6**-Z isomer is mainly formed via the sensitized triplet excited state and not by direct excitation to the singlet. In the presence of oxygen, the triplet state of benzophenone is quenched and only a small amount of the residual absorption, attributable to the Z isomer produced by direct excitation of **BN6**, was observed (Figure 2.13).
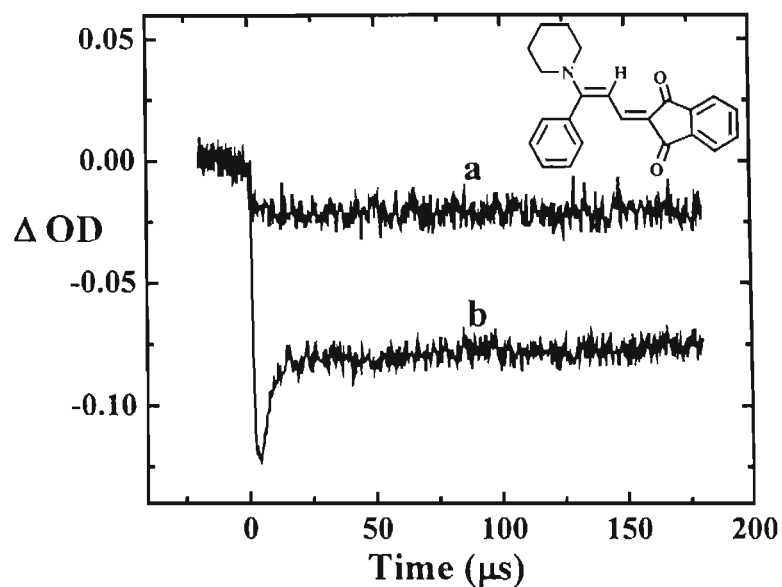
Figure 2.13. Transient absorption-time profiles recorded at 450 nm following 355 nm laser pulse excitation of **BN6** and benzophenone in benzene. (a) oxygen-saturated and (b) argon-purged solutions.

This confirms that the major fraction of the **BN6** isomer generated in the presence of benzophenone arises from the triplet state of **BN6**. The observed processes can be described by the mechanism shown in Scheme 2.5.

$$BP \xrightarrow{h\nu} {}^3BP^*$$

$${}^3BP^* \longrightarrow BP$$

$${}^3BP^* + BN6\text{-}E \longrightarrow {}^3BN6^* + BP$$

$${}^3BN6^* \xrightarrow{\tau = 9\ \mu s} BN6\text{-}Z$$

$$BN6\text{-}Z \xrightarrow{\tau = 3\ ms} BN6\text{-}E$$
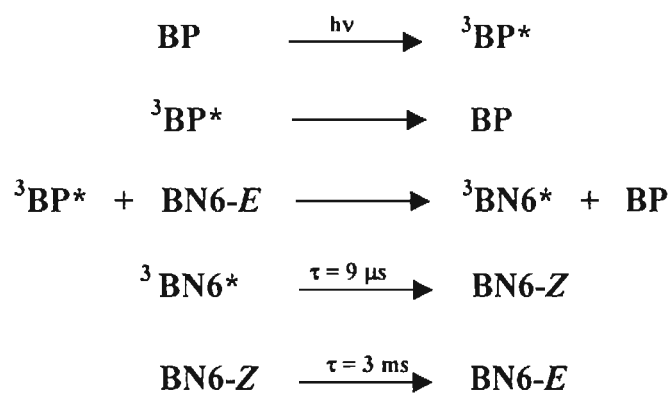
Scheme 2.5. The various steps involved in the photoisomerization of **BN6** through the triplet pathway upon sensitization using benzophenone.

2.3.9. Quantum Yield of Photoisomerization

For estimating the photoisomerization quantum yield on direct excitation of
BN6, the extinction coefficient of the Z isomer at 490 nm was first determined by
the relative actinometry method using tris(2,2'-bipyridyl)ruthenium(II)chloride
hexahydrate (**Rubp**) as actinometer.[44] Solutions of **Rubp** in water and of
benzophenone and **BN6** in benzene (optically matched at 355 nm) were used. The
extinction coefficient was estimated from the following relationship (equation 2.6),

$$\varepsilon(\mathbf{BN6}\text{-}Z) = [\Delta OD_S \, \phi_T(R)/\Delta OD_R \, Y(\mathbf{BN6}\text{-}Z)]\varepsilon_R \qquad (2.6)$$

where, $\varepsilon(\mathbf{BN6}\text{-}Z)$ is the extinction coefficient of **BN6-Z** at 490 nm, ΔOD_S is the
change in ΔOD at 490 nm for solution of **BN6** containing benzophenone, ΔOD_R is
the change in ΔOD at 370 nm for the **Rubp** solution, $\phi_T(R)$ is the triplet quantum
yield of **Rubp**, $Y(\mathbf{BN6}\text{-}Z)$ is the yield of **BN6-Z** and ε_R is the extinction coefficient
of **Rubp** at 370 nm.

For estimating the extinction coefficient of Z isomer of **BN6**, the following
two assumptions were made, (1) benzophenone quenched by **BN6** leads
quantitatively to the triplet state of **BN6**, and (2) ^{3}**BN6*** thus formed is
quantitatively converted to **BN6-Z** isomer. Based on this, the yield $Y(\mathbf{BN6}\text{-}Z)$ of
the **BN6-Z** isomer formed in the presence of varying concentrations of **BN6** was
calculated using the following equation (equation 2.7),

$$Y(\mathbf{BN6}\text{-}Z) = Y(^3\mathbf{BN6}^*) = [(k^1{}_{obs} - k) / k^1{}_{obs}]\phi_T(^3\mathbf{BP}^*) \qquad (2.7)$$

where, $k^1{}_{obs}$ is the observed rate of decay of benzophenone in presence of **BN6** and

k is the rate constant for decay of benzophenone in the absence of quencher,

Y(^{3}BN6*) is the triplet yield of **BN6** formed via energy transfer at different

quencher concentrations, and $\phi(^3$BP*) is the triplet quantum yield of

benzophenone. Using ΔOD_S/Y(**BN6-Z**) = 0.32, obtained from a linear plot of

ΔOD_S versus Y(**BN6-Z**) (Figure 2.14) of solutions containing benzophenone and

varying concentrations of **BN6-Z**, in equation 2.6, the extinction coefficient of

BN6-Z isomer was estimated as 1.3×10^5 $M^{-1}cm^{-1}$ at 490 nm.
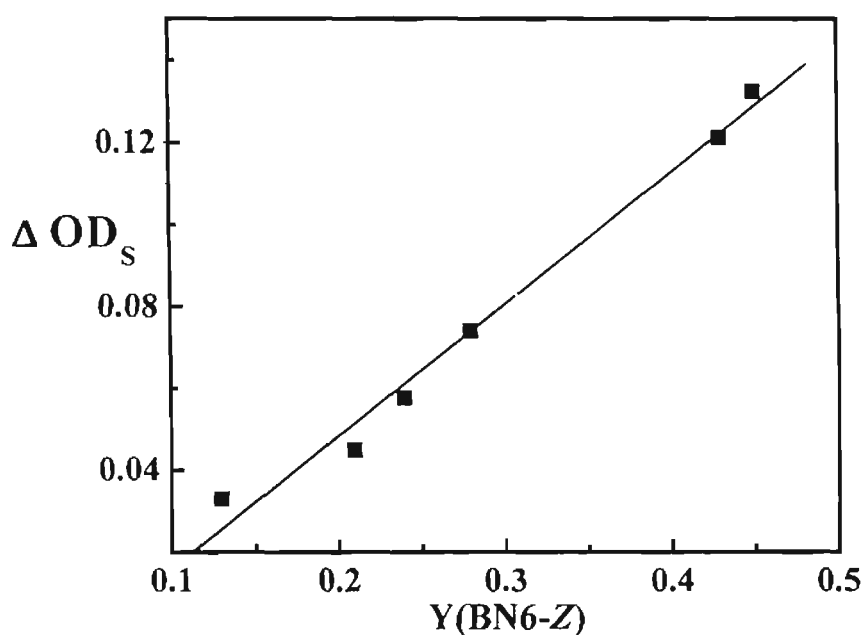
Figure 2.14. Plot of ΔOD_S versus Y(**BN6-Z**) at varying concentrations of **BN6** in acetonitrile in the presence of benzophenone.

Since the amount of **BN6-Z** isomer formed will be equal to the amount

of **BN6-E** isomer depleted, the extinction coefficient of the stable **BN6-E** isomer

at 450 nm can be calculated using equation 2.8.

$$\varepsilon(\textbf{BN6-}E) / \varepsilon(\textbf{BN6-}Z) = \Delta OD(\lambda_{max} E) / \Delta OD(\lambda_{max} Z) \qquad (2.8)$$

This results in a $\varepsilon(\textbf{BN6-}E)$ value of 1.3×10^5 $M^{-1}cm^{-1}$ at 450 nm, which closely matches the value of 1.1×10^5 $M^{-1}cm^{-1}$ for $\varepsilon(\textbf{BN6-}E)$ at 450 nm obtained by using the conventional Beer-Lambert law. The close match in the extinction coefficient of the stable **BN6-**E isomer obtained using two very different methods justifies the assumptions mentioned above, made in estimating the extinction coefficient of the **BN6-**Z isomer. These results also indicate that a very small overlap exists between the absorption spectra of the Z and E isomers of **BN6**. Earlier reports on polyenes have shown that such isomers can have well separated absorption bands with minimal overlap.[36-38]

Using the extinction coefficient of **BN6-**Z isomer obtained above, the photoisomerization quantum yield (ϕ (**BN6-**Z)) of **BN6** from the excited singlet state was estimated as 0.15 by the relative actinometry method, using **Rubp** as actinometer (equation 2.9)

$$\phi(\textbf{BN6-}Z) = [(\Delta OD_S \phi_T(R)) / (\Delta OD_R \varepsilon(\textbf{BN6-}Z))]\varepsilon_R \qquad (2.9)$$

The results of the triplet-mediated photoisomerization of **BNDE** were similar to that of **BN6**. For **BN5**, a different behavior was found. Although **BN5** undergoes photoisomerization from the singlet state in a manner similar to that of **BN6** and **BNDE**, its triplet state properties are markedly different. Figure 2.15 shows the transient absorption profile at 450 nm, on excitation of **BN5** in oxygen-saturated (curve a) and in argon-purged (curve b) benzene solutions containing

benzophenone. In oxygen-saturated solutions, triplets are quenched and hence the transient absorption observed is due to the direct absorption by the substrate. From Figure 2.15 it is clear that the isomerization occurs mainly from the singlet state and that isomerization from the triplet state of **BN5** is very inefficient, unlike what is observed for **BN6** (Figure 2.13).
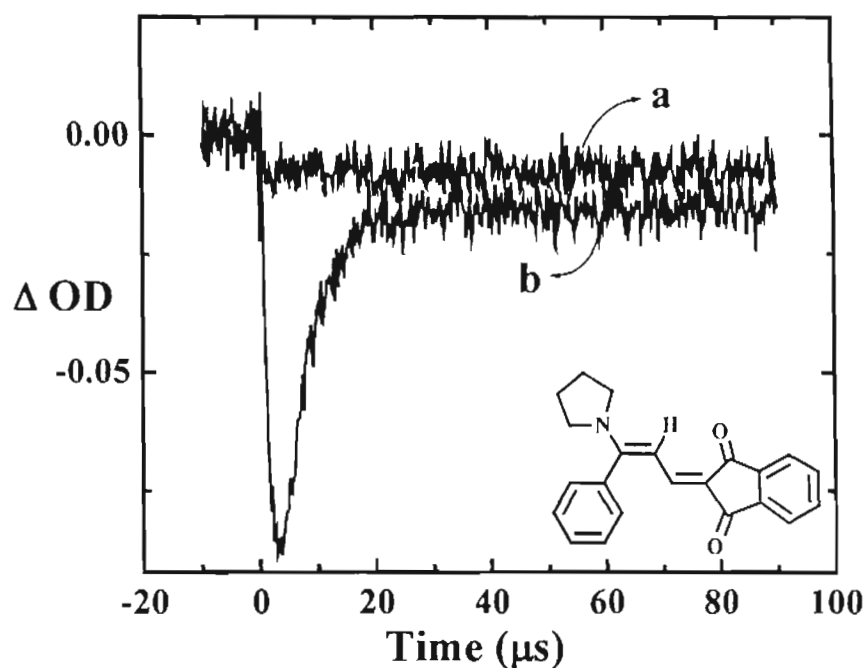
Figure 2.15. Transient absorption-time profiles recorded at 450 nm, following 355-nm laser pulse excitation of **BN5** and benzophenone in benzene, a) oxygen-saturated and b) argon-purged solutions.

In order to estimate the quantum yield of isomerization of **BN5**, the extinction coefficient of its *Z* isomer was determined from the transient absorption spectrum, using equation 2.8, assuming minimum overlap between the absorption bands of *E* and *Z* isomers. The results obtained for **BN6** justify this assumption for the DA-substituted butadiene derivatives under investigation. The quantum yields

of photoisomerization of **BNDE** and **BN5AN** were estimated in a similar manner and the results are summarized in Table 2.3. The triplet excited state properties of the DA-substituted butadienes (Chart 2.1) are also summarized in Table 2.3. The photoisomerization quantum yields were lower in acetonitrile compared to those in benzene.

The thermal *Z-E* isomerization of the DA-substituted butadienes, **BN5**, **BN6**, **BNDE** and **BN5AN**, occurs in the millisecond time domain. The lifetimes of the *Z* isomers were much shorter in acetonitrile than those in benzene. The rate constants for isomerization of DA-substituted olefins are known to increase with increase in solvent polarity, due to the reduction in bond order in such systems.[45]

2.3.10. Photoisomerization of BAN

Laser pulse (532 nm) excitation of a solution of **BAN** in acetonitrile yields a weak transient absorption, which does not decay within 100 ms, indicating the formation of a long-lived species. Steady-state irradiation using a 520 nm band pass filter resulted in a decrease in absorbance at 520 nm and a slight increase at 620 nm (Figure 2.16). This phototransformation is thermally reversible (Figure 2.17). For **BAN**, the all-*trans* (*E*) isomer is expected to be the more stable form, based on comparison with similar compounds reported earlier.[46] Irradiation can lead to *E-Z* isomerization. The quantum yield of isomerization was estimated as 0.09 and 0.02 in benzene and acetonitrile, respectively.

Table 2.3. Photoisomerization data for the butadiene derivatives (Chart 2.1).

Compound	Benzene					Acetonitrile		
	λ_{max} (E) (nm)	λ_{max} (Z) (nm)	$\tau_T(\mu s)$	$\tau_Z(ms)$	$\Phi_{isomerization}$	$\lambda_{max}(Z)$ (nm)	$\tau_Z(\mu s)$	$\Phi_{isomerization}$
BN5	450	475	4	10	0.10	470	30	0.04
BN6	450	490	9	3	0.15	480	13	0.08
BNDE	450	480	4	1.5	0.09	480	22	0.04
BN5AN	460	490	15	0.13	0.11	490	90	0.01
BAN	525	580	15	48 min*	0.09*	620*	8 min*	0.02*

* measured using steady state photolysis

The thermal back reaction for **BAN**, measured by following the recovery of the absorption of the *E* isomer, occurred with lifetimes of 48 and 8 min in benzene and acetonitrile, respectively. This is much slower than those observed for the other butadienes, **BN5**, **BN6**, **BNDE** and **BN5AN**.
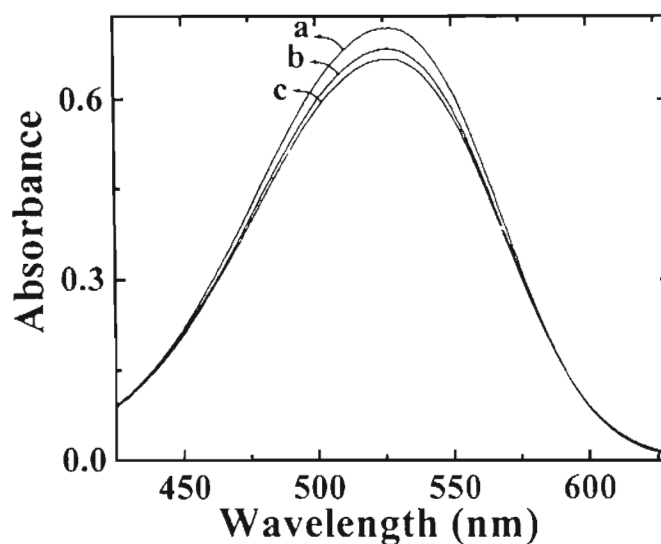
Figure 2.16. Effect of irradiation on the absorption spectrum of **BAN** in acetonitrile. a) before irradiation, b) after 2 min, c) after 5 min.
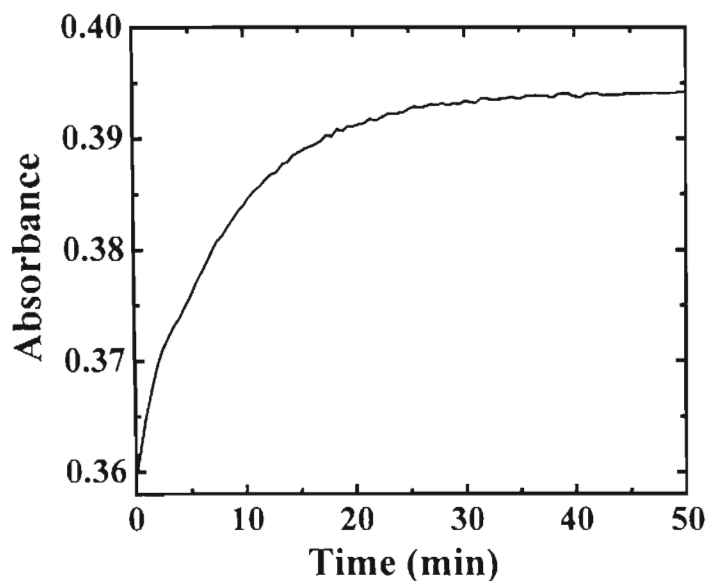
Figure 2.17. Recovery of the absorption at 520 nm, following irradiation of **BAN** in acetonitrile for 3 minutes at 27 °C.

This difference may be attributed to efficient charge transfer from the amino nitrogen directly attached to the butadiene chain (**BN5, BN6, BNDE** and **BN5AN**), which can reduce the bond order of the C=C double bond, thereby making the isomerization process faster. In **BAN**, which does not possess an amino group directly attached to the butadiene chain, the charge transfer from the aromatic amino nitrogen to the indanedione, would be hindered by the energy barrier for the loss of aromaticity required in the formation of the quinonoid structure. The C=C double bond being less affected in this case, would result in slower *Z-E* isomerization of **BAN**.

2.4. Conclusion

Intramolecular charge transfer, triplet state properties and photoisomerization were studied for the D/A-substituted butadienes (Chart 2.1). Compounds, **BN5, BN6, BNDE** and **BN5AN**, which posses an amine substituent directly connected to the butadiene chain show dual fluorescence from a LE state and a more polar ICT state. Compound **BAN**, which contains only an aromatic amine connected to the butadiene chain, does not show dual fluorescence. The quantum yield of fluorescence is very low for these compounds and the intersystem crossing efficiencies are negligible. The compounds undergo *E-Z* photoisomerization from the excited singlet state with a quantum efficiency of about 0.10 in benzene. Internal conversion forms the main pathway for energy dissipation from the excited singlet state for this class of molecules. The triplet

states of the butadienes were generated via energy transfer from the triplet state of benzophenone. Compounds containing diethylamine, **BNDE** and piperidine, **BN6** as substituents undergo *E-Z* isomerization quantitatively from the excited triplet state, whereas for the pyrrolidine substituted derivatives, **BN5** and **BN5AN**, photoisomerization from the excited triplet state is highly inefficient. The rates for thermal *Z-E* isomerization of these derivatives are also highly sensitive to the nature of the amine substituent on the butadiene moiety (**BN6~BNDE>BN5**).

2.5. Experimental Section

2.5.1. Materials

The DA-substituted butadienes, **BN5**, **BN6**, **BNDE** and **BN5AN**, were synthesized using methods reported earlier.[11] **BAN** was synthesized by the condensation of N,N-dimethylaminocinnamaldehyde with 1,3-indanedione. All the compounds were purified by column chromatography, followed by repeated recrystallizations from suitable solvents: **BN5** (from a mixture (1:9) of methanol and chloroform), **BN6**, **BNDE** and **BN5AN** (from benzene) and **BAN** (from a mixture (4:1) of ethyl acetate and hexane). The structures of the butadiene derivatives (Chart 2.1) were confirmed by NMR, IR and high-resolution mass spectral (HRMS) analyses. The purity of these compounds (>99%) was confirmed by high-pressure liquid chromatography. Spectroscopic grade solvents were used for all the spectroscopic studies. Solvents were purified by chromatography over

alumina. Toluene and benzene were purified by refluxing over sodium before distilling.

2.5.2. Optical Measurements

Absorption spectra were recorded on a Shimadzu UV-3101PC spectrophotometer. The excitation and emission spectra were measured on a SPEX Fluorolog F112X spectrofluorimeter. Fluorescence quantum yields were determined by comparison with Rhodamine 6G. Solutions with the same optical density at the excitation wavelength were used.

The fluorescence decay times were determined with a picosecond laser setup (excitation wavelength λ_{exc}, 413 nm).[17,33] The instrument response time has a half-width of 20-35 ps. The analysis of fluorescence decays was carried out as per reported procedures.[17,33]

Nanosecond laser flash photolysis experiments were carried out on an Applied Photophysics model LKS-20 laser kinetic spectrometer with the third harmonic (355 nm) of a Quanta Ray GCR-12 Nd:YAG laser with a pulse duration of 10 ns and energy of 70 mJ/pulse. All solutions were degassed by bubbling argon for a minimum of 15 minutes, before use.

A 200 W high-pressure mercury lamp in combination with an Oriel grating monochromator (model 77250) was used as the light source for steady state photolysis experiments. For estimating the steady state quantum yield of photoisomerization, the intensity of the light absorbed by substrate (I) was

determined by using the Reinecke's salt actinometer.[47] The light intensity (I_0) transmitted through the solvent was first measured using the actinometer solution in a cuvette (1 cm) placed behind the cuvette containing the solvent alone. The solvent was replaced with a solution containing the substrate and a fresh solution of the actinometer was used to estimate the intensity of light (I_1) transmitted through the solution. The intensity of light (I) absorbed by the substrate is equal to the difference between the intensities of light (I_0-I_1).

2.5.3. General Procedure for Synthesis of Donor-Acceptor-Substituted Butadienes, BN5, BN6, BNDE and BN5AN

The donor-acceptor-substituted butadienes, **BN5, BN6, BNDE** and **BN5AN**, were synthesized as per the procedure shown in Scheme 2.1. Detailed description on synthesis and spectral characterization are given in the following sections. Treatment of the appropriate acetophenone with butanethiol in the presence of boron trifluoride-etherate and subsequent Vilsmeier formylation leads to the formation of the intermediate aldehyde, **2a-d**. Aldol type condensation of **2a-d** with indane-1,3-dione gives the butylsulfanyl-substituted butadiene derivatives, **3a-d**. Substitution of the butylsulfanyl group with appropriate donor gives the final compounds, **BN5, BN6, BNDE** and **BN5AN**. The condensation of 4-dimethylaminocinnamaldehyde with indane-1,3-dione in the presence of a base, as described in Scheme 2.2 gave **BAN**. The synthesis of compounds **3a-c** is reported.

elsewhere.[11] All compounds (Chart 2.1) were characterized on the basis of analytical and spectral data.

2.5.3.1. Synthesis of Donor-Acceptor-Substituted Butadiene Derivatives

2-[3-Butylsufanyl-3-(4-N,N-dimethylaminophenyl)prop-2-enylidene]indane-1,3-dione (3d)

Equimolar quantities of the aldehyde **2d** and indane-1,3-dione was stirred in methanol in the presence of KOH for 3 h. The solvent was removed under reduced pressure and the crude product was isolated by column chromatography using silica gel (100-200 mesh) and a mixture (3:7) of ethyl acetate and petroleum ether as the eluent. Compound **3d** was obtained in the form of intense red liquid.

3d (40%): IR ν_{max} (Neat) 2920, 1683, 1610, 1568, 1365, 1333 cm^{-1}; ^{1}H NMR (300 MHz, CDCl$_3$) δ 0.8 (t, 3H, CH$_3$), 1.2-1.7 (m, 4H, CH$_2$CH$_2$), 2.6 (t, 2H, CH$_2$), 3.0 (s, 6H, NMe$_2$), 6.6-7.8 (m, 8H, aromatic), 8.0-8.3 (dd, 2H, vinylic) ppm.

2-(3-Pyrrolidine-3-phenylprop-2-enylidene)indane-1,3-dione (BN5)

Treatment of indane-1,3-dione, **3a** with pyrrolidine in equimolar ratio under reflux conditions in methanol for 12 h gave a reddish brown solid which was further purified by column chromatography using chloroform as eluent. Recrystallization from a mixture (1:9) of methanol and chloroform gave compound **BN5** in the form of reddish brown crystals.

BN5 (88%): mp 274-275 °C; IR ν_{max} (KBr) 2993, 2875, 1684, 1587 cm^{-1}; UV

λmax (CHCl$_3$) 456 nm (ϵ 88900); ^{1}H NMR (300 MHz, CDCl$_3$) δ 1.65-2.25 (m, 4H, CH$_2$), 3.20 (t, 2H, NCH$_2$), 7.00-7.90 (m, 11H, aromatic and vinylic) ppm; ^{13}C NMR (75 MHz, CDCl$_3$): δ 24.95, 25.28, 49.61, 52.02, 102.87, 120.86, 121.32, 128.32, 128.99, 130.02, 132.65, 132.86, 133.59, 140.10, 141.46, 146.54, 167.65, 173.81 ppm; Exact mass calcd for C$_{22}$H$_{20}$NO$_2$ (MH+) 330.1512; found 330.1494 (FAB, HRMS).

2-(3-Piperidine-3-phenylprop-2-enylidene)indane-1,3-dione (BN6)

Treatment of indane-1,3-dione, **3b** with piperidine in equimolar ratio under reflux conditions in methanol for 12 h gave the crude product, which was further purified by column chromatography. Elution with a mixture (3:7) of ethyl acetate and petroleum ether gave a pure sample of **BN6**, after recrystallization from benzene.

BN6 (90%): mp 243-244 °C; IR ν_{max} (KBr): 2939, 2861, 1703, 1659, 1563 cm^{-1}; UV λ_{max} (CHCl$_3$): 458 nm (ϵ 70200 M^{-1}cm^{-1}); ^{1}H NMR (300 MHz, CDCl$_3$): δ 1.4-2.0 (m, 6 H, (CH$_2$)$_3$), 3.1-3.4 (m, 2H, NCH$_2$), 3.7-4.0 (m, 2 H, NCH$_2$), 6.9-7.9 (m, 11 H, aromatic and vinylic) ppm; ^{13}C NMR (75 MHz, CDCl$_3$): δ 23.72, 25.48, 101.88, 114.95, 120.47, 120.89, 128.61, 129.90, 132.37, 132.58, 132.79, 139.74, 141.09, 147.44, 169.40, 191.00, 191.92 ppm. Exact mass calcd for C$_{23}$H$_{22}$NO$_2$ (MH$^+$) 344.1662; found 344.1651 (FAB, HRMS).

2-(3-Diethylamino-3-phenylprop-2-enylidene)indane-1,3-dione (BNDE)

Treatment of indane-1,3-dione, **3c** with diethylamine in equimolar ratio under reflux conditions in methanol for 12 h gave an orange solid, which was further purified by column chromatography using a mixture (3:7) of ethyl acetate and petroleum ether as eluent. The pure sample of **BNDE** was obtained after recrystallization from benzene.

BNDE (85%): mp 172-173 °C; IR v_{max} (KBr): 3060, 2990, 1698, 1651, 1566 cm^{-1}; UV λ_{max} (CHCl$_3$): 455 nm (ε 86500 $M^{-1}cm^{-1}$); ^{1}H NMR (300 MHz, CDCl$_3$): δ 0.90 (t, 3H, CH$_3$), 1.53 (t, 3H, CH$_3$), 3.15 (q, 2H, NCH$_2$), 3.70 (q, 2H, NCH$_2$), 6.80-7.90 (m, 11H, aromatic and vinylic) ppm; ^{13}C NMR (75 MHz, CDCl$_3$): δ 11.96, 14.14, 44.75, 47.26, 102.24, 115.16, 120.71, 121.19, 128.53, 128.76, 129.84, 132.58, 132.79, 139.98, 141.29, 147.41, 169.43, 191.42, 192.37 ppm. Exact mass calcd for $C_{22}H_{22}NO_2$ (MH$^+$) 332.1655; found 332.1651 (FAB, HRMS).

2-[3-(4-N,N-dimethylaminophenyl)-3-pyrrolidinoprop-2-enylidene] indane-1,3-dione (BN5AN)

Equimolar quantities of indane-1,3-dione, **3d** and pyrrolidine was refluxed in methanol for 12 h. The product was isolated by chromatography over silica gel using a mixture (3:7) of ethyl acetate and petroleum ether as the eluent. Recrystallization from benzene gave compound **BN5AN** in the form of yellowish-brown crystals.

BN5AN (90%): mp 255- 256 °C; IR v_{max} (KBr) 2933, 1700, 1683, 1646 cm^{-1}; UV

λ_{max} (CH$_3$CN) 455 nm (ϵ 39000); ^{1}H NMR (Acetone D$_6$) δ 1.96 (t, 2H, CH$_2$), 2.18

(t, 2H, CH$_2$), 3.06 (s, 6H, NMe$_2$), 3.45(t, 2H, NCH$_2$), 3.72 (t, 2H, NCH$_2$), 6.85 (d,

1H, vinylic), 7.16-7.59 (m, 9H, aromatic and vinylic) ppm; ^{13}C NMR (75 MHz,

CDCl$_3$): δ 25.09, 40.18, 49.61, 52.02, 108.10, 109.10, 109.42, 110.77, 111.65,

114.36, 120.61, 121.07, 130.08, 132.35, 132.59, 147.18, 164.31, 182.91 ppm;

Exact mass calcd for C$_{24}$H$_{24}$N$_2$O$_2$ (MH$^+$) 373.1916; found 373.1939 (FAB,

HRMS).

2-[3-(4-N,N-dimethylaminophenyl)prop-2-enylidene] indane-1,3-dione (BAN)

To a solution of 1,3-indanedione in 1,4-dioxane, 2 to 3 drops of

triethylamine were added. To the above mixture, an equimolar amount of

dimethylaminocinnamaldehyde was added and stirred the resulting mixture at

room temperature (30 °C) for 5 h. The reaction mixture was poured into cold water

and filtered out the crude product. The compound was purified through

chromatography over silica gel (100-200 mesh) using a mixture (1:4) of ethyl

acetate and hexane as the eluent. Recrystallization from a mixture (4:1) of ethyl

acetate and hexane gave **BAN** in the form of deep red crystals.

BAN (70%): mp 250-251 °C; IR ν_{max} (KBr) 1675, 1562, 1381, 1286, 1237, 1182

cm^{-1}; ^{1}H NMR (300 MHz, CDCl$_3$) δ 3.18 (s 6H, NMe$_2$), 6.70 (d, 1H, vinylic), 7.60

(d, 1H, vinylic), 7.63-7.90(m, 8H, aromatic), 8.23-8.32(dd, 1H, vinylic) ppm; ^{13}C

NMR (75 MHz, CDCl$_3$): δ 40.10, 108.99, 109.48, 111.75, 111.88, 112.10, 113.68,

113.84, 119.35, 122.38, 122.62, 123.71, 131.34, 134.30, 134.46, 140.75, 146.55, 152.54, 153.66 ppm; Exact mass calcd for $C_{20}H_{17}NO_2$ (MH^+) 303.1259; found 303.1281 (FAB, HRMS).

2.6. References

1) Chemla, D. S.; Zyss, J. *Nonlinear Optical Properties of Organic Molecules and Crystals*; Academic Press: London, 1987; Vol. 1 and 2.

2) Hann, R. A.; Bloor, D. *Organic Materials for Nonlinear Optics;* Royal Society of Chemistry: Oxford, 1989; Vol. Special publication No. 69.

3) Burland, D. M.; Miller, R. D.; Walsh, C. A. *Chem. Rev.* **1994**, *94*, 31.

4) Marder, S. R.; Perry, J. W. *Adv. Mater.* **1993**, *5*, 804.

5) Paley, M. S.; Harris, M. J. *J. Org. Chem.* **1991**, *56*, 568.

6) Stiegman, A. E.; Graham, E.; Perry, K. J.; Khundkar, L. R.; Cheng, L.-T.; Perry, J. W. *J. Am. Chem. Soc.* **1991**, *113*, 7658.

7) Jen, A. K.-Y.; Rao, V. P.; Wang, K. Y.; Drost, K. J. *J. Chem. Soc. Chem. Commun.* **1993**, 90.

8) Ching, K. C.; Lequan, M.; Lequan, R. M. *J. Chem. Soc. Faraday Trans.* 1991, *87*, 2225.

9) Coe, B. J. *Chem. Eur. J.* **1999**, *5*, 2464.

10) Christopher, R. M.; Robert, J. T.; Lee, V. Y.; Swanson, S. A.; Better, , K. M.; Miller, R. D. *J. Am. Chem. Soc.* **1993**, *115*, 12599.

11) Das, S.; George, M.; Mathew, T.; Asokan, C. V. *J. Chem. Soc. Perkin Trans. 2* **1996**, *2*, 731.

12) Singh, A. K.; Darshi, M.; Kanvah, S. *J. Phys. Chem. A* **2000**, *104*, 464.

13) Zachariasse, K. A. *Chem. Phys. Lett.* **2000**, *320*, 8.

14) Rettig, W.; Bliss, B.; Dirnbirger, K. *Chem. Phys. Lett.* **1999**, *305*, 8.

15) Demeter, A.; Druzhnin, S.; George, M.; Haselbach, E.; Roulin, J.-L.; Zachariasse, K. A. *Chem. Phys. Lett.* **2000**, *323*, 351.

16) Chudoba, C.; Kummrow, A.; Dreyer, J.; Strenger, J.; Nibbering, E. T. J.; Elsaesser, T.; Zachariasse, K. A. *Chem. Phys. Lett.* **1999**, *309*, 357.

17) Il'ichev, Y. V.; Kühnle, W.; Zachariasse, K. A. *J. Phys. Chem.* **1998**, *102*, 5670.

18) Rettig, W. *Topics of Current Chemistry,*; Springer: Berlin, 1994; Vol. 169.

19) Takeuchi, S.; Tahara, T. *J. Phys. Chem. A* **1997**, *101*, 3052.

20) Shimojima, A.; Tahara, T. *J. Phys. Chem. B* **2000**, *104*, 9288.

21) Yamaguchi, S.; Hamaguchi, H.-O. *J. Chem. Phys.* **1998**, *109*, 1397.

22) X-ray structure determination was carried out by Dr. M. Noltemeyer, University of Göttingen, Göttingen Germany.

23) Lippert, E.; Mall, F. *Z. Elektrochem.* **1954**, *58*, 718.

24) Lippert, E. *Z. Elektrochem.* **1957**, *61*, 962.

25) Lippert, E. *Z. Naturforsch.* **1955**, *10a*, 541.

26) Kawski, A.; Gryczynski, I.; Jung, C.; Heckner, K.-H. *Z. Naturfosch.* **1977**, *32a*, 420.

27) Il'ichev, Y. V.; Kühnle, W.; Zachariasse, K. A. *Chem. Phys. Lett.* **1996**, *211*, 441.

28) Baumann, W.; Bischof, H.; Brittinger, J.-C.; Rettig, W.; Rotkiewicz, K. *J. Photochem. Photobiol. A: Chem.* **1992**, *64*, 49.

29) Horng, M. L.; Gardecki, J. A.; Papazyan, A.; Maroncelli, M. *J. Phys. Chem.* **1995**, *99*, 17311.

30) Schmidt, M. W.; Baldridge, K. K.; Boatz, J. A.; Elbert, S. T.; Gordon, M. S.; Jensen, J. J.; Koseki, S.; Matsunaga, N.; Nguyen, K. A.; Su, S.; Windus, T. L.; Dupuis, M.; Montgomery, J. A. *J. Comput. Chem.* **1993**, *14*, 1347.

31) Gajewski, J. J.; Gilbert, K. E.; McKelvey, L. *Advances in Molecular Modelling*, 1990; Vol. 2.

32) Zachariasse, K. A. *Trends in Photochemistry and Photobiology* **1994**, *3*, 211.

33) Leinhos, U.; Kühnle, W.; Zachariasse, K. A. *J. Phys. Chem.* **1991**, *95*, 2031.

34) Lewis, F. D.; Weigel, W. *J. Phys. Chem. A:* **2000**, *104*, 8146.

35) Görner, H. *J. Photochem.* **1982**, *19*, 343.

36) Kawski, A.; Kuklinski, B.; Kubicki, A. *Z. Naturfosch.* **1993**, *48a*, 1177.

37) Kawski, A.; Gryczynski, Z.; Gryczynski, I.; Wiczk, W.; Malak, H. *Z. Naturfosch.* **1991**, *46a*, 621.

38) Lewis, F. D.; Yoon, B. A.; Arai, T.; Iwasaki, T.; Tokumaru, K. *J. Am. Chem. Soc.* **1995**, *117*, 3029.

39) Lewis, F. D.; Yoon, B. A. *J. Photochem. Photobiol. A: Chem.* **1995**, *87*, 193.

40) Arai, T.; Moriyama, M.; Tokumaru, K. *J. Am. Chem. Soc.* **1994**, *116*, 3171.

41) Arai, T.; Iwasaki, T.; Tokumaru, K. *Chem. Lett.* **1993**, 691.

42) Lewis, F. D.; Yang, J. S. *J. Phys. Chem.* **1996**, *100*, 14560.

43) Hoshino, H.; Shizuka, H. *Photoinduced Electron Trasfer*; Elsevier: New York, 1988; Vol. Part C.

44) Carmichael, I.; Hug, G. L. **1986**, *15*, 1.

45) Schanze, K. S.; Mattox, T. F.; Whitten, D. G. *J. Am. Chem. Soc.* **1991**, *104*, 1733.

46) Orlandi, G.; Zerbetto, F.; Zgierski, M. Z. *Chem. Rev.* **1991**, *91*, 867.

47) Wegner, E. E.; Adamson, A. W. *J. Am. Chem. Soc.* **1966**, *88*, 394.

Chapter 3

Reversible Photochemical Phase Transition Behaviour of Alkoxy-Cyano-Substituted Diphenylbutadiene Liquid Crystals

3.1. Abstract

The photoisomerizable butadiene chromophore has been utilized for the design of photoresponsive monoalkoxy-cyano-substituted diphenylbutadiene liquid crystals. The EE isomers of these derivatives were found to undergo photoisomerization to yield thermally stable EZ and ZE isomers, which could be transformed back to the EE isomer using light of a different wavelength. The photoisomers were isolated and characterized using ^{1}H-^{1}H COSY and ^{1}H-^{1}H NOESY NMR analyses. Photolysis of the liquid crystalline EE isomers of these derivatives with 360 nm light resulted in an isothermal phase transition to isotropic phase due to the formation of the non-liquid crystalline EZ and ZE isomers. The liquid crystalline state could be regenerated by photolysing the isotropic state using 266 nm light. The thermal stability of the EZ and ZE isomers ensured that the reverse switching of these materials to the liquid crystalline phase remained purely a photon-controlled process. Detailed study on the photoisomerization of these derivatives was carried out in solution, liquid crystalline and solid phases. In the solution phase, the Z-E reverse isomerization reached a photostationary state with the regeneration of only 70% of the EE form. The corresponding process in the solid state was found to be stereospecific and a near quantitative conversion of the EZ and ZE isomers to the EE form (>95%) was observed. Trialkyoxy-cyano-substituted diphenylbutadiene derivatives were also synthesized and their photoisomerization reactions were investigated.

3.2. Introduction

Liquid crystals (LCs) have been extensively used in display devices due to their large optical anisotropies and ability to undergo electric field induced switching.[1-20] Due to the relatively slow switching times for such devices, there has been a growing interest in the development of liquid crystalline materials wherein the optical properties can be reversibly controlled using light activated processes.[10,21,22] Since light induced switching times can be several orders of magnitude faster than electric field induced switching, these materials can play an important role in the development of technologies such as high speed information processing, apart from their use in conventional imaging and display devices. Earlier studies in this area were related to the use of photochromic molecules such as azobenzene[7,8,23] and spiropyrans[24] dissolved in liquid crystalline matrices, where the photochemical transformations of the guest molecules bring about changes in the phase or alignment of the liquid crystalline host. Subsequent studies have shown that the switching times for such processes can be much faster when the liquid crystalline material is inherently photoactive.[8,12,25,26] With a few exceptions, most systems designed for such applications have utilized the *trans-cis* photoisomerization of the azobenzene chromophore, since its rod-shaped *trans* form is known to stabilize the liquid crystalline phase whereas the *cis* isomer destabilizes it.[7,8,23] A drawback connected with the use of the azobenzene chromophore is that *trans-cis* photoisomerization is usually thermally reversible and additional measures such as polymerization[8] or formation of glassy liquid

crystals[27,28] are required for long term storage of information. In view of this, development of photoswitchable liquid crystals using alternate chromophores is desirable. Our interest in the study of the photochemical, photophysical and nonlinear optical properties of some donor-acceptor-substituted butadienes[29,30] led us to explore the use of photoisomerization of the butadiene chromophore for photoswitching in liquid crystals. Although butadiene based liquid crystalline materials have been reported,[31,32] the photoinduced phase transition behavior of these materials have hitherto not been explored. Also, the thermal stability of the photoisomers of donor-acceptor-substituted butadienes largely depend on the strength of the donor and acceptor groups[29,33] and earlier attempts at the isolation and characterization of these isomers have been unsuccessful.[33] Here, we have demonstrated the photoinduced isothermal phase transitions in alkoxy-cyano-substituted diphenylbutadiene liquid crystals (Chart 3.1) with the use of isomerization of the butadiene chromophore. Photoisomerization of these derivatives have been studied both in solution and liquid crystalline phases. The photoisomers were isolated and their detailed spectral characterization has been done. The photoisomerization of some trialkoxy-cyano-substituted diphenylbutadines have also been investigated.
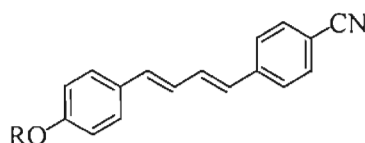
| BC1, R = CH_3 | BC8, R = C_8H_{17} |
| BC4, R = C_4H_9 | BC12, R = $C_{12}H_{25}$ |

Chart 3.1

3.3. Results and Discussion

3.3.1. Synthesis and Structure of Monoalkoxy-Cyano-Substituted Diphenylbutadienes

The alkoxy-cyano-substituted diphenylbutadiene derivatives were synthesized using reported procedures. The detailed synthetic route and spectral data are included in the Experimental Section (3.5). In all cases, the synthetic methodology used yielded purely the *EE* isomer of these derivatives, which was confirmed from the *trans-* ^3J olefinic proton coupling constant values ($^3J_{H,H} = 15$ Hz) in their ^1H NMR spectra.[34] Although the *EE* configuration could be assigned to the synthetically obtained isomer, it was not possible to label each proton in the molecule using the ^1H NMR spectrum. For the ease of representation, the protons in a molecule are labeled as shown in Chart 3.2.
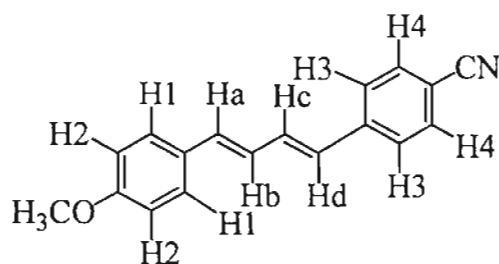
Chart 3.2

The ^1H NMR spectra of the *EE* forms of all derivatives were similar in the aromatic and olefinic regions. In these regions, the ^1H NMR spectra of the *EE* forms showed four doublets (6.91, 7.42, 7.50 and 7.61 ppm) of two protons each, which correspond to aromatic protons. The olefinic protons appeared as two doublets (6.61 and 6.74 ppm) and two double doublets (6.83-6.88 and 7.01-7.08

ppm) with each representing one proton. The two sets of aromatic protons in the

^{1}H NMR spectra of the *EE* isomers could be identified as those appearing on the

methoxyphenyl and cyanophenyl by comparison with ^{1}H NMR spectra of the

model compounds such as 4-methoxycinnamaldehyde and 4-cyanobenzyl bromide,

respectively, as shown in Figure 3.1. Whereas H1 and H2 belong to the

methoxyphenyl moiety, H3 and H4 appear on the cyanophenyl ring.
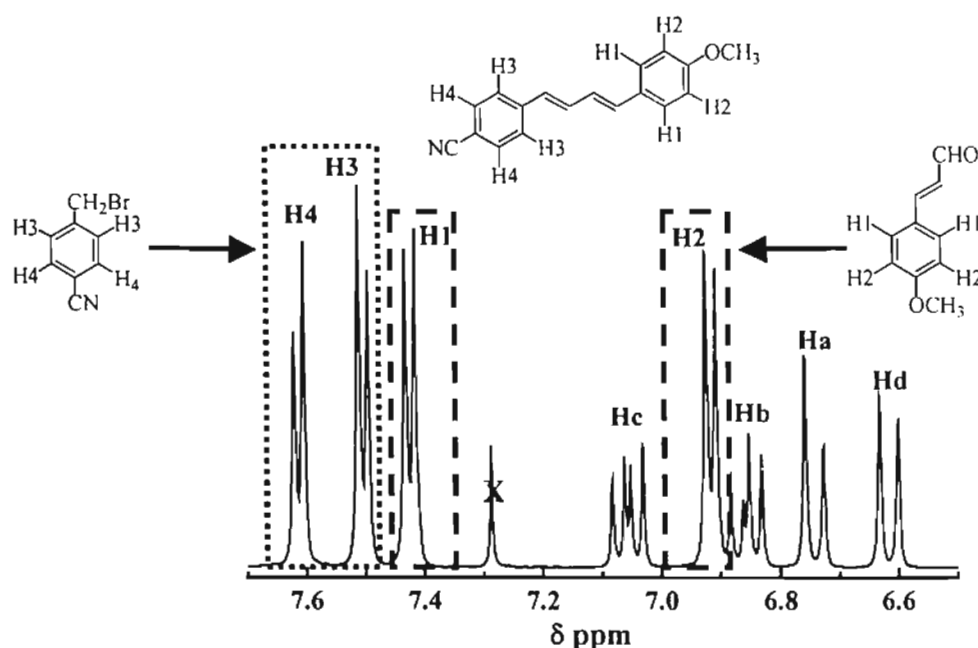
Figure 3.1. Classification of the aromatic protons, H1,H2 (- - -) and H3,H4 (.......) in the ^{1}H NMR spectrum of the *EE* isomer of **BC1**, based on comparison with the ^{1}H NMR spectra of the model compounds.

In order to correctly label the protons in the molecular structure it was

essential to carry out two-dimensional NMR analyses such as ^{1}H-^{1}H NOESY and

^{1}H-^{1}H COSY. In the ^{1}H-^{1}H NOESY spectrum of **BC1-*EE*** (Figure 3.2) a doublet

olefinic proton (Hd, δ 6.61) was found to spatially interact with an aromatic proton

on the cyanophenyl (H3, δ 7.50). This interaction was the basis for labeling the

olefinic proton as Hd and the aromatic proton as H3. Similarly the other olefinic

doublet proton (Ha, δ 6.74) was found to interact with an aromatic proton (H1, δ

7.42) on the methoxyphenyl and thus Ha and H1 could be identified. In the ^{1}H-^{1}H

COSY spectrum (Figure 3.3) Hd was found to couple with a double doublet proton

(Hc, δ 7.01-7.08) clearly indicating the proximity of Hd and Hc. Likewise Ha was

found to couple with the second double doublet (Hb, δ 6.83-6.88) which helped to

fix the position of Hb. ^{1}H-^{1}H COSY also showed the couplings between the two

protons on each aromatic rings ie. H1 with H2 (δ 6.91) and H3 with H4 (δ 7.61).

These proton couplings formed the basis for labeling all the protons of the *EE*

form as shown in Chart 3.2.
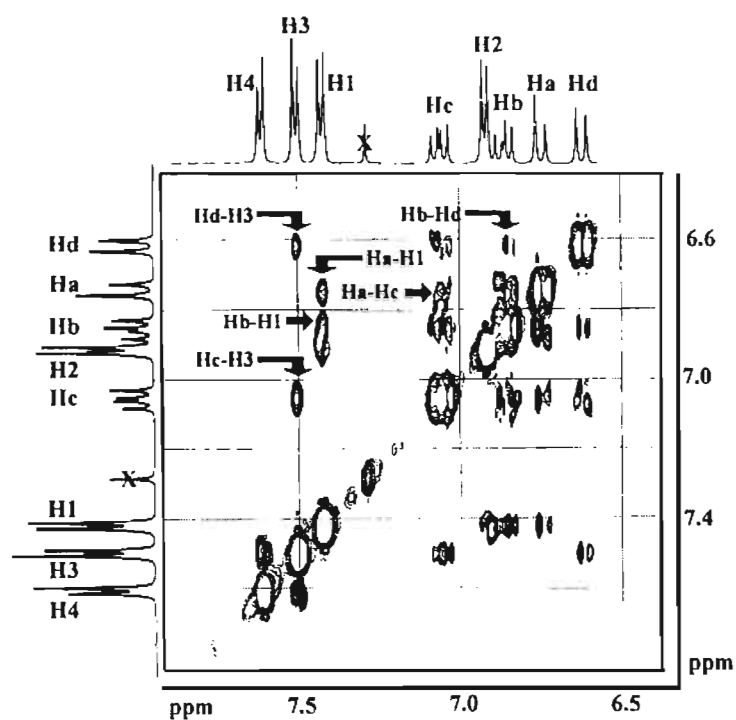
Figure 3.2. ^{1}H-^{1}H NOESY NMR spectrum of **BC1-*EE***.
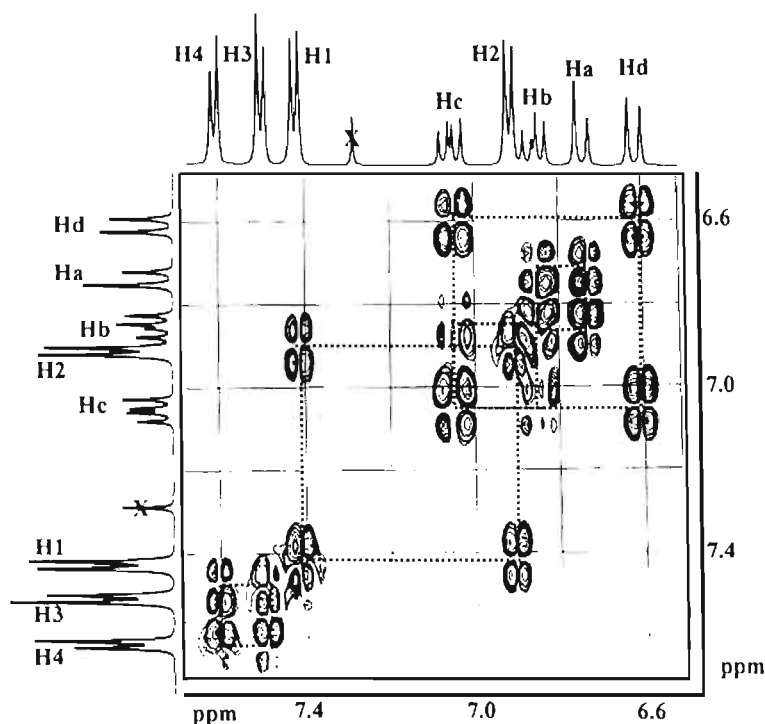
Figure 3.3. ^1H-^1H COSY NMR spectrum of **BC1**-*EE*.

3.3.2. Liquid Crystalline Property of Monoalkoxy-Cyano-Susbstituted Diphenylbutadienes

The liquid crystalline phases of the monoalkoxy-cyano-substituted diphenylbutadiene derivatives (Chart 3.1) were characterized using a polarizing optical microscope (POM) and the sharp phase transitions observed in the heating and cooling cycles were further confirmed by differential scanning calorimetry (DSC). Table 3.1 summarizes their phase transition temperatures and thermodynamic parameters. **BC1** exhibited Schlieren as well as droplet texture characteristic of a nematic (N) phase.[35] Figure 3.4 shows the polarized optical micrograph of **BC1**. The LC phases of **BC4** and **BC8** observed in the present study

were identical to that reported by Brettle *et al.*[31] Whereas **BC4** possessed a nematic LC phase, both nematic and smectic LC phases were observed for **BC8**. The compound **BC12** showed only a smectic A (S_A) phase, which was confirmed by its focal conic texture with homeotropic areas.[35] Figure 3.5 shows the DSC curve obtained for **BC12** during the heating and cooling cycles. With increasing length of the alkoxy chain in these derivatives, the isotropization temperature was found to decrease (Figure 3.6). This observed dependence of phase characteristics and phase transition temperatures on the length of alkoxy chain conforms with the general behaviour of LC molecules.[35]

Table 3.1. Phase transition temperatures and thermodynamic parameters of the diphenyl butadiene derivatives (Chart 3.1)

Compound	Phase transition temperatures (°C)[a]	$\Delta H(kJmol^{-1})$	$\Delta S(JK^{-1}mol^{-1})$
BC1	K 175.3 N 213 I	21.1 (K-N)	47.0 (K-N)
BC4	K 141.5 N 209.1 I	25.8, 0.4	85.1, 0.9
BC8	K 105.3 S 159.6 N 186.6 I	36.2, 0.4 (N-I)	95.7, 0.9 (N-I)
BC12	K 96.9 S 171.9 I	46.2, 3.4	124.7, 7.6

[a] **K = crystalline, N = nematic , S = smectic A and I = isotropic**

Figure 3.4. Polarized optical micrograph (400x) showing Schlieren texture of a nematic phase obtained for **BC1** at 194.7 °C.
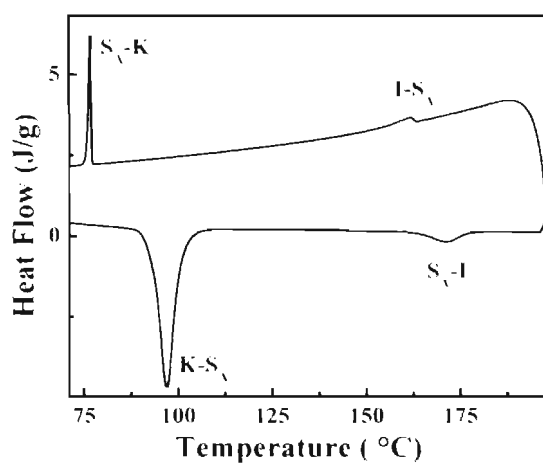
Figure 3.5. DSC curve obtained for **BC12** in the heating and cooling cycles.
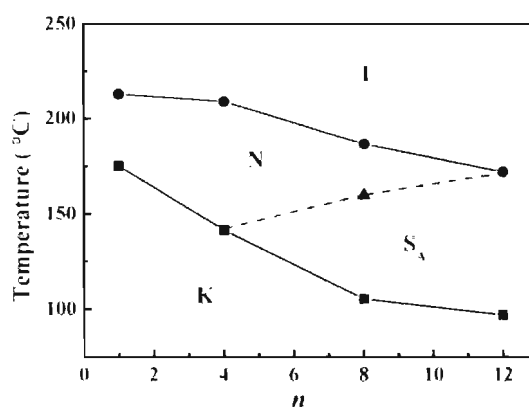
Figure 3.6. A Plot of transition temperatures against the number of carbon atoms (*n*) in the alkoxy chain of the diphenylbutadiene mesogens (Chart 3.1).

3.3.3. Photoisomerization of Monoalkoxy-Cyano-Susbstituted Diphenylbutadienes

In solution, the *EE* isomers of the diphenylbutadiene derivatives possess a strong absorption band with a maximum centered on 360 nm. Photolysis with 360 nm light results in a decrease in intensity of this band and the formation of a new band centered on 265 nm. These changes are marked by the presence of an isosbestic point around 317 nm (Figure 3.7A). Donor-acceptor-substituted diphenylbutadiene derivatives are known to undergo photoisomerization,[33,36-40] to yield *cis-trans* and *trans-cis* photoisomers. In most of the reported systems the isomers are thermally unstable and undergo transformation to their all-*trans*-isomeric form with lifetimes depending on the nature of the donor and the acceptor, thereby making it difficult to characterize the photoisomers using spectroscopic techniques.[29,33] The structural assignments of the photoisomers of all-*trans*-4-dimethylamino-4'-cyano-1,4-diphenylbutadiene, for example, had to be made by quantum-chemical modeling of their absorption spectra.[33] Photolysis of the alkoxy-cyano-substituted diphenylbutadiene derivatives studied here, however, resulted in the formation of. a photostationary state (PSS 1) consisting of the *EE* and thermally stable photoisomers (Figure 3.7 A).
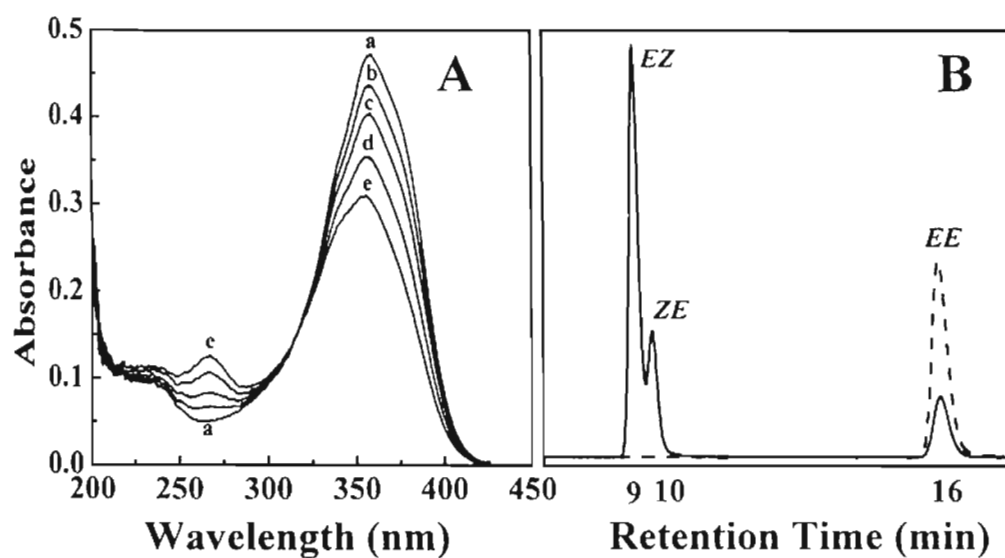
Figure 3.7. (A) Absorption spectral changes of **BC12** in acetonitrile at different time intervals upon photolysis using 360 nm light. Time of photolysis: a) 0 sec, b) 30 sec, c) 60 sec, d) 120 sec and e) 180 sec (PSS1). (B) HPLC traces of **BC12** in acetonitrile: (- - -) before photolysis and (——) after attaining the photostationary state, PSS1.

3.3.4. Isolation and Characterization of Photoisomers of Monoalkoxy-Cyano-Susbstituted Diphenylbutadienes

HPLC analyses of a solution of **BC12** in acetonitrile before and after photolysis (Figure 3.7B) are clearly indicative of the formation of two photoisomers. Similar observations were made for the other derivatives. Isolation and detailed structural characterization of the photoisomers were carried out for **BC1** since the separation between the two photoisomers in HPLC was better than that for the other derivatives. Figure 3.8 shows the ^{1}H NMR spectra of the *EE* and the two isolated photoisomers of **BC1** in the region showing the olefinic and aromatic protons. The detailed ^{1}H NMR data of the photoisomers are provided in the Experimental Section (3.5).
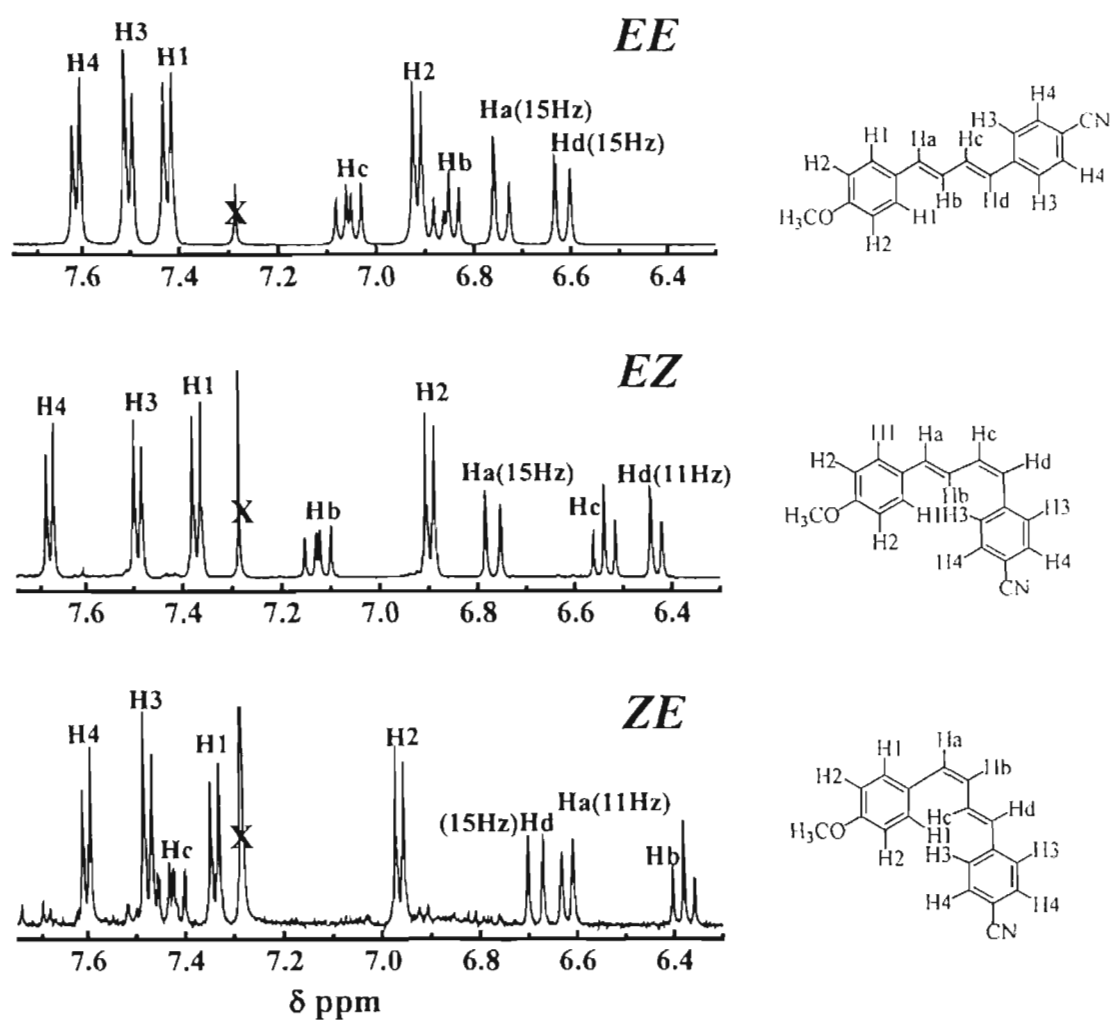
Figure 3.8. ^{1}H NMR spectra of the isomers of **BC1**.

^{1}H NMR spectra of the photoisomers suggest that in each isomer one of the double bonds has undergone isomerization since in both cases the two olefinic doublets (Ha and Hd) possess different ^3J-coupling constant values with one corresponding to an *E* coupling (~15 Hz) and the other to a *Z* coupling (~11 Hz).[34] As in the case of the *EE* isomer it was essential to locate the proximity of the olefinic protons (Ha and Hd) to the aromatic protons in order to assign isomeric configuration to these photoisomers.[36] ^{1}H-^{1}H NOESY and ^{1}H-^{1}H COSY NMR

analyses were carried out to identify which of the double bonds had undergone isomerization in each of the photoisomers.

The structures of the two possible photoisomers (*EZ* and *ZE*) are shown in Figure 3.8. ^{1}H-^{1}H NOESY NMR spectrum (Figure 3.9), which shows a spatial interaction of the *E*-olefinic doublet proton (Ha, δ 6.76 ppm) with one of the protons (H1, δ 7.37 ppm) appearing on the methoxyphenyl group, suggests that the isomer may be assigned an *EZ* configuration. Further confirmation on the assignment was obtained by observing a spatial interaction between the *Z*-olefinic doublet proton (Hd, δ 6.42 ppm) and one of the protons on cyanophenyl ring (H3, δ 7.49 ppm).

In the ^{1}H-^{1}H COSY NMR spectrum (Figure 3.10) of the *EZ* isomer, Ha was found to couple with the double doublet olefinic proton (Hb, δ 7.09-7.15) and similarly Hd coupled with the triplet olefinic proton (Hc, δ 6.54). In the *EZ* isomer, Hc couples with Hb and Hd with identical ^{3}*J*-coupling constant values (~11 Hz) and hence appears as a triplet, unlike in the *EE* isomer. ^{1}H-^{1}H COSY NMR spectrum also showed that the double doublet olefinic proton (Hb, δ 7.09-7.15) coupled with the triplet olefinic proton (Hc, δ 6.54). The couplings between the two types of protons on each aromatic ring was also observed in the ^{1}H-^{1}H COSY NMR spectrum (H1 with H2 and H3 with H4). The observation of these couplings formed the basis for labeling the protons in the ^{1}H NMR spectrum of the *EZ* isomer and its structural assignment.
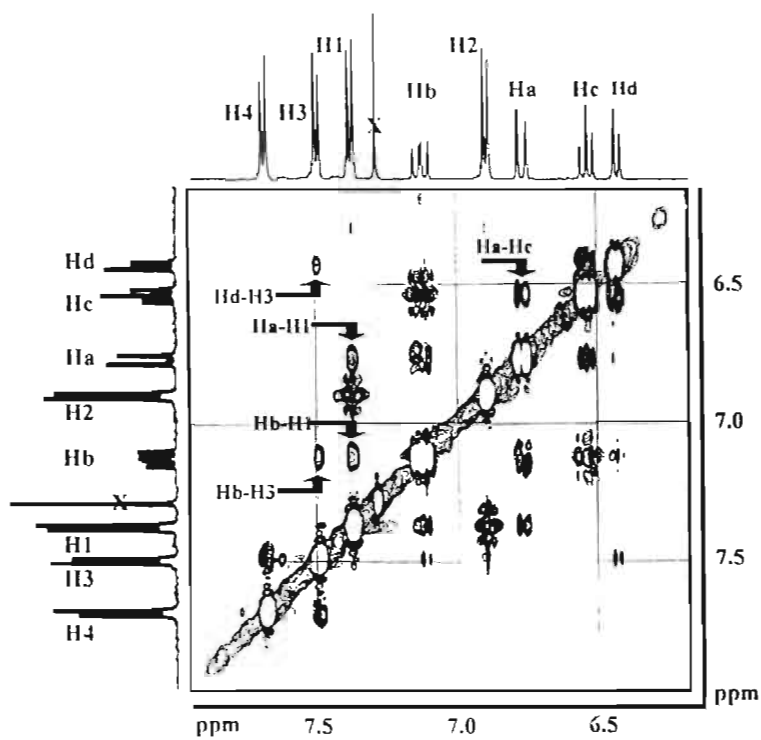
Figure 3.9. ^{1}H-^{1}H NOESY spectrum of **BC1-EZ**.
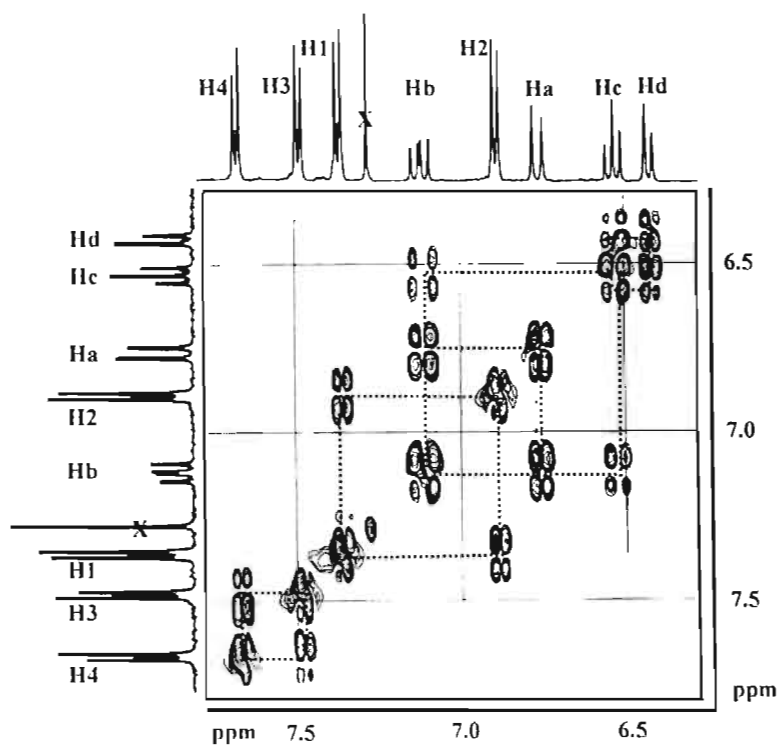
Figure 3.10. ^{1}H-^{1}H COSY spectrum of **BC1-EZ**.

^{1}H-^{1}H NOESY NMR spectrum (Figure 3.11) of the second photoisomer shows a spatial interaction of the *Z*-olefinic doublet proton (Ha, δ 6.62) with one of the protons on the methoxyphenyl ring (H1, δ 7.34) and that of the *E*-olefinic doublet (Hd, δ 6.68) with one of the protons on the cyanophenyl ring (H3, δ 7.47), both confirming the *ZE* configuration of the photoisomer. ^{1}H-^{1}H COSY NMR spectrum (Figure 3.12) of the *ZE* isomer showed that Ha coupled with the triplet olefinic proton (Hb, δ 6.38) and Hd coupled with the double doublet olefinic proton (Hc, δ 7.40-7.45). In the ^{1}H NMR of the *ZE* isomer, the proton Hb appeared as a triplet because its coupling with Ha and Hc had identical ^{3}*J*-coupling constant values (~11 Hz), which was similar to the case of Hc in the *EZ* isomer. The triplet olefinic proton (Hb, δ 6.38) was also found to couple with the double doublet olefinic proton (Hc, δ 7.43). The coupling between the two types of protons on each aromatic ring was also observed (H1 with H2 and H3 with H4).
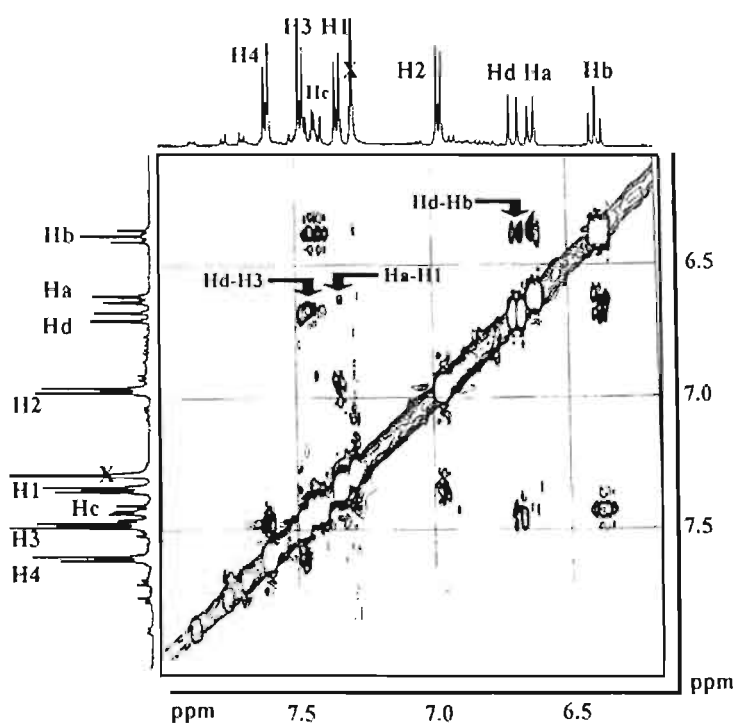
Figure 3.11. ^{1}H-^{1}H NOESY spectrum of **BC1-ZE**.
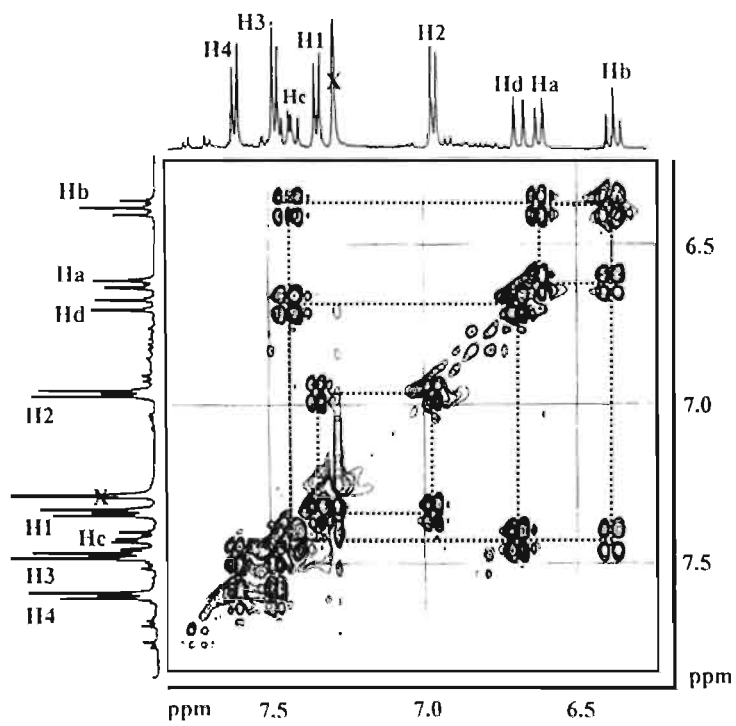
Figure 3.12. ^{1}H-^{1}H COSY spectrum of **BC1-ZE**.

3.3.5. *Photoisomerization of EE, EZ and ZE Isomers of Monoalkoxy-Cyano-Susbstituted Diphenylbutadienes*

HPLC analyses of the photolysed solutions were carried out with the UV-vis spectrophotometer detector set at 317 nm, which corresponds to the isosbestic point observed in the absorption spectral changes upon photolysis of the *EE* isomer. At this wavelength the extinction coefficients of the isomers are the same and hence the HPLC peak areas will be proportional to the relative concentrations of the isomers. The composition of the photostationary state (PSS1) of **BC12**, in acetonitrile upon photolysis using 360 nm at 27 °C, was found to consist of *EZ* (50 %), *ZE* (15%) and *EE* (35%) isomers. The quantum yields of (*EE*-PSS1) photoisomerization of these diphenylbutadiene derivatives ranged from 0.1 to 0.2 (Table 3.2). Although the photoisomers were thermally irreversible, they could be photochemically reverted back to their initial *EE* form by excitation using 265 nm light. Excitation of PSS1 with 265 nm light resulted in an increase in intensity of the 360 nm band and a decrease in that of the 265 nm band, till a new photostationary state (PSS2), rich in the *EE* isomer (*EZ* (20 %) *ZE* (10%) *EE* (70%)) was reached. Complete reversibility could be observed between these two photostationary states. The photoisomerization process of these diphenylbutadiene derivatives may be represented as in Scheme 3.1.

Table 3.2. Quantum yield of photoisomerization of the diphenylbutadienes (Chart 3.1).

Solvent	BC1	BC4	BC8	BC12
Toluene	0.19	0.15	0.13	0.13
Acetonitrile	0.16	0.10	0.19	0.15

Scheme 3.1. Photoisomerization of the diphenylbutadiene derivatives (Chart 3.1).
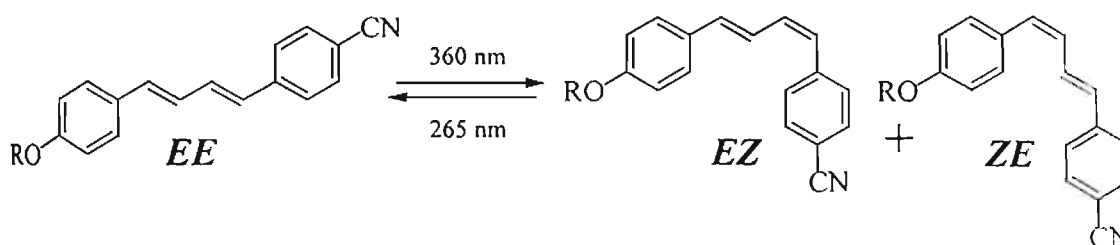
Figure 3.13 shows the absorption spectra of all the isomers of BC1 in acetonitrile. Absorption changes observed upon photolysis of pure solutions of *EZ* and *ZE* isomers using 265 nm light clearly showed their transformation to the *EE* isomer (Figure 3.14).
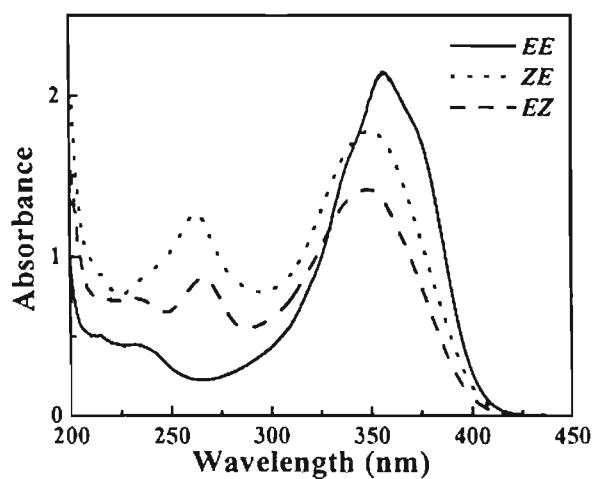
Figure 3.13. Absorption spectra of the isomers of **BC1** in acetonitrile.
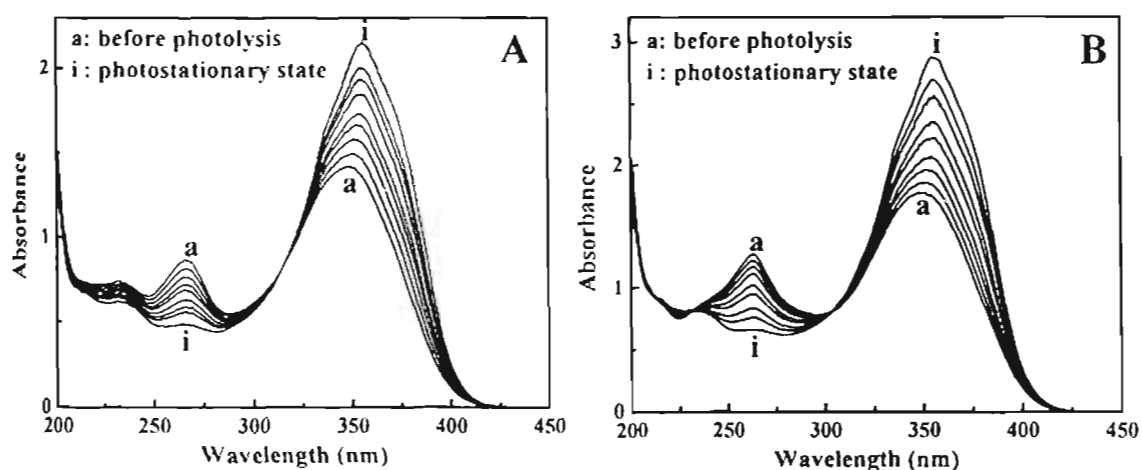
Figure 3.14. Absorption changes upon photolysis using 265 nm light A) acetonitrile solution of **BC1-EZ** and B) acetonitrile solution of **BC1-ZE**.

HPLC traces of pure *EZ* isomer of **BC1**, in acetonitrile, before and after photolysis are shown in Figure 3.15 Trace 'b' in Figure 3.15 represents the photostationary state (PSS3) obtained upon photolysis of pure *EZ* in acetonitrile using 265 nm light. The composition of isomers in PSS3 was found to be *EZ* (20 %), *ZE* (5 %), *EE* (75 %). It is clear from this figure that during the conversion of *EZ* isomer to its *EE* form in solution, there is also the formation of *ZE* isomer, which may be due to the absorption of 265 nm light by the *EE* isomer to give the *ZE* isomer.
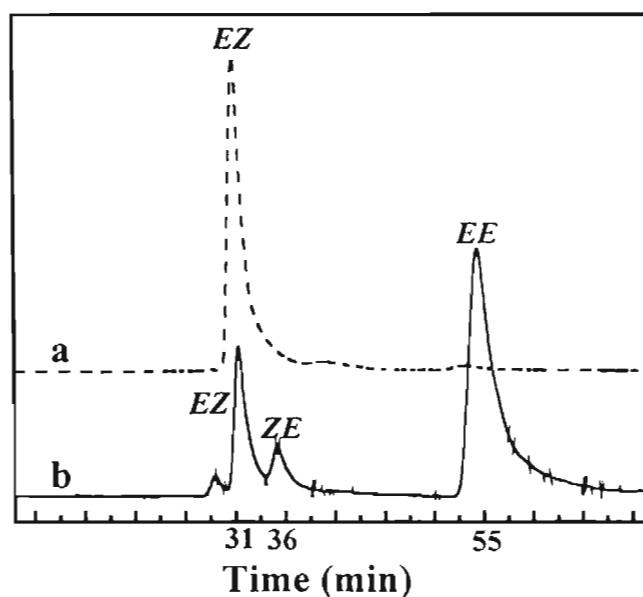
Figure 3.15. HPLC traces of (a) **BC1-*EZ*** before irradiation and (b) **BC1-*EZ*** in acetonitrile upon photolysis using 265 nm until photostationary state (PSS3).

3.3.6. *Photochemical Phase Transitions of Monoalkoxy-Cyano-Susbstituted Diphenylbutadienes*

None of the photoisomers were found to possess liquid crystalline phases. For example the *EZ* isomer of **BC12** showed a sharp crystal to isotropic transformation at 67 °C. Perturbations in molecular structure from linear to a bent shape is known to disrupt long-range ordering leading to breakdown of the liquid crystalline phases.[8] The drastic difference in the phase transition characteristics between the *EE* isomer and the photoisomers make these materials highly suitable for studying photoinduced phase transitions. Photoinduced phase transitions in these materials were investigated in thin liquid crystalline films prepared by slow cooling from their isotropic state between quartz discs. Photolysis of the S_A phase of **BC12** at 120 °C (Figure 3.16a), using 360 nm results in a destruction of the LC texture and isothermal formation of the isotropic phase (Figure 3.16b). HPLC

analysis of the photolysed film (isotropic state) indicated that the isomer composition was similar to that of PSS1 obtained in the corresponding solution phase experiment. The photolysed mixture transforms sharply from its crystalline to isotropic phase at 80 °C and does not posses an LC phase. Similarly, photoinduced isothermal phase transitions were observed for the *EE* isomers of other derivatives also. The photochemically induced isotropic phase was found to be thermally irreversible in all cases.

Photolysis of the isotropic phase held at 120 °C did not lead to recovery of the S_A phase. However, photolysis of the isotropic mixture at room temperature (RT, 27 °C), where it exists in its crystalline form, using 266 nm laser (fourth harmonic of Nd:YAG, pulse width of 10 ns, 15 mJ), for 20 s results in the formation of a material which possesses a clear S_A phase with phase transition temperatures matching that of the *EE* isomer of **BC12** (Figure 3.16c). Steady-state photolysis using low intensity 265 nm light did not result in recovery of the S_A phase. Due to the lowered efficiency of photoconversion in the solid state high intensity light is required for the regeneration of the S_A phase.
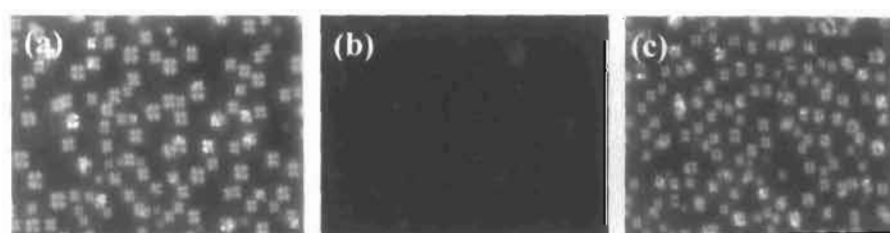
Figure 3.16. Polarized optical micrographs (400x) depicting the photoinduced isothermal phase transition of **BC12**: (a) S_A phase at 120 °C before photolysis, (b) isotropic state at 120 °C obtained upon photolysis using 360 nm, (c) S_A phase at 120 °C regenerated upon photolysis of the same film at room temperature (27°C) using 266 nm laser.

HPLC analysis of the laser photolysed sample of the isotropic mixture in the solid state showed a near complete conversion (>95%) to the *EE* isomer upon photolysis with 266 nm laser, in contrast to PSS2 observed in the corresponding solution phase experiment (Figure 3.17). This can be understood on the basis of the dependence of photoisomerization on the viscosity of the medium. Whereas *trans-cis* isomerization is substantially prevented in viscous and frozen medium, *cis-trans* isomerization remains feasible, resulting in stereospecific isomerization. This aspect of photoisomerization of polyenes is well documented.[38,41-43] For example, the photoisomerization of trans-stilbene decreases rapidly upon increase in solvent viscosity and is stopped upon freezing the sample.[41,42] The photoisomerization of the *cis*-isomer of stilbene on the other hand remains observable even in the frozen media. A similar effect of the viscosity of the medium on the stereoselectivity of photoisomerization of polyenes has been reported.[43]
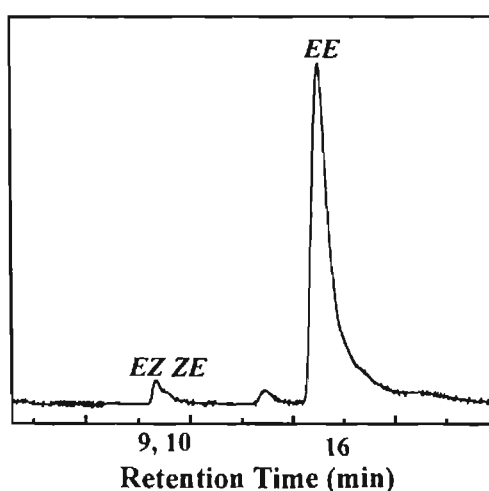
Figure 3.17. HPLC trace of the regenerated LC state (*EE* form >95%) of **BC12** obtained upon 266 nm laser photolysis of the isotropic state.

Photoswitching of the LC phase was further confirmed using the pure *EZ* photoisomer of **BC12**, which does not posses a liquid crystalline phase. Photolysis, using 266 nm laser, of the crystalline state of the *EZ* isomer, results in the formation of a material which shows an S_A phase with phase transition temperatures similar to that of the *EE* isomer of **BC12**.

Photolysis of the *EZ* isomer in its crystalline state, using 266 nm laser, yielded only the *EE* isomer, which was confirmed by HPLC analysis. The HPLC trace showed that there was no formation of the *ZE* isomer unlike the corresponding solution phase experiment (Figure 3.18 and Figure 3.15). This observation further justifies the stereospecificity of the *Z-E* isomerization in the crystalline state. As discussed earlier the high viscosity in the crystalline state prevents isomerization of the *EE* isomer to yield the *ZE* isomer, which results in a stereospecific isomerization of *EZ* isomer to give only the *EE* isomer.
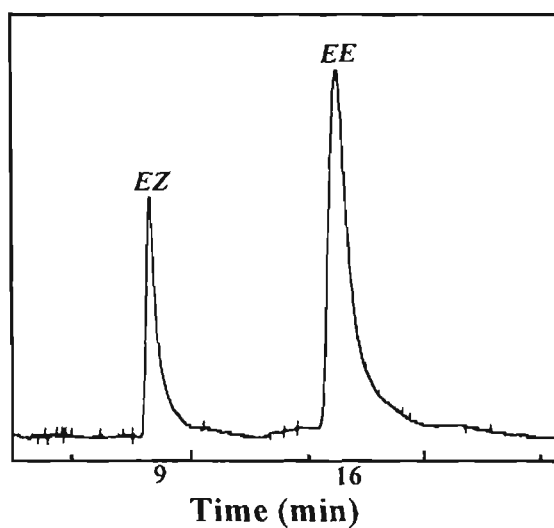
Figure 3.18. HPLC trace of **BC12-*EZ*** upon photolysis using 266 nm laser (15 mJ) in the crystalline state.

3.4. Trialkoxy-Cyano-Substituted Diphenylbutadienes

A series of 3,4,5-triakyloxy-cyano-substituted diphenylbutadiene derivatives (Chart 3.2) were synthezised and studied for their liquid crystalline properties and photoisomerization. The principal objective of synthesizing these derivatives was to investigate the effect of the additional alkoxy groups both on the liquid crystalline and isomerization properties of the butadiene derivatives. The detailed synthetic procedures and spectroscopic characterization data for these derivatives are provided in the Experimental Section (3.5).

TABC1,	R = CH$_3$
TABC4,	R = C$_4$H$_9$
TABC12,	R = C$_{12}$H$_{25}$
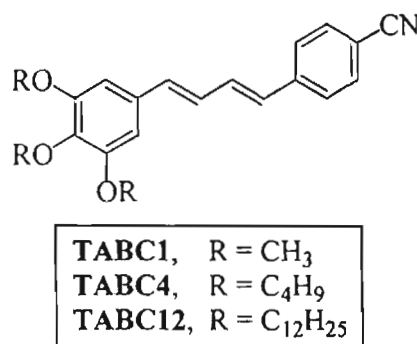
Chart 3.2

None of these derivatives exhibited liquid crystalline nature although there was a considerable decrease in their melting points. This may be attributed to the presence of additional alkoxy groups, which results in the loss in the rod-like shape the molecule. Table 3.2 summarizes the melting points of the trialkyloxy-cyano-substituted diphenylbutadiene derivatives.

Table 3.2. Phase transition temperatures of the trialkyloxy-cyano-substituted diphenylbutadiene derivatives (Chart 3.2).

Compound	Phase transition temperature (°C)
TABC1	K155.7 I
TABC4	K_1 79.0 K_2 85.0 I
TABC12	K_1 46.8 K_2 61.4 I

The photoisomerization reactions of these derivatives were markedly different from that of the monoalkoxy-cyano-substituted derivatives. Figure 3.19 shows the changes in absorption spectrum of trialkyloxy-cyano-substituted diphenylbutadiene derivatives upon photolysis using 360 nm light. The figure also shows the HPLC traces of these derivatives before photolysis and after attaining the photostationary state. Upon photolysis of solutions of the *EE* isomer of the trialkoxy derivatives, using 360 nm light, the intensity of the absorption band at ~360 nm was found to decrease and this was accompanied by an increase in absorption ~265 nm. HPLC analyses of solutions of **TABC1** and **TABC4** showed that in the photostationary state there was only one photoisomer formed, which was attributed to the *EZ* isomer by comparison with the HPLC trace of the photostationary states obtained for the monalkoxy derivatives. In the case of **TABC12** however, the formation of both photoisomers (*EZ* and *ZE*) was observed. The concentration of *EZ* and *ZE* isomers in the photostationary state were nearly the same for **TABC12**, unlike in the case of the monoalkoxy derivatives, where the *ZE* isomer was formed as a minor component.
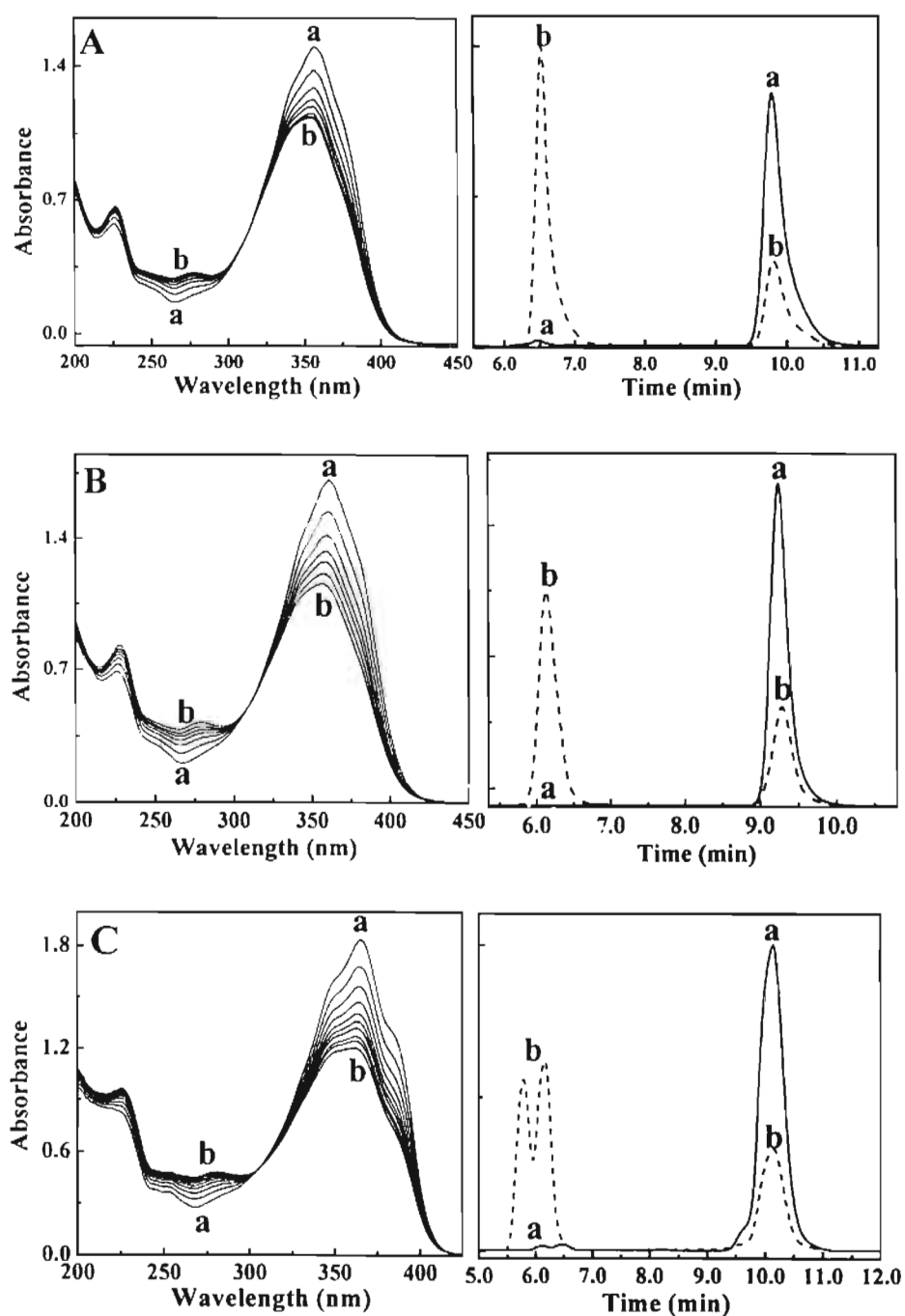
Figure 3.19. Absorption changes and HPLC traces obtained on photolysis of A) **TABC1** in acetonitrile, (B) **TABC4** in acetonitrile and (C) **TABC12** in heptane. In all cases, curve 'a' represent the state before photolysis and curve 'b' represent the photostationary state (PSS1).

Table 3.3 summarizes the composition of isomers in the photostationary state (PSS1) for the trialkyoxy derivatives. Apart from these changes, it is seen that with an increase in the trialkoxy chain length, the net conversion of the *EE* isomer to their photoisomers decreases. This difference in their photoisomerization characteristics may be explained as a consequence of the increase in the bulkiness of the molecule with the increase in the alkoxy chain length.

Table 3.3. Composition of isomers in the photostationary states (PSS1) of the trialkyloxy derivatives.

Compound	*EE (%)*	*EZ (%)*	*ZE (%)*
TABC1	25	75	-
TABC4	35	65	-
TABC12	40	25	35

⟨ The photoisomers generated were found to be thermally irreversible but photochemically reversible just as in the case of the monoalkoxy-cyano-substituted diphenylbutadiene derivatives.

3.5. Experimental Section

3.5.1. Synthesis of mono-alkoxy-cyano-substituted diphenylbutadiene derivatives

The mono-alkoxy-cyano-substituted diphenylbutadienes **BC1**, **BC4** and **BC8** were synthesized as reported earlier[31,32,44] and their structures were

confirmed using NMR, IR, and HRMS analyses. Purification of the compounds was achieved by using column chromatography using silica gel (100-200 mesh) as the stationary phase material and hexane/ethyl acetate mixture (99:1) as the eluent. Recrystallization from hexane/ethyl acetate (99:1) gave pure samples (>99%) of these derivatives as confirmed by HPLC. **BC12** was synthesized as per Scheme 3.2 and its detailed spectral data with that of all intermediates are provided below.
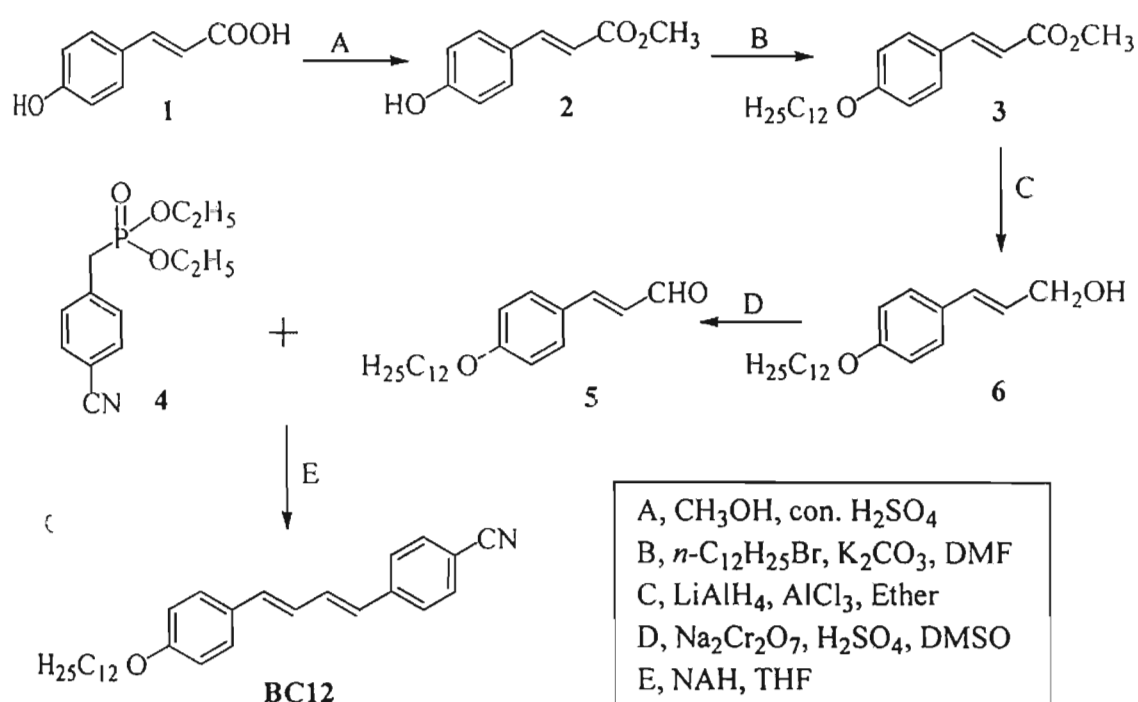
Scheme 3.2

Synthesis of 2

4-hydroxycinnamic acid (2g, 1.22 mol), was dissolved in methanol (30 mL). To the above solution 3 drops of conc. H_2SO_4 was added and the resulting mixture was refluxed for 24 h. Excess methanol was removed under reduced pressure and the reaction mixture was poured into cold water (30 mL). The crude product was

extracted using dichloromethane. The product was purified by column chromatography using silica gel (100-200 mesh) and a mixture (1:4) of ethyl acetate and hexane as the eluent. Recrystallization from a mixture (1:9) of ethyl acetate and hexane gave colorless needle-like crystals of **2**.

2: Yield: 77%; mp: 132-134 °C; IR v_{max} (KBr): 3412, 1696, 1643, 1613, 1587, 1586, 1526, 1443, 1338, 1202, 840, 637 cm^{-1}; ^{1}H NMR (300 MHz, CDCl$_3$): δ 3.79 (s, 3H, OCH$_3$), 6.30 (d, 1H, olefinic), 6.84 (d, 2H, aromatic), 7.44 (d, 2H, aromatic), 7.63 (d, 1H, olefinic) ppm; ^{13}C NMR (75 MHz, CDCl$_3$): δ 51.81, 114.76, 115.93, 126.82, 130.04, 145.09, 158.19, 168.44 ppm.

Synthesis of 4

4-Hydroxymethylcinnamate (654 mg, 3.6 mmol), *n*-dodecylbromide (897 mg, 3.6 mmol) and K$_2$CO$_3$ (1.49g, 10.8 mmol) were dissolved in dry DMF. The mixture was heated at 100 °C for 24 h. The reaction mixture was cooled to room temperature and added to water. The crude product was extracted with ether. The solvent was evaporated. The product was purified by column chromatography using a mixture (1:4) of ethyl acetate and hexane as the eluent. Recrystallization from benzene gave **4** in the form of colourless crystals.

4: Yield: 77%; mp: 70-71 °C; IR v_{max} (KBr): 2936, 2863, 1739, 1696, 1643, 1617, 1567, 1521, 1481, 1445, 1293, 1256, 1211, 1181, 983 cm^{-1}; ^{1}H NMR (300 MHz, CDCl$_3$): δ 0.80 (t, 3H, CH$_3$), 1.19-1.38 (m, 18H, (CH$_2$)$_9$), 1.69-1.73 (m, 2H, CH$_2$), 3.72 (s, 3H, OCH$_3$), 3.90 (t, 2H, OCH$_2$), 6.23 (d, 1H, olefinic), 6.82 (d, 2H, aromatic), 7.38 (d, 2H, aromatic), 7.58 (d, 1H, olefinic) ppm; ^{13}C NMR (75 MHz,

CDCl₃): δ 14.10, 22.68, 25.98, 29.34, 29.56, 29.63, 31.91, 51.55, 68.16, 114.82, 115.04, 126.86, 129.70, 144.63, 161.02, 167.81 ppm.

Synthesis of 3

To LiAlH₄ (0.2 g) in a dry 100 mL two necked round bottom flask equipped with a stirrer, a nitrogen inlet and addition funnel 10 mL ether was added dropwise. The flask was placed in an ice bath (0 °C). To this cooled, stirred suspension of LiAlH₄ a solution of AlCl₃ (0.2 g) in ether (10 mL) was added. The mixture was then allowed to warm up to room temperature (27 °C) and stirred for an additional 30 min. Then a solution of 4-dodecyloxymethylcinnamate (0.5 g, 1.7 mmol) in 20 mL ether was added dropwise via an addition funnel. After the addition was completed, the mixture was stirred for an additional 30 min before it was quenched with 10% aqueous solution of sodium hydroxide. The resulting mixture was then acidified with dilute HCl and the product was extracted using diethylether with the aid of brine. The ether solution was dried over anhydrous sodium sulfate. The crude product was purified by column chromatography using a mixture (1:4) of ethyl acetate and hexane as the eluent and silica gel (100-200 mesh) as the packing material. After recrystallization from a mixture (1:9) of ethyl acetate and hexane 241 mg of pure product was obtained.

3: Yield: 44%; mp: 82-84 °C; IR ν_max (KBr): 3389, 2937, 2862, 1617, 1519, 1470, 1262, 1183, 1025, 972 cm⁻¹; ¹H NMR (300 MHz, CDCl₃): δ 0.86 (t, 3H, CH₃), 1.26-1.44 (m, 18H, (CH₂)₉), 1.77-1.79 (m, 2H, CH₂), 3.95 (t, 2H, OCH₂), 4.29 (d, 2H, C*H*₂OH), 6.18-6.27 (m, 1H, olefinic), 6.54 (d, 2H, aromatic), 7.30 (d, 2H,

aromatic) ppm; ^{13}C NMR (75 MHz, CDCl$_3$): δ 14.11, 22.67, 26.02, 29.34, 29.62, 31.90, 63.96, 68.04, 114.56, 126.01, 127.01, 127.62, 131.08, 158.90 ppm.

Synthesis of 5

To a stirred solution of Na$_2$Cr$_2$O$_7$ (59 mg, 0.2 mmol) in DMSO (10 mL), 4-dodecyloxycinnamyl alcohol (100 mg, 0.31 mmol), conc. H$_2$SO$_4$ (0.04 mL) was added dropwise keeping the temperature below 70 °C. Then the mixture was heated at 70 °C for 1.5 h. The crude product was extracted with ether three times of 50 mL each, washed with NaHCO$_3$ solution and water. The crude product was purified using column chromatography using silica gel (100-200 mesh) and a mixture (1:19) of ethyl acetate and hexane. After purification 40 mg (40 %) of the pure product was obtained.

5: Yield: 40%. mp 40-41 °C. IR ν_{max} (KBr): 3487, 2944, 2869, 1741, 1688, 1609, 1553, 1515, 1470, 1259, 1180, 1131, 976 cm^{-1}; ^{1}H NMR (300 MHz, CDCl$_3$): δ 0.80 (t, 3H, CH$_3$), 1.19-1.38 (m, 18H, (CH$_2$)$_9$), 3.93 (t, 2H, OCH$_2$), 6.50-6.57 (dd, 1H, olefinic), 6.84 (d, 2H, aromatic), 7.32-7.37 (dd, 1H, olefinic) 7.43 (d, 2H, aromatic) 9.57 (d, 1H, CHO) ppm; ^{13}C NMR (75 MHz, CDCl$_3$): δ 14.09, 22.67, 25.96, 29.08, 29.33, 29.61, 31.89, 68.26, 104.74, 114.87, 115.04, 126.35, 126.52, 130.02, 130.34, 152.86, 161.85, 193.75 ppm.

Synthesis of phosphonate ester of *p*-cyanobenzylbromide

To a solution of *p*-tolunitrile (1g, 8.5 mmol) in dry CCl$_4$ (20 mL), NBS (1.51 g, 8.5 mmol) was added. Catalytic amount of benzoylperoxide was added to the mixture and refluxed it for 24 h. After cooling, the reaction mixture was

filtered and the filtrate was concentrated. The residue was washed with a mixture (1:4) of ethyl acetate and hexane. Recrystallization from a mixture (1:4) of ethyl acetate and hexane gave 0.9 g (60%) of *p*-cyanobenzylbromide. A mixture of the obtained *p*-cyanobenzylbromide (235 mg, 1.2 mmol) and excess of triphenylphosphite was heated at 100 °C for 24 h. After cooling the excess triphenylphosphite was distilled out under reduced pressure. The viscous residue was carried over to the next reaction.

Synthesis of 4-(p-Cyanophenyl)-1-(*p*-dodecyloxyphenyl)buta-1*E*,3*E*-diene (BC12)

To the phosphonate ester of *p*-cynaobenzylbromide obtained from the earlier reaction, NaH (57 mg, 2.4 mmol) was added. Dry THF was added to the above mixture with efficient stirring. After about 10 min of stirring, a solution of 4-dodecyloxycinnamaldehyde (380 mg, 1.2 mmol) was added dropwise and the resulting mixture was refluxed for 24 h in argon atmosphere. The solvent was removed under reduced pressure and the resulting residue was washed with water. The crude product was extracted using dichloromethane. The product was purified by column chromatography using silica gel (100-200 mesh) and a mixture (1:99) of ethyl acetate and hexane as the eluent. After recrystallization from the same solvent mixture **BC12** was obtained in the form of yellow crystals.

BC12: Yield: 40%. mp:171.9 °C (clearing temperature). UV-Vis λ_{max} (MeCN): 356 nm ($\varepsilon = 4.4 \times 10^4$ M^{-1} cm^{-1}). IR ν_{max} (KBr): 2926, 2857, 2356, 2230, 1735, 1680, 1603, 1511, 1475, 1306, 1258, 1176, 1027, 984, 857, 800 cm^{-1}; ^{1}H NMR

(300 MHz, CDCl$_3$) (protons labeled as in Chart 3.2): δ 0.88 (t, 3H, CH$_3$), 1.26-1.45 (m, 18H, (CH$_2$)$_9$), 1.73-1.80 (m, 2H, CH$_2$), 3.97 (t, 2H, OCH$_2$), 6.58 (d, 1H, $^3J_{c,d}$ = 15.4 Hz, Hd), 6.71 (d, 1H, $^3J_{a,b}$ = 15.4 Hz, Ha), 6.78-6.86 (dd, 1H, $^3J_{a,b}$ = 15.4 Hz, $^3J_{b,c}$ = 10.2 Hz, Hb), 6.87 (d, 2H, $^3J_{1,2}$ = 8.3 Hz, H2), 6.99-7.07 (dd, 1H, $^3J_{c,d}$ = 15.4, $^3J_{b,c}$ = 10.2 Hz, Hc), 7.38 (d, 2H, $^3J_{1,2}$ = 8.3 Hz, H1), 7.48 (d, 2H, $^3J_{3,4}$ = 8.1 Hz, H3), 7.58 (d, 2H, $^3J_{3,4}$ = 8.1 Hz, H4) ppm; ^{13}C NMR (75 MHz, CDCl$_3$): δ 14.08, 22.65, 25.99, 29.20, 29.31, 29.55, 29.60, 31.88, 68.09, 68.25, 104.72, 109.96, 114.78, 115.03, 119.12, 126.11, 126.45, 127.95, 129.21, 129.35, 130.32, 132.38, 133.21, 135.27, 142.12, 159.39 ppm; HRMS: calcd for C$_{29}$H$_{37}$NO: 415.2875, Found: 415.2887.

3.5.2. Synthesis of 3,4,5-Trialkoxy-Cyano-Substituted Diphenylbutadiene derivatives

The trialkoxy-cyano-substituted diphenylbutadiene derivative **TABC1** was synthesized as shown in Scheme 3.3. **TABC4** and **TABC12** were synthesized as per Scheme 3.4. The structures of these derivatives were confirmed using NMR, IR and CHN analyses. The compounds were purified by column chromatography using silica gel (100-200 mesh) as the stationary phase and hexane/ethyl acetate mixture (9:1) as the eluent. Further purification was done using preparative HPLC to get extrapure (>99%) samples. The detailed synthetic procedures and spectral data of these derivatives and the intermediates involved are provided below.
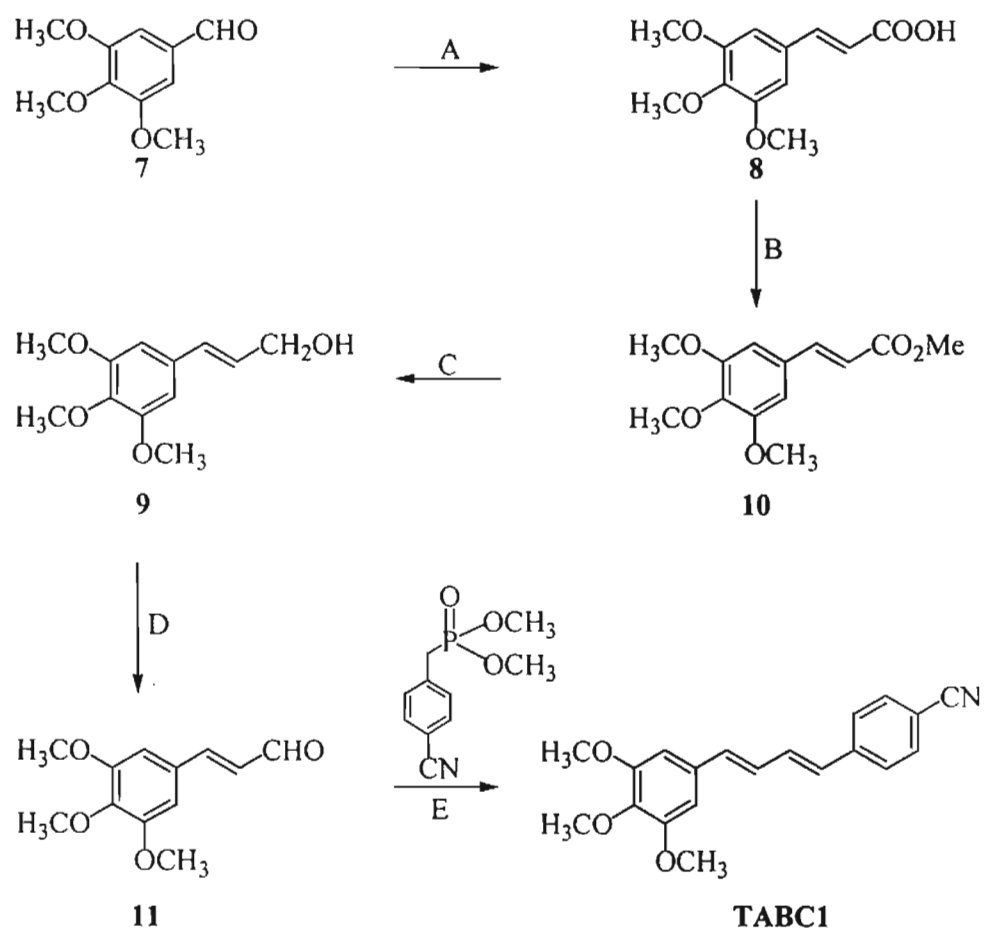
A, Malonic Acid, Pyridine, Piperidine
B, MeOH, H_2SO_4
C, LiAlH$_4$, AlCl$_3$, Diethyl Ether
D, Na$_2$Cr$_2$O$_7$, H$_2$SO$_4$, DMSO
E, NaH, THF

Scheme 3.3

A, LiAlH$_4$, THF
B, PCC, DCM
C, Malonic Acid, Pyridine, Piperidine
D, MeOH, H$_2$SO$_4$
E, LiAlH$_4$, AlCl$_3$, Diethyl Ether
F, Na$_2$Cr$_2$O$_7$, H$_2$SO$_4$, DMSO
G, NaH, THF

a, R=C$_4$H$_9$
b, R=C$_{12}$H$_{25}$

TABC4, R=C$_4$H$_9$
TABC12, R=C$_{12}$H$_{25}$
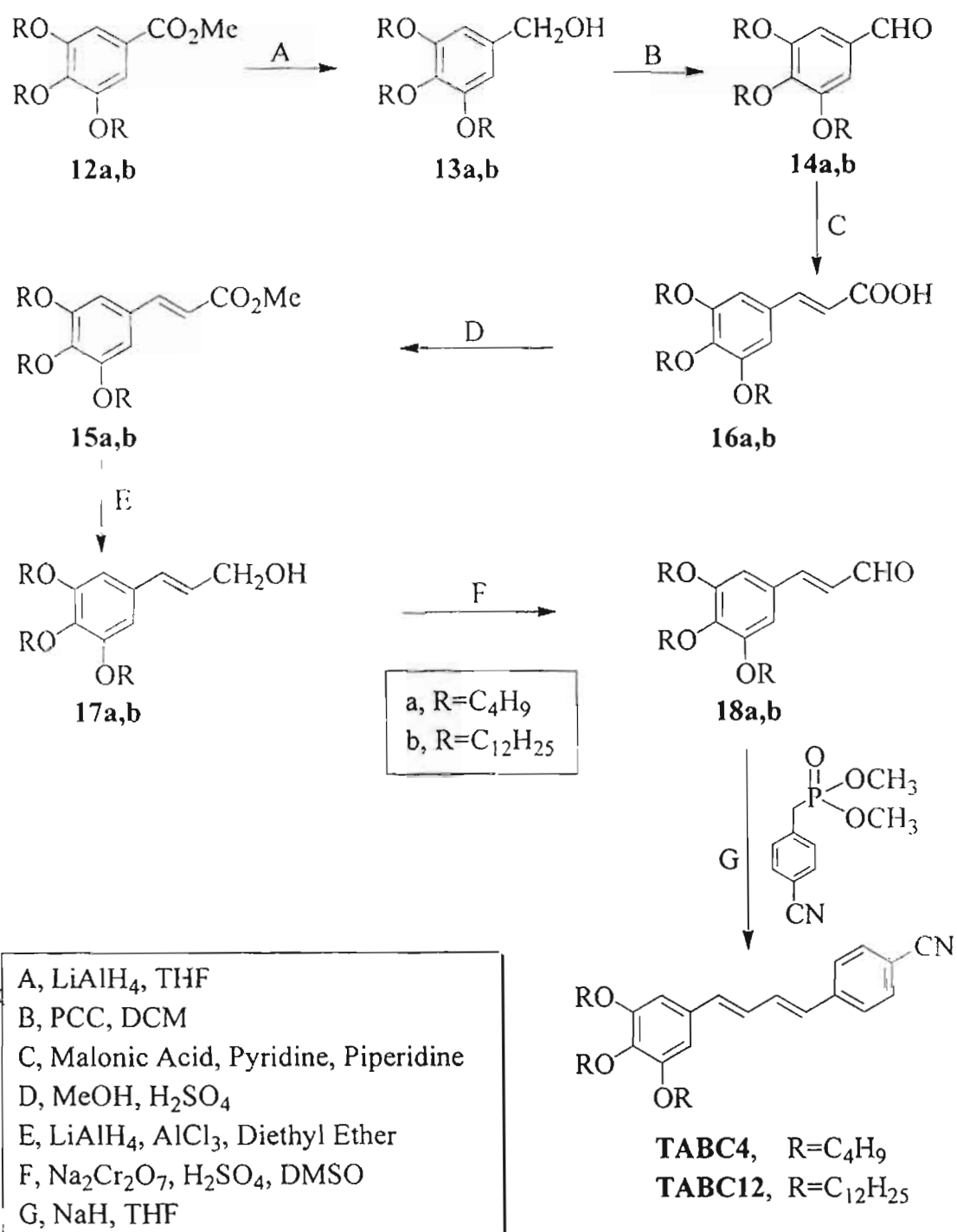
Scheme 3.4

General Procedure for the Preparation of 3,4,5-tri(*n*-alkoxy)benzylalcohol (13a,b)

A suspension of LiAlH$_4$ (3.5eq) in THF was stirred for 20 minutes. To this suspension THF solution of 3,4,5-tris(*n*-alkoxy)methylbenzoate (1eq) was then added dropwise, with the mixture maintained at 0 °C .The resulting mixture was stirred for 3 h at room temperature (27 °C). The reaction mixture was quenched using 10% NaOH solution and was then it was filtered to remove the insoluble materials. The solvent was distilled out and the crude product was extracted with ether. The product was purified by column chromatography using silica gel (100-200 mesh) as the packing material and a mixture (1:20) of ethyl acetate and hexane as the eluent. Recrystallization form the same solvent mixture gave pure samples, **13a,b** in 70% yield.

13a: IR v$_{max}$(neat): 3387, 2962, 2874 2362, 1593, 1445, 1384, 1330, 1249, 1121 cm^{-1}; ^{1}H NMR (300 MHz, CDCl$_3$): 0.92-0.99 (m, 9H, CH$_3$), 1.48-2.02 (m, 12H, CH$_2$), 3.91-3.98 (m, 6H, OCH$_2$), 4.57 (d, 2H, C*H*$_2$OH), 6.54 (s, 2H, aromatic) ppm.

13b: mp 47-48 °C; IR v$_{max}$(KBr): 2921, 2847, 1715, 1593, 1506, 1472, 1445, 1384, 1344, 1222, 1128, 1013, 778, 737 cm^{-1}; ^{1}H NMR (300 MHz, CDCl$_3$): δ 0.84-0.90 (m, 9H, CH$_3$), 1.26-1.86 (m, 60H, CH$_2$), 3.91-3.99 (m, 6H, OCH$_2$), 4.58 (d, 2H, C*H*$_2$OH), 6.56 (s, 2H, aromatic) ppm.

General Procedure for the Preparation of 3,4,5-tri(*n*-alkoxy)benzaldehyde (14a,b)

3,4,5-tris(*n*-alkoxy)benzyl alcohol (1 eq), pyridinium chlorochromate (PCC) (2.5 eq) and dichloromethane were taken in a round bottom flask. The mixture was stirred for 3 h at room temperature (27 °C). The product was then filtered through a silica column using dichloromethane as the eluent to remove the insoluble and inorganic matter. The solvent was removed under reduced pressure to obtain pure samples of the pure product in 50% yield.

14a:IR v_{max} (KBr): 2955, 2876, 1708, 1596, 1449, 1399, 1343, 1292, 1236, 1129, cm^{-1}; ^{1}H NMR (300MHz, CDCl$_3$): δ 0.93-1.01 (m, 9H, CH$_3$), 1.48-1.86 (m, 12H, CH$_2$), 4.02-4.09 (m, 6H, OCH$_2$), 7.09 (s, 2H, aromatic), 9.83 (s, 1H, CHO) ppm. ^{13}C NMR (75 MHz, CDCl$_3$): 13.69, 13.73, 19.01, 19.14, 31.17, 32.22, 68.78, 73.12, 76.58, 77.00, 77.42, 107.71, 131.37, 153.42, 191.17 ppm.

14b:mp 47-48 °C; IR v_{max} (KBr): 3467, 2921, 2854, 2362, 1694, 1587, 1499, 1472, 1445, 1384, 1337, 1229, 1121, 825, 724 cm^{-1}; ^{1}H NMR (300MHz, CDCl$_3$) δ 0.85-0.90 (m, 9H, CH$_3$), 1.26-1.85 (m, 60H, CH$_2$), 4.01-4.07 (6H, m, OCH$_2$), 7.08 (2H, s, aromatic), 9.82 (1H, s, CHO) ppm.

General Procedure for the Preparation of 3,4,5-tri(*n*-alkoxy)cinnamicacid (8 and 16a,b)

3,4,5-tri(*n*-alkoxy)benzaldehyde (1 eq) and malonic (1eq) were dissolved in a mixture of pyridine and piperidine and refluxed for 7 h. The reaction mixture was poured into water and the precipitate was filtered and washed with water. The product was purified by column chromatography using silica gel (100-200 mesh)

and a mixture (3:7) of ethyl acetate and hexane as the eluent. After purification pure product was obtained in 60% yield, in the form of a pale yellow solid.

8:IR ν_{max} (KBr): 3102, 3010, 2663, 2368, 1699, 1627, 1588, 1516, 1424, 1346, 1247, 1136, 998, 841; ^{1}H NMR (300 MHz, CDCl$_3$): 3.90 (s, 9H, OCH$_3$), 6.34-6.39 (d, 1H, vinylic), 6.78 (s, 2H, aromatic), 7.68-7.74 (d, 1H, vinylic) ppm; ^{13}C NMR (75 MHz, CDCl$_3$): δ 29.68, 56.17, 60.98, 105.54, 116.39, 129.48, 136.79, 147.04, 153.46, 172.04 ppm.

16a: ^{1}H NMR (300 MHz, CDCl$_3$): δ 0.93-1.01 (m, 9H, CH3), 1.48-1.83 (m, 12H, CH$_2$), 3.98-4.15 (m, 6H, OCH$_2$), 6.29-6.35 (d, 1H, vinylic), 6.75 (s, 2H, aromatic), 7.65-7.71 (d, 1H, vinylic) ppm; ^{13}C NMR (75 MHz, CDCl$_3$): δ 13.79, 13.84, 19.12, 19.23, 31.33, 32.28, 68.86, 73.20, 106.91, 115.94, 129.01, 140.79, 147.34, 153.33, 172.41 ppm.

16b: mp 41-42 °C; IR ν_{max} (KBr): 2921, 2854, 2362, 1688, 1627, 1580, 1506, 1479, 1438, 1283, 1135; ^{1}H NMR (300 MHz, CDCl$_3$): δ 0.85-0.90 (m, 9H, CH$_3$), 1.26-1.83 (m, 60H, CH$_2$), 3.96-4.01 (m, 6H, OCH$_2$), 6.29-6.34 (d, 1H, vinylic), 6.74 (s, 2H, aromatic), 7.64-7.69 (d, 1H, vinylic) ppm; ^{13}C NMR (75 MHz, CDCl$_3$): δ 14.08, 22.66, 26.07, 29.27, 29.33, 29.49, 30.31, 21.81, 31.89, 69.23, 73.61, 106.98, 115.77, 129.01, 147.33, 153.35, 171.59 ppm.

General Procedure for the Preparation of 3,4,5-tri(*n*-alkoxy) methylcinnamate (10, 15a,b)

A mixture of 3,4,5-tri(*n*-alkoxy)cinnamic acid (2.52g, 4.73 mmol), dry methanol (50 mL) and conc. H$_2$SO$_4$ (2.5 mL) were taken in a 100 mL round

bottom flask and refluxed for 36 h. Excess methanol was distilled out under reduced pressure and residue was added to water. The product was extracted with ether. After recrystallization from a mixture (1:20) of ethyl acetate and hexane gave the pure product (90%) in the form of a viscous liquid.

10: IR v_{max} (KBr): 2948, 2834, 1694, 1580, 1425, 1249, 1121; ^{1}H NMR (300 MHz, CDCl$_3$): δ 3.81 (s, 3H, CO$_2$CH$_3$), 3.89 (s, 9H, OCH$_3$), 6.32-6.38 (d, 1H, vinylic), 6.75 (s, 2H, aromatic), 7.59-7.64 (d, 1H, vinylic) ppm; ^{13}C NMR (75 MHz, CDCl$_3$): δ 22.25, 51.69, 56.13, 60.95, 72.50, 105.19, 117.01, 129.84, 144.83, 153.40, 167.38 ppm.

15a: IR v_{max} (KBr): 2962, 2888, 2362, 1721, 1640, 1587, 1506, 1438, 1276, 1121; ^{1}H NMR (300 MHz, CDCl$_3$): δ 0.93-1.00 (m, 9H, CH$_3$), 1.42-1.84 (m, 12H, CH$_2$), 3.75 (s, 3H, CO$_2$CH$_3$), 3.95-4.00 (m, 6H, OCH$_2$), 6.28 (d, 1H, vinylic), 6.72 (s, 2H, aromatic), 7.56 (d, 1H, vinylic) ppm.

15b: mp 44-45 °C; IR v_{max} (KBr): 2921, 2854, 2362, 1715, 1634, 1580, 1506, 1491, 1465, 1182, 1121, 831. cm^{-1}; ^{1}H NMR (300 MHz, CDCl$_3$): δ 0.85-0.87 (t, 9H, CH$_3$), 1.26-1.46 (m, 54H, (CH$_2$)$_9$), 1.72-1.85 (m, 6H, OCH$_2$CH_2),3.79 (s, 3H, CO$_2$CH$_3$), 3.95-4.00 (m, 6H, OCH$_2$), 6.28-6.33 (d, 1H, vinylic), 6.71 (s, 2H, aromatic), 7.55-7.60 (d, 1H, vinylic) ppm; ^{13}C NMR (75 MHz, CDCl$_3$): δ 14.106, 22.69,26.07, 29.39, 106.69, 109.29,116.48, 140.47, 145.19, 153.31 ppm.

General Procedure for the Preparation of 3,4,5-tri(*n*-alkoxy) cinnamylalcohol (9 and 17a,b)

To a weighed amount of LiAlH$_4$ (3.5 eq) in 100 mL two-necked round bottom flask equipped with a stirrer and argon inlet and addition funnel, 10 mL of diethyl ether was added dropwise. The flask was then placed in an ice bath (0 °C). To this cooled, stirred suspension of LiAlH$_4$, a solution of AlCl$_3$ (1eq) in ether was added dropwise. The mixture was then allowed to warm up to room temperature (27 °C) and then stirred for an additional 30 min. To the above mixture a solution of 3,4,5-tri(*n*-alkoxy)methylcinnamate (1 eq) in ether was added dropwise. The resulting mixture was then stirred for another 30 minutes before it was quenched with 10% aqueous solution of sodium hydroxide. The mixture was filtered to remove the insoluble material and the crude product as extracted from the filtrate using diethyl ether. The ethereal solution was dried over anhydrous sodium sulfate. The product was purified by column chromatography using a mixture (1:9) of ethyl acetate and hexane as the eluent and silica gel (100–200 mesh) as the packing material. After recrystallization from the same solvent mixture pure product was obtained in 70 % yield, in the form of a viscous liquid.

9: IR v_{max} (KBr): 3407, 2957, 2873, 1591, 1507, 1435, 1387, 1339, 1243, 1118, 1034, 974; ^{1}H NMR (300 MHz, CDCl$_3$): δ 3.84 (s, 9H, OCH$_3$), 4.31 (d, 2H, C*H$_2$*OH) 6.23-6.32 (m, 1H, vinylic), 6.50-6.55 (d, 1H, vinylic), 6.60 (s, 2H, aromatic) ppm; ^{13}C NMR (75 MHz, CDCl$_3$): δ 55.99, 60.78, 60.85, 63.46, 103.46, 128.05, 130.89, 132.41, 153.21 ppm.

17a: IR ν_{max} (KBr): 3491, 2945, 2843, 1591, 1507, 1465, 1417, 1345, 1249, 1130;

^{1}H NMR (300 MHz, CDCl$_3$): δ 0.93-0.99 (m, 9H, CH$_3$), 1.46-1.80 (m, 12H, CH$_2$),

3.93-3.99 (m, 6H, OCH$_2$), 4.26 (d, 2H, CH_2OH) 6.19-6.26 (m, 1H, vinylic), 6.47-

6.44 (d, 1H, vinylic), 6.56 (s, 2H, aromatic) ppm; ^{13}C NMR (75 MHz, CDCl$_3$): δ

13.73, 13.79, 19.08, 19.17, 31.34, 32.19, 63.43, 68.69, 73.03, 104.58, 105.00,

127.59, 131.00, 131.05, 131.91, 153.05 ppm.

17b: IR ν_{max} (KBr): 3413, 2928, 2854, 2375, 1742, 1580, 1506, 1465, 1431, 1384,

1330, 1236, 1115, 1020 cm^{-1}; ^{1}H NMR (300 MHz, CDCl$_3$): δ 0.85-0.89 (m, 9H,

CH$_3$), 1.26-1.83 (m, 60H, CH$_2$), 3.92-3.94 (m, 6H, OCH$_2$), 4.29 (d, 2H, CH_2OH),

6.19-6.28 (m, 1H, vinylic), 6.47-6.52 (d, 1H, vinylic), 6.58 (s, 2H, aromatic) ppm;

^{13}C NMR (75 MHz, CDCl$_3$): δ 14.09, 22.68, 26.11, 29.36, 29.41, 29.69, 29.73,

30.32, 31.92, 63.74, 105.23, 127.46, 131.48, 131.83, 153.21 ppm.

General Procedure for the Preparation of 3,4,5-tri(*n*-octyloxy) cinnamaldehyde (11 and 18a,b)

To a stirred solution of Na$_2$Cr$_2$O$_7$ (0.7 eq) in DMSO, 3,4,5-tri(*n*-

alkoxy)cinnamylalcohol (1 eq) was added. Conc. H$_2$SO$_4$ (2.5 eq) was added

dropwise keeping the temperature below 70 °C. The mixture was heated at 70 °C

for 90 minutes. The crude product was extracted with diethyl ether three times of

50 mL each. The ether extract was washed with sodium bicarbonate solution and

water. The product was purified by column chromatography using silica gel (100-

200 mesh) as the packing material and a mixture (1:20) of ethyl acetate and hexane

as the eluent. After purification, pure product (60%) was obtained in the form of a viscous liquid.

11: IR v_{max} (KBr): 3002, 2935, 2827, 2746, 1694, 1613, 1580, 1506. 1458, 1418, 1330, 1249, 1121, 987, 825; ^{1}H NMR (300 MHz, CDCl$_3$): δ 3.90 (s, 9H, OCH$_3$), 6.60-6.68 (m, 1H, vinylic), 6.80 (s, 2H, aromatic), 7.37 (d, 1H, vinylic), 9.67 (d, 1H, CHO) ppm; ^{13}C NMR (75 MHz, CDCl$_3$): δ 56.18, 60.98, 105.67, 127.92, 152.67, 193.38 ppm.

18a:IR v_{max} (KBr): 2955, 2881, 2362, 1681, 1580, 1506, 1445, 1344, 1249, 1121; ^{1}H NMR (300 MHz, CDCl$_3$): δ 0.94-1.01 (m, 9H, CH$_3$), 1.49-1.85 (m, 12H, CH$_2$), 3.98-4.05 (m, 6H, OCH$_2$), 6.57-6.65 (m, 1H, vinylic), 6.77 (s, 2H, aromatic), 7.34 (d, 1H, vinylic), 9.63 (d, 1H, CHO) ppm; ^{13}C NMR (75 MHz, CDCl$_3$): δ 13.62. 13.66, 18.96, 19.06, 31.17, 32.14, 68.70, 73.02, 106.88, 127.38, 128.88, 152.97. 153.24, 193.25 ppm.

18b: IR v_{max} (KBr): 2928, 2859, 1735, 1694, 1573, 1506, 1465, 1425, 1371, 1337, 1121, 966, 744 cm^{-1}; ^{1}H NMR (300 MHz, CDCl$_3$): δ 0.85-0.89 (m, 9H, CH$_3$), 1.26-1.83 (m, 60H, CH$_2$), 3.92-4.00 (m, 6H, OCH$_2$), 6.56-6.64 (m, 1H, vinylic), 6.75 (s, 2H, aromatic), 7.33 (1H, d, vinylic), 9.64 (1H, d, CHO) ppm; ^{13}C NMR (75 MHz, CDCl$_3$): δ 14.11, 22.69, 26.07, 29.32, 29.37, 29.56, 29.63, 29.65, 29.69, 30.33, 31.92, 69.11, 69.28, 73.64, 107.13, 127.59, 128.99, 153.14, 153.45, 193.48 ppm.

General Procedure for the Preparation of 4-(*p*-Cyanophenyl)-1-(3,4,5-tri(alkoxy)phenyl)buta-1*E*,3*E*-diene (TABC1, TABC4 and TABC12)

To the phosphonate ester of *p*-cynaobenzylbromide (1 eq) obtained from the earlier reaction, NaH (5 eq) was added. Dry THF was added to the above mixture with efficient stirring. After about 10 min of stirring, a solution of 4-alkoxycinnamaldehyde (1 eq) was added dropwise and the resulting mixture was refluxed for 24 h in argon atmosphere. The solvent was removed under reduced pressure and the resulting residue was washed with water. The crude product was extracted using dichloromethane. The product was purified by column chromatography using silica gel (100-200 mesh) and a mixture (1:99) of ethyl acetate and hexane as the eluent. After recrystallization from the same solvent mixture the pure product (40%) was obtained in the form of yellow crystals.

TABC1: ^{1}H NMR (300 MHz, CDCl$_3$): δ 3.87-3.90 (m, 9H, OCH$_3$), 3.94-4.02 (m, 6H, OCH$_2$), 6.62 (d, 1H, olefinic), 6.68 (s, 2H, aromatic), 6.71 (d, 1H, olefinic), 6.83-6.91 (dd, 1H, olefinic), 6.99-7.07 (dd, 1H, olefinic), 7.50 (d, 2H, aromatic), 7.59 (d, 2H, aromatic) ppm; Elemental analysis for C$_{20}$H$_{19}$NO$_3$: calc. C(74.74%), H(5.95%), N(4.35%); found C(74.74%), H(5.81%), N(4.85%).

TABC4: ^{1}H NMR (300 MHz, CDCl$_3$): δ 0.93-1.01 (m, 9H, CH$_3$), 1.48-1.85 (m, 12H, CH$_2$), 3.95-4.05 (m, 6H, OCH$_2$), 6.60 (d, 1H, olefinic), 6.65 (s, 2H, aromatic), 6.67 (d, 1H, olefinic), 6.79-6.87 (dd, 1H, olefinic), 6.98-7.06 (dd, 1H, olefinic), 7.49 (d, 2H, aromatic), 7.61 (d, 2H, aromatic) ppm; Elemental analysis

for $C_{29}H_{37}NO_3$: calc. C(77.83%), H(8.33%), N(3.13%); found C(77.83%), H(8.21%), N(5.24%).

TABC12: mp 64-65 °C; IR ν_{max} (KBr): 2921, 2847, 2362, 2220, 1600, 1580, 1506, 1472, 1431, 1324, 1249, 1128, 987, 858, 804 cm^{-1}; ^{1}H NMR (300 MHz, CDCl$_3$): δ 0.88-1.00 (m, 9H, CH$_3$), 1.26-1.83 (m, 60H, CH$_2$), 3.94-4.02 (m, 6H, OCH$_2$), 6.61 (d, 1H, olefinic), 6.64 (s, 2H, aromatic), 6.69 (d, 1H, olefinic), 6.78-6.87 (dd, 1H, olefinic), 6.97-7.06 (dd, 1H, olefinic), 7.48 (d, 2H, aromatic), 7.58 (d, 2H, aromatic) ppm. ^{13}C NMR (75 MHz, CDCl$_3$): δ 14.10, 22.68, 26.10, 29.37, 29.41, 29.60, 29.65, 29.70, 29.74, 30.33, 31.92, 69.20, 73.57, 105.41, 110.18, 119.09, 126.55, 127.38, 129.96, 131.94, 132.42, 132.84, 135.72, 141.96, 153.32 ppm.

3.5.3. Instrumentation

HPLC analyses were carried out on a Shimadzu HPLC using the following conditions: Shimadzu System Controller SCL10AVP, Shimadzu LC-6AD pump, Shimadzu SPD-6AV UV-Vis spectrophotometric detector, Rheodyne injection valve with 20 μL (analytical) and 200 μL (preparative) sample loops; Shimadzu Shim-pack CLC-Sil (4.6 mm x 25 cm) analytical column packed with totally porous, spherical silica particles (5 μm particle diameter 100 Å pore diameter) with chemically modified surfaces and Prep-Sil (20 mm x 25 cm) preparative columns packed with totally porous, irregular-shaped silica particles (15 μm particle diameter, 100 Å pore diameter) with chemically modified surfaces; mobile

phase: hexane-ethylacetate (99:1), flow rate: 2 mL/min (analytical) and 20 mL/min (preparative).

Phase transitions were observed using a Nikon HFX 35A Optiphot-2 polarized light optical microscope, equipped with a Linkam THMS 600 heating and freezing stage connected to a Linkam TP92 temperature programmer. DSC analyses were preformed under air, using Du Pont DSC 2010 Differential Scanning Calorimeter attached to Thermal Analyst 2100 data station.

Absorption spectra were recorded on a Shimadzu UV-3101PC UV-Vis-NIR spectrophotometer. The excitation and emission spectra were recorded on a SPEX Fluorolog F112X spectrofluorimeter. Fluorescence quantum yields, with an estimated reproducibility of around 10%, were determined by comparison with Quinine sulfate in 0.1 N H_2SO_4 ($\Phi_f = 0.515$), which was used as the fluorescence standard. The quantum yield of fluorescence of these derivatives were measured using a modified method[33] due to strong photoisomerization processes of the *EE* forms of these derivatives. Two factors affected the quantum yield measurements of these derivatives; (i) the fluorescence intensity diminishes during the measurement of the fluorescence spectrum due to the disappearance of the *EE* isomer; (ii) the total optical density diminishes because the *EZ* and *ZE* isomers exhibit a smaller extinction coefficient than the *EE* isomer. In order to overcome these factors, at the maximum wavelength of the fluorescence spectrum a time trace of the subsiding intensity is recorded until the photostationary state of the solution is safely reached. The fluorescence spectrum is then recorded in the

photostationary state and the intensity is scaled to the value at time t = 0 using the time trace spectrum. During the whole measurement time the solution is intensely stirred. The applicability of this method results from the absence of the fluorescence of the *EZ* and *ZE* isomers. This was checked using the isolated samples of the *EZ* and *ZE* isomers.

Steady-state photolysis experiments were carried out using a 200 W high-pressure mercury lamp, in combination with a 360 nm Oriel band pass filter. The intensity of light was determined using potassium ferrioxalate actinometry.[45] Laser photolysis was carried out using the third harmonic (355 nm, 60 mJ/pulse, pulse width 10 ns) and fourth harmonic (266 nm, 15 mJ/pulse, pulse width 10 ns) of a Quanta Ray GCR-12 Nd:YAG laser.

IR spectra were recorded on a Nicolet Impact, Bomem MB Series 400 D FT-IR spectrometer. ^{1}H-NMR spectra were measured on Bruker DRX 500 MHz and Bruker DPX 300 MHz spectrometers. ^{1}H-COSY and ^{1}H-NOESY NMR analyses were carried out on Bruker DRX 500 MHz spectrometer. Tetramethylsilane (TMS) was used as the internal standard and chloroform-*d* (CDCl$_3$) was used as the solvent.

3.6. Conclusion

In summary, we have demonstrated for the first time that alkoxy-cyano-substituted diphenylbutadiene derivatives can be utilized for developing reversibly photoswitchable mesogenic materials. Since the phototransformations are thermally irreversible, switching between the mesogenic and isotropic phases

remains purely photon-controlled in these materials. These properties of the alkoxy-cyano-substituted diphenylbutadienes make them uniquely suited for the design of a wide variety of photoactive liquid crystals, including chiral nematic and ferroelectric liquid crystals. Studies on these aspects as well as on enhancing the range of the phase transition temperatures of these materials are in progress.

3.7. References

1) Eich, M.; Wendorff, J. *J. Opt. Soc. Am. B* **1990**, *7*, 1428.

2) Anderle, K.; Wendorff, J. H. *Mol. Cryst. Liq. Cryst.* **1994**, *243*, 51.

3) Gibbons, W. M.; Shannon, P. J.; Sun, S. T. *Mol. Cryst. Liq. Cryst.* **1994**, *251*, 191.

4) Gibbons, W. M.; Kosa, T.; Palffy-Muhoray, P.; Shannon, P. J.; Sun, S. T.; Swetlin, B. J. *Nature* **1995**, *377*, 43.

5) Haas, W.; Adams, J.; Wysocki, J. *Mol. Cryst. Liq. Cryst.* **1969**, *7*, 371.

6) Haas, W. E.; Nelson, K. F.; Adams, J. E.; Dir, G. A. *J. Electrochem. Soc.* **1974**, *121*, 1667.

7) Ikeda, T.; Kanazawa, A. *Molecular Switches*; Wiley-VCH: Weinheim, 2001.

8) Ikeda, T.; Tsutsumi, O. *Science* **1995**, *268*, 1873.

9) Ikeda, T.; Sasaki, T.; Ichimura, K. *Nature* **1993**, *361*, 428.

10) Kurihara, S.; Ikeda, T.; Sasaki, T.; Kim, H.-B.; Tazuke, S. *J. Chem. Soc. Chem. Commun.* **1990**, 1751.

11) Kurihara, S.; Nomiyama, S.; Nonaka, T. *Chem. Mater.* **2000**, *12*, 9.

12) Tsutsumi, O.; Shiono, T.; Ikeda, T.; Galli, G. *J. Phys. Chem. B* **1997**, *101*, 1332.

13) Tamaoki, N.; Moriyama, M.; Matsuda, H. *Angew. Chem. Int. Ed. Engl.* **2000**, *39*, 509.

14) Stumpe, J.; Fischer, T.; Menzel, H. *Macromolecules* **1996**, *29*, 2831.

15) Stumpe, J.; Geue, T.; Fischer, T.; Menzel, H. *Thin Solid Films* **1996**, 606.

16) Ichimura, K. *Chem. Rev.* **2000**, *100*, 1847.

17) Suarez, M.; Schuster, G. B. *J. Am. Chem. Soc.* **1995**, *117*, 6732.

18) Janicki, S. Z.; Schuster, G. B. *J. Am. Chem. Soc.* **1995**, *117*, 8524.

19) Feringa, B. L.; Huck, N. P. M.; Doren, H. A. v. *J. Am. Chem. Soc.* **1995**, *117*, 9929.

20) Huck, N. P. M.; Jager, W. F.; Lange, B. d.; Feringa, B. L. *Science* **1996**, *273*, 1686.

21) Ikeda, T.; Sasaki, T.; Kim, H.-B. *J. Phys. Chem.* **1991**, *95*, 509.

22) Sasaki, T.; Ikeda, T.; Ichimura, K. *Macromolecules* **1992**, *25*, 3807.

23) Mallia, V. A.; George, M.; Das, S. *Chem. Mater.* **1999**, *11*, 207.

24) Kobayashi, T.; Degenkolb, E. O.; Rentzepis, P. M. *J. Phys. Chem.* **1979**, *83*, 2431.

25) Shishido, A.; Tsutsumi, O.; Kanazawa, A.; Shiono, T.; Ikeda, T.; Tamai, N. *J. Am. Chem. Soc.* **1997**, *119*, 7791.

26) Tsutsumi, O.; Demachi, Y.; Kanazawa, A.; Shiono, T.; Ikeda, T.; Nagase, Y. *J. Phys. Chem. B* **1998**, *102*, 2869.

27) Tamaoki, N.; Song, S.; Moriyama. M.; Matsuda. H. *Adv. Mater.* **2000**, *12*, 94.

28) Tamaoki, N. *Adv. Mater.* **2001**, *13*, 1135.

29) Davis, R.; Das, S.; George, M.; Druzhinin. S.; Zachariasse, K. *J. Phys. Chem. A* **2001**, *105*, 4790.

30) Das, S.; George, M.; Mathew, T.; Asokan, C. V. *J. Chem. Soc. Perkin Trans. 2* **1996**, *2*, 731.

31) Brettle, R.; Dunmur, D. A.; Hindley, N. J.; Marson, C. M. *J. Chem. Soc. Chem. Commun.* **1992**, 411.

32) Brettle, R.; Dunmur, D. A.; Hindley. N. J.; Marson, C. M. *J. Chem. Soc. Perkin Trans 1* **1993**, 775.

33) Braatz, H.; Hecht, S.; Seifert, H.; Helm, S.; Bendig, J.; Rettig, W. *J. Photochem. Photobiol. A: Chem.* **1999**, *123*, 99.

34) Neuhaus, D.; Williamson, N. *The Nuclear Overhauser Effect in Structural and Conformational Analysis*; VCH Publishers Inc: New York, 1989.

35) Kelker, H.; Hatz, R. *Hand book of liquid crystals;* Verlag Chemie: Weinheim, 1980.

36) Spalletti, A.; Bartocci, G.; Galiazzo, G.; Macchioni, A.; Mazzucato, U. *J. Phys. Chem. A* **1999**, *103*, 8994.

37) Allen, M. T.; Whitten, D. G. *Chem. Rev.* **1989**, *89*, 1691.

38) Liu, R. S. H. *Acc. Chem. Res.* **2001**, *34*, 555.

39) Arai, T.; Tokumaru, K. *Chem. Rev.* **1993**, *93*, 23.

40) Singh, A. K.; Krishna, T. S. R. *J. Photosci.* **1998**, *5*, 47.

41) Dellinger, B.; Kasha, M. *Chem. Phys. Lett.* **1976**, *38*, 9.

42) Sun, Y.-P.; Saltiel, J.; Hoburg, E. A.; Waldeck, D. *J. Phys. Chem.* **1991**, *53*, 10336.

43) Liu, R. S. H.; Asato, A. E.; Denny, M. *J. Am. Chem. Soc.* **1983**, *105*, 4829.

44) Singh, A. K.; Kanvah, S. *New J. Chem.* **2000**, *24*, 639.

45) Murov, S. L.; Carmichael, I.; Hug, G. L. *Handbook of Photochemistry*; Marcel Dekker Inc.: New York, 1993.

Study of the Fluorescence of Alkoxy-Cyano- and Alkylamino-Cyano-Substituted Diphenylbutadienes in Solution and Crystalline Phases

4.1. Abstract

The fluorescence of some alkoxy-cyano and alkylamino-cyano-substituted diphenylbutadiene derivatives have been examined in solution and crystalline phases. In solutions the monoalkoxy-cyano-substituted diphenylbutadienes (Chart 4.1) exhibit weak fluorescence (ϕ ~0.02) with emission maxima centered on ~450 nm which is fairly independent of the length of the alkoxy group. In contrast, these derivatives possess broad and intense fluorescence bands in the solid state whose emission maxima undergo significant hypsochromic shift with increase in the length of the alkoxy group. Single crystal X-ray diffraction (XRD) studies and powder XRD analyses indicate that this effect can be attributed to the difference in molecular packing, which affects the nature of the intermolecular interactions. The solid state fluorescence of one of the derivatives, **BC8**, undergoes a dramatic change from blue to green when prepared as its freshly cooled melt. Powder XRD analyses indicate that this difference could be attributed to the polymorphic nature of **BC8**. The solid state fluorescence of the trialkyloxy-cyano-substituted diphenylbutadienes has also been investigated. Photoisomerization of the butadiene chromophore in the alkoxy-cyano-substituted diphenylbutadienes result in significant changes in their solid state fluorescence and the use of this property for recording fluorescent images has been explored. The strong temperature dependence of the solid state fluorescence of these compounds which makes potentially useful as temperature sensors has also been investigated. By bringing about suitable structural modifications of the butadiene chromophore it has been possible to tune the solid state fluorescence of these materials almost over the entire visible range, with the alkoxy-cyano-substituted diphenylbutadienes emitting in the blue-green region and the alkylamino-cyano derivatives emitting in the yellow-red region.

4.2. Introduction

The ability to tailor functional properties of materials by controlling the manner in which the constituent molecules self-assemble has been an important advancement in science. More interestingly, if the functional properties of such self-assembled materials can be controlled by external stimuli such as light or heat, they become potential candidates for a number of applications such as in imaging, opto-electronics and development of sensors. Solid state fluorescence is an important functional property of materials, which has been attracting increasing attention due to the current interest in development of organic light emitting diodes (OLEDs).[1-4]

Although the role of molecular packing in controlling solid state photochemical reactions of organic molecules is fairly well understood there has been much less progress in understanding the factors that affect solid state photophysical properties. Very few studies have tried to address the role of molecular packing in controlling the photophysical properties such as fluorescence of solid state materials. Weiss and co-worker have observed that the solid state emission of a series of 4-alkyl-*N*-(4-cyanophenyl)piperidines varied significantly with the length of the alkyl group. They concluded that exciton hopping to energy sinks, namely molecules in a unit cell with lowest excitation energies played an important role in controlling the solid state fluorescence of these materials, whereas energy hopping to defect sites was not important.[5] Lewis and Yang

reported on the fluorescence of secondary amine dicarboxamides in single crystals, powders, melts and ethanol solutions.[6] Their investigations indicate that the excited dimer formation from hydrogen-bonded arrays of arene dicarboamides is dependent on both the ground state structure and arene-arene interactions. The ground state structures of these amides are controlled by hydrogen-bonded scaffolds. The single crystals of some of these amides, which packed in one-dimensional tapes, exhibited dual emission attributed to excited state monomers and dimers. The single crystals of these amides, which pack in two-dimensional sheets however, displayed only monomer emission, whereas melted and resolidified samples displayed a broad and structureless emission attributed to the fluorescence from a mixture of monomers and dimers with differing ground state geometry.

Jenekhe and Osaheni have observed fluorescence from thin films of π-conjugated polymers, which has been attributed to emission from interchain interactions of two or more associated chromophores.[7] Emission from trimers and higher aggregates are generally not observed in single crystals or in solution but has been observed in the case of triple-decker cyclophanes.[8] Lim and co-workers have found that van der Waals clusters containing more than two naphthalene molecules display monomer and dimer emission but not from higher aggregates.[9]

In this chapter we describe our detailed studies on the solid state photochemical and photophysical properties of novel donor-acceptor-substituted diphenylbutadiene (Chart 4.1) based materials.

BC1. R = CH$_3$	BC8. R = C$_8$H$_{17}$
BC4, R = C$_4$H$_9$	BC12, R = C$_{12}$H$_{25}$

TABC1, R = CH$_3$
TABC4. R = C$_4$H$_9$
TABC12, R = C$_{12}$H$_{25}$

DMAB, R = H
DMABE, R = C$_2$H$_5$
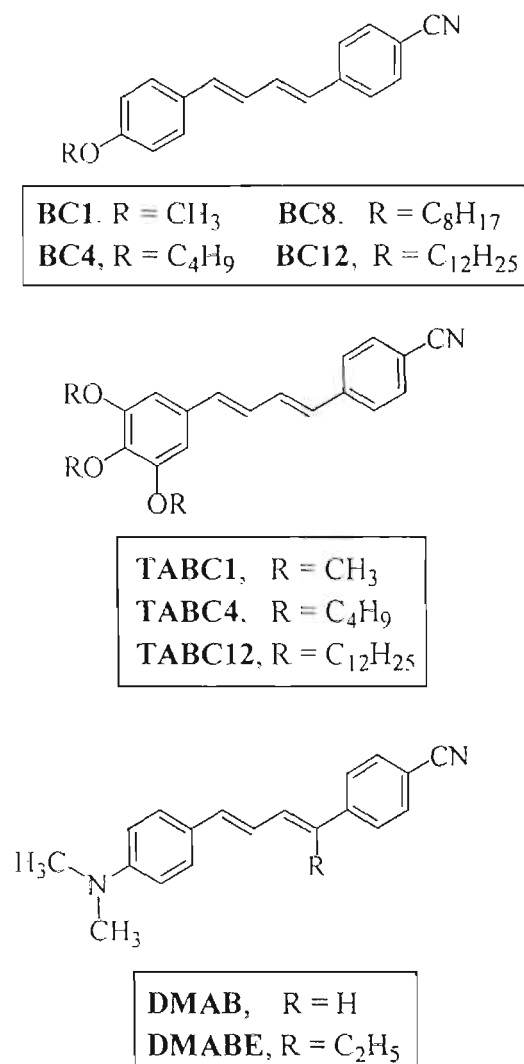
Chart 4.1

4.3. Results and Discussion

4.3.1. Synthesis

The synthesis of the mono- and trialkoxy-cyano-substituted diphenylbutadienes are described in the Experimental Section of Chapter 3. The reported synthesis[10] of (1-(*N,N*-dimethylaminophenyl)-4-(cyanophenyl)buta-1,3-diene, **DMAB**, is as per Scheme 4.1, shown below.
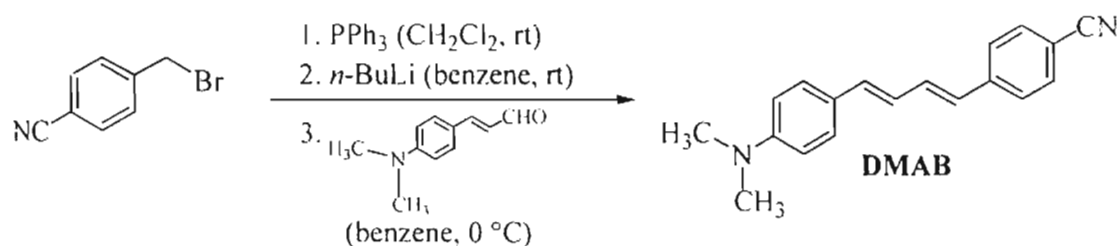
Scheme 4.1. Synthesis of **DMAB** using triphenylphosphine as the Wittig reagent.

We have used a modified procedure where triethyl phosphite was used instead of triphenylphosphine as the Wittig reagent (Scheme 4.2).

DMAB, R = H
DMABE, R = C$_2$H$_5$
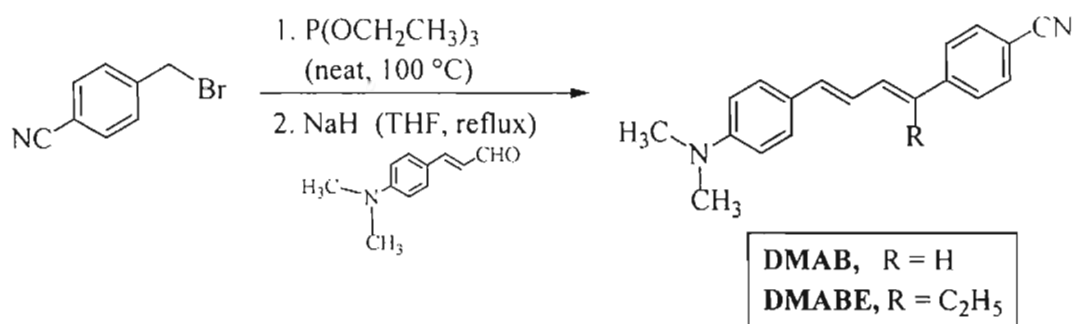
Scheme 4.2. Synthesis of **DMAB** using triethyl phosphite as the Wittig reagent.

In our attempts to modify the procedure for the synthesis of **DMAB** using triethyl phosphite, instead of triphenylphosphine, as shown in Scheme 4.2, we found that besides **DMAB**, an ethyl substituted, (1-(*N,N*-dimethylaminophenyl)-4-(cyanophenyl)-4-ethyl)buta-1,3-diene, **DMABE** was also obtained. In fact **DMABE** was the major product under these reaction conditions.

The structure of **DMABE** was unequivocally established on the basis of spectroscopic techniques and X-ray crystallographic analysis. The characterization

data for **DMABE** is provided in the Experimental Section (4.4) and its X-ray diffraction analysis is discussed in Section (4.3.6).

The formation of both **DMAB** and **DMABE** may be rationalized in terms of the pathways shown in Scheme 4.3. The initial step involves the formation of the phosphonate intermediate, **3**. The structure of **3** was confirmed using ^{1}H NMR, which clearly showed the presence of a two-proton doublet at δ 3.24 that corresponds to the benzylic protons. The phosphorous ylide formed from the intermediate, **3** subsequently reacts with 4-*N,N*-dimethylaminocinnamaldehye leading to the formation of the expected **DMAB**. The formation of **DMABE** will require an ethyl group at the benzylic carbon of the phosphorous ylide. The only source of an ethyl group in the reaction mixture is triethyl phosphite. A probable route to the formation of **DMABE** involves an intermediate, **5** formed through an intramolecular ethyl migration, which could be the precursor for the ethyl substituted phosphorous ylide. In order to examine this possibility the phosphonate ester, **3** was treated with NaH. As expected, the ^{1}H NMR spectrum of the phosphorous intermediate obtained by this reaction corresponded to that of **5**. The NMR showed a single-proton doublet at δ 3.16, corresponding to the benzylic proton, a multiplet (two protons) between δ 3.72-3.77 and a triplet (three protons) at δ 1.04, with the latter two belonging to the migrated ethyl group.

We assume that the base-catalyzed transformation of **3** to **5** involves a four-membered transition state, as shown in Scheme 4.3. In the presence of 4-*N,N*-

dimethylaminocinnamaldehyde, the phosphorous ylide formed from the intermediate, **5** couples with the former as per the conventional Wittig coupling reactions to form **DMABE**.
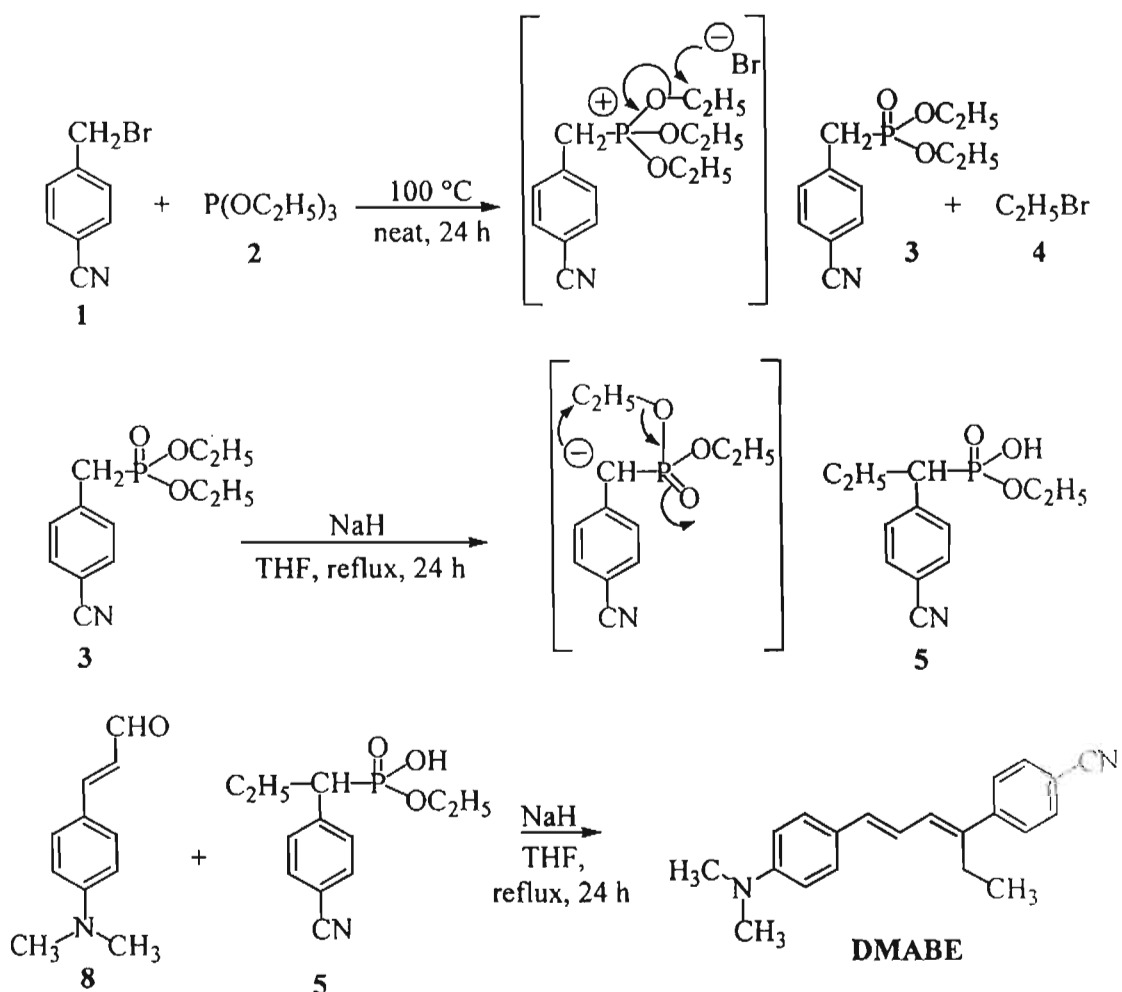
Scheme 4.3. Mechanism for the formation of **DMABE**.

It is interesting to note that the analogous ethyl substituted product was never observed during the synthesis of alkoxy-cyano-substituted diphenylbutadienes using similar reaction conditions. This may be rationalized on the basis of the difference in the donor strengths of the amino and the alkoxy groups, which can have a pronounced effect on the electrophilicity of the carbonyl center in the corresponding cinnamaldehydes. The carbonyl center in 4-N,N-dimethylaminocinnamaldehyde is rendered less electrophilic due to the strong positive mesomeric effect or the stronger electron donating nature of the amino group compared to the alkoxy groups in alkoxycinnamaldehydes. As a result the condensation reaction between the corresponding cinnamaldehydes and the phosphorous ylide obtained from **3** will be more facile in the case of the alkoxycinnamaldehydes. The less facile condensation reaction of the aminocinnamaldehyde with the phosphonate ylide obtained from **3** can result in competitive base-catalyzed formation of the phosphonate ester, **5**, which can eventually lead to the formation of ethyl-substituted derivative, **DMABE**. It is proposed that using this method a variety of alkene substituted polyene chains can be synthesized.

4.3.2. Solution Phase Fluorescence Studies of Alkoxy-cyano-Substituted Diphenylbutadiene Butadienes

Table 4.1 summarizes the absorption and fluorescence properties of the monoalkoxy-cyano-substituted diphenylbutadienes in three different solvents. It

may be noted that in a particular solvent, change in length of the alkoxy group did not bring about any change in its absorption or emission properties. This is along anticipated lines, since the length of the alkoxy group is not expected to affect the butadiene chromophore substantially. The absorption and fluorescence spectra of the monoalkoxy-cyano-susbtituted diphenylbutadiene derivative **BC4** are shown in Figure 4.1. Whereas the absorption spectrum (λ_{max} ~360 nm) was found to be practically independent of the nature of the solvent, a bathochromic shift in the fluorescence was observed with increasing in solvent polarity. For example, the fluorescence maximum was found to shift from ~435 nm in toluene to ~475 nm in acetonitrile.
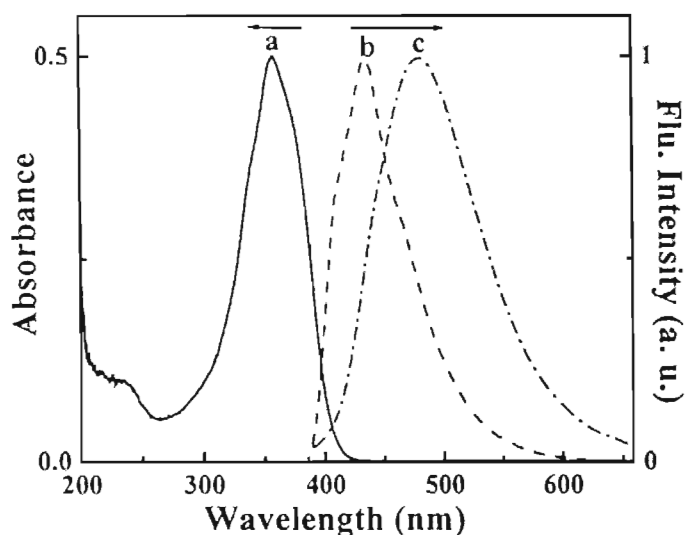
Figure 4.1. Absorption and fluorescence spectra of **BC4**; (a) absorption spectrum in acetonitrile and fluorescence spectra in (b) toluene and (c) acetonitrile.

Table 4.1. Absorption and fluorescence properties of monoalkoxy-cyano-substituted diphenylbutadienes in various solvents.

Solvent	BC1		BC4		BC8		BC12	
	Abs. λ_{max} (nm) ($\varepsilon(M^{-1}cm^{-1})$ x 10^{-4})	Ems. λ_{max} (nm) (Φ_f)	Abs. λ_{max} (nm) ($\varepsilon(M^{-1}cm^{-1})$ x 10^{-4})	Ems. λ_{max} (nm) (Φ_f)	Abs. λ_{max} (nm) ($\varepsilon(M^{-1}cm^{-1})$ x 10^{-4})	Ems. λ_{max} (nm) (Φ_f)	Abs. λ_{max} (nm) ($\varepsilon(M^{-1}cm^{-1})$ x 10^{-4})	Ems. λ_{max} (nm) (Φ_f)
Toluene	363	435	365	435	364	435	364	435
	(4.1)	(0.02)	(4.8)	(0.03)	(5.1)	(0.02)	(5.2)	(0.03)
THF	361	455	363	455	362	455	362	455
		(0.02)		(0.02)		(0.02)		(0.02)
Acetonitrile	356	475	358	480	355	477	356	482
	(4.5)	(0.01)	(5.9)	(0.01)	(4.6)	(0.01)	(4.4)	(0.01)

A similar behaviour was observed for the trialkoxy-cyano-substituted diphenylbutadiene derivatives. Table 4.2 summarizes the absorption and fluorescence properties of these derivatives in various solvents. Their absorption maxima were centered on ~370 nm, which were fairly independent of solvent polarity. Within a particular solvent, the fluorescence of these derivatives were also insensitive to the length of the alkoxy groups. However, their fluorescence spectra showed a significant bathochromic shift with increasing solvent polarity. Whereas the fluorescence maxima of these derivatives were centered on ~440 nm in heptane, in acetonitrile the maxima were centered on ~520 nm.

The absorption and fluorescence spectra of **TABC4** in various solvents are shown in Figures 4.2 and 4.3, respectively. The solvent polarity induced bathochromic shift in fluorescence was much more pronounced for these derivatives and can be visually perceived (Figure 4.4). The fluorescence quantum yields (Φ ~0.3) of the trialkoxy derivatives were also found to be ~10 fold higher than that of the mono-alkoxy derivatives.

Table 4.2. Absorption and fluorescence properties of trialkoxy-cyano-substituted diphenylbutadienes in various solvents.

Solvent	TABC1		TABC4		TABC12	
	Abs. λ_{max} (nm) ($\varepsilon(M^{-1}cm^{-1})$ x 10^4)	Ems. λ_{max} (nm) (Φ_f)	Abs. λ_{max} (nm) ($\varepsilon(M^{-1}cm^{-1})$ x 10^4)	Ems. λ_{max} (nm) (Φ_f)	Abs. λ_{max} (nm) ($\varepsilon(M^{-1}cm^{-1})$ x 10^4)	Ems. λ_{max} (nm) (Φ_f)
Heptane	361	435 (0.23)	361	441 (0.29)	365	440 (0.28)
Toluene	366 (4.5)	443 (0.20)	368 (6.1)	456 (0.24)	368 (5.3)	451 (0.24)
THF	363	500 (0.02)	366	504 (0.23)	366	504 (0.25)
Acetonitrile	358 (6.2)	515 (0.14)	361 (6.0)	522 (0.16)	-	-
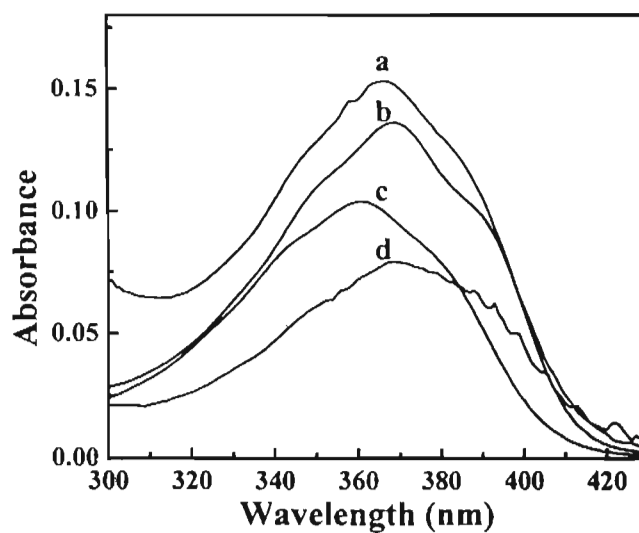
Figure 4.2. The absorption spectra of **TABC4** in various solvents; a) heptane b) toluene, c) THF and d) acetonitrile.
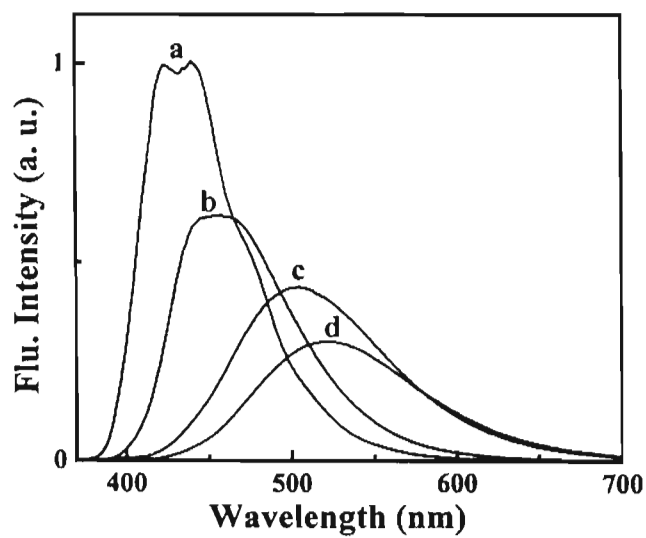
Figure 4.3. Fluorescence spectra of **TABC4** in various solvents; a) heptane, b) toluene, c) THF, d) acetonitrile. Excitation: 360 nm.
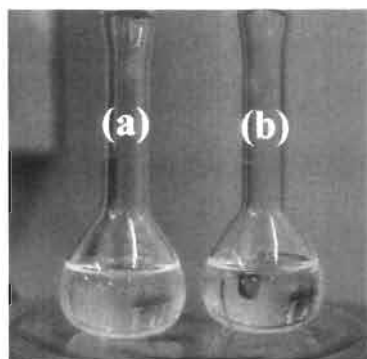
Figure 4.4. Photograph showing the fluorescence of **TABC4** in (a) acetonitrile and (b) toluene.

Table 4.3 summarizes the fluorescence lifetime data obtained for the trialkoxy-cyano substituted diphenylbutadiene derivatives in various solvents. The fluorescence decayed predominantly by a monoexponential process.

Table 4.3. Fluorescence lifetime data of the trialkyloxy-cyano-substituted diphenyl butadiene derivatives in various solvents.

Compound	Solvent	τ_1(ns)	F_1%	τ_2(ns)	F_2%	χ^2
TABC1	Heptane	0.51	100			0.98
	Toluene	0.35	100			1.10
	THF	0.44	99.61	4.60	0.39	1.00
	Acetonitrile	0.34	100			1.10
TABC4	Heptane	0.51	100			1.00
	Toluene	0.39	100			0.98
	THF	0.50	99.2	5.67	0.8	0.92
	Acetonitrile	0.49	100			1.20
TABC12	Heptane	0.58	99.4	5.14	0.6	0.99
	Toluene	0.43	100			1.10
	THF	0.49	99.3	4.80	0.67	0.91
	Acetonitrile	-	-	-	-	-

The effect of solvent polarity on the fluorescence properties of these derivatives was also studied using toluene-acetonitrile mixtures. Figure 4.5 shows

fluorescence spectra of **TABC4** in various toluene-acetonitrile mixtures. Table 4.4

summarizes the fluorescence lifetime data of **TABC4** in various toluene-

acetonitrile mixtures. With increasing content of acetonitrile in the solvent mixture

a bathochromic shift in the fluorescence spectrum which was also associated with

a slight enhancement in the fluorescence lifetime was observed.
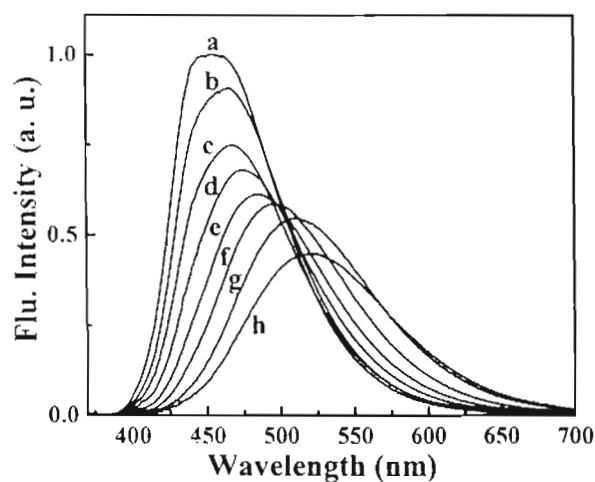
Figure 4.5. Fluorescence spectra of **TABC4** in toluene-acetonitrile mixtures; a) toluene, b) 1% acetonitrile, c) 2% acetonitrile, d) 5% acetonitrile, e) 10% acetonitrile, f) 20% acetonitrile, g) 50% acetonitrile, h) acetonitrile. Excitation wavelength: 360 nm.

Table 4.4. Fluorescence lifetime data for **TABC4** in toluene-acetonitrile mixtures.

Toluene (%)	Ems. (nm)	τ_1(ns)	F_1%	τ_2(ns)	F_2%	χ^2
100	450	0.38	99.4	1.60	0.6	0.97
80	495	0.39	99.7	3.26	0.3	1.12
60	505	0.46	99.2	6.35	0.8	1.01
40	510	0.49	99.8	8.05	0.2	1.04
20	510	0.47	97.1	8.64	2.9	1.19
0	520	0.50	99.1	5.2	0.9	1.10

It is interesting to note that the absorption spectra of the alkoxy-cyano-substituted diphenylbutadienes was not affected by solvent polarity indicating that there is not much difference between the dipole moments of the ground and excited states. The red shift in the fluorescence spectra with increase in solvent polarity suggests however, that there is a significant enhancement in the dipole moment of the excited state compared to the ground state. In order to explain this contradiction it must be assumed that the Franck-Condon (FC) excited state and the emitting states are different. Whereas the FC state may not involve an intramolecular charge transfer (ICT), the emitting state may have formed via an ICT process. Our study on the donor-acceptor-substituted butadienes (Chart 2.1, Chapter 2), which show dual emission indicated that their absorption spectra were unaffected by solvent polarity. In these molecules, emission was observed both from the FC excited state (locally excited state, LE) as well as from the ICT state.[11] Whereas the LE state emission was not significantly affected by solvent polarity, the ICT state emission showed a significant red-shift with increasing solvent polarity.[12] In the present case the absence of dual emission could be due to the FC state being a non-emitting state, with emission occurring only from the ICT state. This can happen if the activation barrier between the FC and ICT states are very low, unlike for the butadiene derivatives which show dual emission as depicted in Figure 4.6.
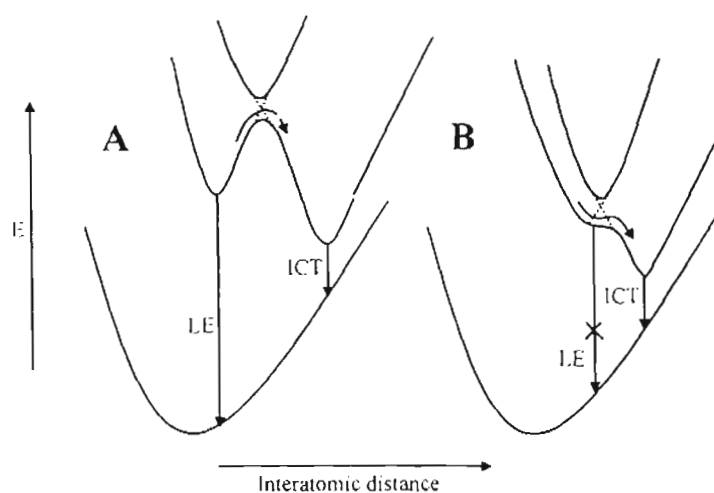
Figure 4.6. Schematic representation of potential energy curves for (A) donor-acceptor-substituted butadienes (Chart 2.1, Chapter 2) showing dual emission from LE and ICT states and for (B) alkoxy-cyano-substituted diphenylbutadienes, where only an ICT emission is observed.

4.3.3. Solid State Fluorescence of Monoalkoxy-Cyano-Substituted Diphenylbutadiene Butadienes (Chart 4.1)

The solid state fluorescence of the alkoxy-cyano-substituted diphenylbutadienes were distinctly different from that solution. All the derivatives exhibited broad and intense fluorescence in the solid state, which was strongly dependent on the length of their alkoxy chain. Figure 4.7 shows the solid state fluorescence of thin films of these compounds prepared by cooling their melts between thin quartz slides. Upon excitation with 360 nm light, the films of **BC1** and **BC4** exhibited green fluorescence (λ_{max} ~520 nm), whereas **BC8** and **BC12** exhibited blue fluorescence (λ_{max} ~450 nm) (Figure 4.7). The solid state fluorescence spectra of these compounds are depicted in Figure 4.8.

BC1   BC4   BC8   BC12
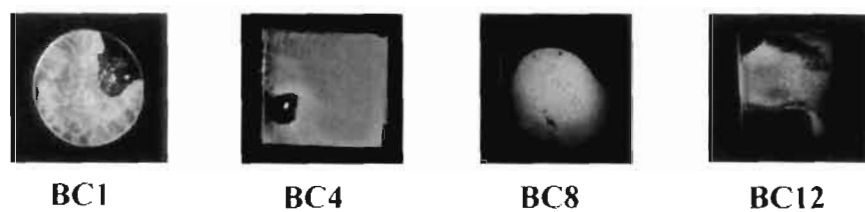
Figure 4.7. Fluorescence observed from solid films of the monoalkoxy-cyano-substituted diphenylbutadiene derivatives sandwiched between quartz slides upon excitation using 360 nm light.
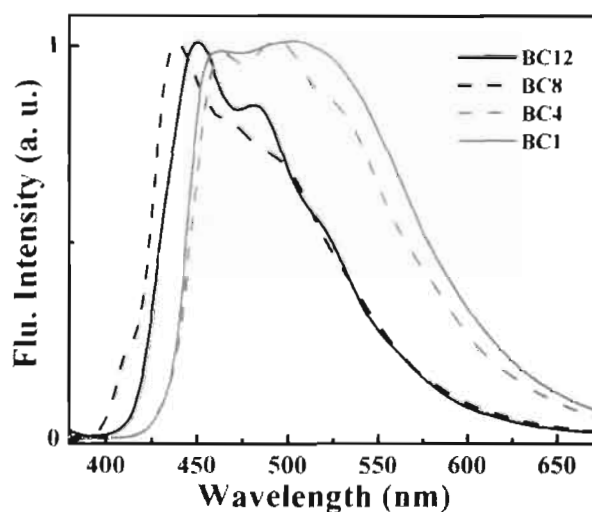
Figure 4.8. Fluorescence spectra of the monoalkoxy-cyano-substituted diphenyl butadiene derivatives upon excitation of solid films using 360 nm light.

The solid state fluorescence lifetimes were determined using the single photon counting technique. Fluorescence decay profiles of all derivatives showed good biexponential fit in all cases. The fluorescence lifetimes τ_1 and τ_2 and their fractional contributions, F_1 and F_2 as well as the fitting parameter, χ^2 are summarized in Table 4.5. For **BC8** and **BC12**, which emit in the blue region, the lifetime analysis indicated that the major component was short-lived with lifetimes of 1.1 ns (89.2%) and 1.4 ns (79.3%), respectively. For **BC4**, which emitted in the green region, the major component was the longer-lived species with a lifetime of

5.4 ns (87.6%). The decay characteristics of **BC1**, which is also green fluorescent, showed that the major component was a short-lived species with a fluorescence lifetime of 1.1 ns (91.2%).

Table 4.5. Fluorescence lifetime data of the monoalkoxy-cyano-substituted diphenyl butadiene derivatives in their solid state.

Compound	τ_1(ns)	F_1%	τ_2(ns)	F_2%	χ^2
BC1	1.12	91.2	4.30	8.8	1.10
BC4	2.38	12.4	5.41	87.6	1.02
BC8	1.17	89.2	3.64	10.8	1.33
BC12	1.38	79.3	3.12	20.7	0.93

The macroscopic properties of solids are controlled by their molecular structure and packing. Whereas the alkoxy chain length did not affect the fluorescence of the butadiene derivatives in solutions, it had a significant on their solid state fluorescence. This difference can be attributed to the difference in molecular packing in the solid state, which can be expected to be controlled by the length of the alkoxy chain. In order to investigate these aspects, we have obtained the powder X-ray diffraction (XRD) patterns of these derivatives. These patterns are indicative of the highly crystalline nature of these materials. All the derivative showed strong diffraction peaks corresponding to interplanar distance (*d*-spacing) of ~4 Å, which can be attributed to π-stacking as observed in several conjugated systems.[13-19] As a typical example, Figure 4.9 shows the XRD pattern obtained for **BC8** where a diffraction peak corresponding to 4 Å is clearly visible.
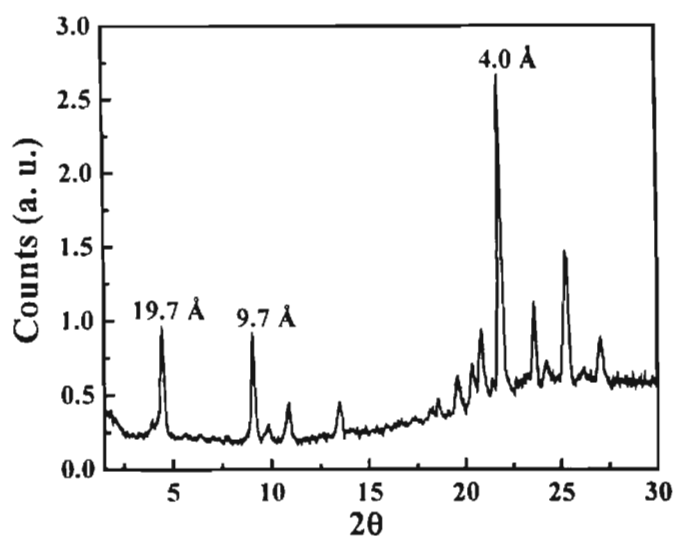
Figure 4.9. XRD pattern obtained for **BC8**.

Single crystal XRD analysis was carried out for **BC8** for which good crystals could be grown from a 2:8 benzene and methanol solvent mixture. Figure 4.10 shows the ORTEP diagram of **BC8**.[20]
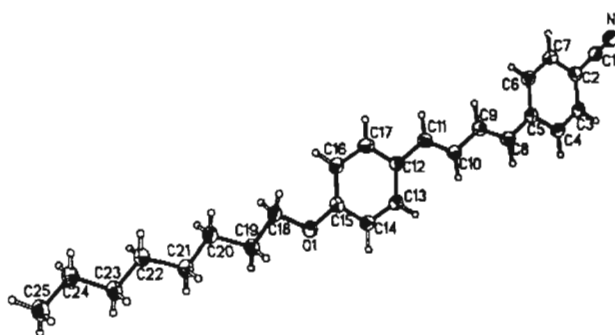
Figure 4.10. ORTEP diagram of **BC8**.

Figure 4.11 shows the packing plot of **BC8** projected on the a-c plane. The molecular packing of **BC8** clearly showed extended π-stacking along the b axis. The molecules in **BC8** were found to pack into a monoclinic crystal structure with a unit cell consisting of four molecules (Annexure A.2).
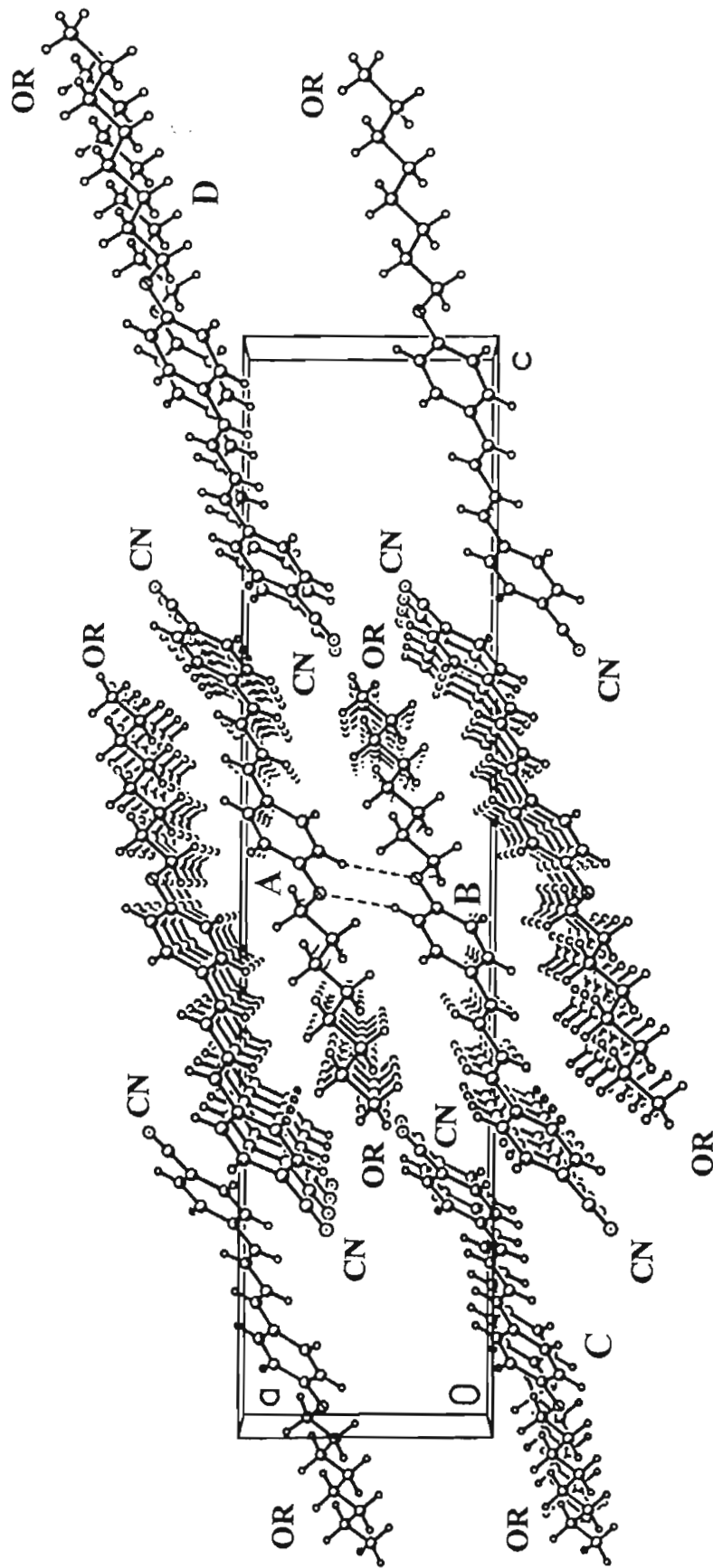
Figure 4.11. Packing plot of **BC8** projected on the a-c plane. The dotted lines represent CH··O interactions.

The supramolecular assembly of these molecules is stabilized by CH--O interactions between the oxygen atom of one molecule (labeled 'A' in Figure 4.11) and a phenyl hydrogen of the adjacent molecule (labeled 'B' in Figure 4.11), which are oriented in mutually opposite directions. Along with this pair, two molecules (labeled as 'C' and 'D' in Figure 4.11) present on either sides, with their cyano ends facing the center form a unit core that extends three-dimensionally into a supramolecular arrangement.

Weiss *et al.* have reported the molecular packing of a series of 4-alkyl-*N*-(4-cyanophenyl)piperidines (Figure 4.12).
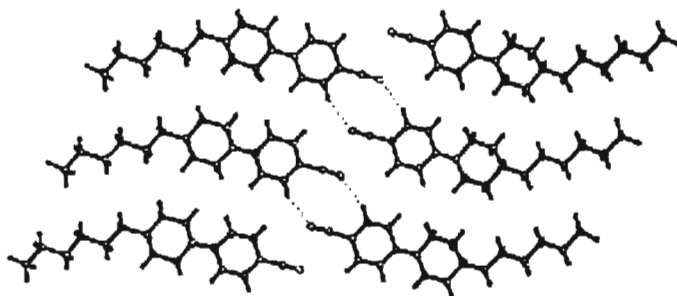
Figure 4.12. Layered molecular arrangement observed for 4-alkyl-N-(4-cyanophenyl) piperidines.

Unlike in the case of the alkoxy-cyano-substituted diphenylbutadiene derivatives, the 4-alkyl-*N*-(4-cyanophenyl)piperidines arrange in a layered fashion without any interdigitation. A schematic representation of the molecular alignment in the two different molecular systems is provided in Figure 4.13 in order to explain the role of the CH--O hydrogen bond in bringing about the interdigitation.
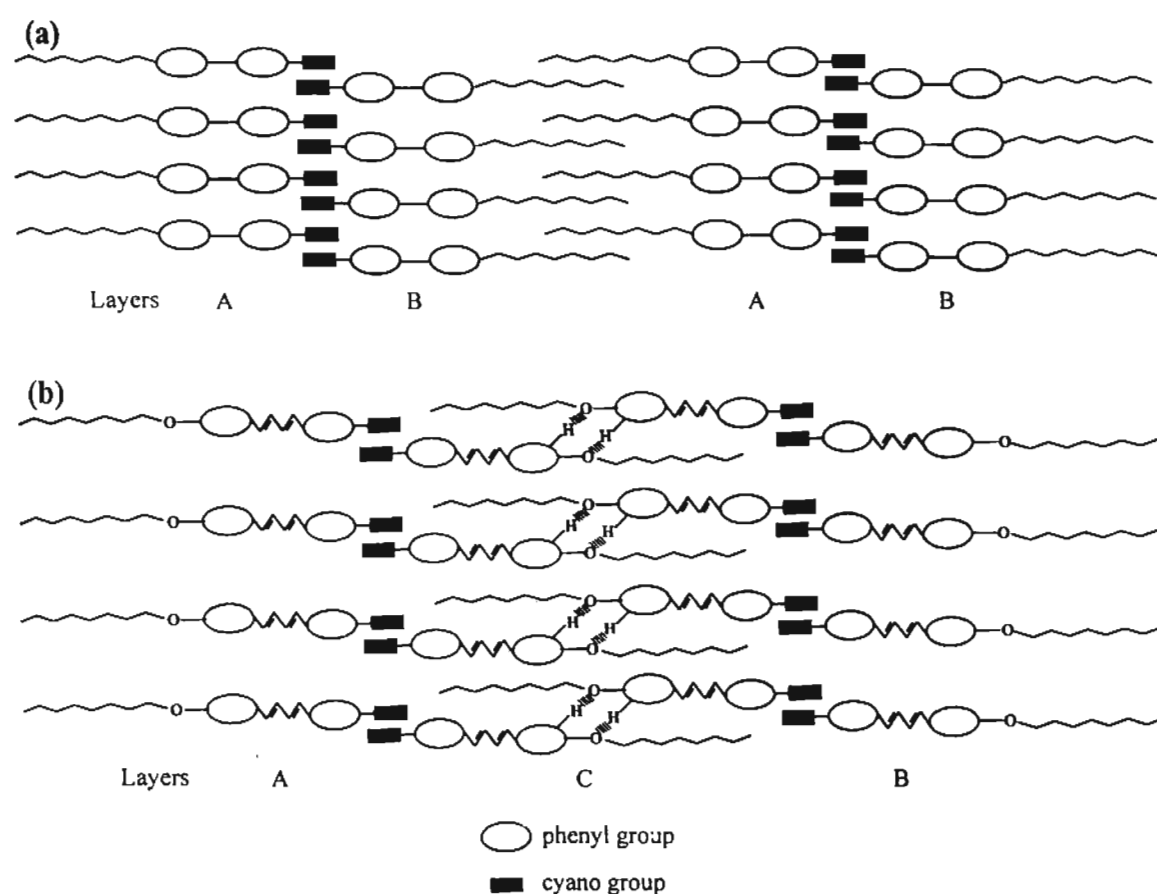
Figure 4.13. Pictorial representation of the molecular packing of (a) alkyl-substituted aromatic systems (b) **BC8**, where molecules are arranged in an interdigitated layered fashion, which is stabilized by the CH--O interactions.

The schematic diagram clearly shows that the 4-alkyl-*N*-(4-cyanophenyl)piperidine molecules have two distinctly different types of layers (A and B, Figure 4.13(a)) in which the cyano groups point in opposite directions. In the case of alkoxy-cyano-substituted diphenylbutadiene an additional layer (layer C, Figure 4.13 (b)) exists due to interdigitation of molecules brought about by the intermolecular CH--O hydrogen bonding. This study provides an interesting example of the role of the CH--O interactions in controlling crystal packing, which has been attracting increasing attention in recent years.[21-24] Although CH--O

interactions are weak compared to the conventional OH--O hydrogen bonding, they are nevertheless considered to be important in deciding crystal structure.

The solid state fluorescence of **BC8** was observed to change from blue to green when it was prepared as a freshly cooled melt. The solid state fluorescence maximum was found to shift from 450 nm (blue) to 520 nm (green) during this process. The fluorescence of the freshly cooled melt changes from green to blue over a period of 6 h at room temperature (27 °C) indicating that the green fluorescence arises from a metastable state. This gradual change was monitored by measuring their fluorescence and reflectance spectrum as well as their fluorescence decay profiles at regular time intervals. Figure 4.14A shows the changes in fluorescence spectrum with time. A shift in the emission maximum from 520 to 450 nm is clearly visible. The reflectance spectra measured during the same time period indicate a decrease in absorption of the band centered on 440 nm and an increase in absorption in the lower wavelength region (Figure 4.14B). These changes are clearly marked by an isosbestic point, indicating an equilibrium between two distinctly different states.
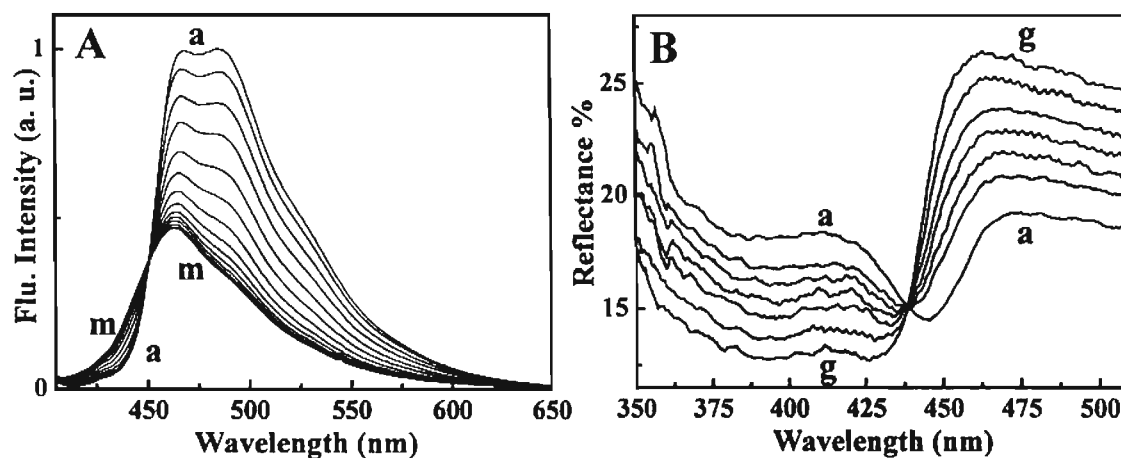
Figure 4.14. Temporal changes in the fluorescence and reflectance spectra of a freshly cooled melt of **BC8**; A) change in fluorescence spectrum (in steps of 30 min); λ_{ex}: 400 nm and B) changes in reflectance spectrum (in steps of 1 h).

Figure 4.15 shows temporal change in fluorescence decay profiles of a freshly cooled melt of **BC8**. The fluorescence decay profiles showed good biexponential fit in all cases and the data are summarized in Table 4.6. In the freshly cooled melt the major contribution to its overall fluorescence is from a long-lived species with a fluorescence lifetime of 6.1 ns (93.8%). With increasing time, a decrease in contribution of the long-lived species and a corresponding increase in that of the short-lived species to the overall fluorescence is observed. When the fluorescence lifetimes stabilize (>6 h) the major contribution to the overall fluorescence is from a short-lived species (1.3 ns, 94.2%).
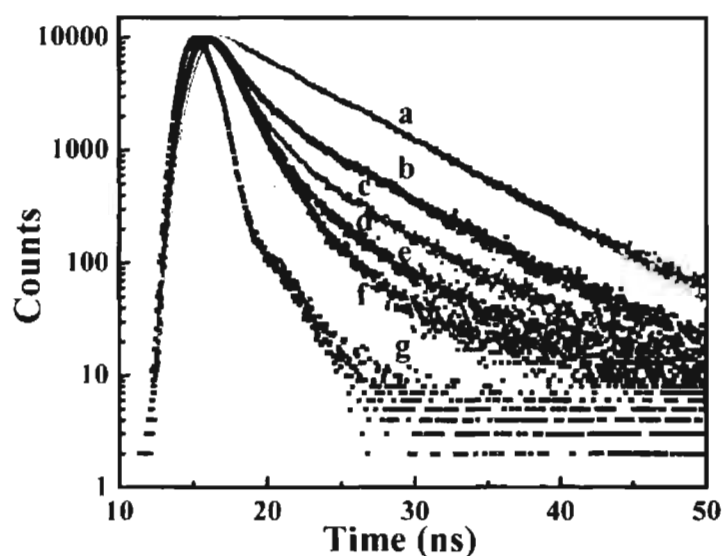
Figure 4.15. Fluorescence decay profiles recorded at regular time interval during the fluorescence change of freshly cooled melt of **BC8**. Time: a) 0 h, b) 1h, c) 2h, d) 3h, e) 4h and f) 6h; g) lamp profile.

Table 4.6. Temporal changes in the fluorescence lifetimes of a solid film of **BC8** obtained as a freshly cooled melt.

Hours (h)	τ_1 (ns)	$F_1\%$	τ_2 (ns)	$F_2\%$	χ^2
0	2.72	6.1	6.11	93.8	1.04
1	1.52	17.7	6.06	82.3	1.05
2	1.27	52.9	5.98	47.1	0.99
3	1.24	73.1	5.87	26.9	0.95
4	1.27	86.9	5.78	13.1	1.16
5	1.29	92.3	5.77	7.7	1.25
6	1.31	94.2	5.92	5.8	1.27

The change in solid state fluorescence properties of **BC8** in its stable state and when prepared as a freshly cooled melt may be attributed to its polymorphic nature. Powder XRD analyses of the stable blue fluorescing and metastable green

fluorescing states were indicative of clearly different crystal packing in the two

states. Figure 4.16 shows the XRD patterns, fluorescence and fluorescence spectra

of **BC8** in its stable and metastable states. The major changes are that the peak

corresponding to a d-spacing of 9.7 Å in the stable state shifts to 8.0 Å in the

metastable state, whereas that of 19.7 Å shifts to 25.3 Å. These changes can affect

the excitonic coupling of the molecules resulting in the changes in the

flouorescence of **BC8**.
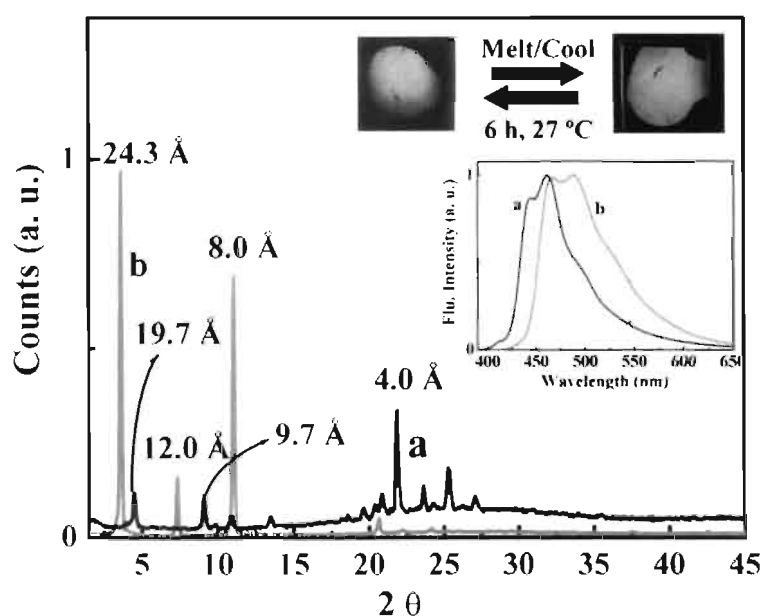
Figure 4.16. The XRD patterns, fluorescence spectra and the fluorescence colour of **BC8**. The green and blue coloured curves represent their respective fluorescent forms.

The solid state fluorescence of these derivatives is highly sensitive to

temperature. The fluorescence intensity of these derivatives was found to decrease

with increasing temperature. This change in fluorescence intensity was reversible

and upon cooling the original fluorescence intensity could be obtained. Figure

4.17A shows the temperature dependence of the solid state fluorescence of **BC4**

temperature induced fluorescence switching is shown in Figure 4.17B. The strong

dependence of fluorescence on temperature makes these materials potentially

useful as temperature sensors specially for mapping the temperature gradients of

surfaces.
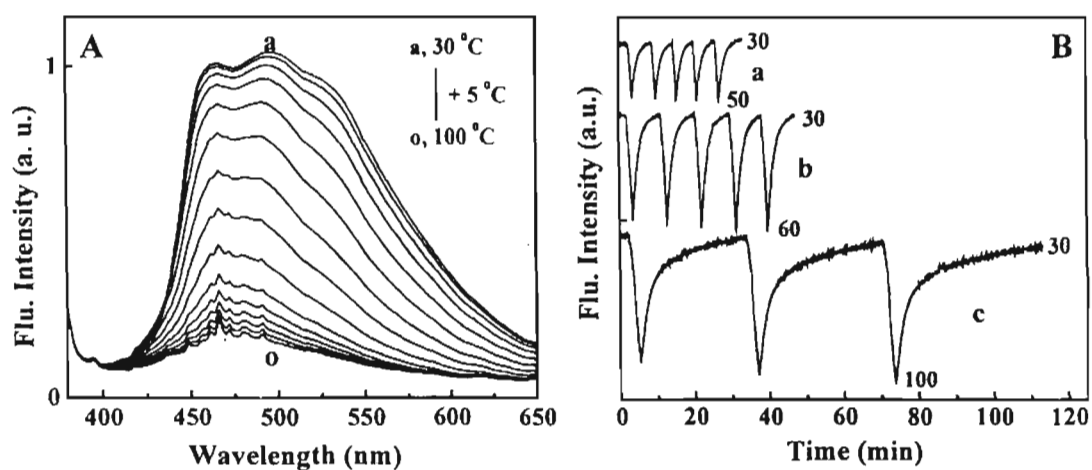
Figure 4.17. Temperature dependence of solid state fluorescence of **BC4**; A) Emission spectra at temperatures from 30 to 100 °C in steps of 5 °C, excitation wavelength: 360 nm, B) solid state fluorescence switching between (a) 30-50 °C, (b) 30-60 °C, (c) 30-100 °C; emission monitored at 520 nm; heating rate 20 °C/min and cooling rate 5 °C/min.

This loss of fluorescence intensity on increasing temperature can be

attributed to a direct consequence of the disruption of the crystal packing due to

increased mobility of the molecules at higher temperatures. **BC4** showed the

widest temperature range of 30-100 °C for fluorescence switching with a

sensitivity of 3 °C. Reports on temperature sensitive solid state fluorescent

materials are relatively rare.[25,26] Recently the use of temperature sensitivity of the

emission from a two component mixture consisting of perylene and *N*-allyl-*N*-

methylaniline (NA) for developing temperature sensors has been reported.[26]

The effect of temperature (Figure 4.17) on solid state fluorescence of these derivatives were studied with the samples exposed to 360 nm radiation throughout the experiment. Even after several cycles of heating and cooling the material do not undergo any permanent change in fluorescence (Figure 4.17B) indicating that the materials are stable and do not undergo any photochemical transformation during the measurement process. This can be attributed to the *EE* to the *EZ* and *ZE* photoisomerization being restricted in the solid state as reported for most polyenes. At elevated temperatures close to their melting point, however, the light from the excitation source brings about *E-Z* photoisomerization leading to a permanent decrease in fluorescence intensity (Figure 4.18).
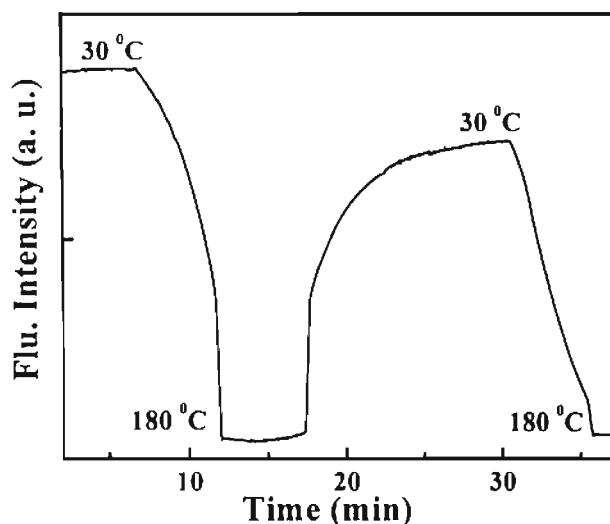
Figure 4.18. Solid state fluorescence switching of **BC4** carried out above its melting point with the sample continuously exposed to the excitation light during the heating and cooling cycles. Excitation: 360 nm; Emission: 520 nm.

By controlling the exposure of the sample to the excitation light fluorescence switching at high temperatures without any permanent loss fluorescence can be achieved. Figure 4.19 shows fluorescence switching of **BC4**

carried out between 30-150 °C. During the heating and cooling cycles the sample was protected from the excitation radiation and was exposed only after the final temperature was attained. Under these conditions permanent loss of fluorescence is not observed.
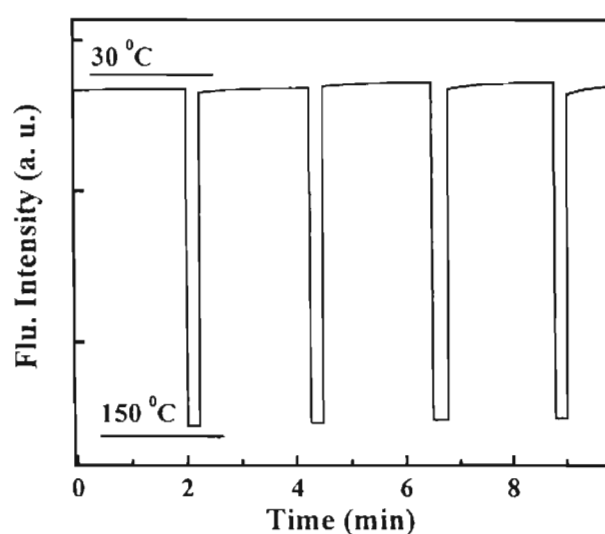
Figure 4.19: Solid state fluorescence switching of **BC4** carried out by raising the temperature of the sample above its melting point. The sample was protected from the excitation radiation during the heating and cooling cycles. Excitation: 360 nm; Emission: 520 nm.

The solid states of these materials could also be utilized for light induced recording of fluorescent images. Although, as described earlier, photoisomerization of the *EE* form does not occur in the solid state at ambient temperatures, this could be brought about at temperatures close to that of their melting point. Upon photolysis using 360 nm radiation of a solid film of **BC4** maintained at 130 °C, the solid state fluorescence colour at the photolysed regions was found to shift from green to blue. This can be attributed to the photoisomerization of the *EE* isomer to the *EZ* and *ZE* isomers. Figure 20 shows a photograph of a solid state photoimage recorded on a solid film of **BC4**.

Figure 4.20. Fluorescent image of the initials of the "Photochemistry Research Unit" recorded on a solid film of **BC4**. The sample was exposed to 360 nm light through an appropriate mask.

A solid film of **BC4** was prepared by cooling its melt between two quartz slides. The sample was photolysed for about 10 minutes, using 360 nm light from a high-pressure Xenon lamp coupled with a monochromator and a suitable photomask placed between the sample and the light source. The unphotolysed portions emit green light whereas the irradiated portions emit blue light when exposed under UV lamp. The fluorescent spectra of solid films of **BC4** before and after irradiation are shown in Figure 4.21.
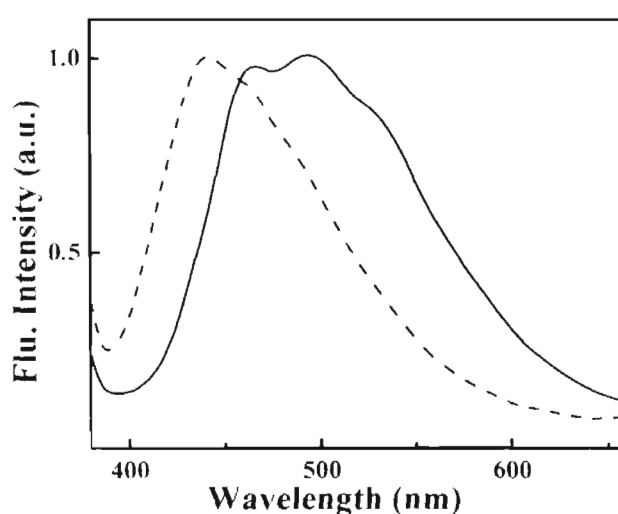
Figure 4.21. Solid state fluorescence spectra of **BC4** before ( ) and after (----) irradiation.

The blue fluorescence can be attributed to the solid state fluorescence of the mixture of *EZ* and *ZE* isomers. This was confirmed by recording the fluorescence in the solid state the pure *EZ* isomers of **BC1** and **BC12**, which emitted strongly in the blue region (Figure 4.22).

(a)   **(b)**
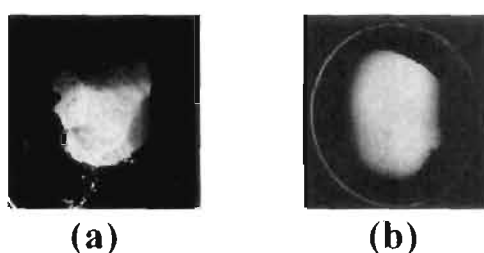
Figure 4.22. Fluorescence of thin solid films of the *EZ* isomers of a) **BC1** and b) **BC12** upon excitation using 360 nm light.

Since the photoisomers are thermally irreversible, the images were stable under ambient conditions. Photochromism has been extensively employed in optical recording of images. A drawback associated with most photochromic systems is that the 'write' and 'read' wavelengths are usually the same. Due to this, recorded images are destroyed by photoreactions initiated during the 'read' process. Tamaoki *et al.* have tried to overcome this limitation using macrocyclic azobenzene dimes containing two azobenzene chromophores.[27] At low intensities only one of the azo chromophores undergo *tran-cis* photoisomerization which rapidly reverts to its *trans* form. Photoisomerization of both the chromophores in the molecule using high intensity light resulted in a more permanent storage of information, since photoisomerization of both chromophores in the molecule brings about a conformational restriction which hinders the thermal *cis-trans*

isomerization in both chromophores. Using this system they have been able to record stable images by using high intensity light.

Light induced images recorded in the solid films of the alkoxy-cyano-substituted diphenylbutadienes do not undergo erasure during the 'read' process. This is because the write process has to be carried out at higher temperatures where the *EE* photoisomerization can occur whereas the 'read' process is carried out at ambient temperatures *EE* photoisomerization cannot occur. Thus, using this procedure stable fluorescent images could be recorded which could be read any number of times without damaging the quality of the image.

An interesting aspect of polyene photochemistry is that although the *EE* photoisomerization is blocked in the solid state, the reverse process namely *EZ* and *ZE* photoisomerization to the *EE* isomer is not restricted.[28-31] This aspect was discussed in Chapter 3 (page). Using this the images could be erased by photolysis of the films at ambient temperatures using 266 nm laser light (15 mJ, fourth harmonic of Nd:YAG, 10 ns pulse width).

4.3.4. Crystalline Phase Fluorescence Studies of Trialkoxy-Cyano-Substituted Diphenylbutadiene Derivatives (Chart 4.1)

The trialkoxy-cyano-substituted diphenylbutadiene derivatives also showed strong solid state fluorescence. Unlike in the case of the monoalkoxy derivatives, solid state fluorescence of these derivatives was not dependent on the length of the alkoxy chain. All the derivatives exhibited intense green solid state fluorescence

with the fluorescence maximum centered on 500 nm (Figure 4.23). Figure 4.24

shows the green fluorescence of the trialkoxy derivatives under a UV lamp.

Fluorescence lifetimes of these derivatives in their solid state were determined and

the data have been summarized in Table 4.7. Whereas the fluorescence decay

profiles of **TABC4** and **TABC12** could be fit using a biexponential equation that

of **TABC1** could only be fit by a triexponential equation. In all cases the major

emitting species was the component with the shortest lifetime.
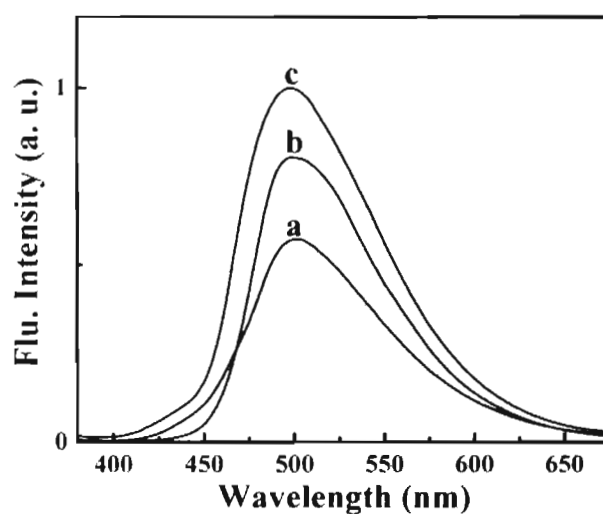
Figure 4.23. Fluorescence spectra of a) **TABC1** b) **TABC4** c) **TABC12**. Excitation: 360 nm.
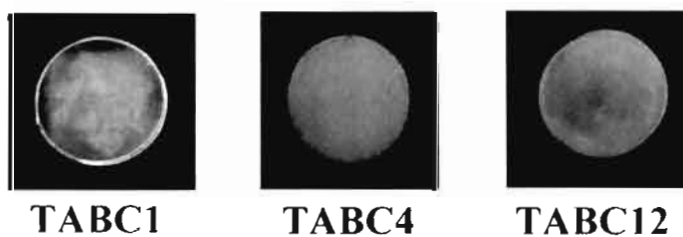
Figure 4.24. Solid state fluorescence of the trialkyloxy-cyano-substituted diphenyl butadiene derivatives. Excitation: 360 nm.

Table 4.7. Fluorescence lifetime data for the solid state fluorescence of the trialkyloxy-cyano-substituted diphenylbutadiene derivatives.

Compound	Ems (nm)	τ_1(ns)	F_1%	τ_2(ns)	F_2%	τ_3(ns)	F_3%	χ^2
TABC1	500	1.19	55.5	3.9	32.1	11.8	12.4	0.96
TABC4	500	3.24	80.0	6.29	20.0	-	-	1.12
TABC12	500	2.76	60.5	4.83	39.5	-	-	1.09

4.3.5. Fluorescence Properties of Alkylamino-cyano-Substituted Diphenylbutadienes

The alkoxy-cyano-substituted diphenylbutadiene derivatives exhibit strong solid state fluorescence in the blue-green portion of the visible range of electromagnetic radiation. In order to try and tune the solid state fluorescence of these butadiene derivatives the alkoxy group was replaced by an amino moiety. This was expected to reduce the HOMO-LUMO energy gap, which should result in a red-shifted fluorescence.

The fluorescence of 4-*N*,*N*-dimethylamino-4-cyano-1,4-diphenylbutadiene (**DMAB**) as well as their *trans-cis* photoisomerization in solution have been extensively studied. Here we report on the solid state fluorescence of this compound. Along with this we also report the solid state fluorescence of (1-(*N*,*N*-dimethylaminophenyl)-4-(cyanophenyl)-4-ethyl)buta-1,3-diene, (**DMABE**).

The solution phase absorption and fluorescence properties of **DMAB** and **DMABE** were indistinguishable. The fluorescence spectrum of **DMABE** in acetonitrile is shown in Figure 4.25.
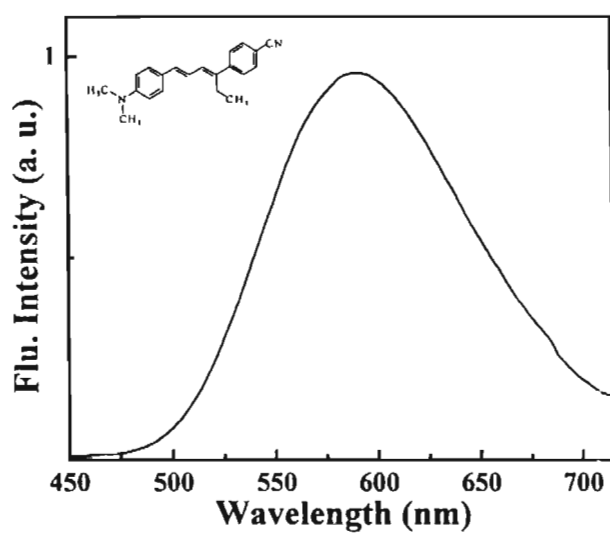
Figure 4.25. Fluorescence spectrum of **DMABE** in acetonitrile.

The fluorescence of **DMABE** in its crystalline form was found to be identical to that of **DMAB**. The emission maxima in both cases were centered on 630 nm Figure 4.26 shows the crystalline state emission spectrum of **DMAB**.
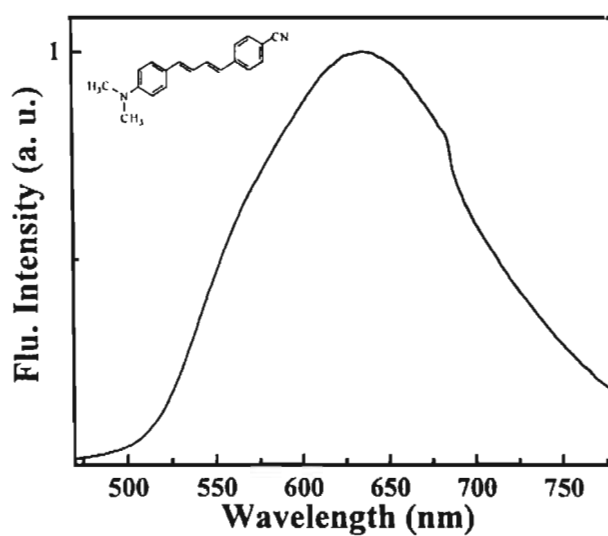
Figure 4.26. Fluorescence spectrum of **DMAB** in crystalline state.

The melting behaviour of the two compounds were very different. Whereas **DMABE** melted sharply between 141-143 °C, **DMAB** melted only at ~250 °C, which was accompanied by decomposition. The melt of **DMABE** could be cooled to form thin solid films. Thin films of **DMABE** obtained in this manner between quartz plates exhibited fluorescence in the yellow region of the spectrum with the fluorescence maximum being centered on 570 nm (Figure 4.27). The fluorescence spectrum of this cooled melt was quite similar to its solution fluorescence indicating that in this case the solid state fluorescence was due to the molecular fluorescence. The red emission observed in the crystalline state could be attributed to exciton coupling arising out of a favourable crystal packing.
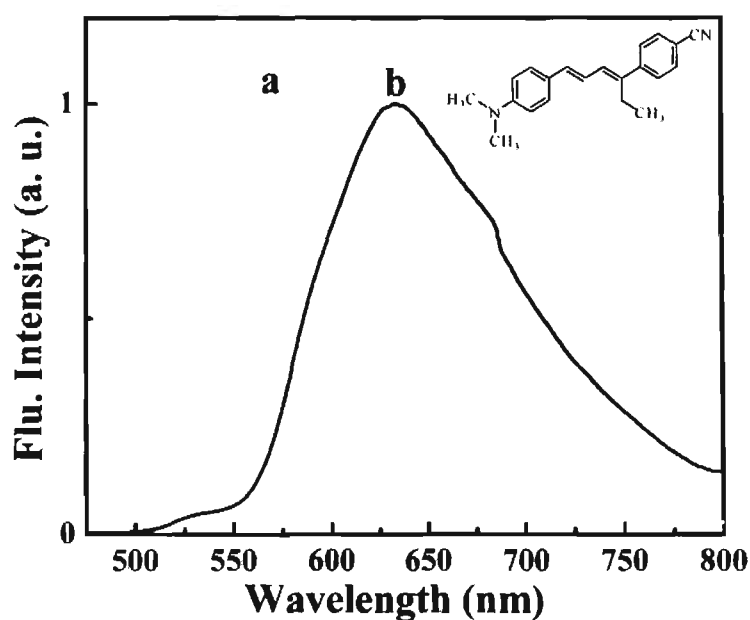
Figure 4.27. Fluorescence spectra of **DMABE** in a) cooled melt and b) crystalline state; Excitation: 400 nm.

The solution and solid state fluorescence lifetime data for the alkylamino-cyano-substituted diphenylbutadienes are summarized in Table 4.8. The fluorescence decay profiles could be fit to a biexponential equation. The major component (>95%) to the overall fluorescence was a short-lived species, with lifetimes of ~0.5 ns in solution and ~1 ns in the solid state.

Table 4.8. Fluorescence lifetime data for the fluorescence of alkylamino-cyano-substituted diphenylbutadiene derivatives.

Compound	Ems. (nm)	τ_1(ns)	F_1%	τ_2(ns)	F_2%	χ^2
DMABE (in acetonitrile)	590	0.52	97.7	5.5	2.3	0.97
DMAB (in acetonitrile)	590	0.58	98.5	5.98	1.5	0.94
DMABE (cooled melt)	570	1.01	97.4	5.43	2.6	1.01
DMABE (Crystalline state)	600	1.09	97.0	6.64	3.0	1.13
DMAB (Crystalline state)	600	1.35	97.0	5.89	3.0	1.14

The studies described in this section of the thesis show that by suitable substitution the solid state fluorescence of donor-acceptor-substituted diphenylbutadienes can be tuned over the entire visible region of electromagnetic spectrum. The monoalkoxy-cyano substituted diphenylbutadiene derivatives exhibited both blue and green luminescence. All trialkoxy-cyano-substituted

diphenylbutadiene derivatives exhibited green fluorescence. By replacing the alkoxy group with an alkylamino group the solid state fluorescence of these diphenylbutadiene derivatives shift to the red region of the spectrum. Both **DMAB** and **DMABE** exhibited red luminescence in their crystal state. Thin films of **DMABE** prepared from their melt however exhibited yellow emission. The solid state fluorescence of these derivatives are shown in Figure 4.28.
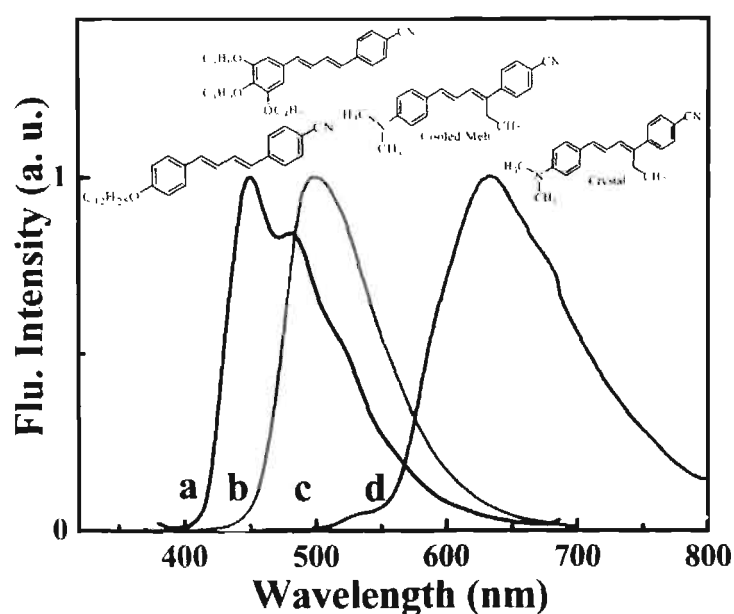
Figure 4.28. Solid state fluorescence exhibited by various diphenylbutadiene derivatives; a) **BC12**, b) **TABC4**, c) **DMABE** film obtained from the melt and d) **DMABE** in the crystalline phase.

4.3.6. Single Crystal X-ray Analysis of DMABE

DMABE was found to crystallize into fairly large good quality crystals. The single crystal XRD analysis of **DMABE** was carried out (Annexure A.3).

Figure 4.29 shows the ORTEP diagram obtained for **DMABE**.[20] The ethyl group in **DMABE** was found to protrude out of the plane, which contained the rest of the molecule.
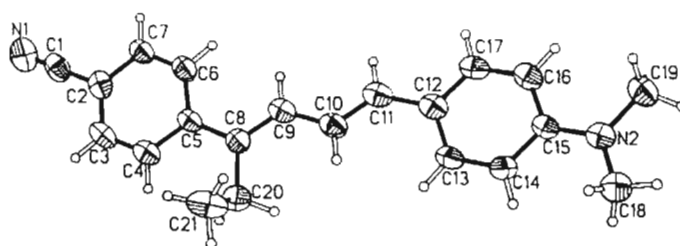
Figure 4.29. ORTEP diagram of **DMABE**.

Figure 4.30 shows the molecular packing plot of **DMABE** projected on the b-c plane. The molecules in the packing plot have been indicated as green or red depending upon their orientation. From the figure it becomes evident that two distinctly different types of molecular arrangements exist. A clear difference from the alkoxy-cyano-substituted diphenylbutadienes is the absence of π-stacking in **DMABE**. The presence of the ethyl group, which sticks out of the molecular plane, may play a role in preventing π-stacking in **DMABE**. This may also explain the difference in melting behaviour of **DMAB** and **DMABE**. In the absence of π-stacking in **DMABE**, the energy required to break the crystal lattice could be lower, thereby resulting in a substantially lower melting point.
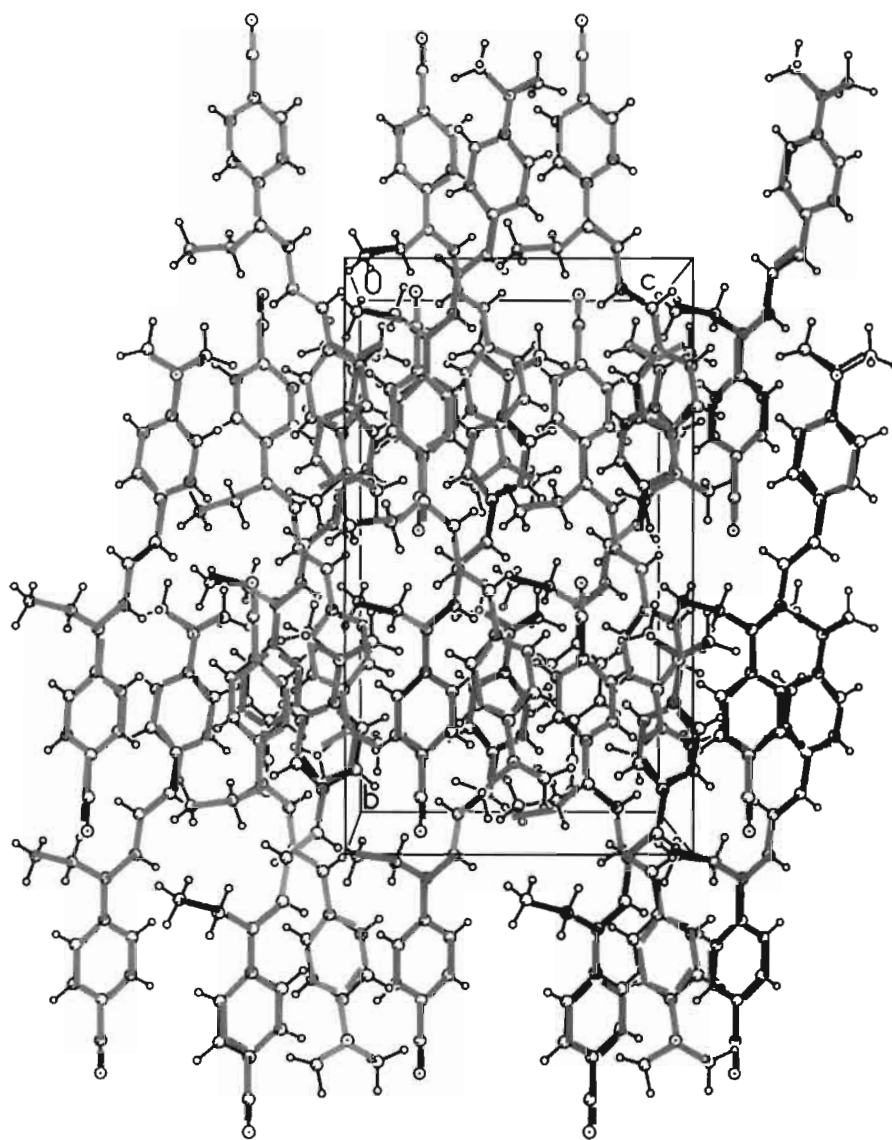
Figure 4.30. Packing plot of **DMABE** projected on the b-c plane. The red and green colours represent oppositely oriented molecules.

4.4. Experimental Section

Powder X-ray diffraction (XRD) patterns were recorded on a Rigaku Miniflex diffractometer using Cu-Kα radiation (λ = 1.540 Å) with Ni-filter. Solid state emission spectra were recorded using a front face emission scan mode on a SPEX Fluorolog spectrometer. Reflectance spectra were recorded using a Shimadzu integrating sphere assembly attached to a Shimadzu UV-Vis-NIR 3101 PC spectrophotometer. $BaSO_4$ was used as the 100% reflectance standard. Temperature variation of the sample for the solid state fluorescence switching experiment was done using a Linkam THMS 600 heating and freezing stage connected to a Linkam TP92 temperature programmer. Laser photolysis was carried out using the fourth harmonic (266 nm, 15 mJ/pulse, pulse width 10 ns) of a Quanta Ray GCR-12 Nd:YAG laser. Color photographs of samples were taken using a digital camera and the colors corrected in Adobe PhotoDeluxe Business Edition 1.1 software to match the visual appearance.

Single crystal molecular structure and packing analyses were carried out on a Siemens SMART-1K CCD diffractometer with Mo source and graphite monochromator.

Characterization of (1-(*N,N*-dimethylaminophenyl)-4-(cyanophenyl)-4-ethyl)buta-1,3-diene (DMABE)

DMABE: Yield: 40%; mp: 142-143 °C; IR v_{max} (KBr): 3744, 3036, 2921, 2355, 2213, 1573, 1512, 1357, 1175, 960, 811 cm^{-1}; ^{1}H NMR (CDCl$_3$, 300 MHz):δ 1.10 (t, 3H, CH$_3$), 2.69-2.77 (q, 2H, CH$_2$), 2.99 (s, 6H, N(CH$_3$)$_2$), 6.59-6.68 (m, 2H,

olefinic), 6.69 (d, 2H, aromatic), 6.92-7.01 (dd, 1H, olefinic), 7.36 (d, 2H, aromatic), 7.52 (d, 2H, aromatic), 7.59 (d, 2H, aromatic) ppm; ^{13}C NMR (CDCl$_3$, 75 MHz): δ 14.01, 22.73, 40.36, 109.57, 112.33, 119.26, 120.70, 125.59, 126.22, 127.80, 130.50, 132.12, 135.83, 138.60, 146.87, 150.35 ppm.

4.5. Conclusion

The solid state fluorescence of some alkoxy-cyano and alkylamino-cyano-substituted diphenylbutadienes have been studied. By bringing about suitable structural modifications of the butadiene chromophore it has been possible to tune the solid state fluorescence of these materials almost over the entire visible range, with the alkoxy-cyano-substituted diphenylbutadienes emitting in the blue-green region and the alkylamino-cyano-substituted derivatives emitting in the yellow-red region. The role of molecular packing in determining the solid state fluorescence of these compounds has been examined. The use of these materials for recording fluorescent images and as temperature sensors has also been explored.

4.6. References

1) Service, R. F. *Science* **1996**, *273*, 878.

2) Sheats, J. R.; Antoniadis, H.; Hueshcen, M.; Leonard. W.; Miller. J.; Moon. R.; Roitman, D.; Stocking, A. *Science* **1996**, *273*, 884.

3) Chen, C. H.; Shi, J.; Tang, C. W. *Macromol. Symp.* **1997**, *125*, 1.

4) Kraft, A.; Grimsdale, A. C.; Holmes, A. B. *Angew. Chem. Int. Ed.* **1998**, *37*, 403.

5) Sheikh-Ali, B. M.; Rapta, M.; Jameson, G. B.; Cui, C.; Weiss, R. G. *J. Phys. Chem.* **1994**, *98*, 10412.

6) Lewis, F. D.; Yang, J.-S. *J. Phys. Chem. B* **1997**, *101*, 1775.

7) Jenekhe, S. A.; Osaheni, J. A. *Science* **1994**, *265*, 765.

8) Otsubo, T.; Kohda, T.; Misumi, S. *Bull. Chem. Soc. Jpn.* **1980**, *53*, 512.

9) Saigusa, H.; Lim, E. C. *Acc. Chem. Res.* **1996**, *29*, 171.

10) Braatz, H.; Hecht, S.; Seifert, H.; Helm, S.; Bendig, J.; Rettig, W. *J. Photochem. Photobiol. A: Chem.* **1999**, *123*, 99.

11) Davis, R.; Das, S.; George, M.; Druzhinin, S.; Zachariasse, K. *J. Phys. Chem. A* **2001**, *105*, 4790.

12) Demeter, A.; Druzhnin, S.; George, M.; Haselbach, E.; Roulin, J.-L.; Zachariasse, K. A. *Chem. Phys. Lett.* **2000**, *323*, 351.

13) Stevens, B. *Spectrochimica Acta 439* **1962**, *18*, 439.

14) Cotrait, M.; Marsau, P.; Kessab, L.; Grelier, S.; Nourmamode, A.; Castellan, A. *Aust. J. Chem.* **1994**, *47*, 423.

15) Munakata, M.; Wu, L. P.; Yamamoto, M.; Kuroda-Sowa, T.; Maekawa, M. *J. Am. Chem. Soc.* **1996**, *118*, 3117.

16) Shetty, A. S.; Zhang, J.; Moore, J. S. *J. Am. Chem. Soc.* **1996**, *118*, 1019.

17) Graf, D. D.; Duan, R. G.; Campbell, J. P.; Miller, L. L.; Mann, K. R. *J. Am. Chem. Soc.* **1997**, *119*, 5888.

18) Yamamoto, T.; Komarudin, D.; Arai, M.; Lee, B. L.; Suganuma, H.; Asakawa, N.; Inoue, Y.; Kubota, K.; Sasaki, S.; Fukuda, T.; Matsuda, H. *J. Am. Chem. Soc.* **1998**, *120*, 2047.

19) Azumi, R.; Götz, G.; Debaerdemaeker, T.; Bäuerle, P. *Chem. Eur. J.* **2000**, *6*, 735.

20) X-ray structure determination was carried out by Dr. Nigam P. Rath, D. o. C., University of Missourie St. Louis, MO 63121, USA .

21) Desiraju, G. R. *Acc. Chem. Res.* **1996**, *29*, 441.

22) Kuduva, S. S.; Craig, D. C.; Nangia, A.; Desiraju, G. R. *J. Am. Chem. Soc.* **1999**, *121*, 1936.

23) Gu, Y.; Kar, T.; Scheiner, S. *J. Am. Chem. Soc.* **1999**, *121*, 9411.

24) Scheiner, S.; Grabowski, S. J.; Kar, T. *J. Phys. Chem. A* **2001**, *105*, 10607.

25) Engeser, M.; Fabbrizzi, L.; Licchelli, M.; Sacchi, D. *Chem. Commun.* **1999**, 1191.

26) Chandrasekharan, N.; Kelly, L. A. *J. Am. Chem. Soc.* **2001**, *123*, 9898.

27) Tamaoki, N.; Yoshimura, S.; Yamaoka, T. *Thin Solid Films* **1992**, *221*, 132.

28) Liu, R. S. H. *Acc. Chem. Res.* **2001**, *34*, 555.

29) Dellinger, B.; Kasha, M. *Chem. Phys. Lett.* **1976**, *38*, 9.

30) Sun, Y.-P.; Saltiel, J.; Hoburg, E. A.; Waldeck, D. *J. Phys. Chem.* **1991**, *53*, 10336.

31) Liu, R. S. H.; Asato, A. E.; Denny, M. *J. Am. Chem. Soc.* **1983**, *105*, 4829.

ANNEXURE

A.1. X-ray Crystallographic Data for BN5

Empirical formula	C22 H19 N O2
Formula weight	329.38
Temperature	200(2) K
Wavelength	0.71073 Å
Crystal system	Orthorhombic
Space group	Pbca
Unit cell dimensions	a = 13.756(2) Å α= 90°.
	b = 14.839(3) Å β= 90°.
	c = 16.821(2) Å γ = 90°.
Volume	3433.7(10) Å^3
Z	8
Density (calculated)	1.274 Mg/m^3
Absorption coefficient	0.081 mm^{-1}
F(000)	1392
Crystal size	0..90 x 0.80 x 0.70 mm^3
Theta range for data collection	3.66 to 25.03°.
Limiting indices	0≤h≤16, -3≤k≤17, -20≤l≤20
Reflections collected	3052
Independent reflections	3052 [R(int) = 0.0190]
Refinement method	Full-matrix least-squares on F^2
Data / restraints / parameters	3021 / 0 / 227
Goodness-of-fit on F^2	1.043
Final R indices [I>2sigma(I)]	R1 = 0.0647, wR2 = 0.1591
R indices (all data)	R1 = 0.0833, wR2 = 0.1838
Largest diff. peak and hole	0.278 and -0.282 e.Å^{-3}

Table A.1.1. Selected torsion angles for **BN5**.

1.	-175.24 (0.24)	N15 - C1 - C2 - C3
2.	3.00(0.24)	C20 - C1 - C2 - C3
3.	175.58 (0.24)	C1 - C2 - C3 - C4
4.	-1.77 (0.45)	C2 - C3 - C4 - C5
5.	179.65 (0.25)	C2 - C3 - C4 - C12
6.	1.76 (0.44)	C3 - C4 - C5 - O14
7.	-179.50 (0.24)	C12 - C4 - C5 - O14
8.	-179.31 (0.24)	C3 - C4 - C5 - C6
9.	-0.58 (0.27)	C12 - C4 - C5 - C6
10.	1.35 (0.41)	O14 - C5 - C6 - C17
11.	-177.64 (0.24)	C4 - C5 - C6 - C7
12.	-179.95 (0.23)	O14 - C5 - C6 - C11
13.	1.07 (0.26)	C4 - C5 - C6 - C11
14.	-1.87 (0.37)	C11 - C6 - C7 - C8
15.	176.70 (0.24)	C5 - C6 - C7 - C8
16.	1.55 (0.41)	C6 - C7 - C8 - C9
17.	0.04 (0.45)	C7 - C8 - C9 - C10
18.	-1.31 (0.44)	C8 - C9 - C10 - C11
19.	1.00 (0.40)	C9 - C10 - C11 - C6
20.	-175.42 (0.26)	C9 - C10 - C11 - C12
21.	0.60 (0.37)	C7 - C6 - C11 - C10
22.	-178.24 (0.23)	C5 - C6 - C11 - C10
23.	177.72 (0.22)	C7 - C6 - C11 - C12
24.	-1.12 (0.27)	C5 - C6 - C11 - C12
25.	-3.22 (0.44)	C3 - C4 - C12 - O13
26.	177.94 (0.28)	C5 - C4 - C12 - O13
27.	178.76 (0.23)	C3 - C4 - C12 - C11
28.	-0.08 (0.27)	C5 - C4 - C12 - C11

29.	-0.57 (0.46)	C10 - C11 - C12 - O13
30.	-177.32 (0.27)	C6 - C11 - C12 - O13
31.	177.51 (0.27)	C10 - C11 - C12 - C4
32.	0.76 (0.28)	C6 - C11 - C12 - C4
33.	1.30 (0.39)	C2 - C1 - N15 - C16
34.	-177.04 (0.23)	C20 - C1 - N15 - C16
35.	-177.88 (0.24)	C2 - C1 - N15 - C19
36.	3.78 (0.36)	C20 - C1 - N15 - C19
37.	175.61 (0.26)	C1 - N15 - C16 - C17
38.	-5.11 (0.33)	C19 - N15 - C16 - C17
39.	-9.78 (0.38)	N15 - C16 - C17 - C18
40.	21.37 (0.44)	C16 - C17 - C18 - C19
41.	-163.12 (0.28)	C1 - N15 - C19 - C18
42.	17.61 (0.34)	C16 - N15 - C19 - C18
43.	-23.82 (0.40)	C17 - C18 - C19 - N15
44.	79.88 (0.29)	N15 - C1 - C20 - C25
45.	-98.45 (0.29)	C2 - C1 - C20 - C25
46.	-96.51 (0.28)	N15 - C1 - C20 - C21
47.	85.15 (0.31)	C2 - C1 - C20 - C21
48.	-0.90 (0.37)	C25 - C20 - C21 - C22
49.	175.50 (0.23)	C1 - C20 - C21 - C22
50.	-0.42 (0.41)	C20 - C21 - C22 - C23
51.	1.25 (0.42)	C21 - C22 - C23 - C24
52.	-0.76 (0.40)	C22 - C23 - C24 - C25
53.	-0.55 (0.39)	C23 - C24 - C25 - C20
54.	1.38 (0.37)	C21 - C20 - C25 - C24
55.	-175.09 (0.23)	C1 - C20 - C25 - C24

Table A.1.2. Atomic coordinates (x 10^4) and equivalent isotropic displacement parameters (Å^2x 10^3) for **BN5**. U(eq) is defined as one third of the trace of the orthogonalized U^{ij} tensor.

C(1)	11629(2)	665(2)	8098(2)	40(1)
C(2)	11012(2)	1132(2)	7583(2)	43(1)
C(3)	11015(2)	978(2)	6770(2)	42(1)
C(4)	10397(2)	1355(2)	6206(1)	40(1)
C(5)	9597(2)	1971(2)	6318(1)	38(1)
C(6)	9172(2)	2152(2)	5512(1)	39(1)
C(7)	8422(2)	2712(2)	5291(2)	47(1)
C(8)	8204(2)	2791(2)	4485(2)	57(1)
C(9)	8720(2)	2297(2)	3925(2)	62(1)
C(10)	9457(2)	1718(2)	4149(2)	54(1)
C(11)	9685(2)	1655(2)	4950(1)	42(1)
C(12)	10473(2)	1145(2)	5359(2)	46(1)
O(13)	11075(2)	668(2)	5030(1)	72(1)
O(14)	9300(1)	2312(1)	6942(1)	47(1)
N(15)	11578(2)	768(1)	8885(1)	45(1)
C(16)	10870(2)	1355(2)	9280(2)	57(1)
C(17)	11027(3)	1204(2)	10161(2)	69(1)
C(18)	11686(3)	430(3)	10226(2)	90(1)
C(19)	12221(2)	325(2)	9469(2)	52(1)
C(20)	12363(2)	4(2)	7805(1)	39(1)
C(21)	13277(2)	281(2)	7553(2)	49(1)
C(22)	13963(2)	-359(2)	7337(2)	56(1)
C(23)	13753(2)	-1264(2)	7373(2)	52(1)
C(24)	12843(2)	-1533(2)	7612(2)	51(1)
C(25)	12147(2)	-909(2)	7824(2)	45(1)

Table A.1.3. Bond lengths [Å] and angles [°] for **BC5**.

C(1)-N(15)	1.334(3) ·	N(15)-C(1)-C(2)	121.8(2)
C(1)-C(2)	1.396(3)	N(15)-C(1)-C(20)	116.1(2)
C(1)-C(20)	1.492(3)	C(2)-C(1)-C(20)	122.1(2)
C(2)-C(3)	1.387(4)	C(3)-C(2)-C(1)	122.0(2)
C(3)-C(4)	1.391(3)	C(2)-C(3)-C(4)	127.2(2)
C(4)-C(5)	1.443(3)	C(3)-C(4)-C(5)	129.2(2)
C(4)-C(12,	1.462(3)	C(3)-C(4)-C(12)	122.4(2)
C(5)-O(14)	1.234(3)	C(5)-C(4)-C(12)	108.5(2)
C(5)-C(6)	1.500(3)	O(14)-C(5)-C(4)	128.5(2)
C(6)-C(7)	1.376(3)	O(14)-C(5)-C(6)	124.5(2)
C(6)-C(11)	1.392(3)	C(4)-C(5)-C(6)	107.0(2)
C(7)-C(8)	1.395(4)	C(7)-C(6)-C(11)	121.1(2)
C(8)-C(9)	1.389(4)	C(7)-C(6)-C(5)	130.1(2)
C(9)-C(10)	1.382(4)	C(11)-C(6)-C(5)	108.8(2)
C(10)-C(11)	1.386(4)	C(6)-C(7)-C(8)	118.3(3)
C(11)-C(12)	1.490(4)	C(9)-C(8)-C(7)	120.4(3)
C(12)-O(13)	1.223(3)	C(10)-C(9)-C(8)	121.2(3)
N(15)-C(16)	1.465(3)	C(9)-C(10)-C(11)	118.3(3)
N(15)-C(19)	1.477(3)	C(10)-C(11)-C(6)	120.7(2)
C(16)-C(17)	1.513(4)	C(10)-C(11)-C(12)	130.4(2)
C(17)-C(18)	1.467(5)	C(6)-C(11)-C(12)	108.9(2)
C(18)-C(19)	1.478(4)	O(13)-C(12)-C(4)	127.8(3)
C(20)-C(25)	1.388(3)	O(13)-C(12)-C(11)	125.3(2)
C(20)-C(21)	1.389(4)	C(4)-C(12)-C(11)	106.9(2)
C(21)-C(22)	1.387(4)	C(1)-N(15)-C(16)	123.6(2)
C(22)-C(23)	1.375(4)	C(1)-N(15)-C(19)	125.3(2)
C(23)-C(24)	1.373(4)	C(16)-N(15)-C(19)	111.1(2)
C(24)-C(25)	1.379(4)	N(15)-C(16)-C(17)	105.2(2)
		C(18)-C(17)-C(16)	106.1(3)
	.	C(17)-C(18)-C(19)	109.1(3)
		N(15)-C(19)-C(18)	103.1(2)
		C(25)-C(20)-C(21)	119.3(2)
		C(25)-C(20)-C(1)	119.3(2)
		C(21)-C(20)-C(1)	121.3(2)
		C(22)-C(21)-C(20)	119.5(2)
		C(23)-C(22)-C(21)	121.0(3)
		C(24)-C(23)-C(22)	119.2(3)
		C(23)-C(24)-C(25)	120.9(2)
		C(24)-C(25)-C(20)	120.0(2)

Table A.1.4. Anisotropic displacement parameters $(\text{Å}^2 \text{x } 10^3)$ for **BN5**. The anisotropic

displacement factor exponent takes the form:$-2\pi^2[h^2 a^{*2}U^{11} + ... + 2 h k a^* b^* U^{12}]$

	U^{11}	U^{22}	U^{33}	U^{23}	U^{13}	U^{12}
C(1)	45(1)	33(1)	43(1)	3(1)	-5(1)	-1(1)
C(2)	50(1)	36(1)	43(1)	2(1)	-3(1)	4(1)
C(3)	45(1)	39(1)	43(1)	4(1)	0(1)	1(1)
C(4)	47(1)	39(1)	35(1)	3(1)	1(1)	4(1)
C(5)	50(1)	31(1)	32(1)	2(1)	0(1)	-3(1)
C(6)	48(1)	34(1)	34(1)	3(1)	-3(1)	-5(1)
C(7)	53(2)	42(1)	47(1)	1(1)	-8(1)	0(1)
C(8)	61(2)	57(2)	53(2)	10(1)	-19(1)	0(1)
C(9)	75(2)	73(2)	38(2)	7(1)	-17(1)	-12(2)
C(10)	61(2)	66(2)	34(1)	-4(1)	0(1)	-10(1)
C(11)	47(1)	44(1)	34(1)	1(1)	2(1)	-6(1)
C(12)	49(1)	49(1)	40(1)	-3(1)	6(1)	2(1)
O(13)	69(1)	93(2)	53(1)	-9(1)	11(1)	29(1)
O(14)	64(1)	45(1)	33(1)	-3(1)	2(1)	11(1)
N(15)	54(1)	42(1)	40(1)	0(1)	-7(1)	11(1)
C(16)	66(2)	54(2)	51(2)	-2(1)	0(1)	18(1)
C(17)	75(2)	86(2)	45(2)	-6(2)	-4(2)	21(2)
C(18)	122(3)	104(3)	43(2)	6(2)	7(2)	54(3)
C(19)	59(2)	52(2)	44(1)	3(1)	-11(1)	8(1)
C(20)	46(1)	36(1)	35(1)	2(1)	-6(1)	0(1)
C(21)	54(2)	44(1)	48(1)	2(1)	-4(1)	-7(1)
C(22)	44(2)	71(2)	53(2)	-1(1)	2(1)	-1(1)
C(23)	56(2)	58(2)	42(2)	-7(1)	-7(1)	14(1)
C(24)	65(2)	38(1)	50(2)	-4(1)	-10(1)	5(1)
C(25)	47(1)	39(1)	48(1)	2(1)	-4(1)	-1(1)

A.2. X-ray Crystallographic Data for BC8

Empirical formula	C25 H29 N O
Formula weight	359.49
Temperature	220(2) K
Wavelength	0.71073 Å
Crystal system	Monoclinic
Space group	$P2_1/c$
Unit cell dimensions	a = 8.8931(8) Å $\quad \alpha = 90°$.
	b = 6.1431(5) Å $\quad \beta = 91.066(6)°$.
	c = 37.907(3) Å $\quad \gamma = 90°$.
Volume	2070.5(3) Å^3
Z	4
Density (calculated)	1.153 Mg/m^3
Absorption coefficient	0.069 mm^{-1}
F(000)	776
Crystal size	0.34 x 0.20 x 0.08 mm^3
Theta range for data collection	2.15 to 26.00°.
Index ranges	$-10 \leq h \leq 10, -7 \leq k \leq 7, -46 \leq l \leq 46$
Reflections collected	17785
Independent reflections	4072 [R(int) = 0.078]
Completeness to theta = 26.00°	99.7 %
Absorption correction	None
Max. and min. transmission	0.9945 and 0.9769
Refinement method	Full-matrix least-squares on F^2
Data / restraints / parameters	4072 / 0 / 244
Goodness-of-fit on F^2	0.999
Final R indices [I>2sigma(I)]	R1 = 0.0563, wR2 = 0.1050
R indices (all data)	R1 = 0.1320, wR2 = 0.1305
Largest diff. peak and hole	0.173 and -0.221 e.Å^{-3}

Table A.2.1. Atomic coordinates (x 10^4) and equivalent isotropic displacement parameters ($Å^2$x 10^3) for **BC8**. U(eq) is defined as one third of the trace of the orthogonalized U^{ij} tensor.

	x	y	z	U(eq)
O(1)	3186(2)	6873(2)	10066(1)	36(1)
N(1)	-3597(2)	-9079(3)	7228(1)	47(1)
C(1)	-2883(2)	-7975(4)	7409(1)	34(1)
C(2)	-1998(2)	-6610(4)	7642(1)	29(1)
C(3)	-642(2)	-7375(4)	7784(1)	29(1)
C(4)	166(2)	-6116(4)	8024(1)	30(1)
C(5)	-363(2)	-4084(3)	8131(1)	26(1)
C(6)	-1714(2)	-3321(4)	7980(1)	31(1)
C(7)	-2526(2)	-4559(4)	7739(1)	32(1)
C(8)	489(2)	-2861(4)	8400(1)	32(1)
C(9)	83(2)	-985(4)	8550(1)	31(1)
C(10)	908(2)	131(3)	8826(1)	30(1)
C(11)	446(2)	2013(4)	8967(1)	31(1)
C(12)	1164(2)	3259(3)	9253(1)	27(1)
C(13)	2485(2)	2621(4)	9429(1)	31(1)
C(14)	3110(2)	3850(4)	9696(1)	32(1)
C(15)	2431(2)	5775(4)	9803(1)	29(1)
C(16)	1121(2)	6454(4)	9637(1)	35(1)
C(17)	506(2)	5197(4)	9364(1)	37(1)
C(18)	2521(2)	8778(3)	10217(1)	32(1)
C(19)	3694(2)	9809(3)	10456(1)	32(1)
C(20)	3084(2)	11743(3)	10660(1)	32(1)
C(21)	4264(2)	12862(4)	10893(1)	33(1)
C(22)	3627(2)	14716(4)	11109(1)	34(1)
C(23)	4773(2)	15927(4)	11339(1)	35(1)
C(24)	4111(2)	17865(4)	11529(1)	35(1)
C(25)	5257(3)	19087(4)	11759(1)	45(1)

Table A.2.2. Bond lengths [Å] and angles [°] for **BC8**.

O(1)-C(15)	1.370(2)	C(11)-C(12)	1.463(3)
O(1)-C(18)	1.435(2)	C(12)-C(17)	1.396(3)
N(1)-C(1)	1.148(3)	C(12)-C(13)	1.396(3)
C(1)-C(2)	1.440(3)	C(13)-C(14)	1.373(3)
C(2)-C(3)	1.393(3)	C(14)-C(15)	1.391(3)
C(2)-C(7)	1.396(3)	C(15)-C(16)	1.378(3)
C(3)-C(4)	1.386(3)	C(16)-C(17)	1.392(3)
C(4)-C(5)	1.397(3)	C(18)-C(19)	1.509(3)
C(5)-C(6)	1.403(3)	C(19)-C(20)	1.523(3)
C(5)-C(8)	1.465(3)	C(20)-C(21)	1.523(3)
C(6)-C(7)	1.383(3)	C(21)-C(22)	1.519(3)
C(8)-C(9)	1.338(3)	C(22)-C(23)	1.522(3)
C(9)-C(10)	1.441(3)	C(23)-C(24)	1.517(3)
C(10)-C(11)	1.342(3)	C(24)-C(25)	1.526(3)
C(15)-O(1)-C(18)	119.40(16)	C(14)-C(13)-C(12)	121.6(2)
N(1)-C(1)-C(2)	178.9(2)	C(13)-C(14)-C(15)	120.7(2)
C(3)-C(2)-C(7)	119.7(2)	O(1)-C(15)-C(16)	125.7(2)
C(3)-C(2)-C(1)	119.9(2)	O(1)-C(15)-C(14)	114.86(19)
C(7)-C(2)-C(1)	120.3(2)	C(16)-C(15)-C(14)	119.5(2)
C(4)-C(3)-C(2)	120.0(2)	C(15)-C(16)-C(17)	119.2(2)
C(3)-C(4)-C(5)	121.1(2)	C(16)-C(17)-C(12)	122.4(2)
C(4)-C(5)-C(6)	118.05(19)	O(1)-C(18)-C(19)	107.19(17)
C(4)-C(5)-C(8)	119.22(19)	C(18)-C(19)-C(20)	112.56(18)
C(6)-C(5)-C(8)	122.7(2)	C(19)-C(20)-C(21)	113.50(18)
C(7)-C(6)-C(5)	121.3(2)	C(22)-C(21)-C(20)	113.04(18)
C(6)-C(7)-C(2)	119.8(2)	C(21)-C(22)-C(23)	114.97(18)
C(9)-C(8)-C(5)	126.6(2)	C(24)-C(23)-C(22)	113.20(19)
C(8)-C(9)-C(10)	125.5(2)	C(23)-C(24)-C(25)	113.38(19)
C(11)-C(10)-C(9)	123.0(2)		
C(10)-C(11)-C(12)	127.9(2)		
C(17)-C(12)-C(13)	116.7(2)		
C(17)-C(12)-C(11)	119.4(2)		
C(13)-C(12)-C(11)	123.9(2)		

Table A.2.3. Anisotropic displacement parameters $(\text{Å}^2 \times 10^3)$ for **BC8**. The anisotropic

displacement factor exponent takes the form:$-2\pi^2[\ h^2\ a^{*2}U^{11} + ... \ + 2\ h\ k\ a^*\ b^*\ U^{12}\ ]$

	U^{11}	U^{22}	U^{33}	U^{23}	U^{13}	U^{12}
O(1)	38(1)	31(1)	40(1)	-11(1)	-7(1)	6(1)
N(1)	39(1)	48(1)	55(1)	-16(1)	-4(1)	0(1)
C(1)	31(1)	36(2)	35(1)	-3(1)	2(1)	2(1)
C(2)	26(1)	32(1)	27(1)	-2(1)	2(1)	-6(1)
C(3)	30(1)	25(1)	32(1)	-2(1)	5(1)	-1(1)
C(4)	28(1)	30(1)	31(1)	2(1)	1(1)	4(1)
C(5)	26(1)	26(1)	27(1)	1(1)	2(1)	-2(1)
C(6)	31(1)	27(1)	35(1)	-3(1)	0(1)	2(1)
C(7)	27(1)	34(1)	36(1)	1(1)	-1(1)	2(1)
C(8)	29(1)	31(1)	36(1)	-1(1)	-2(1)	1(1)
C(9)	31(1)	32(1)	30(1)	1(1)	-1(1)	2(1)
C(10)	28(1)	30(1)	33(1)	-2(1)	-2(1)	1(1)
C(11)	30(1)	32(1)	33(1)	-1(1)	-2(1)	-1(1)
C(12)	28(1)	27(1)	27(1)	0(1)	1(1)	1(1)
C(13)	32(1)	26(1)	34(1)	-3(1)	2(1)	6(1)
C(14)	31(1)	29(1)	37(1)	-4(1)	-5(1)	5(1)
C(15)	32(1)	28(1)	26(1)	-1(1)	0(1)	-1(1)
C(16)	36(1)	29(1)	40(1)	-8(1)	-2(1)	7(1)
C(17)	31(1)	38(2)	43(1)	-6(1)	-7(1)	6(1)
C(18)	36(1)	27(1)	33(1)	-7(1)	3(1)	5(1)
C(19)	35(1)	30(1)	32(1)	-2(1)	1(1)	2(1)
C(20)	38(1)	29(1)	30(1)	-2(1)	1(1)	4(1)
C(21)	39(1)	28(1)	31(1)	-1(1)	4(1)	0(1)
C(22)	39(1)	33(1)	29(1)	-2(1)	4(1)	-2(1)
C(23)	45(1)	28(1)	31(1)	-3(1)	1(1)	-1(1)
C(24)	43(1)	30(1)	33(1)	-1(1)	4(1)	-3(1)
C(25)	57(2)	38(2)	42(2)	-9(1)	-3(1)	1(1)

Table A.2.4. Hydrogen coordinates (x 10^4) and isotropic displacement parameters ($\mathring{A}^2$x 10^3) for **BC8**.

	x	y	z	U(eq)
H(3)	-275	-8745	7716	35
H(4)	1085	-6639	8116	36
H(6)	-2075	-1940	8044	37
H(7)	-3431	-4022	7641	38
H(8)	1416	-3455	8474	38
H(9)	-817	-339	8468	37
H(10)	1811	-488	8911	36
H(11)	-447	2601	8871	38
H(13)	2958	1320	9362	37
H(14)	4005	3387	9808	39
H(16)	649	7749	9706	42
H(17)	-385	5672	9252	45
H(18A)	1632	8380	10351	38
H(18B)	2212	9799	10030	38
H(19A)	4541	10292	10314	39
H(19B)	4072	8714	10624	39
H(20A)	2261	11244	10808	38
H(20B)	2670	12807	10492	38
H(21A)	4717	11784	11053	39
H(21B)	5063	13432	10744	39
H(22A)	2845	14129	11262	40
H(22B)	3144	15761	10948	40
H(23A)	5200	14916	11514	42
H(23B)	5594	16431	11191	42
H(24A)	3291	17360	11678	42
H(24B)	3682	18873	11354	42
H(25A)	5680	18105	11935	68
H(25B)	4765	20291	11876	68
H(25C)	6054	19641	11613	68

A. 3. X-ray Crystallographic Data for DMABE

Empirical formula	C21 H22 N2
Formula weight	302.41
Temperature	120(2) K
Wavelength	0.71073 Å
Crystal system	Orthorhombic
Space group	Pna2$_1$
Unit cell dimensions	a = 16.1420(3) Å $\alpha = 90°$.
	b = 18.9857(4) Å $\beta = 90°$.
	c = 11.1379(2) Å $\gamma = 90°$.
Volume	3413.40(11) Å^3
Z	8
Density (calculated)	1.177 Mg/m^3
Absorption coefficient	0.069 mm^{-1}
F(000)	1296
Crystal size	0.24 x 0.20 x 0.16 mm^3
Theta range for data collection	2.12 to 26.00°.
Index ranges	-19<=h<=19, -23<=k<=23, -13<=l<=13
Reflections collected	51849
Independent reflections	6697 [R(int) = 0.079]
Completeness to theta = 26.00°	99.9 %
Absorption correction	None
Max. and min. transmission	0.9890 and 0.9836
Refinement method	Full-matrix least-squares on F^2
Data / restraints / parameters	6697 / 1 / 415
Goodness-of-fit on F^2	0.971
Final R indices [I>2sigma(I)]	R1 = 0.0609, wR2 = 0.1277
R indices (all data)	R1 = 0.1577, wR2 = 0.1658
Absolute structure parameter	7(4)
Largest diff. peak and hole	0.234 and -0.165 e.Å^{-3}

Table A.3.1. Atomic coordinates (x 10^4) and equivalent isotropic displacement parameters ($Å^2$x 10^3) for **DMABE**. U(eq) is defined as one third of the trace of the orthogonalized U^{ij} tensor.

	x	y	z	U(eq)
N(1)	3799(2)	14525(2)	2000(4)	70(1)
N(2)	3439(2)	6451(2)	4884(3)	53(1)
C(1)	3847(2)	13919(3)	2025(4)	51(1)
C(2)	3922(2)	13164(2)	2072(4)	44(1)
C(3)	4449(2)	12814(2)	1290(4)	48(1)
C(4)	4534(2)	12094(2)	1360(4)	47(1)
C(5)	4103(2)	11682(2)	2195(3)	37(1)
C(6)	3561(2)	12058(2)	2965(4)	45(1)
C(7)	3473(2)	12769(2)	2915(3)	44(1)
C(8)	4204(2)	10915(2)	2246(4)	40(1)
C(9)	3835(2)	10520(2)	3112(3)	42(1)
C(10)	3872(2)	9770(2)	3238(4)	45(1)
C(11)	3535(2)	9407(2)	4152(4)	44(1)
C(12)	3548(2)	8650(2)	4352(4)	43(1)
C(13)	3989(2)	8171(2)	3622(4)	44(1)
C(14)	3955(2)	7466(2)	3794(4)	45(1)
C(15)	3486(2)	7160(2)	4736(3)	38(1)
C(16)	3072(2)	7634(2)	5496(3)	45(1)
C(17)	3104(2)	8350(2)	5315(3)	42(1)
C(18)	3745(3)	5980(2)	3938(5)	69(1)
C(19)	2909(2)	6149(2)	5797(4)	55(1)
C(20)	4734(2)	10582(2)	1289(4)	56(1)
C(21)	4293(3)	10512(2)	91(5)	72(1)
N(1')	8395(2)	4870(2)	7086(4)	68(1)
N(2')	8452(2)	-3207(2)	9774(3)	60(1)
C(1')	8558(2)	4283(2)	7098(4)	49(1)
C(2')	8732(2)	3544(2)	7143(4)	44(1)
C(3')	9241(2)	3221(2)	6322(4)	55(1)
C(4')	9403(2)	2516(2)	6368(3)	48(1)
C(5')	9043(2)	2078(2)	7250(4)	42(1)
C(6')	8516(2)	2405(2)	8067(4)	45(1)

C(7')	8361(2)	3114(2)	8026(4)	51(1)
C(8')	9209(2)	1314(2)	7290(3)	45(1)
C(9')	8860(2)	885(2)	8127(4)	46(1)
C(10')	8934(2)	137(2)	8233(4)	43(1)
C(11')	8565(2)	-242(2)	9104(4)	47(1)
C(12')	8566(2)	-996(2)	9271(3)	42(1)
C(13')	8997(2)	-1465(2)	8543(4)	47(1)
C(14')	8973(2)	-2185(2)	8690(4)	45(1)
C(15')	8503(3)	-2484(2)	9625(4)	46(1)
C(16')	8088(2)	-2016(2)	10407(4)	44(1)
C(17')	8127(2)	-1305(2)	10215(4)	44(1)
C(18')	8779(3)	-3680(2)	8857(4)	70(1)
C(19')	7952(2)	-3517(2)	10704(4)	61(1)
C(20')	9768(2)	991(2)	6352(3)	50(1)
C(21')	9299(2)	814(2)	5197(4)	65(1)

Table A.3.2. Bond lengths [Å] and angles [°] for **DMABE**.

N(1)-C(1)	1.153(5)	C(12)-C(17)	1.410(5)
N(2)-C(15)	1.360(4)	C(12)-C(13)	1.413(5)
N(2)-C(19)	1.447(5)	C(13)-C(14)	1.353(5)
N(2)-C(18)	1.466(5)	C(14)-C(15)	1.417(5)
C(1)-C(2)	1.441(6)	C(15)-C(16)	1.404(5)
C(2)-C(3)	1.387(5)	C(16)-C(17)	1.375(5)
C(2)-C(7)	1.402(5)	C(20)-C(21)	1.518(6)
C(3)-C(4)	1.376(5)	N(1')-C(1')	1.145(5)
C(4)-C(5)	1.400(5)	N(2')-C(15')	1.385(5)
C(5)-C(6)	1.418(5)	N(2')-C(19')	1.438(5)
C(5)-C(8)	1.466(5)	N(2')-C(18')	1.459(5)
C(6)-C(7)	1.358(5)	C(1')-C(2')	1.432(6)
C(8)-C(9)	1.359(5)	C(2')-C(3')	1.373(5)
C(8)-C(20)	1.506(5)	C(2')-C(7')	1.412(5)
C(9)-C(10)	1.432(5)	C(3')-C(4')	1.366(6)
C(10)-C(11)	1.345(5)	C(4')-C(5')	1.412(5)
C(11)-C(12)	1.454(5)	C(5')-C(6')	1.392(5)

C(5')-C(8')	1.475(5)	C(12')-C(13')	1.391(5)
C(6')-C(7')	1.369(5)	C(12')-C(17')	1.398(5)
C(8')-C(9')	1.360(5)	C(13')-C(14')	1.376(5)
C(8')-C(20')	1.511(5)	C(14')-C(15')	1.408(6)
C(9')-C(10')	1.430(5)	C(15')-C(16')	1.413(5)
C(10')-C(11')	1.347(5)	C(16')-C(17')	1.368(5)
C(11')-C(12')	1.444(5)	C(20')-C(21')	1.530(5)
C(15)-N(2)-C(19)	120.7(3)	C(17)-C(16)-C(15)	121.8(4)
C(15)-N(2)-C(18)	119.8(4)	C(16)-C(17)-C(12)	122.0(4)
C(19)-N(2)-C(18)	117.6(3)	C(8)-C(20)-C(21)	113.1(3)
N(1)-C(1)-C(2)	178.8(5)	C(15')-N(2')-C(19')	121.6(4)
C(3)-C(2)-C(7)	118.8(4)	C(15')-N(2')-C(18')	120.3(4)
C(3)-C(2)-C(1)	120.3(4)	C(19')-N(2')-C(18')	117.1(4)
C(7)-C(2)-C(1)	120.9(4)	N(1')-C(1')-C(2')	177.6(5)
C(4)-C(3)-C(2)	120.1(4)	C(3')-C(2')-C(7')	117.4(4)
C(3)-C(4)-C(5)	122.9(4)	C(3')-C(2')-C(1')	122.0(4)
C(4)-C(5)-C(6)	115.3(3)	C(7')-C(2')-C(1')	120.5(4)
C(4)-C(5)-C(8)	121.7(4)	C(4')-C(3')-C(2')	121.8(4)
C(6)-C(5)-C(8)	123.0(3)	C(3')-C(4')-C(5')	121.6(4)
C(7)-C(6)-C(5)	122.7(4)	C(6')-C(5')-C(4')	116.3(4)
C(6)-C(7)-C(2)	120.3(4)	C(6')-C(5')-C(8')	122.0(4)
C(9)-C(8)-C(5)	121.8(4)	C(4')-C(5')-C(8')	121.7(4)
C(9)-C(8)-C(20)	121.3(3)	C(7')-C(6')-C(5')	122.0(4)
C(5)-C(8)-C(20)	116.9(3)	C(6')-C(7')-C(2')	120.8(4)
C(8)-C(9)-C(10)	126.9(4)	C(9')-C(8')-C(5')	122.3(4)
C(11)-C(10)-C(9)	124.5(4)	C(9')-C(8')-C(20')	118.6(4)
C(10)-C(11)-C(12)	128.1(4)	C(5')-C(8')-C(20')	119.1(4)
C(17)-C(12)-C(13)	115.7(4)	C(8')-C(9')-C(10')	128.0(4)
C(17)-C(12)-C(11)	120.6(4)	C(11')-C(10')-C(9')	123.6(4)
C(13)-C(12)-C(11)	123.7(4)	C(10')-C(11')-C(12')	128.5(4)
C(14)-C(13)-C(12)	122.3(4)	C(13')-C(12')-C(17')	115.1(4)
C(13)-C(14)-C(15)	122.1(4)	C(13')-C(12')-C(11')	124.0(4)
N(2)-C(15)-C(16)	122.3(4)	C(17')-C(12')-C(11')	120.9(4)
N(2)-C(15)-C(14)	121.7(4)	C(14')-C(13')-C(12')	123.5(4)
C(16)-C(15)-C(14)	116.0(4)	C(13')-C(14')-C(15')	120.3(4)

N(2')-C(15')-C(14')	121.4(4)	C(17')-C(16')-C(15')	120.1(4)
N(2')-C(15')-C(16')	121.4(4)	C(16')-C(17')-C(12')	123.7(4)
C(14')-C(15')-C(16')	117.2(4)	C(8')-C(20')-C(21')	112.0(3)

Table A.3.3. Anisotropic displacement parameters (Å^2 x 10^3) for DMABE. The anisotropic displacement factor exponent takes the form: $-2\pi^2[h^2 a^{*2}U^{11} + \dots + 2 h k a^* b^* U^{12}]$

	U^{11}	U^{22}	U^{33}	U^{23}	U^{13}	U^{12}
N(1)	85(3)	65(3)	59(3)	6(3)	-6(3)	-9(2)
N(2)	51(2)	52(2)	57(2)	2(2)	15(2)	2(2)
C(1)	46(2)	68(3)	39(3)	7(3)	-4(2)	-14(2)
C(2)	43(2)	49(3)	40(3)	3(2)	-11(2)	-11(2)
C(3)	48(3)	63(3)	34(2)	1(2)	6(2)	-15(2)
C(4)	46(2)	58(3)	37(2)	0(2)	6(2)	-4(2)
C(5)	31(2)	50(3)	29(2)	1(2)	0(2)	-6(2)
C(6)	42(2)	55(3)	38(2)	8(2)	1(2)	-4(2)
C(7)	40(2)	57(3)	35(2)	5(2)	1(2)	-5(2)
C(8)	31(2)	51(3)	38(2)	5(2)	-5(2)	-1(2)
C(9)	34(2)	57(3)	34(2)	-1(2)	-2(2)	-5(2)
C(10)	40(2)	59(3)	36(2)	2(2)	1(2)	-1(2)
C(11)	34(2)	60(3)	37(2)	-4(2)	-3(2)	-4(2)
C(12)	30(2)	56(3)	42(3)	-1(2)	-6(2)	-7(2)
C(13)	33(2)	61(3)	37(2)	2(2)	7(2)	1(2)
C(14)	39(2)	48(3)	46(3)	2(2)	7(2)	6(2)
C(15)	32(2)	49(3)	34(2)	-1(2)	1(2)	-3(2)
C(16)	40(2)	61(3)	33(2)	1(2)	-1(2)	-5(2)
C(17)	34(2)	62(3)	30(2)	-6(2)	-1(2)	1(2)
C(18)	76(3)	60(3)	71(3)	4(3)	24(3)	9(2)
C(19)	52(3)	65(3)	47(3)	10(2)	3(2)	-6(2)
C(20)	42(2)	59(3)	67(3)	10(3)	9(2)	3(2)
C(21)	56(3)	91(4)	70(3)	-21(3)	18(3)	-8(3)
N(1')	83(3)	55(3)	65(3)	3(2)	-5(2)	-15(2)
N(2')	59(2)	62(3)	58(2)	-5(2)	21(2)	6(2)
C(1')	54(3)	52(3)	41(3)	0(3)	-9(2)	-13(2)
C(2')	41(2)	59(3)	33(2)	-4(2)	-1(2)	-7(2)

C(3')	56(3)	64(3)	46(3)	-3(3)	0(2)	-17(2)
C(4')	38(2)	77(3)	28(2)	-4(2)	6(2)	-14(2)
C(5')	32(2)	56(3)	37(2)	-1(2)	-6(2)	-1(2)
C(6')	39(2)	59(3)	37(2)	-3(2)	11(2)	-1(2)
C(7')	47(2)	63(3)	43(3)	-4(2)	8(2)	-2(2)
C(8')	32(2)	75(3)	28(2)	-1(2)	-1(2)	3(2)
C(9')	38(2)	62(3)	37(2)	-6(2)	-1(2)	9(2)
C(10')	36(2)	59(3)	35(2)	-3(2)	-1(2)	9(2)
C(11')	38(2)	58(3)	44(3)	-10(2)	-4(2)	8(2)
C(12')	33(2)	59(3)	32(2)	-6(2)	-3(2)	8(2)
C(13')	40(2)	58(3)	41(3)	-4(2)	2(2)	5(2)
C(14')	36(2)	61(3)	38(2)	-6(2)	10(2)	9(2)
C(15')	42(2)	50(3)	47(3)	-1(2)	-5(2)	4(2)
C(16')	34(2)	62(3)	37(2)	-11(2)	4(2)	5(2)
C(17')	43(2)	51(3)	39(2)	-12(2)	0(2)	6(2)
C(18')	90(4)	58(3)	64(3)	-2(3)	14(3)	17(3)
C(19')	65(3)	65(3)	53(3)	6(3)	-3(2)	3(2)
C(20')	41(2)	67(3)	43(2)	-1(2)	6(2)	10(2)
C(21')	56(3)	79(4)	60(3)	-22(3)	10(3)	-2(2)

Table A.3.4. Hydrogen coordinates (x 10^4) and isotropic displacement parameters (Å^2x 10 ^{3}) for **DMABE**.

	x	y	z	U(eq)
H(3)	4751	13072	704	58
H(4)	4902	11867	819	57
H(6)	3247	11803	3540	54
H(7)	3106	13000	3452	53
H(9)	3519	10768	3695	50
H(10)	4155	9511	2633	54
H(11)	3254	9678	4741	52
H(13)	4321	8350	2987	52
H(14)	4255	7166	3267	53
H(16)	2762	7455	6153	54
H(17)	2818	8651	5855	50

H(18A)	4351	5993	3923	104
H(18B)	3529	6135	3160	104
H(18C)	3558	5498	4100	104
H(19A)	2332	6276	5632	82
H(19B)	3070	6332	6586	82
H(19C)	2967	5635	5792	82
H(20A)	4908	10109	1564	67
H(20B)	5239	10870	1178	67
H(21A)	4187	10981	-241	108
H(21B)	3766	10265	206	108
H(21C)	4642	10244	-466	108
H(3')	9487	3497	5705	66
H(4')	9767	2315	5791	57
H(6')	8257	2129	8670	54
H(7')	7998	3319	8600	61
H(9')	8525	1111	8715	55
H(10')	9261	-105	7657	52
H(11')	8266	21	9685	56
H(13')	9326	-1279	7911	56
H(14')	9274	-2480	8159	54
H(16')	7781	-2196	11067	53
H(17')	7839	-1005	10755	53
H(18D)	9385	-3650	8847	106
H(18E)	8560	-3544	8070	106
H(18F)	8611	-4165	9039	106
H(19D)	7374	-3373	10598	92
H(19E)	8151	-3357	11489	92
H(19F)	7991	-4031	10658	92
H(20C)	10019	556	6680	60
H(20D)	10222	1324	6164	60
H(21D)	9122	1251	4804	98
H(21E)	8811	528	5392	98
H(21F)	9662	549	4656	98